ISSN: 2408-2384 (Online)
ISSN: 1686-5456 (Print)

Environment and Natural Resources Journal

Volume 21, Number 3, May - June 2023

Environment and Natural Resources Journal (EnNRJ)

Volume 21, Number 3, May - June 2023

ISSN: 1686-5456 (Print)

ISSN: 2408-2384 (Online)

AIMS AND SCOPE

The Environment and Natural Resources Journal is a peer-reviewed journal, which provides insight scientific knowledge into the diverse dimensions of integrated environmental and natural resource management. The journal aims to provide a platform for exchange and distribution of the knowledge and cutting-edge research in the fields of environmental science and natural resource management to academicians, scientists and researchers. The journal accepts a varied array of manuscripts on all aspects of environmental science and natural resource management. The journal scope covers the integration of multidisciplinary sciences for prevention, control, treatment, environmental clean-up and restoration. The study of the existing or emerging problems of environment and natural resources in the region of Southeast Asia and the creation of novel knowledge and/or recommendations of mitigation measures for sustainable development policies are emphasized.

The subject areas are diverse, but specific topics of interest include:

- Biodiversity
- Climate change
- Detection and monitoring of polluted sources e.g., industry, mining
- Disaster e.g., forest fire, flooding, earthquake, tsunami, or tidal wave
- Ecological/Environmental modelling
- Emerging contaminants/hazardous wastes investigation and remediation
- Environmental dynamics e.g., coastal erosion, sea level rise
- Environmental assessment tools, policy and management e.g., GIS, remote sensing, Environmental Management System (EMS)
- Environmental pollution and other novel solutions to pollution
- Remediation technology of contaminated environments
- Transboundary pollution
- Waste and wastewater treatments and disposal technology

Schedule

Environment and Natural Resources Journal (EnNRJ) is published 6 issues per year in January-February, March-April, May-June, July-August, September-October, and November-December.

Publication Fees

There is no cost of the article-processing and publication.

Ethics in publishing

EnNRJ follows closely a set of guidelines and recommendations published by Committee on Publication Ethics (COPE).

Environment and Natural Resources Journal (EnNRJ)

Volume 21, Number 3, May - June 2023

ISSN: 1686-5456 (Print)
ISSN: 2408-2384 (Online)

Editorial Office Address
Research Management and Administration Section,
Faculty of Environment and Resource Studies, Mahidol University
999, Phutthamonthon Sai 4 Road, Salaya, Phutthamonthon, Nakhon Pathom, Thailand, 73170
Phone +662 441 5000 ext. 2108 Fax. +662 441 9509-10
Website: https://ph02.tci-thaijo.org/index.php/ennrj/index
E-mail: ennrjournal@gmail.com

Environment and Natural Resources Journal (EnNRJ)
Volume 21, Number 3, May - June 2023
ISSN: 1686-5456 (Print)
ISSN: 2408-2384 (Online)

CONTENT

Identification of Potential Groundwater Recharge Zones Using GIS Based Multi-Criteria and AHP Technique: A Case Study of Pune City, Western Maharashtra

Natraj Vaddadi[1*], Chaiwiwat Vansarochana[2], and Venkatesh Raghavan[3]

[1]*Centre for Education and Research in Geosciences, Aundh, Pune 411007, India*
[2]*Faculty of Agriculture Natural Resources and Environment, Naresuan University, Phitsanulok 65000, Thailand*
[3]*Graduate School of Science, Osaka Metropolitan University, Osaka 558-8585, Japan*

ARTICLE INFO

Received: 1 Dec 2022
Received in revised: 23 Jan 2023
Accepted: 5 Feb 2023
Published online: 13 Mar 2023
DOI: 10.32526/ennrj/21/202200257

Keywords:
Groundwater Recharge Potential/ Rainwater Harvesting/ Multi Criteria Analysis/ Analytic Hierarchy Process/ Weighted Overlay Analysis/ Pune City

*** Corresponding author:**
E-mail: natraj@cerg.org.in

ABSTRACT

With dwindling supply of surface water, Ground water is increasingly being used as a source of fresh water in many cities across the world. Consequently, there is an increasing need to evaluate groundwater potential of an area. Over the past few decades, Remote Sensing and GIS have been used for systematic investigations on potential recharge of aquifers. As in major cities of the world, the demand for water in Pune City is also increasing every year and demand outstrips the supply of surface water. This study delineated potential zones for artificial recharge across Pune City by using Multi-criteria analysis and the Analytical Hierarchy Process (AHP) techniques.

Artificial recharge techniques especially the use of rainwater harvesting (RWH) are being deployed globally to augment supply of fresh water. Ground-water recharge is directly influenced by surface characteristics such as rainfall, geology, soil types, Land Use/Land Cover (LULC), drainage, lineaments/fractures, etc. Hence, six such parameters, namely, LULC, Slope, Soil texture, Rainfall, Drainage density, and Geology were considered to generate a groundwater recharge potential map. Based on the analysis, the study area was zoned into five classes, namely, low, moderate, good, very good and high groundwater potentials. About 45% of the city shows good to high potential for recharge. The results reveal that the high and good potential recharge zones lie to the western part of the city, whereas the central part (inner city) and the eastern part show medium to low potential for recharge. The results can help to identify areas for recharge and formulate a framework for systematic recharge of the existing aquifers in the area under study.

1. INTRODUCTION

Water scarcity is increasingly becoming a global phenomenon in urban growth centers, even in developed countries. Population growth and rapid urbanization have led to increased demand of water and over exploitation of groundwater and consequently water stress. In this scenario, maintaining the groundwater balance assumes immense importance. Artificial recharge of groundwater using different techniques such as roof-top rainwater harvesting, recharge pits, check dams, percolation tanks, and injection wells is therefore crucial for the restoration of the hydrological balance (Rao et al., 2022).

Research carried out by several workers (Senanayake et al., 2016; Adham et al., 2016; Paul et al., 2020) on rainwater harvesting (RWH) have focused on identifying potential sites for surface recharge to the aquifers in non-urban areas. Recharge of groundwater from rainfall has been studied extensively and numerous methods like Thiessen polygon (Kim et al., 2003), Agricultural non-point source (Mohammed et al., 2004), water balance approach (Jasrotia et al., 2009) and Soil Conservation Service Curve Number (SCS-CN) (Kadam et al., 2012) have been suggested to identify potential sites for groundwater recharge.

Citation: Vaddadi N, Vansarochana C, Raghavan V. Identification of potential groundwater recharge zones using GIS based multi-criteria and AHP technique: A case study of Pune City, Western Maharashtra. Environ. Nat. Resour. J. 2023;21(3):198-210. (https://doi.org/10.32526/ennrj/21/202200257)

Besides these conventional techniques, integrated application of Remote Sensing (RS), Geographic Information Systems (GIS) and Multi Criteria Decision Analysis (MCDA) techniques for the delineation of recharge zones/sites have drawn attention in recent times. The use of thematic layers and techniques like Weighted Overlay Method (WOA) based on Analytic Hierarchy Process (AHP) are increasingly being used for identification of ground water potential recharge zones, exploitation, and management of ground water resources.

The MCDA and WOA workflow incorporating different parameters, such as geology, geomorphology, soil type, land use/land cover, and slope was applied by Kadhem and Zubari (2020) to identify optimal locations for managed aquifer recharge in Bahrain. The use of MCDA was found useful in assessing potential groundwater zones in Sidhi area of India (Tiwari et al., 2020) and to identify suitable sites for potential recharge in West Medinipur district of West Bengal by Chowdhury et al. (2010). Paul et al. (2020) used multi-criteria evaluation technique for assessment of groundwater potential zones in the Paisuni River Basin, India. They suggested that proper technical design and identification of suitable sites are crucial to efficient RWH.

The AHP method applied using thematic layers like slope, drainage, lithology, LULC, and soil type has been used by several other researchers like Nasiri et al. (2013), Jamali et al. (2014), Akter and Ahmed (2015), Singh et al. (2017), Çelik (2019), and Benjmel et al. (2020). Akter and Ahmed (2015) evaluated potentiality of RWH systems in Chittagong city (urban catchment) of Bangladesh applying the AHP approach and using roof area, slope, drainage density and runoff coefficient as themes. Das and Pal (2019) used AHP and WOA to delineate potential groundwater zones in Puruliya District of West Bengal in India. Kumar et al. (2020) used RS, GIS and AHP techniques to identify potential groundwater zones in parts of the Deccan Volcanic Province. Venkatarao et al. (2019) calculated the groundwater recharge potential zones using a cross-correlation technique between groundwater levels in wells and rainfall events. Vaddadi et al. (2022) estimated the potential for ground water recharge available from roof-top rainwater harvesting for Pune city to be 49.05 million cubic meters (MCM) and that effective recharge using RWH techniques could supplement the groundwater annually by about 22-25 MCM.

The demand for Pune City in 2020 was 424 MCM and the budget for the year 2021-2022 was 568.31 MCM. With growth in population, the annual water demand will increase to 23.34 TMC (660.91 MCM) by 2031-2032. (Pune Municipal Corporation, 2021). The gap between demand and supply necessitates looking for alternative sources of potable water to cater to the shortfall. The objective of this study, therefore, was to delineate potential zones for artificial recharge across Pune city considering urban factors like land-use by using GIS, Multi-criteria analysis, and the Analytical Hierarchy process (AHP) techniques. Six parameters, namely, LULC, Slope, Soil texture, Rainfall, Drainage density, and Geology were considered to generate a groundwater recharge potential map.

2. THE STUDY AREA

Pune City, a part of the Pune urban area is a plateau region set on the western margin of the Deccan Volcanic Province. The Pune Municipal Corporation (PMC, Pune City) covers about 331.26 km^2. Pune City is the second largest city in Maharashtra state and ninth largest in India with a population of 3,124,458. (Census India - Population Census, 2011). The study area lies between 18°27’ and 18°40’ N - 74°39’ and 74°00’ E (Figure 1) and is within the Deccan Volcanic Province. Of the total area of the city, the study area covers about 250 km^2. The average annual precipitation is 780 mm with maximum rainfall occurring in the month of July. The area experiences three seasons - summer, monsoon and winter and usually faces a shortage of water if the monsoon has failed in the previous year.

2.1 Geology and hydrogeology

The area falls in the Western part of the Deccan Volcanic Province and is underlain by basalts of upper Cretaceous to Eocene age. The city is bounded by hills on the West and in the South. Mula and Mutha Rivers are the main rivers in the study area. Two more rivers, Pavana and Indrayani flow from North-western direction. The drainage is dendritic, sub-dendritic and sub-parallel. Structural control in the drainage is evident at many places.

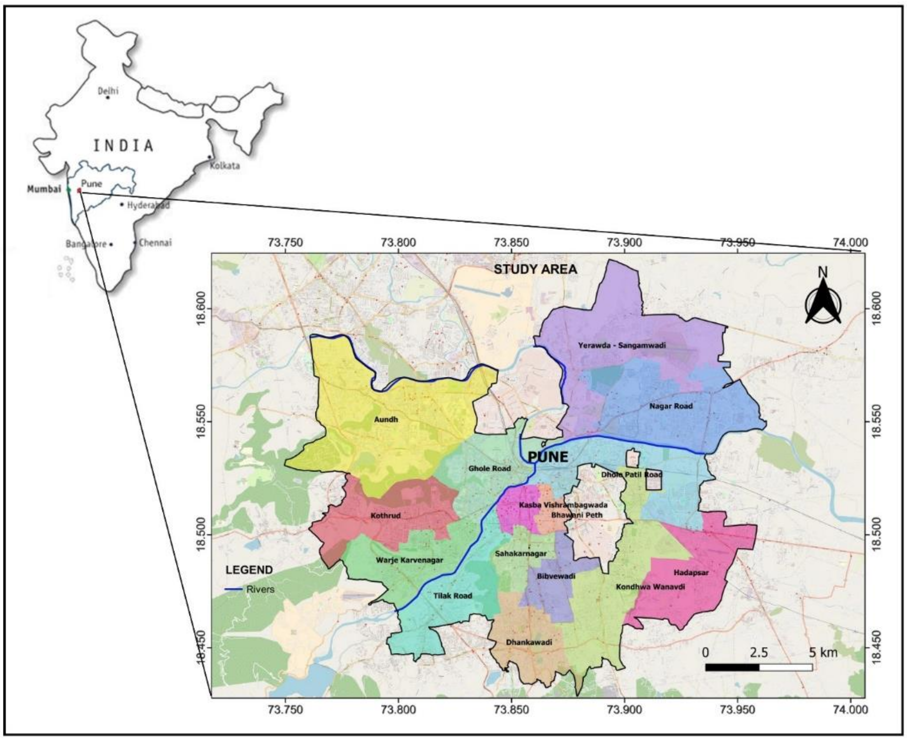

Figure 1. Location map of study area

Based on lithostratigraphy, the lava flow sequence seen in the area have been divided into four Formations - Indrayani, Karla, Diveghat and Purandargarh Formations. The flows belonging to Indrayani, Diveghat and Purandargarh Formations are dominantly of simple nature, while those of Karla Formation show a compound nature.

Based on field characteristics, the lava flows are broadly classified into two types, namely, simple and compound flows. The simple flows are characterized by a fragmented top, a thin brecciated base (basal clinker) and a compact, jointed massive core. The compound flows are vesicular and amygdaloidal at the top and show a certain amount of weathering at places. The middle portion is hard, compact, fractured, and jointed. The basal sections of these flows are characterized by pipe amygdales. The thickness of the flows varies on an average from 10 to 20 meters.

The water bearing capacity of the rock formations is mainly governed by the porosity which determines the volume available for storage of water. Due to their compact nature the basalt flows show very low primary porosity and permeability. Secondary porosity developed due the presence of openings and cavities, vertical joints and horizontal sheet joints, weathering, and flow contacts impart the water holding and transmission capacity to these flows.

The weathered parts of the flows exhibit higher porosity and permeability when compared to the fresh units. The secondary porosity is also higher in the flows exhibiting columnar joints, sheet joints, brecciated and vesicular flow tops.

In terms of hydro-geological properties, the flows are usually classified as vesicular/amygdular basalt (which also includes the Flow Top Breccia (FTB)), jointed basalt, and massive, compact basalt. The vesicular/amygdular basalt, jointed basalt, and weathered basalt act as aquifers as they have better porosity while the massive compact basalts act as aquifuges or aquitards. The clayey tuffaceous layers occurring between the flows act as an aquiclude.

Groundwater circulation happens through the fractured portions in the massive basalt, the vesicular upper sections and through the weathered portion of the flows. Recharge to deeper horizons occurs mainly through deep fractures and fractured dykes.

3. METHODOLOGY

In the present study, a MCDA approach using AHP was used for delineation of potential ground water recharge zones. Physiographic elements have a close relationship with groundwater recharge (Doke et al., 2021). According to Choudhari et al. (2018) the level of groundwater varies according to elements such as geology, drainage density, lineament, rainfall, and land-use. Many researchers have used criteria like lithology, geomorphology, geology, drainage density, soils, lineament, rainfall, land-use, and distance from the river for delineation of groundwater zone (Das and Pal, 2019; Maity and Mandal, 2019). Rao (2006) computed a groundwater potential index (GPI) considering factors such as rainfall, slope, run-off, infiltration, soil cover, moisture content, lineaments, weathered and fractured rocks, drainage, groundwater levels, and vegetation with relation to geomorphological units.

3.1 Thematic layers

The present study uses multi-criteria, namely, LULC, slope, geology, soil, drainage density, and rainfall which are some factors known to affect the recharge of groundwater. Thematic maps were prepared using QGIS for these factors for further AHP and WOA studies.

Survey of India toposheets were used as the reference map by georeferencing and digitisation and for generating the drainage density. Geological data obtained from the District Resource Map of Geological Survey of India (GSI, 2001), was geo-referenced and digitized to obtain the geological map of the area. Landsat 8 was used for generating LULC layer (Vaddadi et al., 2022) and classified into four classes. The slopes for the area were calculated in degrees from Cartosat DEM image of 5 m resolution. Soil data was obtained from the soil map of the Indian National Bureau of Soil Survey and Land Use Planning (NBSS and LUP). The classification of soils given by NBSS and LUP is used in this study. High Spatial Resolution (0.25×0.25 degree) ‘Gridded Rainfall Data Set Over India’ data available from India Meteorological Department was used to create the rainfall map (Pai et al., 2014) (https://imdpune.gov.in/cmpg/Griddata/Rainfall_25_Bin.html). Drainage was digitized from toposheet, and the density was calculated using point density method in QGIS.

Geospatial data (Table 1) was processed using QGIS software, while weight generation and associated functions like Consistency Index and Consistency Ratio were calculated by the AHP method in Microsoft Excel. The input thematic layer data for the different layers was reclassified to obtain four or more discrete classes based on the available data and literature survey. The workflow used for the study is shown in Figure 2.

Table 1. Data sources

Data type	Resolution/Scale	Thematic layer	Data source
Landsat 8 OLI/TM	30 m	Land use/land cover	Earth Explorer - USGS
Cartosat DEM	5 m	Slope, drainage density	Bhuvan ISRO
District Resource Map - Geology	1:250,000	Geology (Lithology)	Geological Survey of India
Rainfall data	0.25×0.25 degree	Rainfall	India Meteorological Department
Soil map	1:250,000	Soil distribution	National Bureau of Soil Sciences and Land Use Planning

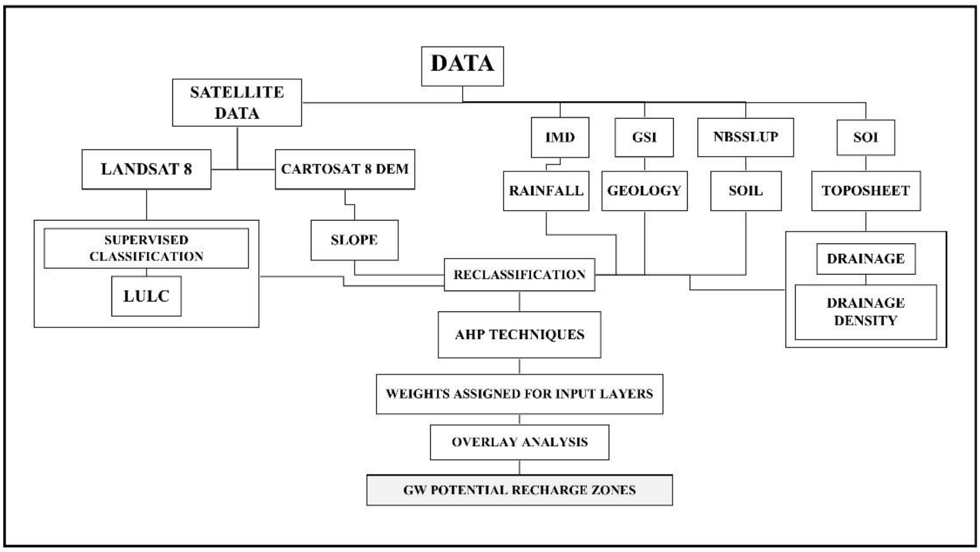

Figure 2. Workflow used in the analysis

3.2 AHP analysis

AHP is a decision-making procedure widely used in management for establishing priorities in multicriteria decision problems. It uses a structured mathematical process based on expert knowledge. AHP was first developed by Saaty (1987). Though introduced as a management tool, it has been used across disciplines as an effective tool for dealing with complex decision-making. AHP converts multi-dimensional complexity into a single dimension scale of priorities (Choosumrong et al., 2012).

The AHP process has also been widely used in GIS to normalize the assigned weights of different thematic layers. In this study, the weights of different thematic layers were assigned based on literature survey, published data and expert opinion for different environmental and geological conditions (Table 2).

Table 2. Input parameters

Rank	Thematic layer	Class	Class description	Weight/Sub rank	Area (km^2)	Area (%)	Normalized weight
1	LULC	4	Vegetation	4	36.42	15.00	0.41
		3	Water	3	2.08	1.00	
		2	Barren land	2	86.37	34.00	
		1	Construction	1	125.65	50.00	
2	Slope	0-5°	Flat surface	6	189.52	75.28	0.23
		5-10°	V. gentle slope	5	44.39	17.63	
		10-15°	Gentle slope	4	12.06	4.79	
		15-20°	Moderate slope	3	4.37	1.73	
		20-25°	Steep slope	2	1.07	0.42	
		<25°	Very steep slope	1	0.36	0.14	
3	Drainage density	<80	Very low drainage	4	9.83	4	0.14
		80-160	Low drainage	3	78.89	32	
		160-240	Moderate drainage	2	115.06	46	
		>240	High drainage	1	46.62	19	
4	Rainfall	>4.8 mm/day	High rainfall	4	29.62	11.83	0.11
		4.1-4.5 mm/day	Moderate rainfall	3	142.63	56.95	
		3.8-4.13 mm/day	Low rainfall	2	55.28	22.07	
		<3.8 mm/day	Very low rainfall	1	22.93	9.16	
5	Soil	Type 1 (118*)	Loamy, mixed and iso-hyperthermic, moderate stoniness	5	104.44	42	0.07
		Type 2 (76*)	Clayey skeletal, strongly calcareous, strong stoniness	4	0.36	0	
		Type 3 (216*)	Fine, clayey, moderately calcareous, moderate stoniness	3	4.96	2	
		Type 4 (266*)	Fine, strongly Calcareous, clayey, montmorillonitic	2	4.89	2	
		Type 5 (244*)	Clayey, calcareous, moderate salinity, fine	1	135.86	54	
6	Geology	Karla formation	Dominantly compound pahoehoe flows	4	128.59	51	0.04
		Diveghat formation	Dominantly Aa' and simple flows with thick FTB (Fragmented tops)	3	61.67	25	
		Indrayani formation	Aa' flows with thick FTB (Fragmented tops)	2	58.91	24	
		Purandargarh formation	Aa' and simple flows with thin FTB (Fragmented tops)	1	1.35	1	

*Soil types - Figures in parentheses indicate Index number as per NBSS and LUP map.

After the ranking of the criteria, the weight for each criterion was determined by using AHP to get a Pairwise Comparison Matrix (PCM) for the main decision criteria being used (Table 3). In doing a pairwise comparison, the relative importance of a set of criteria is decided for determining the suitability for a given objective. The comparison and rating between criteria are conducted using a 9-point continuous scale. (Saaty, 2008).

The following steps were adapted to allocate and normalize weights of the thematic layers using the AHP technique - (1) Defining the criteria; (2) Defining scaled rank (weights) for each criterion based on expert opinion and literature survey; (3) Establishment of pairwise comparison metrics (P) based on scaled ranks; (4) Calculation of the geometric mean; (5) Calculation of normalized weights; and (6) Calculation of consistency ratio to verify the coherence of judgments.

AHP process involves a PCM of the various criteria which influence a particular process to derive priority weightages. The influencing factors or themes are based on expert judgement.

The PCM is calculated on basis of assigned weightages and, shows how a particular criterion is significant when compared to the others Saaty (1987), Saaty (1990), and Saaty (2008). Based on PCM, the relative weight matrix and the normalized principal eigenvalue were derived to determine the percentage of contribution of each criterion.

Table 3. Pair-wise comparison matrix for the six themes and calculation of normalized weights by the analytic hierarchy process

Matrix	LULC	Slope	Drainage density	Rainfall	Soil	Geology	Normalized principal eigenvector
LULC	1	3	5	3	5	5	0.41
Slope	1/3	1	3	3	3	5	0.23
Drainage density	1/5	1/3	1	2	3	5	0.14
Rainfall	1/3	1/3	1/2	1	3	3	0.11
Soil	1/5	1/3	1/3	1/3	1	3	0.07
Geology	1/5	1/5	1/5	1/3	1/3	1	0.04

Each of the six thematic layer has four or more sub-classes, thereby making the relationships between these interdependent classes complex. The relationship between the factors and their relative importance is derived using the AHP. The result of the AHP is assignment of normalized weights which are then used in the weighted overlay analysis.

3.3 Overlay analysis

The final weights are obtained from the computation of the principal Eigenvector of the PCM. To evaluate the consistency of the pair-wise comparison in AHP, the Consistency Index (CI) is determined based on the maximum Eigen value, λmax.

λmax is calculated by summing up the product of each element in the relative weights (the Eigen vector) by the respective column total of the original comparison matrix.

The CI is determined by the equation below.

$$CI = -(\lambda max - n)/n - 1 \tag{1}$$

Where; λmax is the largest Eigen value of the matrix and can easily be determined from the matrix mentioned, and n is the number of factors or criteria being considered. In this case, the λmax obtained is 6.539 and the CI is 0.108.

To verify whether the CI is appropriate, Saaty (1990) suggests the Consistency Ratio (CR) which is determined as the ratio between the CI and the Random Consistency Index (RCI). The value of RI for selected 'n' values are as per the Consistency Index suggested by Saaty (1990).

$$CR = CI / RCI \tag{2}$$

The comparison matrix is consistent if the resulting CR is less than 10% (Saaty, 1990). If the CR exceeds 10%, it is necessary to rework the comparison matrix and recalculate the weights to get a better weighting scheme.

The CR obtained was 0.87 (8.8%) which is less than the threshold limit (0.1). This indicates that the weight assignment for the parameters used in this study is consistent.

4. RESULTS AND DISCUSSION

Anthropogenic alterations, which are a result of increasing urbanization lead to a major impact on the natural resources like water especially in terms of recharge potential. The quantitative impacts of urbanization include a general decline in groundwater level, a reduction of the areal extent of the aquifer, and a change in groundwater flow direction (Khazaei et al., 2004).

4.1 Thematic layers

To implement effective artificial recharge methods, it is important to determine potential recharge zones especially in urban areas. Several spatial factors come into play when considering potential zones for recharge by RWH. Besides rainfall, other factors like slope of the land and soil texture also play a crucial role in the recharge. The ranking of the criteria used in the study are summarized in Table 2.

Land use/land cover impacts the rate of surface runoff, infiltration, and utilization of the groundwater (Senanayake et al., 2016). Urbanization, especially concretisation leads to increased run-off and surface flow thereby reducing the water available for recharge. The LULC of an area is thus a particularly important influencing factor in recharge in an urban context. The greater the concretisation, the less is the recharge and hence LULC was given the highest attribute rank. Within LULC, the built-up area was given the lowest weight. Vegetated areas, wetlands and water bodies are considered to have high infiltration rates.

LULC was derived from Landsat 8 Satellite of 30 m Resolution for year 2019 (Vaddadi et al., 2022). The study area was classified into four classes Barren Land, Settlement, Water Bodies and Vegetation based on a Supervised Classification study (Figure 3). The analysis shows that a major part of the study area is occupied by constructions or built-up area which occupies about 125 km^2 (50%). About 86 km^2 (34%) is occupied by barren land. Vegetated areas and water bodies which are very good for infiltration together constitute 39 km^2 (16%).

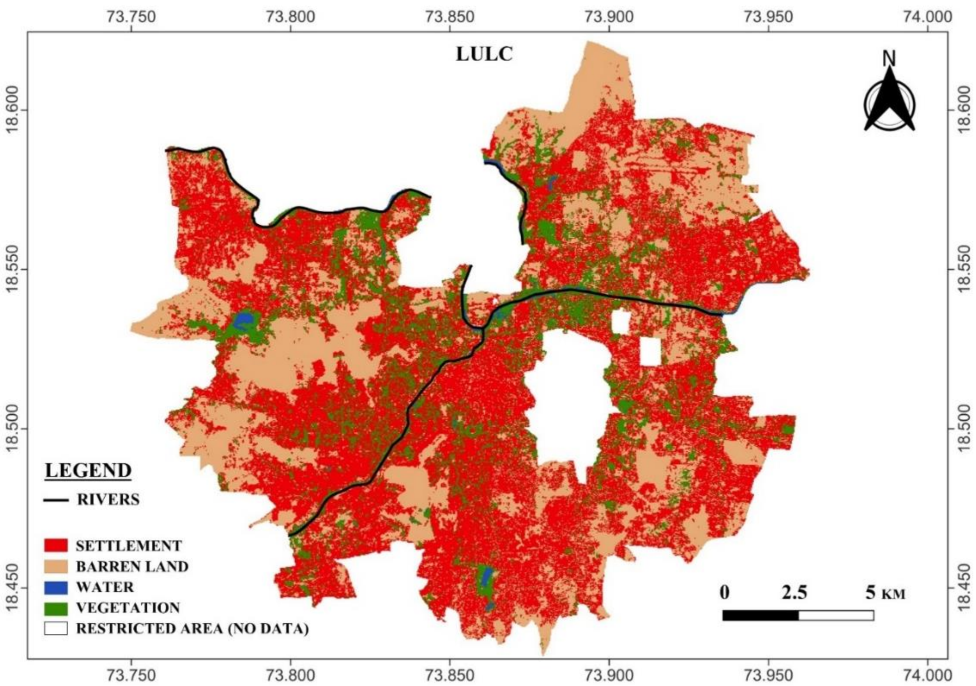

Figure 3. LULC map

The slope of an area influences rainfall infiltration and is an important parameter in recharge potential. Infiltration will be higher in low-slope areas where surface flow and run-off are less and where it takes more time to travel downstream, as compared to high slope areas where the run-off is higher and quicker (Rajaveni et al., 2015).

The slopes for the area were calculated in degrees from Cartosat DEM image of 5 m resolution. The slopes were classified into six classes with slope from 0-31°. The maximum areal extent in the study area was for range 1-5° (Flat surface). About 189 km^2 (75%) of the study area is flat and conducive to infiltration (Figure 4).

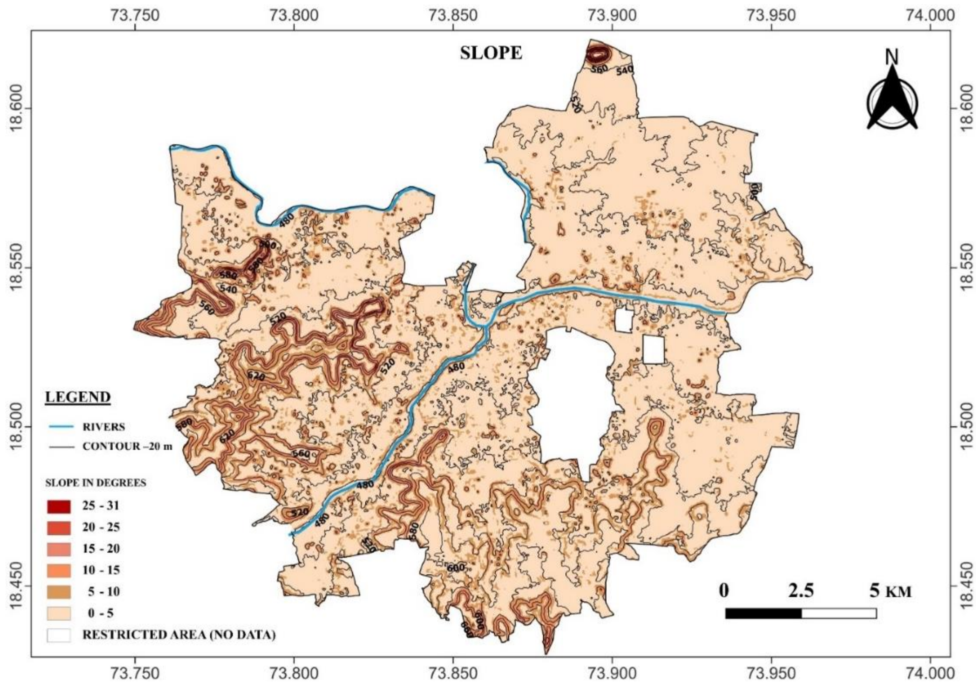

Figure 4. Slope map

Drainage density is a significant parameter which affects the groundwater recharge potential. A low drainage density region causes more infiltration and results in good groundwater potential zones as compared to a high drainage density region (Shekhar and Pandey, 2014). Drainage was digitized from toposheet, and the density was calculated using point density method in QGIS. The obtained densities were classified into four classes which ranged from 0.43-306.80. Of these classes, the areas occupying low and very low density which are good for ground water infiltration occupy about 162 km^2 (65%) of the area. Area with moderate density occupies an area of 79 km^2 (32%) and is also suitable for recharge. Drainage class with least density was assigned the highest weightage on account of the lower number of drainages per unit area (Figure 5).

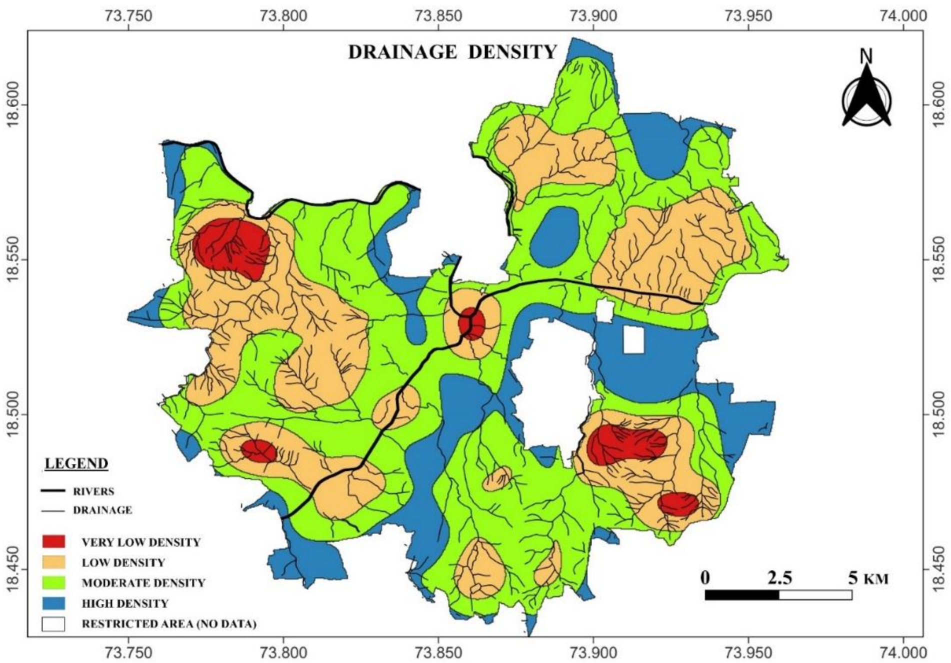

Figure 5. Drainage density map

Rainfall is essential to recharge. Groundwater is formed by rain infiltrating the ground. Using tritium injection studies, Rangarajan and Athavale (2000) estimated a linear relation between rainfall and natural recharge for major hydrogeological units like granites, basalt, sediments and alluvium. According to Mondal and Ajaykumar (2022), rainfall is the primary source of groundwater recharge, whereas irrigation areas, rivers, ponds, lakes, etc., are the secondary sources of groundwater recharge. Grid based rainfall data with a resolution 0.25×0.25 degrees was downloaded from India Metrological Department (IMD) site (https://imdpune.gov.in/cmpg/Griddata/Rainfall_25_Bin.html). This data was then converted to Rainfall point data by using the IMD data converter. This point data was then interpolated to create the Rainfall Map (Figure 6). Though rainfall is a key factor for assessing the suitability of a region for harvesting it was ranked much lower than LULC and slope since it was found that a major part of the city area is built up leading to run-off instead of infiltration.

The rainfall in the area ranged between a high of 4.79 and a low of 3.47 mm/day. Based on this, the study area was re-classified into four classes of high, moderate, low, and very low rainfall. These occupy 11.83%, 56.95%, 22.07%, and 9.16%, respectively.

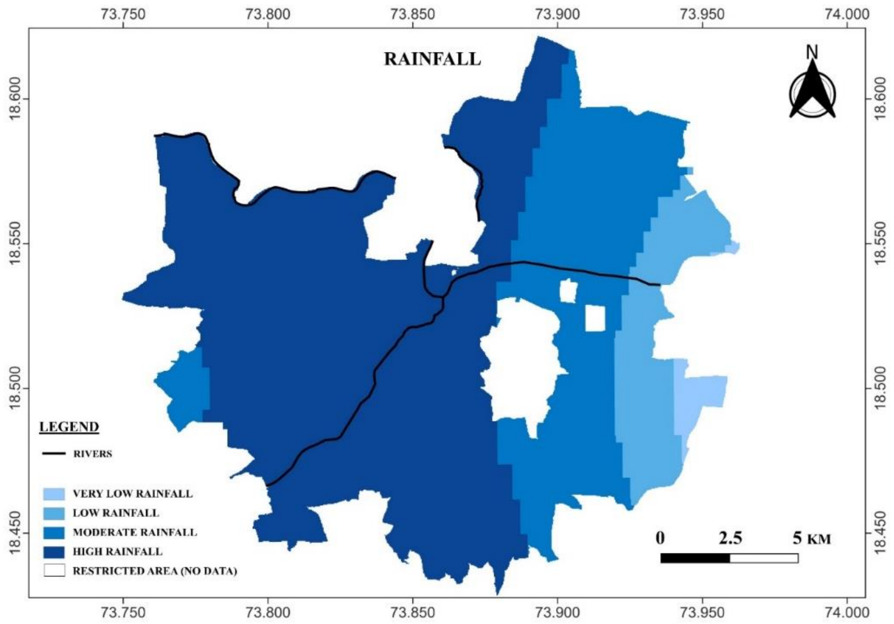

Figure 6. Rainfall map

Soil texture is another important parameter that influences rainfall infiltration into the ground. The rate and amount of infiltration depend on grain structure, size, and shape. Soil texture and hydraulic characteristics (permeability) influence rate of infiltration.

The soil map was obtained from NBSS and LUP. It was then clipped to the study area and used to create the soil type vector data. The classification of soils given by NBSS and LUP is used in this study. The study area exhibits five broad textural classes or types of soil (Figure 7). About 42% (104 km^2) of the area is occupied by loamy, mixed and iso-hyperthermic, moderate stoniness soil which is good for infiltration. Fine Clayey and calcareous soil occupies 136 km^2 (54%) of the area. The other layers together constitute only about 4% of the area. According to Cornell University (2010), Sandy loams, Loams, Clay loams or Clay soils have an infiltration capacity of 0.4 to 0.8, 0.2 to 0.4, and less than 0.2 inches per hour, respectively. Considering the texture and its sand content, Type 1 soil (loamy, mixed, and iso-hyperthermic soil) was given the highest rank and the Type 5 soil (clayey soil) the lowest rank.

The lithology of an area determines the infiltration capacity as different rocks exhibit different properties. Porosity differs from one type to another and has an essential effect on the recharging capacity (Senanayake et al., 2016). The lithology was derived from the District Resource Map of the Geological Survey of India (GSI, 2001). The resource map was georeferenced and digitized to obtain the geological map of the area. The area contains basaltic flows belonging to four different formations, namely, Karla,

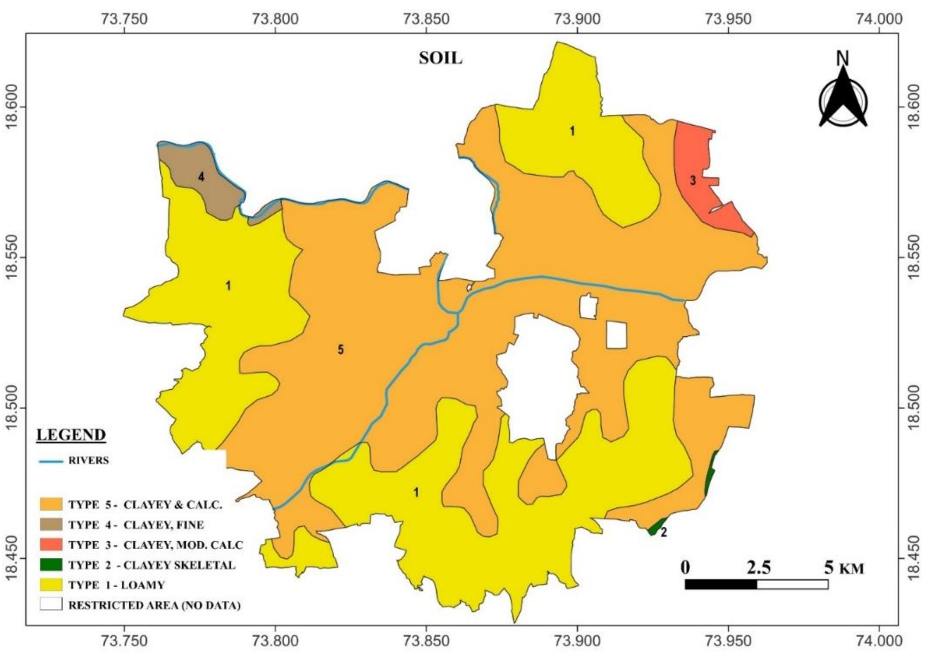

Figure 7. Soil map

Diveghat, Indrayani, and Purandargarh formations, each exhibiting distinctive characteristics (Figure 8) A major part, about 129 km^2 (51%) of the area is occupied by the Karla Formation constituted of dominantly compound pahoehoe flows. Other lithologies like aa' and simple flows with thick fragmented tops, known as Flow Top Breccia (FTB), predominantly aa' flows with thick FTB and aa' and simple flows with thin FTB constitute 25%, 24%, and 1% of the area, respectively. Being vesicular in nature, the compound pahoehoe flows show maximum recharge potential. According to Kulkarni et al. (2000), the weathering and jointing of the vesicular amygdaloidal basalt and the joints within the compact basalt create the aquifers. Aa' flows being compact and dense in nature do not exhibit much infiltration capacity.

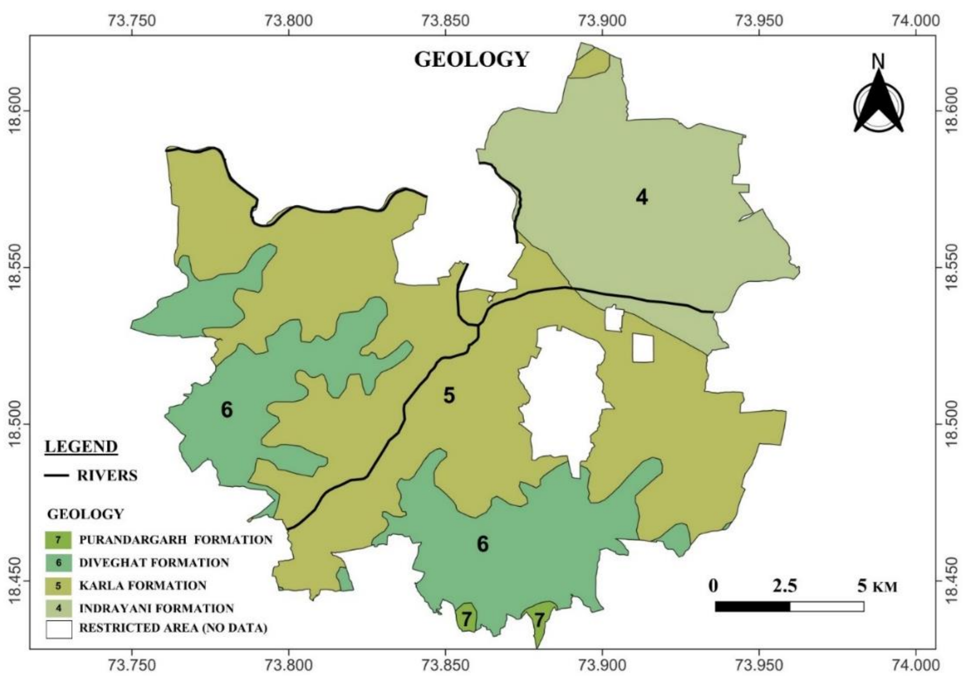

Figure 8. Geological map of the area

4.2 Groundwater recharge potential zones

After obtaining the weights from the AHP analysis, the six thematic layer maps were integrated using Weighted Overlay Analysis in the open source QGIS software to determine the Groundwater Recharge Potential (GRP). The following equation was used to estimate the groundwater potential.

$$GRP = \sum_{i=1}^{6}(MC_i \times w_i \times r_i) \quad (3)$$

Where; MC_1 and MC_6 are the 6 main criteria, w_1-w_6 are the normalized weights generated using AHP method and r_1-r_6 are the ranks given to the main criteria.

The groundwater recharge potential map of the study area generated through this weighted overlay analysis has been categorized into five zones, viz., low, moderate, good, high and very high potential. The Groundwater potential map (Figure 9) shows a coverage of 13.24 km^2 (5%), 124.71 km^2 (50%), 72.92 km^2 (29 %), 8.11 km^2 (3%), and 30.27 km^2 (12%) for the above zones, respectively.

Assessment of potential zones within the study area reveals that the high and good potential zones lie to the western part of the city. The central part or inner city, which is mainly built-up area, shows low potential for recharge. Earlier studies by Vaddadi et al. (2022) on roof top rainwater harvesting estimated the total water available for Rainwater harvesting in Pune city to be 49.05 Million Cubic Metres (MCM) and that effective recharge using RWH techniques could supplement the groundwater annually by about 22-25 MCM. The present study, when used in conjunction with the RWH studies, can provide effective strategies to manage systematic groundwater recharge of the shallow aquifers.

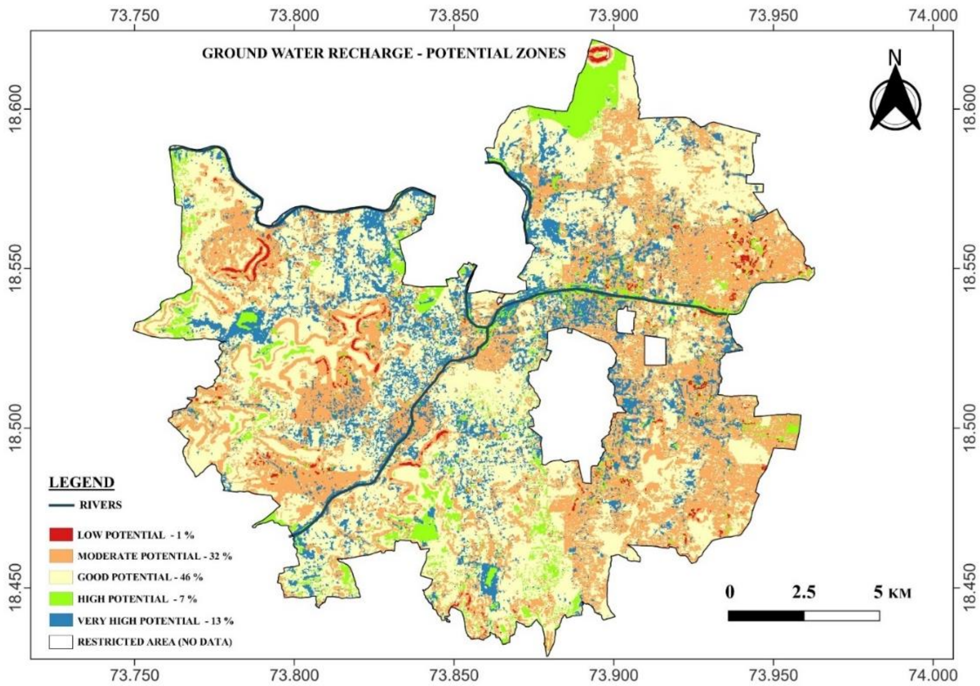

Figure 9. Map of ground water recharge potential zones

5. CONCLUSION

Use of rainwater harvesting for recharge of groundwater has become an effective method globally to maintain the water balance, overcome water crisis and to ensure sustainable water resources management, especially in urban growth areas. For effective recharge to happen, it is vital that the mapping and identification of groundwater potential zones in an area are done on a systematic and scientific basis.

The recharge potential for ground water zones was mapped using thematic layers, MCDA and AHP techniques. Groundwater in the study area is mainly controlled by the Land cover and use (LULC), Slope, Rainfall, Soil and Drainage Density, and lithological factors. Based on the study, the study area is classified into five classes, namely, low, moderate, good, very good and high groundwater potential. The results show a coverage of 5%, 50%, 29%, 3%, and 12% for the above zones, respectively. This indicates that nearly half (45%) of Pune city has good to high potential for recharge. Assessment of potential zones within the study area reveals that the high and good potential zones lie to the western part of the city. The central part or inner city which is mainly built-up area shows low potential for recharge. Though the city has seen rapid urbanisation in the last decade resulting in concretisation, major parts of the city show good potential for recharge. The prospective zones were also cross-checked with groundwater priority recharge maps published by the state's Groundwater Survey and Development Agency (GSDA, 2017). Comparison of the maps of representative areas show a good relationship between the two. The study is of immense importance, as the results when used in conjunction with the roof top RWH studies can help to identify effective sites/areas for recharge and to formulate a framework for systematic recharge of the existing aquifers in the area under study. Further, the workflow has been implemented using Open-Source Software and Open Data and is thereby applicable to other urban areas too.

ACKNOWLEDGEMENTS

We acknowledge with thanks Mr. Job Thomas for his help in the processing of data. The authors also thank Mr. Jeff McKenna, Gateway Geomatics, Canada for agreeing to review and suggest changes to the language and grammar for improving the manuscript. We also acknowledge with thanks the invaluable suggestions from the anonymous reviewers.

REFERENCES

Adham A, Riksen M, Ouessar M, Ritsema CJ. A methodology to assess and evaluate rainwater harvesting techniques in (semi-) arid regions. Water 2016;8(5):1-23.

Akter A, Ahmed S. Potentiality of rainwater harvesting for an urban community in Bangladesh. Journal of Hydrology 2015; 528:84-93.

Benjmel K, Amraoui F, Boutaleb S, Ouchchen M, Tahiri A, Touab A. Mapping of groundwater potential zones in techniques, and multicriteria data analysis (Case of the Ighrem Region, Western Anti-Atlas, Morocco). Water 2020;12: Article No. 471.

Çelik R. Evaluation of groundwater potential by GIS-based multicriteria decision making as a spatial prediction tool: Case study in the Tigris River Batman-Hasankeyf Sub-Basin, Turkey. Water 2019;11:Article No. 12.

Choosumrong S, Raghavan V, Bozon N. Multi-criteria emergency route planning based on analytical hierarchy process and pgRouting. Geoinformatics 2012;23(4):159-67.

Choudhari PP, Nigam GK, Singh SK, Thakur S. Morphometric based prioritization of watershed for groundwater potential of Mula River Basin, Maharashtra, India. Geology, Ecology, and Landscapes 2018;2(4):256-67.

Chowdhury A, Jha MK, Chowdary VM. Delineation of groundwater recharge zones and identification of artificial recharge sites in West Medinipur District, West Bengal, using RS, GIS and MCDM techniques. Environmental Earth Sciences 2010;59:1209-22.

Cornell University. Certified Crop Advisor study resources (Northeast region) [Internet]. 2010 [cited 2022 Jun 22]. Available from: https://nrcca.cals.cornell.edu/soil/CA2/CA0211.1.php/.

Das B, Pal C. Combination of GIS and fuzzy-AHP for delineating groundwater recharge potential zones in the critical Goghat-II block of West Bengal, India. HydroResearch 2019;2:21-30.

Doke AB, Zolekar AB, Patel H, Das S. Geospatial mapping of groundwater potential zones using multi-criteria decision-making AHP approach in a hardrock basaltic terrain in India. Ecological Indicators 2021;127:Article No. 107685.

Geological Survey of India (GSI). District Resource Map: Pune District, Maharashtra. Publications and Cartography Division, GSI; 2001.

Jamali I, Mörtberg U, Olofsson B, Muhammad S. A spatial multi-criteria analysis approach for locating suitable sites for construction of subsurface dams in Northern Pakistan. Water Resources Management 2014;28(14):5157-74.

Jasrotia AS, Majhi A, Singh S. Water balance approach for rainwater harvesting using remote sensing and GIS techniques, Jammu Himalaya, India. Water Resource Management 2009; 3(14):3035-55.

Kadam AK, Kale SS, Pande NN, Pawar NJ, Sankhua RN. Identifying potential rainwater harvesting sites of a semiarid, Basaltic Region of Western India, using SCS-CN method. Water Resource Management 2012;26:2537-54.

Kadhem GM, Zubari WK. Identifying optimal locations for artificial groundwater recharge by rainfall in the Kingdom of Bahrain. Earth Systems and Environment 2020;4(3):551-66.

Khazaei E, Mackay R, Warner JW. The effects of urbanization on groundwater quantity and quality in the Zahedan Aquifer, Southeast Iran. Water International 2004;29(2):178-88.

Kim SJ, Kwon HJ, Jung IK, Park GA. A comparative study on grid-based storm runoff prediction using Thiessen and spatially distributed rainfall. Paddy Water Environment 2003;1:149-55.

Kulkarni H, Deolankar SB, Lalwani A, Joseph B, Pawar S. Hydrogeological framework for the Deccan basalt ground-water systems, west-central India. Hydrogeology Journal 2000;8(4):368-78.

Kumar VA, Mondal NC, Ahmed S. Identification of groundwater potential zones using RS, GIS and AHP Techniques: A case study in a Part of Deccan Volcanic Province (DVP), Maharashtra, India. Journal of the Indian Society of Remote Sensing 2020;48(3):497-511.

Maity DK, Mandal S. Identification of groundwater potential zones of the Kumari River Basin, India: An RS and GIS based semi-quantitative approach. Environment, Development and Sustainability 2019;21:1013-34.

Mohammed H, Yohannes F, Zeleke G. Validation of agricultural non-point source (AGNPS) pollution model in Kori Watershed, South Wollo, Ethiopia. International Journal of Applied Earth Observation and Geoinformation 2004;6:97-109.

Mondal NC, Ajaykumar V. Assessment of natural groundwater reserve of a morphodynamic system using an information-based model in a part of Ganga basin, Northern India. Scientific Reports 2022;12:Article No. 6191.

Nasiri H, Boloorani AD, Sabokbar HAF, Jafari HR, Hamzeh M, Rafii Y. Determining the most suitable areas for artificial groundwater recharge via an integrated PROMETHEE II-AHP method in GIS environment (Case study: Garabaygan Basin, Iran). Environmental Monitoring and Assessment 2013; 185:707-18.

Pai DS, Sridhar L, Rajeevan M, Sreejith OP, Satbhai NS, Mukhopadhyay B. Development of a new high spatial resolution (0.25° × 0.25°) long period (1901-2010) daily gridded rainfall data set over India and its comparison with existing data sets over the region. Mausam 2014;65(1):1-18.

Paul RS, Rawat U, Sengupta D, Biswas A, Tripathi S, Ghosh P. Assessment of groundwater potential zones using multi criteria evaluation technique of Paisuni River Basin from the combined state of Uttar Pradesh and Madhya Pradesh, India. Environmental Earth Sciences 2020;79(340):1-24.

Pune Municipal Corporation. Water budget 2021 [Internet]. 2021 [cited 2022 Jun 3]. Available from: https://pmc.gov.in/sites/default/files/waterbudget-2021-2022.pdf.

Rajaveni SP, Brindha K, Elango L. Geological and geomorphological controls on groundwater occurrence in a hard rock region. Applied Water Science 2015;7(3):1377-89.

Rangarajan R, Athavale RN. Annual replenishable ground water potential of India: An estimate based on injected tritium studies. Journal of Hydrology 2000(234);38-53.

Rao N. Groundwater potential index in a crystalline terrain using remote sensing data. Environmental Geology 2006;50: 1067-76.

Rao N, Gugulothu S, Das R. Deciphering artificial groundwater recharge suitability zones in the agricultural area of a river basin in Andhra Pradesh, India using geospatial techniques and analytical hierarchical process method. Catena 2022; 212:Article No. 106085.

Saaty RW. The analytic hierarchy process: What it is and how it is used. Mathematical Modelling 1987;9(3-5):161-76.

Saaty TL. How to make a decision: The Analytic Hierarchy Process. European Journal of Operational Research 1990; 48:9-26.

Saaty TL. The analytic network process. Iranian Journal of Operations Research 2008;1(5):1-27

Senanayake IP, Dissanayake DMDOK, Mayadunna BB, Weerasekera WL. An approach to delineate groundwater recharge potential sites in Ambalantota, Sri Lanka using GIS techniques. Geoscience Frontiers 2016;7:115-24.

Shekhar S, Pandey AC. Delineation of groundwater potential zone in hard rock terrain of India using remote sensing, geographical information system (GIS) and analytic hierarchy process (AHP) techniques. Geocarto International 2014; 30(4):402-21.

Singh LK, Jha MK, Chowdary VM. Multi-criteria analysis and GIS modelling for identifying prospective water harvesting and artificial recharge sites for sustainable water supply. Journal of Cleaner Production 2017:142(4):1436-56.

Tiwari RN, Vikash K, Kushwaha VK. An integrated study to delineate the groundwater potential zones using geospatial approach of Sidhi Area, Madhya Pradesh. Journal Geological Society of India 2020;95:520-6.

Vaddadi N, Vansarochana C, Raghavan V. Estimation of groundwater recharge potential using rooftop rainwater harvesting: Case study from Pune Urban Area, India. International Journal of Geoinformatics 2022;18(2):55-69.

Venkatarao AK, Mondal NC, Ahmed S. Investigating groundwater recharge potential zones using a cross-correlation technique in a part of Deccan Volcanic Province (DVP), Central India. Environmental Earth Sciences 2019;78:Article No. 704.

A Combined DPSIR Framework and Logical Framework Approach for Sustainable Water Resources Management in the Lagoon Floodplain

Benchawan Teerakul[1], Chaiwat Rongsayamanont[1,2], Rotchanatch Darnsawasdi[1], and Peerapat Kosolsaksakul[1*]

[1]*Faculty of Environmental Management, Prince of Songkla University, Songkhla 90110, Thailand*
[2]*Southern Natural Disaster Research Center, Prince of Songkla University, Songkhla 90110, Thailand*

ARTICLE INFO

Received: 3 Sep 2022
Received in revised: 6 Feb 2023
Accepted: 8 Feb 2023
Published online: 13 Mar 2023
DOI: 10.32526/ennrj/21/202200170

Keywords:
Water management/ DPSIR/ LFA/ Lagoon floodplain/ Sathing Phra peninsula

*** Corresponding author:**
E-mail: k.peerapat@gmail.com

ABSTRACT

This article describes a combination of the driver-pressure-state-impact-response (DPSIR) framework and the logical framework approach (LFA) to develop water management strategies for a lagoon floodplain in Thailand. The DPSIR framework identified the cause-effect relationship between water and anthropogenic activities. LFA developed management strategies based on a systematic and logical approach. DPSIR analysis for the issue of water shortages for irrigated areas revealed the need for income from agriculture is a major driver, as indicated by agricultural development policy. The driver exerted pressure on increasing irrigation water demand, which increased the risk of a water shortage. The impact of water shortage was indicated by loss of farmer income. Existing responses led to inadequate problem-solving, for example, the promotion of mixed farming. Using data captured from DPSIR analysis for LFA analysis, proposed strategies to address the root causes of "ineffective irrigation water allocation" focused on improving (1) the performance of rotating irrigation systems; (2) monitoring water allocation; and (3) water use efficiency. The strategies developed using the combined DPSIR framework and LFA are effective because: (1) this method provides insight into complex water systems; (2) the strategies are developed logically to solve the problem at its root cause; and (3) there is intensive stakeholder participation and in-depth study of the area. This method is a helpful tool for developing a management strategy for a complex water system and is suitable for application by decision-makers. Stakeholder verification is required for future research to ensure that the strategies are appropriate and capable of being implemented.

1. INTRODUCTION

Water-related issues are often complex and challenging to address. Understanding the entire system associated with water management is required to manage water effectively (Enteshari and Safavi, 2021). Therefore, tools that can be used to structure problems and help policymakers address complex water issues are required. Previous studies have shown that the DPSIR framework is an analytical framework essential in promoting policy and regulation design to manage ecosystems effectively (Gari et al., 2015; Roy et al., 2017; Chen et al., 2022). DPSIR was developed in the late 1990s by the Organisation of Economic Cooperation and Development and the European Environment Agency to help decision-makers structure and organise cause-effect relationships between environmental and human systems (OECD, 1993; EEA, 1999; Tscherning et al., 2012). It identifies the cause-effect relationships in five economic and social development categories: driving forces (D) that exert pressure (P) on the environment; changes in the state of the environment (S) and impacts (I) on the ecosystem, human health, and other materials; and society's preventive, adaptive, or curative solution responses (R) to the driving forces, pressures, states, or impacts (Jago-on et al., 2009). DPSIR has been wildly used for analysing environmental problems emanating from human

Citation: Teerakul B, Rongsayamanont C, Darnsawasdi R, Kosolsaksakul P. A combined DPSIR framework and logical framework approach for sustainable water resources management in the lagoon floodplain. Environ. Nat. Resour. J. 2023;21(3):211-221. (https://doi.org/10.32526/ennrj/21/202200170)

activities in policy-making and research (Gari et al., 2018; Lu et al., 2022; Agramont et al., 2022), including water issues (Kagalou et al., 2012; Hashemi et al., 2014; Gari et al., 2018; Ashfaq et al., 2018; Lu et al., 2022). Hashemi et al. (2014) found the framework useful for analysing the changing state of floods, structuring data, and examining leverage points at which appropriate responses can be exerted.

Although DPSIR was widely applied, oversimplifying the complex reality of socio-ecological systems was criticised (Wang et al., 2018; Agramont et al., 2022). As the complexity of the socio-environmental systems relies on several layers of social, political, and economic institutions and the environmental consequences behind their interactions (Teodosiu et al., 2009), the simplicity of DPSIR can be misguiding, ignoring the possible synergistic relations existing between DPSIR categories (Maxim et al., 2009). Thus, the responses defined by DPSIR analysis governed by a standardised framework may disregard such aspects. In addition, DPSIR does not explicitly prioritise responses and cannot individually determine the effectiveness of each response when working with complex systems (Gari et al., 2015; Malmir et al., 2021). To define responses that consider relevant layers under D-P-S-I-R categories and determine the effectiveness of DPSIR responses, there is a need to use other tools with this framework.

The logical framework approach (LFA) is a strategic planning and project management methodology that guides the systematic and logical analysis of key interrelated elements that constitute well-designed management interventions (The World Bank, 2000). LFA was developed in the 1960s to assist the US Agency of International Development (USAID) in improving project planning and evaluation systems (Republic of Serbia Government European Integration Office, 2011). LFA has been used in many development projects (Musiyarira et al., 2019). The problem tree, objective tree, and analysis of strategies is an LFA methodology for identifying main problems and their causes and effects, helping project planners formulate clear and manageable objectives and strategies for achieving them. The problem tree can identify the underlying causes of D-P-S-I-R categories, that is, the layers that cannot be identified using DPSIR. The underlying causes will be translated into solutions and formulated logically to formulate management interventions.

The combination of DPSIR and LFA will form water management tools for comprehensively analysing the water resources system and formulating logical and effective management interventions. This article demonstrates a combination of the driver-pressure-state-impact-response (DPSIR) framework and the logical framework approach (LFA) to develop water management strategies for the Sathing Phra peninsula lagoon floodplain.

2. METHODOLOGY

2.1 Study area

Floodplains are defined as areas periodically inundated by the lateral overflow of rivers and lakes. Floodplains support diverse ecosystems which provide critical benefits to people, especially in agricultural development (Binh et al., 2022). Floodplains are among the most threatened ecosystems in which the annual flood cycle critically impacts productivity (Islam and Braden, 2006). Threats are severe in lagoon floodplains because the hydrological regime is highly dynamic and impacted by salt water (López-Juambeltz et al., 2020).

The Sathing Phra peninsula, a lagoon floodplain in Thailand was selected as a study area. It is an important rice production area, holding approximately 31% of the rice field area in Southern Thailand. Water shortages occasionally occur during the dry season. Floods occur in the wet season. In 2013, severe floods caused damage to 10,654 households, affecting 36,725 people (Songkhla Provincial Disaster Prevention and Mitigation Office, 2017). Ban Khao Sub-District was selected to demonstrate a combined DPSIR and LFA (Figure 1).

2.2 Method

2.2.1 Historical water resource development and management

Participatory Rapid Appraisal (PRA) (Chambers, 1994) was applied to study the history of water resource development and management. PRA tools, including secondary data reviews, semi-structured interviews, and focus group discussions, were conducted during 2012-2019. Sixty-nine people from government organisations, local administrative organisations, communities, academics, private sectors, and NGOs participated.

The communities and community leaders provided information and jointly surveyed the area to understand its context and suggested management guidelines. Relevant government agencies share information about water management, analyse problems, and discuss appropriate management. The qualitative data was validated by triangulation.

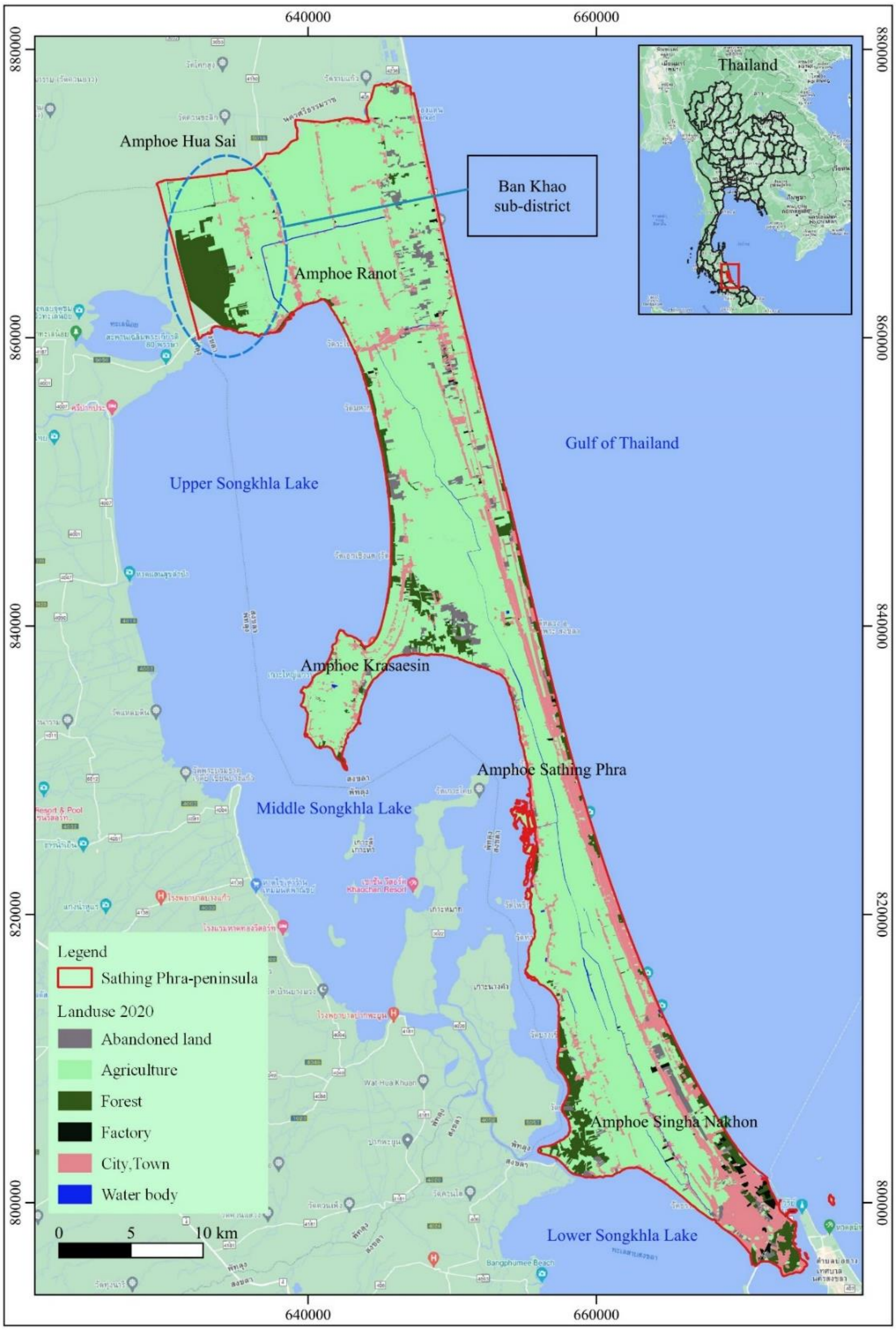

Figure 1. Sathing Phra peninsula floodplain

2.2.2 DPSIR framework

DPSIR was used to describe water resource problems using data from the PRA step. The cause-effect relationship between the water resources systems and anthropogenic activities was identified in terms of the following elements:

- Drivers (D) are the driving forces acting on water resources systems comprising human needs.

- Pressures (P) include all human activities undertaken due to increased needs, which apply pressure on the stage.

- Stage (S) is the current status of water resources.

- Impacts (I) are categorised as loss of functions or services of water resources to humans.

- Response (R) included management practices for managing water resources in the area (Ashfaq et al., 2018).

This study first identified water resources problems (S) and their impacts (I). Next, pressures (P) and drivers (D) were analysed. Finally, existing responses (R) were analysed. The link between categories is shown in the diagram. Statistics for analysing water resource status are descriptive statistics data such as mean, percentage, etc.

DPSIR indicators for agriculture's water shortage are shown in Table 1.

2.2.3 LFA

LFA was applied to analyse the underlying layers/causes of D-P-S-I-R categories and formulate water management strategies and measures. The indicators in Table 1 were also used. Data captured from DPSIR analysis were transferred into a problem tree and disaggregated into causes, root causes, and consequences. State (S) was placed as a problem at the centre of the problem tree diagram. Major causes and root causes that contribute to the problem were replaced with drivers (D), pressures (P), and causes of ineffective responses (R). The effects were replaced with Impacts (I). Negative situations were converted into objectives in the objective tree diagram. The means to achieve the objectives of the root causes were determined as management strategies.

Table 1. The DPSIR indicators for agriculture's water shortage

DPSIR framework	DPSIR component	Indicators	Unit
Drivers	Need of income from agriculture (rice)	Existence of policies that support agricultural development	Yes/no
Pressures	Intensive irrigation water demand	Irrigated area (off-season rice farming)	km^2
	Climate variation	Annual rainfall	mm/year
State	Water shortage for irrigated area	Number of years in which salt water intrudes during off-season rice cultivation	Year
		Uncultivated irrigated paddy field	km^2
Impacts	Loss of income	Income from the sale of off-season rice products	baht/year
	Conflict on irrigation water use	Level of conflict	Level (low, medium, violence)
Responses	Activities to prevent water shortage for irrigated area		
	- Promotion of mixed agriculture/ oil palm	- Rice field area promoted to mixed agriculture/ oil palm	km^2
	- Promotion of less water rice farming	- Rice field area promoted to less water farming	km^2
	- Improving irrigation canals	- The distance of irrigation canals has been improved	km/year
	- Establishing water user groups for managing irrigation water	- The existence of water user groups	Yes/no
	Activities to reduced impact from water shortage		
	- Compensation for rice farming damage	Amount of compensation	baht/rai (equivalent to 0.0016 km^2)
	- Conflict mediation	The existence of a conflict mediator	Yes/no

3. RESULTS

3.1 Historical water resources management in the Sathing Phra peninsula

Timelines of Ban Kao Sub-District water resources management are shown in Figure 2.

Pre-irrigation development, the main activity was rainfed rice farming. Water shortages were common in the dry season. In the second phase, irrigation systems were developed to address the water shortage. The Thung Ranod Irrigation Project supported 136 km^2 of rice fields (RID, 2012). Farmers conduct rice farming twice a year, with some increasing to five times in two years. The off-season rice fields in Ranod district increased steadily from 29.2 km^2 in 1988 to 182.7 km^2 in 2004.

The third phase involved community adaptation. In 2005, a severe flood destroyed much of the in-season rice, after which most farmers shifted the in-season rice farming period to after the rainy season and postponed their off-season rice farming. The adaptation increased the dependence on irrigation water, resulting in more severe water shortages.

3.2 DPSIR water resources system analysis

The water resources system of the Sathing Phra peninsula is depicted in Figure 3, which shows two linked causal loops: (a) water shortage for the irrigated area; and (b) flooding. This study only describes causal loop (a) (Table 2).

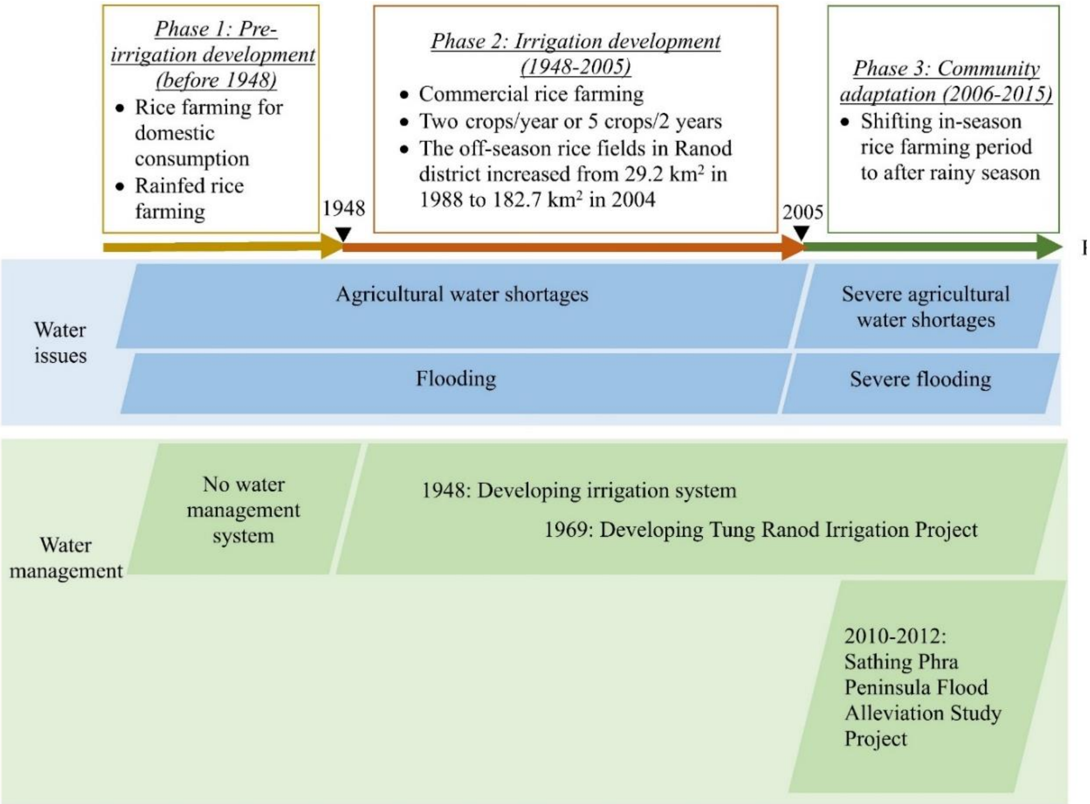

Figure 2. Timelines of water resources development and management in the Ban Kao Sub-District

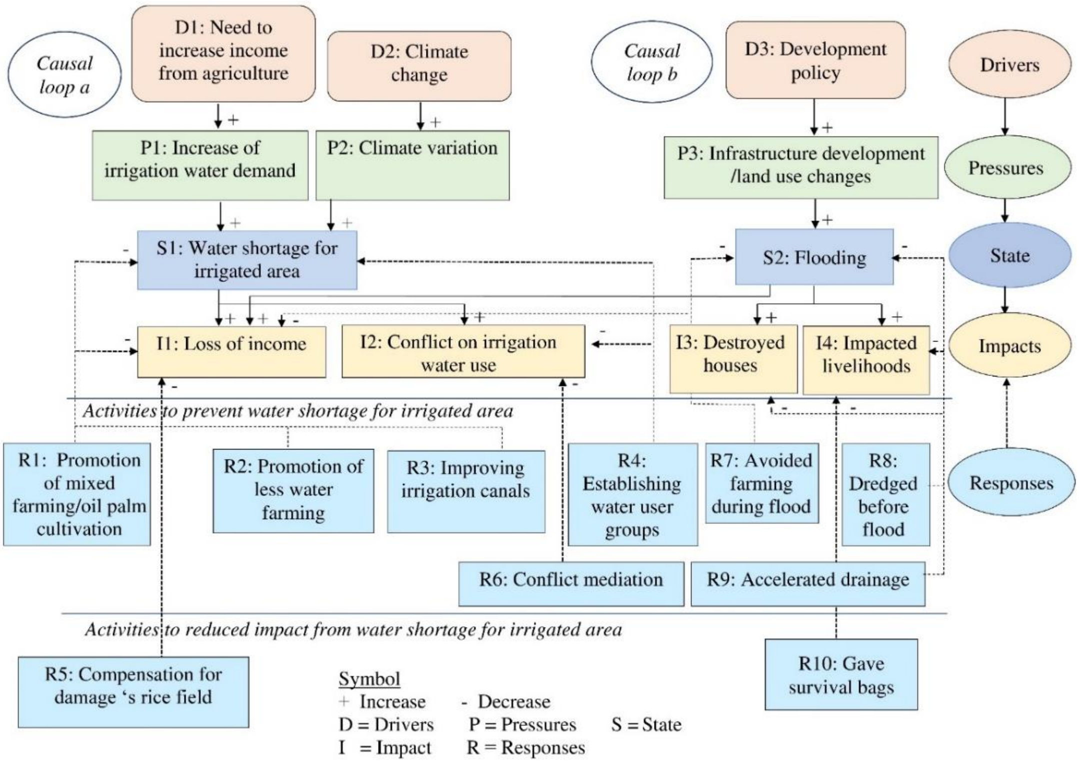

Figure 3. DPSIR analysis for the Sathing Phra peninsula

Table 2. DPSIR for causal loop (a) water shortage for the irrigated area

			Phase		
DPSIR framework	DPSIR component	Indicators	Phase 1: pre-irrigation development (before 1948)	Phase 2: Irrigation development (1948-2005)	Phase 3: Community adaptation to water shortage (2005-2015)
Drivers	Need to increase income from agriculture (D1)	Existence of policy that supports agricultural development	Most rice farming was rainfed	Policy to increase agricultural productivity through irrigation development	Policy to promote mixed agriculture/oil palm and less water farming
Pressures	Increasing of irrigation water demand (P1)	Irrigated rice farming area (Off-season rice farming)	0 rai	Increase of 100% from phase 1	Increase of 100% from phase 1
	Climate variation (P2)	Annual rainfall	n/a	During 1974-2005, annual rainfall below 1,500 mm/year for 3 years	During 2006-2011, no annual rainfall below 1,500 mm/year
State	Water shortage for irrigated area (S1)	Number of years in which salt water intrudes during off-season rice cultivation	n/a	4 years during 1992-2005	1 year during 2006-2010
		Uncultivated irrigated paddy field	None	20.64 km^2 for 4 years (1992-2005)	20.64 km^2 for 1 year (2006-2010)
Impacts	Loss of income (I1)	Income from the sale of off-season rice products	-	23.5 million baht (0.71 million USD)/year (for 4 years)	45.9 million baht (1.39 million USD)/ year (for 1 year)
	Conflict on irrigation water use (I2)	Level of conflict	None	Low	Low
Responses	Activities to prevent water shortage for irrigated area				
	- Promotion of mixed farming/oil palm cultivation (R1)	- Rice field area promoted to mixed agriculture/oil palm	None	n/a	1% of the total area of irrigated rice farming
	- Promotion of less water rice farming (R2)	- Rice field area promoted to less water farming	None	None	None
	- Improving irrigation canals (R3)	- The distance of irrigation canals has been improved	n/a	n/a	n/a
	- Establishing water user groups (R4)	- The existence of water user groups	No	Yes	Yes
	Activities to reduce impact from water shortage				
	- Compensation for rice farming damage cause by water shortage (R5)	Amount of compensation	No	Insufficient	Insufficient
	- Conflict mediation (R6)	The existence of conflict mediator	No (no conflict)	Yes	Yes

n/a=not available

From Figure 3 and Table 2, in developing the area from phase 1 to phase 2, farmers' poverty led to needing to increase income from agriculture which is described as a first driver (D1). This driver was investigated based on the existence of policies to support agricultural development. In phase 2, under the 2nd National Economic and Social Development Plan, the important policy regarding agricultural development focused on increasing productivity via developing irrigation systems (National Economic and Social Development Board, 1967). Therefore, the Thung Ranod irrigation project was developed.

The pressure reflected by the driver is increasing irrigation water demand (P1) which is considered based on irrigated rice farming area. In the second phase, the irrigated rice farming area increased 100% from the first phase, increasing irrigation water demand (RID, 2012). The change in the state due to pressures is water shortage for the irrigated area (S1) which one indicator is the number of years that saltwater intrusion caused uncultivated rice farming, which occurred in 1991, 1992, 1993, 2005, and 2010. The other indicator is the uncultivated irrigated rice farming area, which indicated 20.64 km^2 in the four years that the aforementioned saltwater intrusion occurred (Regional Irrigation Office 16, 2011).

The impacts of water shortage caused loss of income (I1) and conflict in irrigation water use (I2), which is quantified by indicators including income from the sale of irrigated rice products and level of conflict between water users. Inability to do irrigated rice farming in 1991, 1992, 1993, 2005, and 2010, caused the area a loss of income of approximately 23.5 million baht (0.71 million USD)/year (Songkhla Provincial Agriculture and Cooperatives Office, 2022). In addition, because irrigation water supply is limited, conflicts between farmers occurred almost every year.

In the second phase, the results from the study indicated that the existence of the water user group (R4) helped prevent water shortages as the water user group set rules for equitable allocation of limiting irrigation water among users, while other responses did not show clear results due to lack of information. The compensation for rice field damage from water shortage (R5) is insufficient as the cost of compensation was only 28% of the actual cost (actual cost 2,700 baht (81 USD)/rai (Regional Irrigation Office 16, 2011) and compensation 1,113 baht (34 USD)/rai (Songkhla Provincial Agriculture and Cooperatives Office, 2020).

For the third phase, policy regarding agricultural development changed to promoting mixed agriculture/oil palm and less water rice farming. However, the off-season rice farming area is similar to the second phase. This indicated that the new policies have little impact on the water resource system. The reason is that new policies have implementation limitations, for example, inappropriate area, farmer budget, and land tenure problems.

3.2 LFA

Taking causal loop (a) as an example for the LFA analysis, the problem tree analysis showed three significant causes of water shortage for the irrigated area: (1) insufficient water in the dry season, which the indicator showed that during 1992-2005 there were four years that the area of uncultivated irrigated rice farming was 20.64 km^2/year; (2) increased water demand for rice farming which is indicated by an increase of irrigated rice farming area of 100% compare to the pre-irrigation development phase; and (3) ineffective irrigation water allocations which is indicated by the area of uncultivated irrigated rice farming mentioned above. The root causes of each major cause are also shown in Figure 4.

The major causes were then transformed into objectives which were: (1) sufficient water; (2) water demand for rice farming appropriate to the water available; and (3) effective irrigation water allocations (Figure 5).

After the desired future situation, the most feasible strategies and measures were identified. In this study, only the third chain of the objective tree in Figure 5 (effective irrigation water allocation) was selected as an example. The target of management strategies for this chain is at least 70% of farmers having enough water for off-season rice farming. This is achieved by:

1) Improving the performance of the rotating irrigation systems through developing an automatic water-level monitoring system and strengthening the water user groups.

2) Improving the monitoring and evaluation of irrigation water allocation and delivery through participatory monitoring and evaluation of irrigation water allocation and delivery.

3) Improving irrigation water use efficiency through applying economic instruments.

The details of management strategies and indicators are shown in Supplementary Table S1.

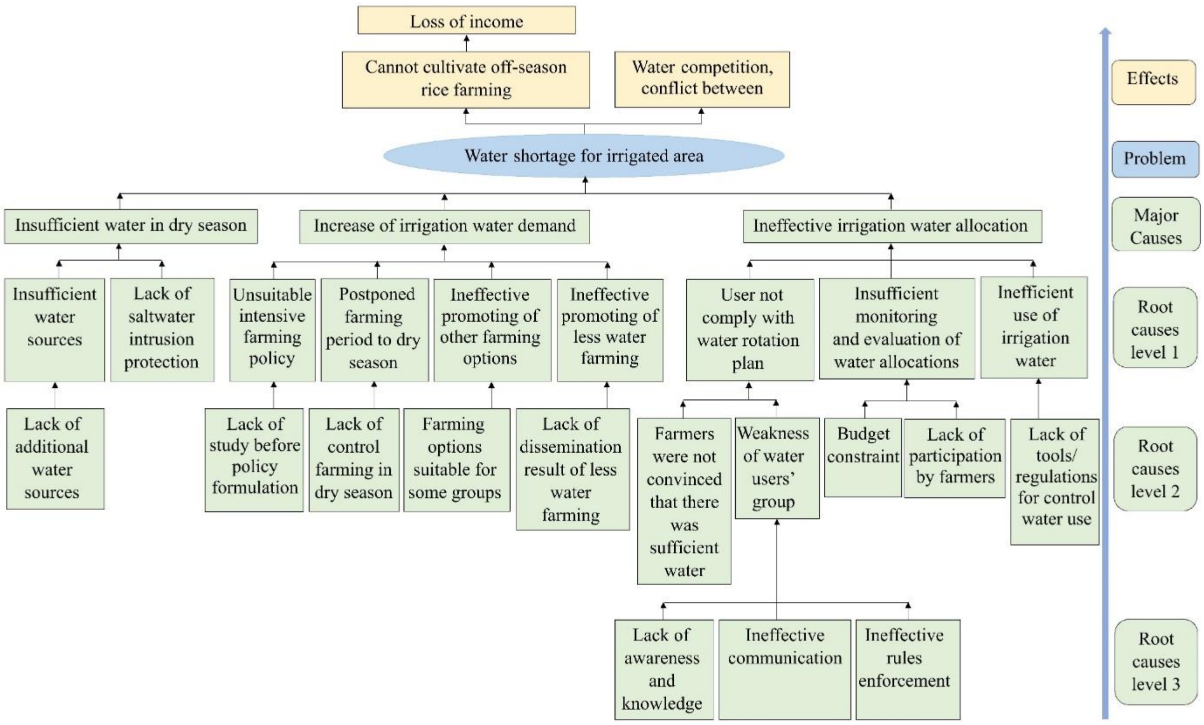

Figure 4. Problem tree analysis for causal loop (a) water shortage for the irrigated area

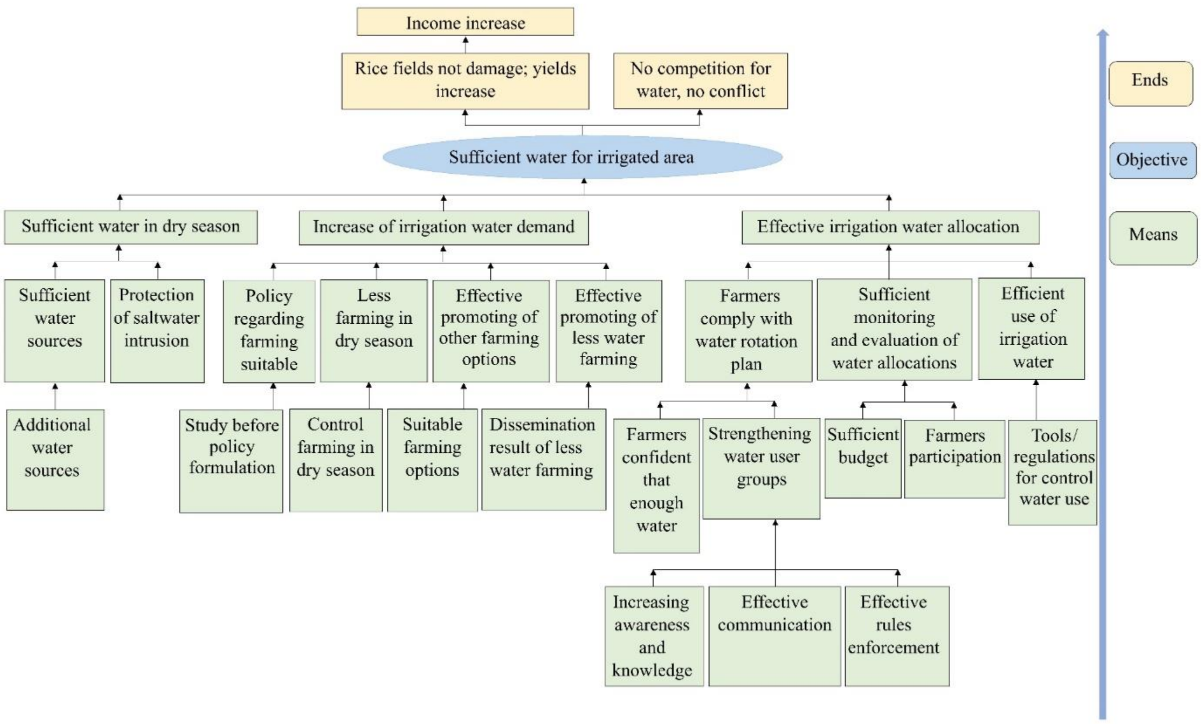

Figure 5. Objective tree analysis for causal loop (a) water shortage for the irrigated area

4. DISCUSSION

Water management strategies for the Sathing Phra peninsula were developed using the combined DPSIR framework and LFA. DPSIR analysis showed the important driver for the issue of water shortage in irrigated areas is the need for income from agriculture, which is associated with water user groups and is difficult to change. Growing demand for irrigation water, combined with natural factors, posed a risk of water shortages. Current responses, such as government policies to promote the transition from rice farming to mixed farming and the promotion of less water rice farming, which have very little application, are ineffective and unable to mitigate water shortages and their impacts. The results illustrated that DPSIR analysis allowed understanding the variables affecting the system, the weights of the variables, the roles of stakeholders, and evaluating the effectiveness of existing responses. This study's findings are consistent with Agramont et al. (2022), who discovered that DPSIR allows understanding the sources of socio-ecological distress and reveals the ineffectiveness of policy responses in Bolivia's Katari River Basin. However, the root cause of the problem, which is useful for developing management strategies, is difficult to identify by DPSIR analysis.

Using the results from the DPSIR analysis to formulate strategies to resolve the root causes using LFA, three strategies to increase the efficiency of irrigation water allocation were proposed. First, improving the rotating irrigation systems' performance by developing an automatic water-level monitoring system and strengthening water user groups. The system provides real-time data that helps water managers and users track transmission and conveyance losses and take decisions to improve water use efficiency (Reddy et al., 2016). Strengthening the water user group will lead to continuous, more efficient, and concrete management of water resources, consistent with the study of Teamsuwan and Satoh (2009), which concluded that the Water User Organisations (WUOs) in the Chao Phraya Delta, Thailand, demonstrate successful long-term management because of the clear definition of the WUOs' common management activities and a budget to guarantee the activities. Second, improving monitoring and evaluating the irrigation system through participatory monitoring and evaluation of irrigation water allocation and delivery. The advantage of this strategy is collaborative problem-solving through the generation and use of knowledge that leads to corrective action by involving all levels of stakeholders in shared decision-making. Uprety et al. (2019) also suggested that the principles of citizen science can help improve the spatial coverage of data, aiding local decision-makers in the water resource management realm. Third, improving water use efficiency in irrigated agriculture by applying economic instruments is instrumental in achieving efficient and equitable use and encouraging conservation and protection of water resources (Rey et al., 2019).

The proposed strategies differ from strategies suggested by the Royal Irrigation Department using rational planning (RID, 2012). Regarding the IWRM component (Global Water Partnership, 2000), for the institutional roles, this study suggests strategies related to water user groups, while RID emphasises the functions of regulators. For the management instruments, this study proposed economic instruments for optimising water use, while the RID proposed guidelines on the effective use of irrigation water and public relations to educate farmers. The result indicated that strategies proposed by this study focus on improving management mechanisms of water user groups differently from those proposed by the rational planning method, which focuses on the function of regulators. The reason is that DPSIR helps structure the information on water resources issues and clearly explains the relationship between DPSIR categories. From this study, DPSIR analysis showed that the important driver is the need for income from agriculture which is associated with water user groups, as mentioned above. While the rational planning method does not analyse the system-wide problem, it is too narrow in focus due to the focus on water management by the responsible authorities and the emphasis on infrastructure development.

Our results demonstrated that the combined DPSIR and LFA enable the development of appropriate and realistic water management solutions. DPSIR provides a framework for comprehensively analysing cause-effect relationships, factors, and actors' influences in the complex water resource system. Analysing the data with stakeholders and revising the DPSIR diagram several times gives us an in-depth and comprehensive understanding of the relationships among variables affecting water systems. In addition, an intermediary study with no interest in the area resulted in facts that reflected water management problems in the area better than studies by agencies or decision-makers due to the embarrassment of the informants in providing information. From the comprehensive understanding of the water system obtained from DPSIR analysis, when further analysed using LFA, it is possible to identify root causes contributing to the problem, which enables the development of feasible solutions/ strategies to solve at the leverage point. Combined DPSIR and LFA is a modified method for analysing water resource systems, an essential step in planning. DPSIR has been used with other tools for analysing water resource systems; for example, Zare et al. (2019)

applied DPSIR as an analytical framework to support the problem scoping and structuring phase in the SD modelling process, and Apostolaki et al. (2019) combined DPSIR with the ecosystem services approach and scenario assessment for developing programs of measures and river basin management plans.

5. CONCLUSION

Applying the combined DPSIR framework and LFA effectively developed water management strategies for a complex water system, including a lagoon floodplain in Thailand. The strategies developed using this method are more effective than those developed using other tools that do not analyse the water system comprehensively and let the responsible authorities focus only on their duties. The effectiveness of the strategies is due to: (1) this method provides insight into complex water systems, stakeholder relationships, key factors influencing the system, and root causes; (2) the strategies developed systematically and logically solve the problem at its root cause, which is the real problem; and (3) intensive stakeholder participation in problem-cause analysis and in-depth study of the area. This method is appropriate for decision-makers because it provides a framework for in-depth analysis of problems and their causes and root causes, covering socioeconomic and environmental aspects. It aids in formulating logical management approaches to solving problems at their root cause. For future research, verifying strategies by stakeholders is needed to ensure the strategies are suitable and applicable.

ACKNOWLEDGEMENTS

This work was partially supported by the Thesis Research Grant from Graduate School, Prince of Songkla University, Thailand.

REFERENCES

Agramont A, Cauwenbergh NV, Griesven AV, Craps M. Integrating spatial and social characteristics in the DPSIR framework for the sustainable management of river basins: Case study of the Katari River Basin, Bolivia. Water International 2022;47:8-29.

Apostolaki S, Koundouri P, Pittis N. Using a systemic approach to address the requirement for integrated water resource management within the Water Framework Directive. Science of the Total Environment 2019;679:70-9.

Ashfaq MY, Al-Ghouti MA, Qiblawey H, Zouari N, Rodrigues DF, Hu Y. Use of DPSIR framework to analyze water resources in Qatar and overview of reverse osmosis as an environment friendly technology. Environmental Progress and Sustainable Energy 2018;38:1-13.

Binh NT, Tien LVT, Tang LT, Tu NM, Dung TD, Quan NH. Resilience of various innovative water management practices: The case of rice production in the Vietnamese Mekong Delta floodplains. Agricultural Water Management 2022;270: Article No. 107739.

Chambers R. The origins and practice of participatory rural appraisal. World Development 1994;22:953-69.

Chen M, Chen F, Tang C, Lu Y, Feng Y. Integration of DPSIR framework and TOPSIS model reveals insight into the coastal zone ecosystem health. Ocean and Coastal Management 2022;226:Article No. 106285.

European Environment Agency (EEA). Environmental Indicators: Typology and Overview: Technical Report No 25. Copenhagen, Denmark: European Environment Agency; 1999.

Enteshari S, Safavi HR. Development of system dynamics for holistic conceptualization of water resources problems using grounded theory: A case study of the Zayandehrud River Basin. Iranian Journal of Science and Technology, Transactions of Civil Engineering 2021;45:413-28.

Gari SR, Newton A, Icely JD. A review of the application and evolution of the DPSIR framework with an emphasis on coastal social-ecological system. Ocean and Coastal Management 2015;103:63-77.

Gari SR, Guerrero CEO, A-Uribe B, Icely JD, Newton A. A DPSIR-analysis of water uses and related water quality issues in the Colombian Alto and Medio Dagua Community Council. Water Science 2018;32:318-37.

Global Water Partnership. Integrated Water Resources Management: Technical Advisory Committee (TAC) Background Paper No. 4. Stockholm, Sweden: Global Water Partnership; 2000.

Hashemi MS, Zare F, Bagheri A, Moridi A. Flood assessment in the context of sustainable development using the DPSIR framework. International Journal of Environmental Protection and Policy 2014;2:41-9.

Islam M, Braden JB. Bio-economic development of floodplains: Farming versus fishing in Bangladesh. Environment and Development Economics 2006;11:95-126.

Jago-on KAB, Kaneko S, Fujikura R, Fujiwara A, Imai T, Matsumoto T, et al. Urbanization and subsurface environmental issues: An attempt at DPSIR model application in Asian cities. Science of the Total Environment 2009; 407:3089-104.

Kagalou I, Leonardos I, Anastasiadou C, Neofytou C. The DPSIR approach for an integrated river management framework: A preliminary application on a Mediterranean site (Kalamas River- NW Greece). Water Resources Management 2012; 26:1677-92.

López-Juambeltz F, Rodríguez-Gallego L, Dabezíes JM, Chreties C, Narbondo S, Conde D. A GIS-based assessment combined with local ecological knowledge to support the management of *Juncus acutus* L. spreading in the floodplain of a protected coastal lagoon. Journal for Nature Conservation 2020; 57:Article No. 125891.

Lu M, Wang S, Wang X, Liao W, Wang C, Lei X, et al. An assessment of temporal and spatial dynamics of regional water resources security in the DPSIR framework in Jiangxi Province, China. International Journal of Environmental Research and Public Health 2022;19:Article No. 3650.

Malmir M, Javadi S, Moridi A, Neshat A, Razdar B. A new combined framework for sustainable development using the DPSIR approach and numerical modeling. Geoscience Frontiers 2021;12:Article No. 101169.

Maxim L, Spangenberg JH, O'Connor M. An analysis of risks for biodiversity under the DPSIR framework. Ecological Economics 2009;69:12-23.

Musiyarira HK, Pillalamarry M, Tesh D, Nikowa N. Formulating strategic interventions for the coloured gemstone industry in Namibia by utilising the logical framework approach. The Extractive Industries and Society 2019;6:1017-29.

National Economic and Social Development Board. The Second National Economic and Social Development Plan (1967-1971). Bangkok, Thailand: Office of the Prime Minister; 1967.

Organisation for Economic Co-operation and Development (OECD). OECD Core Set of Indicators for Environmental Performance Reviews: Environmental Monograph. Paris, France: Organisation for Economic Co-operation and Development; 1993.

Reddy K, Reddy LN, Nagothu S, Nakka SBR. Sensors for water monitoring for improved on farm water management. Proceedings of the 2nd World Irrigation Forum (WIF2); 2016 Nov 6-8; Chiang Mai International Convention and Exhibition Center, Chiang Mai: Thailand; 2016.

Regional Irrigation Office 16. Ranod-Krasasin Operation and Maintenance of Irrigation Project. Songkhla, Thailand: Royal Irrigation Department; 2011.

Republic of Serbia Government European Integration Office. Guide to Logical Framework Approach. Belgrade, Republic of Serbia: Global Print; 2011.

Rey D, Pérez-Blanco CD, Escriva-Bou A, Girard C, Veldkamp TIE. Role of economic instruments in water allocation reform: Lessons from Europe. International Journal of Water Resources Development 2019;35:206-39.

Roy K, Gain AK, Mallick B, Vogt J. Social, hydro-ecological and climatic change in the southwest coastal region of Bangladesh. Regional Environmental Change 2017;17:1895-906.

Royal Irrigation Department (RID). Sathing Phra Peninsula Flood Alleviation Study Project: Final Report. Bangkok, Thailand: Ministry of Agriculture and Cooperatives; 2012.

Songkhla Provincial Agriculture and Cooperatives Office. Agricultural Information of Songkhla Province in 2019. Songkhla, Thailand: Department of Agricultural Extension; 2020.

Songkhla Provincial Disaster Prevention and Mitigation Office. Statistics of disasters for the year 2015 [Internet]. 2017 [cited 2017 Jan 10]. Available from: https://kb.psu.ac.th/psukb/handle/2016/13642.

Songkhla Provincial Agriculture and Cooperatives Office. Basic information of important agricultural products of Songkhla province (rice): Under the BCG Model for agriculture in Songkhla Province for 2022 [Internet]. 2022 [cited 2022 Dec 10]. Available from: https://www.opsmoac.go.th/songkhla-dwl-preview-441291791020.

Teamsuwan V, Satho M. Comparative analysis of management of three water users' organizations: Successful cases in the Chao Phraya Delta, Thailand. Paddy and Water Environment 2009;7:227-37.

Teodosiu C, Ardeleanu C, Lupu L. An overview of decision support systems for integrated water resources management. Environmental Engineering and Management Journal 2009;8:153-62.

The World Bank. The Logframe Handbook: A Logical Framework Approach to Project Cycle Management. Washington DC, USA: The World Bank; 2000.

Tscherning K, Helming K, Krippner B, Sieber S, Paloma SG. Does research applying the DPSIR framework support decision making? Land Use Policy 2012;29:102-10.

Uprety M, Orchoa-Tocachi B, Paul JD, Regmi S, Buytaert W. Improving water resources management using participatory monitoring in a remote mountainous region of Nepal. Journal of Hydrology: Regional Studies 2019;23:Article No. 100604.

Wang W, Sun Y, Wu J. Environmental warning system based on the DPSIR model: A practical and concise method for environmental assessment. Sustainability 2018;10:Article No. 1728.

Zare F, Elsawah S, Bagheri A, Nabavi E, Jakeman AJ. Improved integrated water resource modeling by combining DPSIR and system dynamics conceptual modeling techniques. Journal of Environmental Management 2019;246:27-41.

Do Managed Hill Sal (*Shorea robusta)* Community Forests of Nepal Sequester and Conserve More Carbon than Unmanaged Ones?

Subash Gautam[1], Sachin Timilsina[1], Manish Shrestha[2*], Bina Adhikari[1], Binay Bahadur Adhikari Khatri[3], and Jagadish Timsina[4]

[1]*Tribhuvan University, Institute of Forestry, Pokhara Campus, Pokhara 33700, Nepal*
[2]*Tribhuvan University, School of Forestry and Natural Resource Management, Institute of Forestry, Kathmandu 44600, Nepal*
[3]*Ministry of Forest, Environment and Soil Conservation Gandaki Province, Division Forest Office, Tanahun 33900, Nepal*
[4]*Institute for Study and Development Worldwide, Sydney and Global Evergreening Alliance, Melbourne, Australia*

ARTICLE INFO

Received: 3 Dec 2022
Received in revised: 4 Feb 2023
Accepted: 14 Feb 2023
Published online: 16 Mar 2023
DOI: 10.32526/ennrj/21/202200259

Keywords:
Carbon stock/ Community forests/ Forest management activities/ Soil Organic Carbon/ Tree and soil biomass

*** Corresponding author:**
E-mail:
manish.shrestha1979@gmail.com

ABSTRACT

Nepalese community forests are globally recognized for sustainable forest management and improving the livelihoods of forest-dependent communities, but their contribution to carbon sequestration in trees and soil is rarely studied. This study was performed to understand the effect of management practices on carbon stock of two community forests (CFs) - Taldanda (managed) and Dangdunge (unmanaged) - dominated by Sal (*Shorea robusta*) in the mid-hills of Nepal. Twenty-one concentric sample plots, each of 250 m^2, were laid out in each forest to estimate different carbon pools and a stratified random sampling intensity of 0.5% used to collect data. Results showed significant ($p<0.05$) differences in above and below-ground biomass and carbon sequestration potential between the two CFs. The managed and unmanaged forests had total carbon stock of 269.3±27.4 and 150.0±22.7 ton/ha, respectively, demonstrating 1.79 times higher carbon stock in the former than the latter. The managed forest had significantly ($p<0.05$) greater mean soil organic carbon (SOC) stock than the unmanaged forest. The SOC was highest in the upper soil layer (0-10 cm), with a steady decrease as the soil depth increased. All other measured carbon pools values were higher in managed compared to unmanaged forest. The difference in carbon stock was due to the manipulation of different forest management activities, including thinning, timber extraction, fire control, grazing, and fuel wood/fodder extraction. The study suggests that the implementation of proper forest management would be necessary for enhancing carbon stock in forest trees and soils.

1. INTRODUCTION

Carbon sequestration refers to the removal, capture, or sequestration of carbon dioxide (CO_2) from the atmosphere by condensing and storing it in a sink in a benign manner (Kirschbaum, 2003). It is the prolonged deposition of carbon in soils, plants, oceans, and atmosphere (Selin, 2019). Carbon sequestration in the forest is the process of removing CO_2 from the atmosphere and accumulating it in trees (Jindal et al., 2008). Trees and other plants in a forest absorb CO_2 during photosynthesis and then sequester it as biomass, which comprises standing timber, branches, foliage and roots, as well as all of the plant organisms (Jana et al., 2009). Forest trees and soils account for about 60% of the world's terrestrial carbon (Lal, 2004; Bajracharya et al., 2018); thus, they are the principal carbon pools in the forest ecosystem (Amir et al., 2018). Forests stock up to 70% to 80% of world's carbon and play a crucial role in mitigating greenhouse gas (GHG) emissions and climate change (Batjes, 2014; Vance, 2018). Furthermore, soil organic carbon (SOC) is the most influential carbon pool (Ali et al., 2019; Hou et al., 2019), and its increase has been recognized as a viable strategy for mitigating climate change through increased soil carbon sequestration (Alidoust et al., 2018). Based on the United Nations Framework Convention on Climate Change (UNFCCC) and the Kyoto Protocol, IPCC (2003), five terrestrial carbon pools (soil, litter, under-ground and above-ground biomass, and deadwood) and their

Citation: Gautam S, Timilsina S, Shrestha M, Adhikari B, Khatri BBA, Timsina J. Do managed Hill Sal (*Shorea robusta*) community forests of Nepal sequester and conserve more carbon than unmanaged ones? Environ. Nat. Resour. J. 2023;21(3):222-231. (https://doi.org/10.32526/ennrj/21/202200259)

dynamics are considered to estimate carbon stocks. Following the UNFCCC and its subsequent agreements, nations that are required to report on GHG emissions and removals must estimate the amount of carbon sequestration related to forestry, land use changes, and other land use-related activities (Di Cosmo et al., 2022).

In Nepal, forest covers about 45.3% of the total land area (FRTC, 2022) accumulating 1,055 million tons of carbon, which has a substantial contribution to mitigating the adverse consequences of climate change (DFRS, 2015). Forest ecosystems are being spoiled globally by different biotic and abiotic factors such as human encroachment, road constructions, wildfires, community reliance on forests, desertification, and mining (Arnold, 2022). In tropical and subtropical forests, carbon stocks are declining at the rate of 1-2 billion tons/year (Subedi et al., 2014). Based on the degree of disturbances, Nepalese forests are categorized into degraded and non-degraded forests (Jina et al., 2008). Bhattarai et al. (2012) mentioned that forest management practices influence carbon sequestration in both trees and soil. Therefore, effective forest management not only slows down deforestation and forest degradation rates (Nagendra et al., 2008) but also benefits the forest's carbon store and carbon sequestration (Chhatre and Agrawal, 2009; Pandey et al., 2014; Solomon et al., 2017). Presently, 2.4 million ha of forests are being operated by 22,682 local communities across the country as community forests (CFs) (GoN, 2022). These forests are either fully or partially managed or unmanaged by the local communities and have great potential to increase the carbon sequestration and mitigate the climate change. Moreover, agroforestry systems practiced within and outside the CFs also store carbon in trees and soil (Dhakal et al., 2022) and provide a range of ecosystems services (ES) that need to be considered in CF management (Ojha et al., 2022).

In unmanaged forests, occasional large-scale disturbances and frequent small-scale disturbances allow late-successional phases to develop, resulting in a fine-grained mosaic of different developmental phases (Bengtsson et al., 2000). Thus, unmanaged forests display typical features, such as large amounts of dead wood and decaying trees, old and large trees, and pits and mounds around root plates (Spies and Yurner, 1999). On the other hand, managed forest landscapes are characterized by frequent disturbances with low variability in disturbance size and display more homogeneous tree composition, vertical stratification, age structure, and successional dynamics but lack senescent phases (Kuuluvainen et al., 1996; Commarmot et al., 2005). At the local scale, unmanaged forests in general are said to contain more species than managed forests (Okland et al., 2003).

Sal (*Shorea robusta)* forests dominate both in hills and plains of Nepal and are managed by both government and local communities. Sal forests have been heavily exploited either to generate state revenue or to meet the forest product demand of the ever-increasing population (Acharya et al., 2002). Though the role of CFs in improving the livelihoods and ecosystems services have been studied (Dhakal et al., 2022; Ojha et al., 2022), their contribution in terms of carbon sequestration in trees and soil has rarely been reported. Though a few researchers have assessed the carbon stocks for a variety of land-use classes, species, and physiographic regions in CFs, most of them have no records of carbon stocks (Shrestha and Singh, 2008). Moreover, the soil carbon sequestration potential under CFs and agroforestry systems is still underappreciated (Kafle, 2020; Joshi et al., 2021; Dhakal et al., 2022). There is also a knowledge gap on the variation in carbon stock between managed and unmanaged forests in the same geographic region, climate, altitude, and within same species. Thus, this study assesses the above- and below-ground carbon stocks in trees and soil under managed and unmanaged Hill Sal CFs of Nepal. The study also illustrates the influence of management activities on Sal biomass and carbon stock, as well as the association between SOC and bulk density with depth. Additionally, this study offers fundamental knowledge on the association between altitude and carbon stock and provides the baseline information for the carbon sequestration potential of managed and unmanaged Hill Sal CFs of Nepal.

2. METHODOLOGY

2.1 Study area

The study was conducted in a managed Taldanda and an unmanaged Dangdunge CFs of Tanahun District in Nepal's Gandaki Province (27°74′-28°13′ N and 83°94′-84°56′ E) (Figure 1). Taldanda and Dangdunge CFs, with respective land areas of 100.12 ha and 81.98 ha, are both Sal-dominated. These CFs were chosen because they are nearly identical in terms of the growing stock observed 10 years ago (154 m^3/ha), altitude, climatic zone, and aspect, but differ in their management practices.

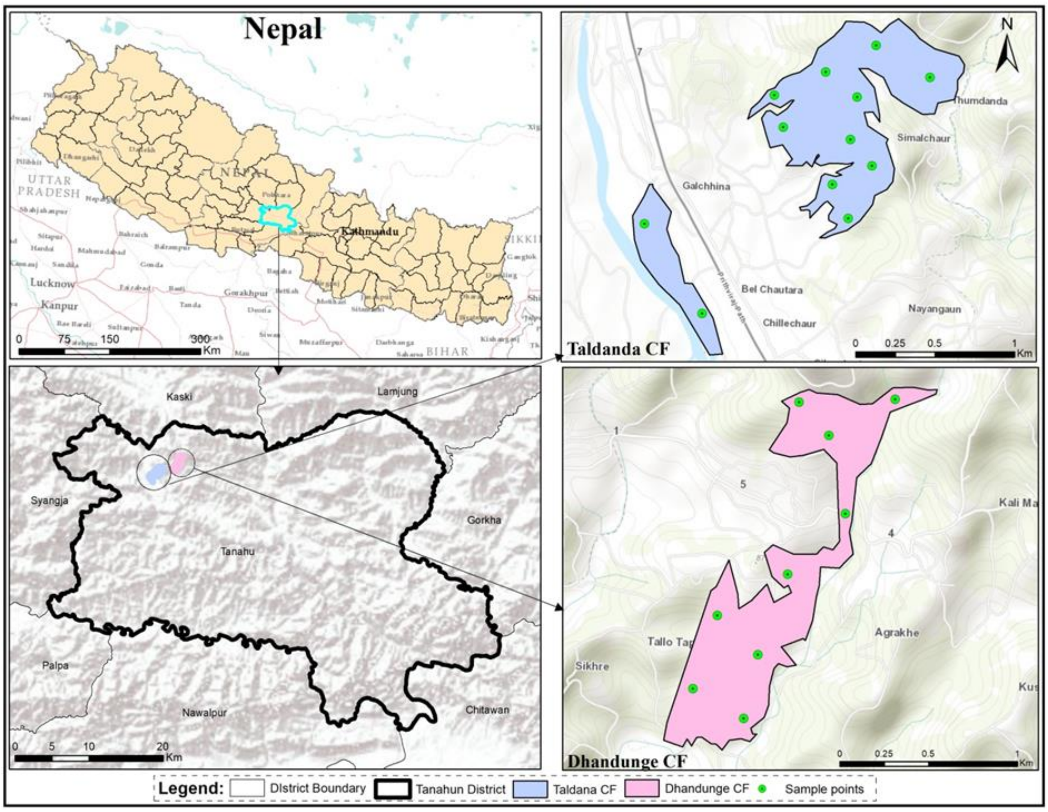

Figure 1. Map of Nepal showing study area with two community forests

2.2 Selection criteria

The criteria for managed and unmanaged CFs are shown in Table 1. Based on these criteria, Taldanda was considered as 'managed CF' and Dangdunge as an 'unmanaged CF'.

2.3 Sampling design and procedure

The majority of the data was gathered through a direct field survey of biophysical measurements. The diameter at breast height (DBH) and height of the tree were measured with a diameter tape (D-tape) and an Abney's level, respectively. A linear tape in the plot was laid out according to the sampling design (Figure 2). According to the guidelines for measuring carbon stocks in CF, 12 and nine sample plots were laid out in Taldanda and Dangdunge CF, respectively (ANSAB, 2010). Due to complex geology and variable altitude, a stratified random sampling method was used for measurements. Based on the Ministry of Forest and Soil Conservation's inventory guidelines, a sampling intensity of 0.5% was used (DoF, 2004).

Due to moderately dense woody vegetation, trees were measured within a circular plot of 250 m^2 with radius of 8.92 m to quantify above ground tree biomass (AGTB) (MacDicken, 1997). The DBH was measured at 1.3 m (DBH≥5 cm was considered as tree) and tree height was measured in each circular plot of 250 m^2 (Figure 2). For sapling measurements, a nested subplot of 100 m^2 with a radius of 5.64 m was established within larger plots (ANSAB, 2010). For assessing regeneration, smaller nested subplots with a 1 m radius were established within the larger nested plots. Saplings with diameters ranging from 1 to 5 cm were measured at 1.3 m above ground level, while saplings with diameter <1 cm were counted as regenerated. The regeneration data were used to observe the quality of regeneration.

The SOC was determined using samples collected from the IPCC (2006) recommended depth of 30 cm. A single 30 cm deep pit was dug at the center of each plot of both managed and unmanaged forests. To calculate bulk density, three soil samples from three depths (0-10 cm, 10-20 cm, and 20-30 cm) of approximately 300 cm^3 were collected from each plot using a standardized 300 cm^3 metal soil sampling core. Likewise, three samples from the same depths were collected to determine the organic carbon concentration in each depth. In addition, secondary data sources like published literature on carbon estimation were also used.

Table 1. Selection criteria of managed and unmanaged CFs

Criteria	Activities	Remarks
Thinning and Timber extraction	• Implementation of guidelines prescribed by respective CF operation plan (OP)	If Yes, Managed If No, Unmanaged
Weeding and cleaning	• Weeding at seedling stage • Cleaning at sapling stage	If Yes, Managed If No, Unmanaged
Fire	• Fire line construction • Controlled or prescribed burning • Legal measures to prevent fire (Sharma et al., 2011; Mathema, 2016)	If Yes, Managed If No, Unmanaged
Grazing	• Hoofmarks and dungs of livestock • Broken tops of seedlings and saplings • Signs of trampling (Joshi et al., 2020)	If Absence, Managed If Presence, Unmanaged
Fuel wood/fodder collection	• Restriction (Jina et al., 2008)	If Yes, Managed If No, Unmanaged

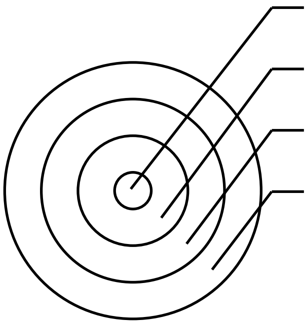

Figure 2. Sampling design of circular plots

2.4 Measurements and data collection

2.4.1 Above ground tree biomass

Above-ground tree biomass (AGTB) was estimated by using the following allometric equation devised by Chave et al. (2005):

$$AGTB = 0.0509 \times \rho D^2 H \quad (1)$$

Where; AGTB=above-ground tree biomass (kg); ρ=wood specific gravity (g/cm^2); D=tree diameter (m); and H=tree height (m).

The biomass stock density (kg/m^2) was calculated by adding the individual tree weight (kg) in the sampling plot and dividing by sampling plot area (250 m^2) and multiplying by 10 to convert to ton/ha. Biomass stock density was then converted to carbon stock density by multiplying by the default carbon fraction of 0.47 (IPCC, 2006).

2.4.2 Above-ground sapling biomass

Above-ground sapling biomass (AGSB) consisted of foliage, branch, and stem. The following regression model was used to calculate the AGSB.

$$\text{Log (AGSB)} = a + b \log (D) \quad (2)$$

Where; log=natural log (dimensionless); a=intercept of allometric relationship for saplings (dimensionless); b=slope allometric relationship for saplings (dimensionless); and D=over bark diameter at breast height (measured at 1.3 m above ground) (cm).

To evaluate the AGSB, national allometric biomass tables was utilized, which was generated by the Department of Forest (DoF), the Department of Forest Research and Survey (DFRS), Tree Improvement and Silviculture Component (TISC) (Tamrakar, 2000). Biomass stock density was then converted to carbon stock density by multiplying by the default carbon fraction of 0.47 (IPCC, 2006).

2.4.3 Below-ground biomass

The below-ground biomass (BGB) included the biomass of all live roots except fine roots with <2 mm diameter (Chavan and Rasal, 2012). The BGB was calculated by multiplying the AGB by 0.26 (constant factor) as per the Good Practice Guidelines of IPCC (2006) and Mandal and Joshi (2015):

$$BGB = AGB \times 0.26 \quad (3)$$

Where; BGB=below-ground biomass and AGB=above-ground biomass.

2.4.4 Deadwood biomass

The deadwood biomass (DWB) was evaluated by adding AGB and BGB and then multiplying by 0.11 (constant factor) as prescribed by IPCC (2006):

$$DWB = (AGB + BGB) \times 0.11 \quad (4)$$

Where; BGB=below-ground biomass and AGB=above-ground biomass.

2.4.5 Soil organic carbon and soil bulk density

Soil samples from 0-10, 10-20, and 20-30 cm depths from two replications were used to calculate bulk density and the carbon content of each plot in the laboratory.

Bulk density: Sixty-three soil samples were taken to the soil lab of the College of Natural Resource Management (CNRM), Puranchaur, Nepal. Samples were oven-dried at 105°C for 24 h and dried soils were passed through a 2 mm sieve. The sieved soils were weighed and the volume of stones was measured by water displacement method for stone correction. The following formula was employed to compute the bulk density (Pearson et al., 2005).

$$\text{Bulk density (g/cm}^3\text{)} = \frac{\text{Oven dry mass (g/cm}^3\text{)}}{\text{Core volume (cm}^3\text{)} - \frac{\text{Mass of coarse fragments (g)}}{\text{Density of rock fragment (g/cm}^3\text{)}}} \quad (5)$$

Carbon concentration (%): Sixty-three soil samples from each plot were dried at room temperature for three days and then quantified for carbon measurement by clearing stones and plant residue of >2 mm in size. Then they were taken to the Soil and Fertilizer Testing Laboratory (SAFTL), Gandaki Province, Pokhara where the titrimetric method based on Walkley and Black (1934) was employed for determination of carbon concentration.

Carbon stock density of soil organic carbon was calculated following Pearson (2007):

$$SOC = \rho \times d \times \%C \quad (6)$$

Where; SOC=soil organic carbon stock per unit area (ton/ha); ρ=soil bulk density (g/cm^3); d=soil depth at which the sample was taken (cm); and %C=carbon concentration (%).

2.5 Statistical analysis

To compare the carbon stock density between managed and unmanaged CFs at 5% level of significance, T-tests were performed using SPSS software. Correlation and regression analysis was conducted to establish the relationships between altitude and carbon stock for both managed and unmanaged CFs.

3. RESULTS AND DISCUSSION

3.1 Properties of forest stand

The mean diameter and height of trees was 29.28 cm and 18.36 m, respectively, in Taldanda CF, while they were 16.71 cm and 7.95 m respectively in Dandunge CF. Similarly, the mean diameter (dbh) of saplings was 2.63 cm and 1.89 cm respectively in Taldanda and Dangdunge CFs. On the other hand, tree and sapling density CF were 366 and 1,151 per ha, respectively in Taldanda, while they were 662 and 1,649 per ha, respectively, in Dangdunge CF. The results demonstrate that diameter, dbh, and height of the tree were higher in the managed CF while tree and sapling densities were higher in unmanaged CF. Managed CF had also more regeneration (10,896 per ha) than unmanaged CF (6,719 per ha) (Table 2). Dominant tree species in managed and unmanaged CFs are presented in Table 3.

Table 2. Properties of forest stand under the managed and unmanaged CFs in Nepal

CF	No. of plots	Tree							Sapling				Regeneration
		dbh (cm)			height (m)			trees /ha	dbh (cm)			Saplings/ ha	Seedlings/ha
		Min	Max	Mean	Min	Max	Mean		Min	Max	Mean		
Taldanda CF	12	5.5	55.8	29.28	5.3	27.5	18.36	366	1.3	4.9	2.63	1,151	10,896
Dangdunge CF	9	5.3	46.1	16.71	1.3	21.1	7.95	662	1.1	4.6	1.89	1,649	6,719

Table 3. Dominant tree species in managed and unmanaged CFs

Dangdunge CF	Taldanda CF
Shorea robusta	*Shorea robusta*
Schima wallichii	*Schima wallichii*
Castanopsis indica	*Dalbergia sissoo*
Lagerstroemia parviflora	*Acacia catechu*
Wrightia arborea	*Melastoma malabathricum*
Photinia integrifolia	*Colebrookea oppositifolia*

3.2 Vegetative biomass and carbon stock

The above-ground tree biomass (AGTB) and carbon stock in Taldanda CF were 294.17 ton/ha and 138.26±19.47 ton/ha, respectively, compared to 145.37 ton/ha and 68.33±16.88 ton/ha in Dangdunge CF. Similarly, the above-ground sapling biomass (AGSB) and carbon stock in Taldanda CF were 18.65 ton/ha and 8.77±0.83 ton/ha, respectively, compared to 4.65 ton/ha and 2.18±0.39 ton/ha in Dangdunge CF. The below-ground biomass (BGB) and carbon stock in Taldanda CF were 81.33 ton/ha and 38.22±5.03 ton/ha, respectively, compared to 39.00 ton/ha and 18.33±4.37 ton/ha, respectively, in Dangdunge CF. Likewise, the deadwood biomass (DWB) and carbon stock in Taldanda CF were 43.35 ton/ha and 20.37±2.68 ton/ha, respectively, compared to 20.79 ton/ha and 9.77±2.33 ton/ha, respectively, in Dandunge CF. The data reveal that all biomass and carbon parameters had higher values for managed CF compared to unmanaged CF.

3.3 Soil organic carbon stock

Taldanda CF had higher mean SOC than Dangdunge CF, with 63.72±5.11 ton/ha and 51.38±4.76 ton/ha, respectively. The maximum SOC was in the upper layer (0-10 cm) in both managed and unmanaged CFs and gradually decreased with increasing soil depth. In both CFs, as the soil depth increased, SOC decreased (Figure 3(a)) but bulk density increased (Figure 3(b)). Taldanda CF also had a higher bulk density than Dangdunge CF on average.

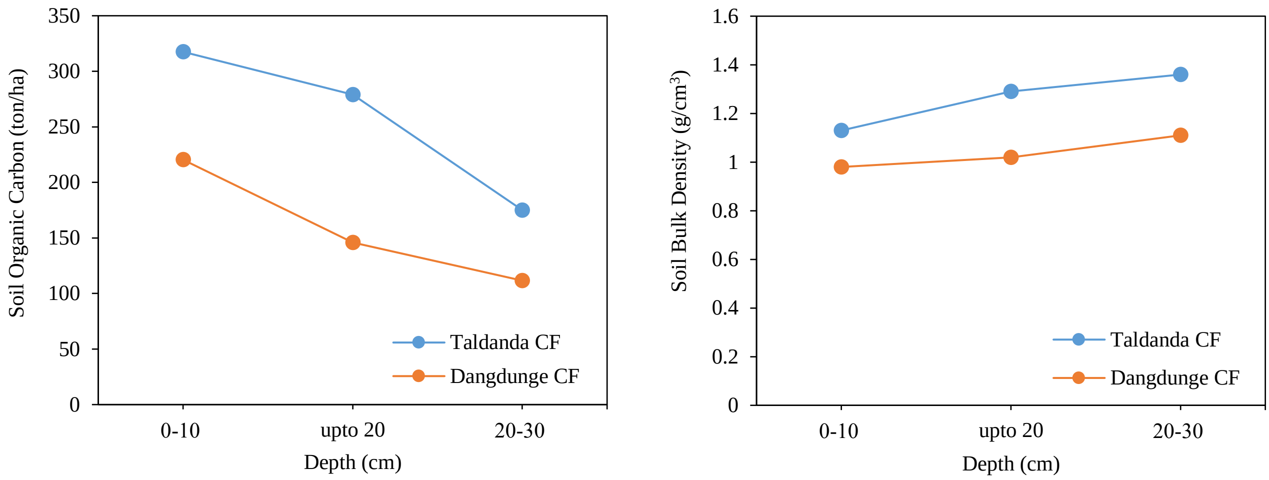

Figure 3. Amount and trend of (a) soil organic carbon stock (b) soil bulk density in each soil depth

3.4 Total biomass and carbon stock

The total carbon stock density was computed by summing the carbon stock density of the individual carbon pools (Table 4). The Taldanda CF had a total carbon stock of 269.34±27.44 ton/ha compared to only 149.98±22.69 ton/ha in Dangdunge CF (Table 4). In Taldanda CF, the total C stock partitioned to 51% in above-ground trees, 3% in above-ground saplings, 14% in below-ground biomass, 8% in the deadwood, and 24% in the soil. In Dangdunge CF, it partitioned to 45% in above-ground tree, 2% in above-ground saplings, 12% in below-ground biomass, 7% in deadwood and 34% in soil. The data reveal that partitioning of total C in Taldanda was higher in plant biomass while in Dandunge it was higher in soil biomass.

3.5 Altitude, aspect and carbon stock

In both managed and unmanaged CFs, plots were allotted without consideration of aspect, so the majority of the plots were located in south facing slope (29%) followed by east (28%), north (24%), and west (19%) facing slopes. Altogether, the altitude ranged from 473 m to 1,090 m from the mean sea level. There were negative correlations between altitude and total C and aspect and total C, suggesting that the carbon stock density decreases with an increase in altitude or aspect (Figure 4).

Table 4. Carbon pools and total carbon stock in Taldanda and Dangdunge CFs

Carbon pools	Carbon stock (ton/ha)		p-value
	Taldanda CF	Dangdunge CF	
Above ground tree carbon	138.26±19.47	68.33±16.88	0.0253
Above ground sapling carbon	8.77±0.83	2.18±0.39	0.0168
Below ground carbon	38.22±5.03	18.33±4.37	0.0498
Deadwood carbon	20.37±2.68	9.77±2.33	0.0012
Soil organic carbon	63.72±5.11	51.37±4.76	0.0327
Total	269.34±27.44	149.98±22.69	0.0287

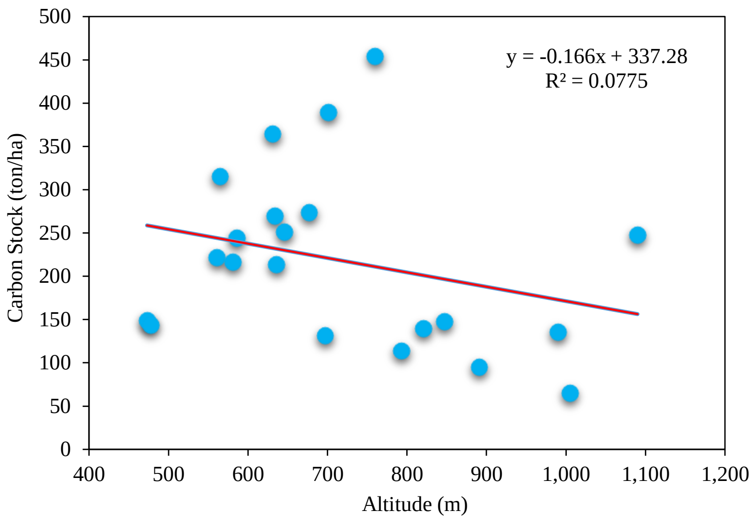

Figure 4. Altitude vs. carbon stock in both managed and unmanaged forests

4. DISCUSSION

Total carbon stock and tree biomass were significantly higher for the Taldanda CF than Dangdunge CF (Table 4) due to the absence of disturbances, including grazing, fuel wood/fodder collection, and timber harvesting (Joshi et al., 2020). Agro-forestry practices, grazing management, restoration of degraded land, mixing fertilizers, and inclusion of grass species are the best strategies for carbon storage under the fodder production system (Prasad et al., 2018). Also, the differences in above-ground carbon stock in the two CFs might be due to variations in forest age, plant species, and local factors (Bohara et al., 2021). The proper management activities lead to more effective stand productivity, and greater increment and assemblage of biomass (Jati, 2012). Joshi et al. (2020) also mentioned both the tree and sapling carbon stock were higher in non-degraded (managed) forests. Furthermore, there was better decomposition of leaf, litter, and tree branches, and below ground fine roots in Taldanda CF due to the protection of the forest from fire, grazing, and fodder/fodder extraction restriction. In contrast, due to lack of such protections, such advantages were not observed in Dangdunge CF which might have affected the BGB and carbon stock (Singh et al., 1987). Kafle et al. (2019) found a deadwood biomass of 22.39 ton/ha and deadwood carbon of 10.74 ton/ha in Parsa National Park, Nepal. Site parameters such as stand establishment and quantity, grade, age, and management activities may affect the deadwood carbon stock in the forest. Our study found a deadwood carbon stock value of 20.37±2.68 in Taldanda and 9.77±2.33 in Dangdunge CF, which was much less than other estimates, e.g., 0 to >600 ton/ha (Bastienne and Pablo, 2008).

Higher SOC in the managed CF was a result of the prevention of forest fires and livestock grazing. The presence of decomposable organic matter from branches and litter fall can boost the soil carbon in forests (Jati, 2012; Bhatta et al., 2021). Such boosting can occur significantly in the managed forest. However, in an unmanaged forest, forest fire always imbibes aboveground biomass and forest floor carbon, and based on the extent of the fire, belowground roots and soil carbon may be adversely impacted (Joshi et al., 2020). Tarus and Nadir (2020) predicted that when exposed to excessive fire, the carbon retained in the forest floor litter and branches undergoes prompt oxidation, permitting it to transfer to a gaseous phase. Forest management practices affect the rate as well as the intensity of carbon stock and SOC (Mandal et al., 2013).

There were differences in the average bulk density of the two forests -1.26 g/cm^3 in Taldanda CF and 1.03 g/cm^3 in Dangdunge CF (Figure 3(b)). Higher soil compaction in Taldanda CF could be due to management activities like thinning, weeding, and cleaning. On the other hand, intensive grazing, movement of local people to the forest for livestock grazing and leaf, litter, fuel wood and fodder collection might be the causes for soil compaction in Dangdunge CF. Animal trampling can cause changes in bulk density, infiltration rate, soil moisture, and soil mechanical properties (Chaichi et al., 2005; Dunne et al., 2011). Grazing influences the soil nutrient release and availability, degradation of leaf litter and roots, and the organic matter (Cornwell et al., 2008; He et al., 2012). Hence, forest management activities have an impact on soil carbon sequestration and emissions (Jandl et al., 2007). Finally, in agreement with findings of this study, Thong et al. (2020) mentioned that soil carbon sequestration can be significantly affected by aspect and altitude.

5. CONCLUSION

Taldanda CF had a total carbon stock of 269.3±27.4 ton/ha and a CO_2 sequestration of 987.6 ton/ha, whereas Dangdunge CF had a total carbon stock of 145.0±22.7 ton/ha with CO_2 sequestration of 549.9 ton/ha. SOC constituted 24% of total C stock in managed forest, while 34% in unmanaged forest. The SOC decreased gradually as soil depth increased, whereas bulk density increased in both CFs. Furthermore, carbon density had a negative correlation with altitude and aspect in both CFs. This study shows that managed CFs have a higher capacity to store CO_2 in forest biomass than unmanaged forests but soil C sequestration is higher in unmanaged CF. The study suggests that the implementation of proper forest management activities is of utmost important not only for the enhancement of carbon stock in tree and soil but also for sustainable forest management and mitigating climate change. The study recommends that the growing biomass stock and carbon stock need to be estimated and updated on a regular basis nation-wide to ensure accurate estimates of carbon emissions and carbon sequestrations necessary for reporting requirements and meeting the net zero target.

ACKNOWLEDGEMENTS

We would like to extend our sincere gratitude to Mr. Suman Bhattarai, Dr. Dhruba Bijaya G.C., Mr. Supuspha Regmi, Mr. Rabindra Adhikari, and Ms. Pratikshya Paneru who guided us from data collection to analysis and interpretation. We also like to thanks Mr. Saurav Shrestha and Mr. Shankar Tripathi for their help during map preparation. Additionally, we appreciate the assistance of the anonymous reviewers and editors, whose insightful comments and recommendations helped us to improve our manuscript.

REFERENCES

Acharya KP, Tamrakar PR, Gautam G, Regmi R, Adhikari A, Acharya B. Managing tropical Sal Forests (*Shorea robusta*) in Nepal in short rotations: Findings of a 12-year long research. Banko Janakari 2002;12(1):71-5.

Ali A, Ashraf MI, Gulzar S, Akmal M, Ahmad B. Estimation of soil carbon pools in the forests of Khyber Pakhtunkhwa Province, Pakistan. Journal of Forestry Research 2019; 31(6):2313-21.

Alidoust E, Afyuni M, Hajabbasi MA, Mosaddeghi MR. Soil carbon sequestration potential as affected by soil physical and climatic factors under different land uses in a semiarid region. Catena 2018;171:62-71.

Amir M, Liu X, Ahmad A, Saeed S, Mannan A, Muneer MA. Patterns of biomass and carbon allocation across chronosequence of chir pine (*Pinus roxburghii*) forest in Pakistan: Inventory-based estimate. Advances in Meteorology 2018;2018:Article No. 3095891.

Arnold H. Biotic and abiotic factors that affecting forest ecosystem. Journal of Forest Research 2022;11:Article No. 325.

Asia Network for Sustainable Agriculture and Bio-resources (ANSAB). Forest Carbon Stock Measurement: Guidelines for Measuring Carbon Stocks in Community-Managed Forests. Kathmandu, Nepal: Asia Network for Sustainable Agriculture and Bio-resources (ANSAB), Federation of Community Forest User Groups and International Centre for Integrated Mountain Development; 2010.

Bajracharya RM, Lal R, Kimble JM. Soil organic carbon distribution in aggregates and primary particle fractions as influenced by erosion phases and landscape position. In: Soil Processes and the Carbon Cycle. CRC Press; 2018. p. 353-67.

Bastienne CS, Pablo JD. Effects of forest type and stand structure on coarse woody debris in old-growth rainforests in the Valdivian Andes, south-central Chile. Forest Ecology and Management 2008;255(5-6):1906-14.

Batjes NH. Total carbon and nitrogen in the soils of the world. European Journal of Soil Science 2014;65(1):10-21.

Bengtsson J, Nilsson SG, Franc A, Menozzi P. Biodiversity, disturbances, ecosystem function and management of European forests. Forest Ecology and Management 2000; 132(1):39-50.

Bhatta S, Poudel A, Kc YB. A comparative study of carbon stocks in the Sal Forest (*Shorea robusta*) in core and buffer zones of Shuklaphanta National Park, Nepal. Forestry: Journal of Institute of Forestry, Nepal 2021;18(1):52-60.

Bhattarai TP, Skutsch M, Midmore DJ, Rana EB. The carbon sequestration potential of community-based forest management in Nepal. International Journal of Climate Change: Impacts and Responses 2012;3(2):233-53.

Bohara B, Miya MS, Timilsina S, Gautam D, Regmi S. Biomass and carbon stock variation along slopes in tropical forest of Nepal: A case of Depard Community Forest, Makwanpur, Nepal. Journal of Multidisciplinary Applied Natural Science 2021;1(2):89-99.

Chaichi MR, Saravi MM, Malekian AR. Effects of livestock trampling on soil physical properties and vegetation cover (Case study: Lar Rangeland, Iran). International Journal of Agriculture and Biology 2005;7:904-8.

Chavan BL, Rasal GB. Comparative status of carbon dioxide sequestration in *Albizia lebbek* and *Delonix regia*. Universal Journal of Environmental Research and Technology 2012; 2(1):85-92.

Chave J, Andalo C, Brown S, Cairns MA, Chambers JQ, Eamus D, et al. Tree allometry and improved estimation of carbon stocks and balance in tropical forests. Oecologia 2005; 145(1):87-99.

Chhatre A, Agrawal A. Trade-offs and synergies between carbon storage and livelihood benefits from forest commons. Proceedings of the National Academy of Sciences 2009; 106(42):17667-70.

Commarmot B, Bachofen H, Bundziak Y, Bürgi A, Ramp B, Shparyk Y, et al. Structures of virgin and managed beech forests in Uholka (Ukraine) and Sihlwald (Switzerland): A comparative study. Forest Snow and Landscape Research 2005;79(1/2):45-56.

Cornwell WK, Cornelissen JH, Amatangelo K, Dorrepaal E, Eviner VT, Godoy O, et al. Plant species traits are the predominant control on litter decomposition rates within biomes worldwide. Ecological Letters 2008;11(10):1065-71.

Department of Forest (DoF). Community Forest Inventory Guideline. Kathmandu, Nepal: DoF; 2004.

Department of Forest Research and Survey (DFRS). State of Nepal's Forests: Forest Resource Assessment (FRA) Nepal. Kathmandu, Nepal: DFRS; 2015.

Dhakal A, Maraseni TN, Timsina J. Assessing the potential of agroforestry in Nepal: Socio-economic and environmental perspectives. In: Agriculture, Natural Resources and Food Security. Springer Cham; 2022. p. 375-94.

Di Cosmo L, Gasparini P, Floris A. Forest carbon stock. In: Italian National Forest Inventory: Methods and Results of the Third Survey. Springer Cham; 2022. p. 503-43.

Dunne T, Western D, Dietrich WE. Effects of cattle trampling on vegetation, infiltration, and erosion in a tropical rangeland. Journal of Arid Environments 2011;75(1):58-69.

Forest Research and Training Centre (FRTC). National Land Cover Monitoring System of Nepal. Babarmahal, Kathmandu, Nepal: Forest Research and Training Centre, Government of Nepal; 2022.

Government of Nepal (GoN). Economic survey. Singh Durbar, Kathmandu [Internet]. 2022 [cited 2023 Feb 8]. Available from: https://www.mof.gov.np/site/publication-detail/3170.

He WM, Shen Y, Cornelissen JHC. Soil nutrient patchiness and plant genotypes interact on the production potential and decomposition of root and shoot litter: Evidence from short-term laboratory experiments with *Triticum aestivum*. Plant and Soil 2012;353(1):145-54.

Hou G, Delang CO, Lu X, Gao L. Soil organic carbon storage varies with stand ages and soil depths following afforestation. Annals of Forest Research 2019;62(2):3-20.

Intergovernmental Panel on Climate Change (IPCC). Good Practice Guidance for Land Use, Land Use Change and Forestry. Kanagawa, Japan: Institute for Global Environmental Strategies, IPCC; 2003.

Intergovernmental Panel on Climate Change (IPCC). IPCC Guidelines for National Greenhouse Gas Inventories, (Volume 4: Agriculture, Forestry and Other Land Use). Hayanma, Japan: Institute of for Global Environmental Strategies, IPCC; 2006.

Jana BK, Biswas S, Majumder M, Roy PK, Mazumdar A. Carbon sequestration rate and aboveground biomass carbon potential of four young species. Journal of Ecology and Natural Environment 2009;1(2):15-24.

Jandl R, Lindner M, Vesterdal L, Bauwens B, Baritz R, Hagedorn F, et al. How strongly can forest management influence soil carbon sequestration? Geoderma 2007;137(3-4):253-68.

Jati R. Comparative Study of Carbon Assessment: A Study on Carbon Stock in Kumvakarna Conservation Community Forest [dissertation]. Department of Environmental Science, Khwopa College, Tribhuwan University; 2012.

Jina BS, Sah P, Bhatt MD, Rawat YS. Estimating carbon sequestration rates and total carbon stockpile in degraded and non-degraded sites of Oak and Pine Forest of Kumaun Central Himalaya. Ecoprint: An International Journal of Ecology 2008;15:75-81.

Jindal R, Swallow B, Kerr J. Forestry-based carbon sequestration projects in Africa: Potential benefits and challenges. In: Natural Resources Forum. Oxford, UK: Blackwell Publishing Ltd; 2008.

Joshi R, Singh H, Chhetri R, Poudel SR, Rijal S. Carbon sequestration potential of community forests: A comparative analysis of soil organic carbon stock in community managed forests of Far-Western Nepal. Eurasian Journal of Soil Science 2021;10(2):96-104.

Joshi R, Singh H, Chhetri R, Yadav K. Assessment of carbon sequestration potential in degraded and non-Degraded community forests in Terai Region of Nepal. Journal of Forest and Environmental Science 2020;36(2):113-21.

Kafle G, Timilsina YP, Sharma RP, Rijal ML, Bartaula B, Pokhrel B, et al. Contribution of dead wood and forest soil to carbon sequestration in Parsa National Park, Nepal. Journal of Agriculture and Forestry University 2019;3:113-23.

Kafle G. Carbon sequestration and soil properties in forests of Nepal. Agriculture and Forestry Journal 2020;4(2):91-5.

Kirschbaum MU. To sink or burn? A discussion of the potential contributions of forests to greenhouse gas balances through storing carbon or providing biofuels. Biomass and Bioenergy 2003;24(4-5):297-310.

Kuuluvainen T, Penttinen A, Leinonen K, Nygren M. Statistical opportunities for comparing stand structural heterogeneity in managed and primeval forests: An example from boreal spruce forest in southern Finland. Silva Fennica 1996;30(2-3):315-28.

Lal R. Soil carbon sequestration to mitigate climate change. Geoderma 2004;123(1-2):1-22.

MacDicken KG. A Guide to Monitoring Carbon Storage in Forestry and Agroforestry Projects. USA: Winrock International Institute for Agricultural Development; 1997.

Mandal G, Joshi SP. Biomass accumulation and carbon sequestration potential of dry deciduous forests. International Journal of Ecology and Development 2015;30(1):64-82.

Mandal RA, Dutta IC, Jha PK, Karmacharya S. Relationship between carbon stock and plant biodiversity in collaborative forests in Terai, Nepal. International Scholarly Research Notices 2013;2013:Article No. 625767.

Mathema P. Forest Fire and its management strategies in Nepal. Banko Janakari 2016;23(2):1-2.

Nagendra H, Pareeth S, Sharma B, Schweik CM, Adhikari KR. Forest fragmentation and regrowth in an institutional mosaic of community, government and private ownership in Nepal. Landscape Ecology 2008;23(1):41-54.

Ojha H, Paudel NS, Timsina J, Chaudhary S, Baral H. Ecosystems services from community forestry: Prospects and challenges for improving local livelihoods in Nepal. In: Timsina J, Maraseni TN, Gauchan D, Adhikari J, Ojha H, editors. Agriculture, Natural Resources and Food Security. Sustainable Development Goals Series. Springer Cham; 2022. p. 337-56.

Okland T, Rydgren K, Okland RH, Storaunet KO, Rolstad J. Variation in environmental conditions, understorey species number, abundance and composition among natural and managed *Picea abies* forest stands. Forest Ecology and Management 2003;177(1-3):17-37.

Pandey SS, Maraseni TN, Cockfield G. Carbon stock dynamics in different vegetation dominated community forests under REDD+: A case from Nepal. Forest Ecology and Management 2014;327:40-7.

Pearson TR, Brown S, Ravindranath NH. Integrating Carbon Benefit Estimates into GEF Projects: Guidelines. New York, USA: Global Environment Facility, United Nations Development Programme; 2005.

Pearson TR. Measurement Guidelines for the Sequestration of Forest Carbon. USA: United States Department of Agriculture, Forest Service; 2007.

Prasad M, Chaudhary M, Srinivasan R. Role of fodder production systems to improve carbon sequestration and environmental sustainability. Global Journal of Bioscience and Biotechnology 2018;7(1):81-7.

Selin NE. Carbon sequestration. Encyclopedia Britannica [Internet]. 2019 [cited 2023 Feb 8]. Available from: https://www.britannica.com/technology/carbon-sequestration.

Sharma CM, Gairola S, Baduni NP, Ghildiyal SK, Suyal, S. Variation in carbon stocks on different slope aspects in seven major forest types of temperate region of Garhwal Himalaya, India. Journal of Biosciences 2011;36(4):701-8.

Shrestha BM, Singh BR. Soil and vegetation carbon pools in a mountainous watershed of Nepal. Nutrient Cycling in Agroecosystems 2008;81(2):179-91.

Singh AK, Kumar VK, Singh J. Forest Resource, Economy, and Environment. Nepal: Concept Publishing Company; 1987.

Solomon N, Birhane E, Tadesse T, Treydte AC, Meles K. Carbon stocks and sequestration potential of dry forests under community management in Tigray, Ethiopia. Ecological Processes 2017;6(1):1-11.

Spies TA, Yurner MG. Dynamic forest mosaics. In: Hunter M, editor. Maintaining Biodiversity in Forest Ecosystems. Cambridge University Press; 1999. p. 95-160.

Subedi M, Matthews RB, Pogson M, Abegaz A, Balana BB, Oyesiku-Blakemore J, et al. Can biogas digesters help to reduce deforestation in Africa? Biomass and Bioenergy 2014;70:87-98.

Tamrakar PR. Biomass and Volume Tables with Species Description for Community Forest Management. Kathmandu, Nepal: MoFSC and NARMSAP-TISC; 2000.

Tarus GK, Nadir SW. Effect of forest management types on soil carbon stocks in Montane Forests: A case study of Eastern Mau Forest in Kenya. International Journal of Forestry Research 2020;2020:Article No. 8862813.

Thong P, Sahoo UK, Thangjam U, Pebam R. Pattern of forest recovery and carbon stock following shifting cultivation in Manipur, North-East India. PLoS ONE 2020;15(10):e0239906.

Vance ED. Conclusions and caveats from studies of managed forest carbon budgets. Forest Ecology and Management 2018;427:350-4.

Walkley A, Black IA. An examination of the Degtjareff method for determining soil organic matter, and a proposed modification of the chromic acid titration method. Soil Science 1934;37(1):29-38.

Seed Osmopriming Improves Germination, Physiological, and Root Anatomical Attributes of Red Amaranth (*Amaranthus tricolor* L.) in Salinity Stress Condition

Deby Rossa Amalia and Diah Rachmawati*

Department of Tropical Biology, Faculty of Biology, Universitas Gadjah Mada, Jl. Teknika Selatan Sekip Utara, Yogyakarta 55281, Indonesia

ARTICLE INFO

Received: 2 Dec 2022
Received in revised: 9 Feb 2023
Accepted: 21 Feb 2023
Published online: 10 Apr 2023
DOI: 10.32526/ennrj/21/202200258

Keywords:
Osmopriming/ NaCl/ PEG/ Proline/ Red amaranth

*** Corresponding author:**
E-mail: drachmawati@ugm.ac.id

ABSTRACT

Salinity stress is a form of abiotic stress that threatens the sustainability of agriculture in almost all countries in the world. It has an impact in reducing plant productivity. Red amaranth (*Amaranthus tricolor* L.) is a vegetable crop that has high nutritional value, but extensive saline land area can cause red amaranth yields to decline. Osmopriming is a seed priming method in which seeds are immersed in a solution that has a high osmotic potential, such as PEG (polyethylene glycol) in order to increase germination under unfavorable conditions. This study determined the effect of osmopriming on germination, physiological, and root anatomical attributes of red amaranth roots under salinity stress conditions. The research design used a completely randomized design with two types of treatment, namely, osmopriming and salinity stress. Each treatment used three concentrations, seed osmopriming with 0%, 5%, and 10% of PEG and salinity stress of 0 mM, 50 mM, and 100 mM of NaCl. The measured parameters were germination, growth, physiological, and root anatomical characters. Osmopriming of seeds with 10% PEG increased germination as indicated by the germination percentage, time, and rate reaching 95.55%, 1.393 day, and 71.98%/day, respectively. Red amaranth plants that had been osmoprimed with 10% PEG grew faster when exposed to salinity stress. Application of PEG 5% and 10% increased total chlorophyll levels while decreasing proline levels and Ca-oxalate crystal density. Under salinity stress conditions, PEG application improved the root anatomical characters of red amaranth as shown by increased epidermis thickness, cortex thickness, and stele diameter. Priming application with 10% PEG has the potential to increase the tolerance of red amaranth to salinity stress.

1. INTRODUCTION

The need for vegetables continues to increase along with increasing public awareness of the importance of a well-balanced nutrition in building immunity. Red amaranth (*Amaranthus tricolor* L.) is a highly nutritious leafy vegetable crop. Amaranth leaves and stems are rich in protein including the essential amino acids lysine, arginine, histidine as well as vitamins (A, C, K, B2, B3, and B6), minerals such as magnesium, calcium, potassium, iron, phosphorus, zinc, and iron (da Silva et al., 2019) and a red color in the form of betacyanins, which acts as an antioxidant (Li et al., 2019). Environmental stresses such as salinity stress decrease water availability (drought) and nutrients, and limit efforts to increase plant productivity.

Salinity stress occurs when an excessive amount of dissolved salt in the soil causes a decrease in plant growth and productivity. Salinity causes osmotic stress which is followed by ion toxicity, nutrient imbalance, impaired ROS detoxification ability, decreased photosynthetic rate, and disturbances in the mechanism of stomata opening and closing (Menezes et al., 2017). The capacity of the root system to absorb water declines during the early stages of stress, whereas the transpiration rate of the leaves increases dramatically.

Citation: Amalia DR, Rachmawati D. Seed osmopriming improves germination, physiological, and root anatomical attributes of red amaranth (*Amaranthus tricolor* L.) in salinity stress condition. Environ. Nat. Resour. J. 2023;21(3):232-244. (https://doi.org/10.32526/ennrj/21/202200258)

The presence of ROS causes oxidative damage to various cellular components, such as proteins, lipids, and DNA (Boughalleb et al., 2017).

Seed germination is a critical stage of the plant life cycle. Priming is a seed treatment that allows seeds to carry out the process of imbibition and activation of early metabolic processes during seed germination while inhibiting growth and emergence of radicles (Arjmand et al., 2014). Seed priming as a pre-planting treatment technique is carried out to increase germination and growth under non optimal environmental conditions (Chen et al., 2021). Priming prepares the process of seed metabolism, making the seeds more ready to germinate. Priming serves several purposes, including the production of healthier and stronger seedlings, which allow plants to grow faster in the field, as well as seedlings are protected from disease or other stresses during the development process. Typically, seed priming results in seedlings having a more developed root system, which allows them to survive stressful conditions.

Osmopriming is one of the most common used priming methods by immersing seeds in a solution with a high osmotic potential which allows pre-germination metabolic activity to continue while preventing the emergence of radicles (Debbarma and Das, 2017). Polyethylene glycol (PEG) is an osmopriming agent that is often used because it is non-toxic and has a high molecular weight. The use of PEG can improve physiological and biochemical processes in seeds by controlled addition of water to imbibition media with low osmotic potential (Pallaoro et al., 2016). Osmopriming can boosts crop yields in addition to increasing the percentage of seed germination. Osmopriming with PEG has been shown to alleviate the effects of drought stress on *Ipomoea reptans* (Latifa and Rachmawati, 2020).

The purpose of this research is to discover the role of osmopriming in increasing the growth and resistance of red amaranth (*Amaranthus tricolor* L.) under salinity stress conditions in terms of germination, physiological, and anatomical characteristics of red amaranth roots. Through the study of germination, physiological and root anatomical characters, the role of osmopriming to alleviate the negative effect of salinity stress can be determined.

2. METHODOLOGY

2.1 Experimental site and design

This experiment was conducted in the greenhouse at the Karanggayam Research Station, Laboratory of Plant Physiology and Laboratory of Plant Structure and Development, Faculty of Biology, Universitas Gadjah Mada from February 2022 to July 2022.

Complete randomized design was used to arrange this research containing two variables: seed osmopriming and salinity stress. Seed osmopriming was performed with three levels of PEG concentration of 0%, 5%, and 10%, and salinity stress with three level of NaCl concentration of 0 mM, 50 mM, and 100 mM. Each treatment combination consisted of three replications. Osmopriming was carried out by soaking red amaranth seeds in PEG solution with three different concentrations (0%, 5%, and 10%) for 24 h. Subsequently, the seeds were dried at room temperature for 24 h and then the primed seeds were germinated in a petri dish. Three replications of 15 red amaranth seeds each were placed on petri dishes Ø 9 cm on one layer of filter paper. The seeds were supplied daily with distilled water during the germination trial which lasted four days (Amalia, 2022). Seed germination was characterized by the appearance of a radicle with a length of ±1 mm. Germination characters including germination percentage, mean germination time, mean germination rate and germination rate index were observed based on the method of Al-Mudaris (1998). Germination percentage was calculated according the formula as follows:

$$\text{Germination percentage} = \frac{\text{Number of germinated seeds}}{\text{Total number of seeds for germination}} \times 100$$

The germination rate provides a measure of the time course of seed germination. Mean germination rate (MGR)=CV/100=1/T; where T is mean germination time and CV: coefficient of velocity. Mean germination time (MGT)=ΣFx/ΣF; where F is the number of seeds germinated on day x. Germination rate index is calculated as the ratio between the sum of the number of seeds germinated each day and the number of days elapsed between sowing and germination. Germination rate index (GRI)= G1/1+G2/2+...+Gi/i; where; G1 is the germination percentage on day 1, G2 is the germination percentage at day 2; and so on (Al-Mudaris, 1998).

Germinated seeds were grown in tray pots for 14 days. The 14-days old individual seedling of each cultivar was transferred into a pot consisting of 2 kg growing media (compost and soil with a ratio of 1:3, respectively) and acclimated for seven days before being treated with salinity stress at NaCl concentration of 0 mM, 50 mM, and 100 mM. Application of salinity stress was carried out for 21 days every two days and the dose given is 150 mL per polybag. The red amaranth plants were harvested at 35 days after transplanted (DAP).

2.2 Growth and physiological analysis

Growth parameters including plant height was measured from the base to the shoot tip every three days from the 14 DAP to 35 DAP, and root length was measured from the base to the tip of the longest root at 35 DAP. Dry weight of shoots and roots were recorded at 35 DAP.

Physiological parameters observed include total chlorophyll content, proline content, oxalic acid content, and Ca-oxalate crystal density. The total chlorophyll content was analyzed from 0.1 g leaf samples. Samples were homogenized in 80% cold acetone and the absorbance of supernatants was measured using GENESYS 10 UV Scanning, Thermo Scientific at the multi-wavelength of 645 nm and 664 nm according to the method of Yoshida (1976). The chlorophyll content was expressed in mg/g FW (fresh weight).

The proline level of samples was measured according to the Bates method (Bates et al., 1973). Leaf samples about 0.25 g were homogenized in 5 mL of 3% sulfosalicylic acid, and 1 mL of filtered supernatant was reacted with 1 mL of CH_3COOH, 1 mL of ninhydrin acid then incubated at 94°C for 1 h and chilled in an icebox. Two mL of toluene were added to separate the proline from the organic phase. The absorbances were measured at 520 nm and the proline content was determined by comparing the results with a standard curve of proline.

The oxalic acid content was determined with the principle of permanganometry titration according to Fitriani et al. (2016). Two grams of red amaranth leaves was crushed to a fine powder and then added to 100 mL aquadest. The extract was heated for 20 min and then filtered. The filtrate was diluted with aquadest up to 250 mL. Then, 50 mL diluted filtrate was added with 1 mL of H_2SO_4 and titrated with 0.01 N of $KMnO_4$ until the equivalent point was reached. Oxalic acid content is calculated using the following formula:

$$\text{Oxalic acid normality} \quad V_K \times N_K = V_o \times N_o$$

$$V_o \times N_o = \frac{\text{Oxalic acid mass (mg)}}{\text{EW}}$$

$$\text{Oxalic acid content (mg/g)} = \frac{\text{Oxalic acid mass (mg)}}{\text{Sample weight (g)}}$$

Where; V_K=Volume of potassium permanganate (mL); N_K=Normality of potassium permanganate (N); V_O=Volume of sample (mL); N_O=Normality of oxalic acid (N); EW=Equivalent weight of oxalic acid=63.

Ca-oxalate Crystal Density was determined according to the method described by Harijati (Harijati et al., 2011). The stem was free-hand sectioned, and the sections were placed in 70% alcohol before being examined under a microscope and documented with an optilab. Formula for calculating Ca-oxalate Crystal Density as follow:

$$\underset{(\text{Crystal/mm}^2)}{\text{Ca-Oxalate Crystal Density}} = \frac{\text{Total observed crystals}}{\text{View area (mm}^2)}$$

2.3 Root anatomical analysis

A cross section of the root 5 cm from the base was prepared using the embedding method (Ruzin, 1999). The root anatomical structure including epidermis thickness, cortex thickness and stele diameter were observed using a binocular light microscope (BOECO BM-180) with an optilab. Measurements of epidermis thickness, cortex thickness and stele diameter were performed using Image Raster software.

2.4 Data analysis

The significant differences of the data between all treatments in each parameter were tested and obtained from the ANOVA test, were then followed by the Duncan multiple range test with a significance level of 5% using SPSS Software (IBM-SPSS Ver 25.00.US).

3. RESULTS AND DISCUSSION

3.1 Germination attributes

Osmopriming with PEG had a positive and significant effect ($p<0.05$) (Table 1) on germination parameters by increasing germination percentage, mean germination rate, and germination rate index, and decreased mean germination time of red amaranth seeds compared to control seeds without osmopriming treatment. Table 1 showed that the highest percentage of germination, mean germination rate, and germination rate index were found in the 10% PEG priming treatment with values of 95.55%, 71.98%, and 80.37%, respectively. These results were not significantly different ($p\geq0.05$) with 5% of PEG but significantly different ($p<0.05$) with control without

PEG treatment. The control seeds showed the lowest results compared to the application of 5% and 10% of PEG with the germination percentage of 82.22%, mean germination time of 2.132 days and mean germination rate of 46.94%/day.

Table 1. Seed germination attributes *A. tricolor* after osmopriming treatment

Osmopriming (% PEG)	Germination percentage (%)	Mean germination time (day)	Mean germination rate (%/day)	Germination rate index
0	82.22±3.85^{a}	2.132±0.085^{a}	46.94±1.83^{a}	45.92±0.64^{a}
5	91.11±3.84^{b}	1.386±0.054^{b}	71.67±2.88^{b}	74.81±5.13^{b}
10	95.55±3.85^{b}	1.393±0.095^{b}	71.98±5.08^{b}	80.37±2.31^{b}

The number followed by the same letter in the same column has no significant difference based on DMRT α=0.05, n=3.

These results are in line with the results of Kim et al. (2022) which showed an increase in germination properties of *Aruncus dioicus*, such as germination percentage, rate, and time to achieve 50% germination (T_{50}) compared to unprimed seeds. Improvement in germination properties caused by PEG could be facilitating water absorption and protein synthesis. Besides that, priming treatments with PEG prolongs phase II (activation) in the germination process where membrane and DNA repair occurs, accumulation of β-tubulin, and mobilization of food reserves (Ghiyasi and Tajbakhsh, 2013). Prolongs phase II (activation) in the germination process where membrane and DNA repair occurs, accumulation of β-tubulin, and mobilization of food reserves (Ghiyasi and Tajbakhsh, 2013). Starch degradation and greater sugar accumulation in primed seeds contributed positively to the attributes of better germination and stress tolerance (Lei et al., 2021). During the osmopriming treatment, the enzymes ATPase, ACC synthetase and isocitrate lyase which play a role in membrane repair also increased, thus increasing membrane integrity, and reducing metabolic leakage (Rachma et al., 2016; Raj and Raj, 2019).

Osmopriming also contributes to increase the expression of aquaporin proteins that facilitate the transport of water across cell membranes (Alleva et al., 2012). The potential for seed germination is increased by increased aquaporin expression because it enhances the water supply to the growing tissue (Raj and Raj, 2019). Additionally, osmopriming increases the accumulation of LEA (Late Embryogenesis Abundant) protein which is important for maintaining macromolecules and cell structure. This can increase seed tolerance when grown under abiotic stress conditions, such as salinity stress (Battaglia and Covarrubias, 2014).

3.2 Growth and physiological attributes

Salinity stress significantly decreased the height of red amaranth plants (Figure 1), particularly in those that had not received osmopriming treatment. Meanwhile, osmopriming-treated plants exhibited better growth than control plants despite being subjected to salinity stress, especially when treated with 10% PEG.

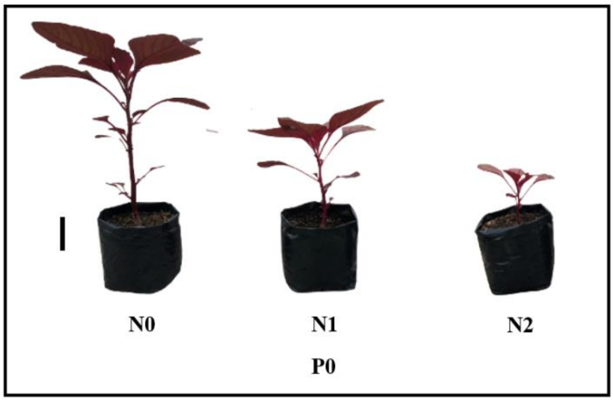

Figure 1. Plant height of red amaranth (*A. tricolor*) plants aged 5 weeks after osmopriming application with PEG (P0: 0%; P1: 5%; P2: 10%) and NaCl stress (N0: 0 mM; N1: 50 mM; N2: 100 mM). Bar=5 cm.

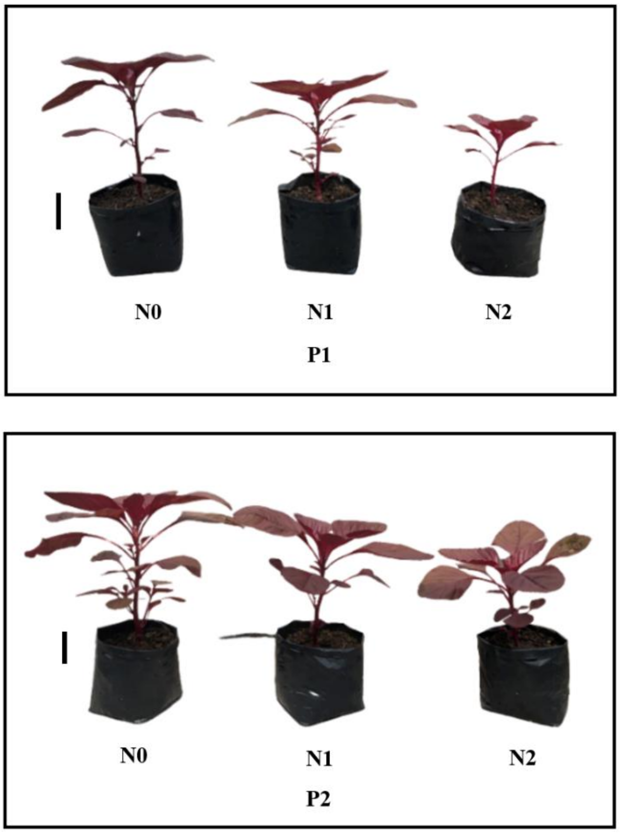

Figure 1. Plant height of red amaranth (*A. tricolor*) plants aged 5 weeks after osmopriming application with PEG (P0: 0%; P1: 5%; P2: 10%) and NaCl stress (N0: 0 mM; N1: 50 mM; N2: 100 mM). Bar=5 cm (cont.).

Plant height decreased as the concentration of NaCl increased. This is caused by increased osmotic pressure which inhibits the absorption and transport of water. Another negative effect of excess NaCl is a decrease in water potential due to stomatal guard cells losing turgor pressure causing disruption of the regulation of opening and closing of stomata. This situation hampers the gas exchange of CO_2 and O_2 and ultimately reduces the rate of photosynthesis. Another impact is the distribution of assimilates, such as carbohydrates and the distribution of various growth hormones (Kotagiri and Viswanatha, 2017). In addition, the excess concentration of NaCl causes the production of ROS (Reactive Oxygen Species) in plants to increase. Excess ROS production causes a series of oxidative damage to chlorophyll, carbohydrates, lipids, DNA and proteins that significantly affect cellular components and cell membranes (Alzahrani et al., 2019). Meanwhile, plants that were given osmopriming treatment showed good tolerance in salinity stress conditions as indicated by the increased height in red amaranth plants. Osmopriming stimulates gene expression to produce various antioxidant compounds that can protect plant cells from oxidative damage, therefore the process of division and expansion of plant cells becomes more optimal even when plants are under stress (Kubala et al., 2015). The presence of antioxidant compounds can reduce oxidative damage by reducing lipid peroxidation and increasing the stability of plant cell membranes. Osmopriming also increases the effectiveness of mobilizing several compounds, such as proteins, amino acids, and dissolved sugars from sources organ to various plant sink tissues during plant exposure to stress. Additionally, osmopriming stimulates plant growth through the mechanism of modification of sucrose metabolizing enzymes. Osmopriming increases the activity of the enzyme sucrose synthase (SS) which causes an increase in plant growth under various stress conditions. Since sucrose is the primary assimilate form transported in plants, sucrose metabolism is thought to be the primary factor in determining the sink strength. Sink strength describes the ability of sink organs to distribute assimilate to support plant growth, development, and maintenance (Kaur et al., 2005).

The increase in plant height under salinity stress in the osmopriming treatment was related to the root system (Figure 2). The plant height and root length significantly decreased as the NaCl concentration increased. According to Menezes et al. (2017), plants experienced osmotic stress due to salinity stress which will decrease their ability to absorb water and nutrients and gradually reduce the rate of photosynthesis and result in decreased of photosynthate. This affects the translocation of photosynthate from source to sink and carbohydrate metabolism in leaves, causing a reduction in overall plant growth (Morales et al., 2012). On the other hand, osmopriming stimulates plant growth through modification of sucrose metabolic enzymes by increasing the activity of sucrose synthase, which acts as a sucrose cleavage enzyme. Sucrose acts as the main carbon link between sources and sinks and is the main form of assimilate transported in plants (Kaur et al., 2005).

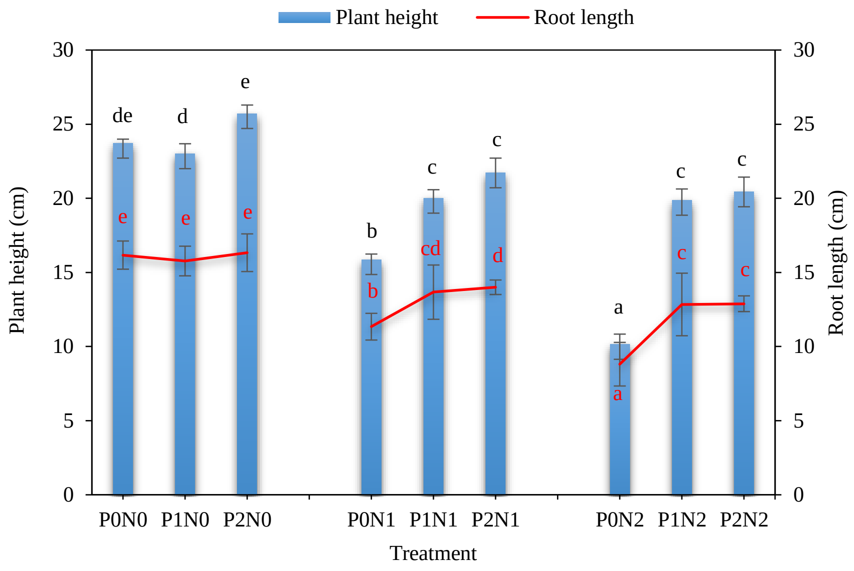

Figure 2. Plant height and root length of red amaranth (*A. tricolor*) aged 5 weeks after osmopriming application with PEG (P0: 0%; P1: 5%; P2: 10%) and NaCl stress (N0: 0 mM; N1: 50 mM; N2: 100 mM). Mean with the same letter in each character has no significant difference based on DMRT α=0.05, n=3.

The increase in root length due to osmopriming was caused by increased metabolic activity at the beginning of the germination period which overall had a valuable effect on the plant growth and development. Osmopriming has a positive effect on several biochemical activities including the breakdown of hydrolytic enzymes, protein and RNA synthesis, and DNA replication. Decomposition of food reserves and synthesis of metabolites for earlier germination of seed priming led to faster sugar availability for embryonic development. Faster sugar availability has a positive impact on plant growth and development, one of which is forming a stronger root system (Hussian et al., 2014). In contrast to the root system is related to the capacity of plants to obtain water and nutrients from the deepest layers of the soil, the growth of plant height shows the capacity of plants to obtain and use resources obtained from the soil (Price et al., 2014). As a result, roots determine growth and development of above-ground plant (Fort et al., 2013).

Salinity stress causes a decrease in several growth parameters. Salinity stress significantly reduced root and shoot dry weight, also root to shoot ratio, especially at 100 mM NaCl concentration (Table 2). These results were in line with the finding of Omami et al. (2006) where shoot growth was reduced and at 50 and 100 mM NaCl the reduction was greater in *A. tricolor* and Accession '83 than in *A. hypochondriacus* and *A. cruentus*. Additionally, Hoang et al. (2019) stated that applying a NaCl concentration of 100 mM to *Amaranthus tricolor* L. caused a 34% decrease in plant height, 40% in leaf number, and 58% in leaf area index. Because of osmotic stress, high NaCl concentrations can induce a decrease in plant water content. This condition correlates with a decrease in the rate of photosynthesis which leads to a reduction in CO_2 fixation, which in turn reduces assimilate production and has a negative impact on the accumulation of plant biomass (Benincasa et al., 2013). A decrease in the dry weight of a plant, both roots and shoots, also indicates an increase in metabolic energy demands and a decrease in carbon availability as a form of plant response to salinity stress (Puvanitha and Mahendran, 2017).

Table 2. Root and shoot dry weight of red amaranth (*A. tricolor*) aged 5 weeks after PEG osmopriming and NaCl stress

Parameters	Osmopriming (% PEG)	NaCl concentration (mM)			Average
		0	50	100	
Root dry weight (g)	0	1.39±0.36^{de}	0.67±0.57^{b}	0.41±0.35^{a}	0.82±0.43^{p}
	5	1.42±0.42^{de}	1.03±0.19^{c}	0.72±0.05^{b}	1.06±0.22^{q}
	10	1.52±0.35^{e}	1.30±0.17^{d}	0.73±0.57^{b}	1.18±0.36^{r}
	Average	1.44±0.38^{z}	1.33±0.31^{y}	0.62±0.32^{x}	
Shoot dry weight (g)	0	7.50±0.34^{bc}	5.70±0.15^{b}	2.61±0.21^{a}	5.27±0.70^{p}
	5	7.87±0.30^{c}	6.82±1.01^{bc}	3.84±2.60^{a}	6.18±1.30^{p}
	10	8.28±0.52^{c}	7.05±0.29^{bc}	6.53±0.24^{bc}	7.29±0.35^{q}
	Average	7.88±0.39^{z}	6.52±0.48^{y}	4.32±1.01^{x}	
Root to shoot ratio (g)	0	0.10±0.02^{ab}	0.09±0.02^{ab}	0.07±0.01^{a}	0.08±0.01^{p}
	5	0.11±0.01^{b}	0.10±0.02^{ab}	0.08±0.02^{ab}	0.09±0.01^{p}
	10	0.11±0.01^{b}	0.15±0.01^{c}	0.08±0.01^{ab}	0.11±0.01^{q}
	Average	0.10±0.01^{y}	0.11±0.01^{y}	0.07±0.01^{x}	

The number followed by the same letter in row and column of each parameter has no significant difference based on DMRT α=0.05, n=5.

Osmopriming increased root dry weight, shoots dry weight, and root to shoot ratio under various conditions (Table 2). The dry weight of roots and shoots, as well as root to shoot ratio, increased as the PEG concentration increased. Under conditions of salinity stress, the application of PEG 10% was able to significantly increase the dry weight of roots and shoots ($p<0.05$) compared to PEG 5% and PEG 0%. The increase in root dry weight, shoots dry weight, and root to shoot ratio in plants due to osmopriming correlated with the increase in root length. These results are in line with those of Latifa and Rachmawati (2020) which found a positive correlation between root length and dry weight of osmopriming *Ipomoea reptans* plants. A well-developed root system increases the reach of the roots in absorbing wider water so that more water and nutrients are available. These conditions increase photosynthetic activity and contribute positively to the accumulation of plant dry weight (Khan et al., 2015). Additionally, osmopriming improves the ability of plants to make osmotic adjustments, enabling them to retain their stomata, photosynthetic activity, and cellular turgor potential (Abid et al., 2017). Osmopriming also increases the rate of metabolic processes involved in germination processes, such as the synthesis of RNA, protein, and DNA during hydration of the embryo. The increase in the amount of nucleic acid caused by RNA synthesis occurs at the time of priming and after priming. In addition, the respiration process and ATP production were higher in seeds that were given primed seeds compared to those that were not given priming treatment, thereby supporting the accumulation of plant dry weight (Parera and Cantliffe, 1994).

Salinity stress results the lower chlorophyll content (Table 3). The decrease in total chlorophyll of salt-stressed plants is a result of either slow synthesis or fast breakdown, indicating that there was a photoprotection mechanism through reducing light absorbance by decreasing chlorophyll contents (Kibria and Hoque, 2019). From the research of Mane et al. (2010) has stated that at concentrations of NaCl 50 mM, the level of chlorophyll a and b was significantly reduced, followed by a decrease in the net photosynthetic rate. Chlorophyll plays an important role in carbon assimilation and maintains photo-synthetic capacity. The decrease in chlorophyll levels occurred due to an increase in chlorophyllase activity and chlorophyll degradation. In order to reduce the amount of ROS produced by chloroplasts, plants limit the amount of chlorophyll in their systems. This is one of their adaptive methods to prevent oxidative stress (Pospíšil, 2016).

The decrease in chlorophyll content at high NaCl concentrations occurs because plants experience a deficiency of magnesium ions. Magnesium functions as a key atom for chlorophyll synthesis which plays a role in the activity of the pigment-protein complex to collect photons in photosystem I (PSI) and photosystem II (PSII) (Chaudhry et al., 2021). Reduced chlorophyll pigment can also be associated with the formation of ROS, such as H_2O_2 which causes lipid peroxidation and chlorophyll damage (Nxele et al., 2017). Decreasing chlorophyll levels due to salinity stress can reduce turgor pressure on leaves, causing water deficits, closing of stomata, and decreased stomatal conductance which ultimately reduces the rate of photosynthesis and inhibits photoassimilate transport (Wulandari et al., 2021). The PEG osmopriming effect increased total chlorophyll levels when compared to controls (Table 3). This is related to the osmopriming effect which can increase the concentration of important ions, one of which is the Mg^{2+} ion which acts as the main mineral constituent in the formation of chlorophyll (Lei et al., 2021). Increasing chlorophyll levels can increase the performance of photosystem II in the photosynthetic process resulting in an increase in the net CO_2 photosynthetic rate which overall has a positive impact on plant yields (Abdelhamid et al., 2019).

Table 3. Total chlorophyll and proline levels of red amaranth (*A. tricolor*) aged 5 weeks after PEG osmopriming and NaCl stress

Parameters	Osmopriming (% PEG)	NaCl concentration (mM)			Average
		0	50	100	
Total chlorophyll (mg/g)	0	3.490±0.10^{c}	3.162±0.05^{b}	2.523±0.02^{a}	3.058±0.06^{p}
	5	3.749±0.07^{cd}	3.474±0.14^{c}	3.569±0.36^{cd}	3.597±0.19^{q}
	10	3.878±0.07^{d}	3.632±0.04^{c}	3.552±0.07^{c}	3.687±0.06^{q}
	Average	3.705±0.08^{c}	3.422±0.08^{b}	3.215±0.15^{a}	
Proline (μmol/g)	0	0.653±0.25^{ab}	0.811±0.09^{bc}	0.957±0.03^{c}	0.807±0.12^{q}
	5	0.626±0.03^{ab}	0.513±0.14^{a}	0.740±0.12^{abc}	0.626±0.10^{p}
	10	0.616±0.10^{ab}	0.739±0.15^{abc}	0.628±0.08^{ab}	0.661±0.11^{p}
	Average	0.632±0.13^{x}	0.688±0.13^{xy}	0.775±0.08^{z}	

The number followed by the same letter in row and column of each parameter has no significant difference based on DMRT α=0.05, n=3.

Increasing the concentration of NaCl enhanced proline levels, while osmopriming with PEG significantly reduced proline levels ($p<0.05$) (Table 3). Proline levels in the osmopriming treatment with 5% and 10% PEG concentrations were lower than 0% PEG. The proline level increased as the increase in NaCl concentration the highest proline level was shown in the 100 mM NaCl concentration treatment. Proline accumulation is related to plant response to external osmotic changes. The increase in proline levels under salinity stress was caused by the breakdown of proline rich proteins (PRPs) (Abdelaziz et al., 2018). Proline acts as an osmoprotectant which is produced to protect cells from the adverse effects of salinity stress (Ahmad et al., 2013). Proline acts as a protective enzyme combats the effects of free radicals, maintains protein structure, as well as nitrogen reserves. (Abid et al., 2020). The decrease in proline levels due to osmopriming treatment showed that the application of osmopriming with PEG could reduce the level of salinity stress in plants. This is related to the accumulation and synthesis of antioxidant enzymes, such as peroxide enzymes (POD) and superoxide dismutase (SOD). Peroxidase enzymes play a role in catalyzing the reduction of H_2O_2, peroxynitrite, and various other organic hydroperoxides that can trigger oxidative stress in plants (Uddin et al., 2021), while SOD is able to catalyze the elimination of ROS by reducing them to O_2 and H_2O_2 so that the levels of free radicals in cells are reduced within the safe range (Das and Roychoudhury, 2014).

Increases in dissolved oxalate levels under salinity stress were accompanied by increases in the density of calcium oxalate crystals (Figure 3). Control plants (P0) showed higher levels of dissolved oxalate and calcium oxalate crystal density compared to plants that treated with 5% (P1) and 10% (P2) of PEG osmopriming treatments. The lowest levels of dissolved oxalate and calcium oxalate crystal density were found in red amaranth which was primed with 10% PEG.

In general, the application of osmopriming reduces the dissolved oxalic acid levels and the density of calcium oxalate crystals (Figure 3). The decrease in oxalate due to osmopriming may be due to an increase in the activity of the enzyme oxalate oxidase, an enzyme involved in the breakdown of oxalate to CO_2 and H_2O_2 (Maksimov et al., 2004). The CO_2 compounds formed can be used as a carbon source in photosynthesis, while H_2O_2 compounds will be degraded into H_2O and O_2 by ROS scavenger compounds (Tooulakou et al., 2016). The reduction in oxalate levels can also happen through the decarboxylase mechanism in addition to the oxidation process. Oxalate decarboxylase catalyzes the decarboxylation of oxalate to produce formic acid and CO_2 (Cai et al., 2018).

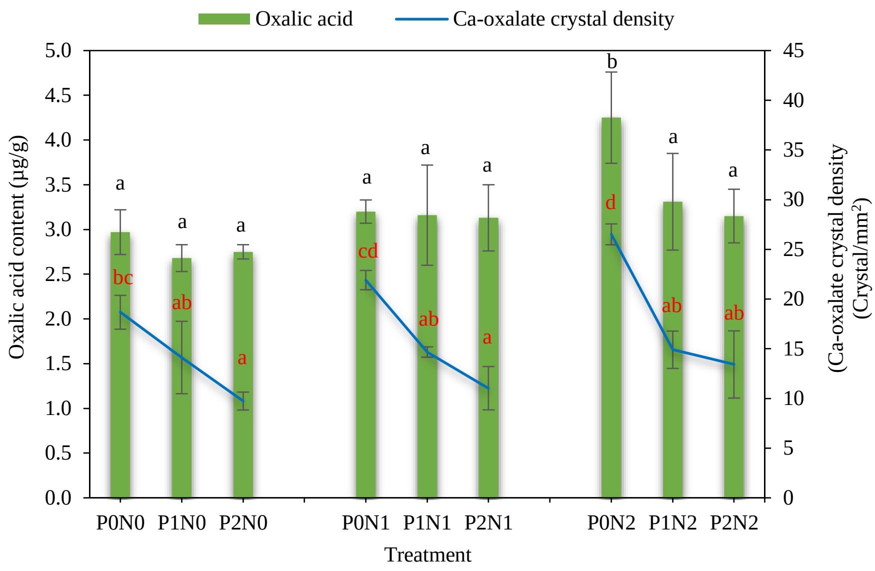

Figure 3. Ca-oxalate crystal density and oxalic acid content of red amaranth (*A. tricolor*) aged 5 weeks after osmopriming application with PEG (P0: 0%; P1: 5%; P2: 10%) and NaCl stress (N0: 0 mM; N1: 50 mM; N2: 100 mM). Mean with the same letter in each character has no significant difference based on DMRT α=0.05, n=3.

Based on research by Wang et al. (2011), plants accumulate various organic acids, such as citric, formic, lactic, acetic, succinic, malic, and oxalic acids under salinity stress. Organic acids are important intermediaries in carbon metabolism in plant cells and play a role in controlling cell physiology, including signaling messengers and absorbing nutrients from the soil. Overall, it can increase plant resistance to a certain extent in less than optimum environmental conditions (Fang et al., 2021). Oxalic acid crystals, particularly calcium oxalate crystals, are formed for the regulation of calcium, metal detoxification, and herbivore defense (Nakata, 2021). Oxalic acid can bind minerals, such as calcium which can trigger the formation of crystals (Xu et al., 2006).

3.3 Root anatomical attributes

Roots are organs that are directly affected by the salinity stress of the growing media. Salinity stress has a negative impact on plant structure and root systems. From Table 4, increasing the concentration of NaCl decreased the thickness of the epidermis, cortex thickness, and diameter of the stele. A NaCl concentration of 100 mM caused the most significant decrease in decreasing epidermal thickness, cortex thickness, and stele diameter. These results are in line with the research of Yildiz et al. (2020) which reported that excess concentration of NaCl in the root area causes the roots to be unable to absorb water and nutrients optimally due to external conditions of low water potential. This condition inhibits the process of cell expansion and growth in the plant root area. It was also reported by Boughalleb et al. (2009) that NaCl stress caused a decrease in root cortex thickness in *Nitraria retusa* L. plants and a reduction in stele and xylem areas in *Medicargo arborea* L. given a NaCl stress of ≥200 mM. The decrease in the cortex thickness is caused by cells that experience a decrease in size under stress conditions. The structure of the epidermis as a protective tissue can also be affected by high concentrations of NaCl. In addition, the toxicity of Na^+ causes inhibition of photosynthate transport to the root area, water dan solute transport, causing a significant decrease in root volume and diameter (Hasanuzzaman et al., 2022). The decrease in the value of each parameter is also due to the negative effect of salinity stress which causes changes in the shape of the cells to become flatter when compared to the control. Excessive NaCl accumulation causes changes in the uptake process of various important elements, such as Al, Ca, Fe, and Mg (Hasan and Miyake, 2017).

Meanwhile, osmopriming with PEG tended to significantly increase epidermal thickness, cortex thickness, and stele diameter ($p<0.05$) under salinity stress conditions, especially osmopriming with 10% PEG concentration. The osmoprimed plants showed better root anatomical structure, both under normal and stressed conditions. This can be related to the early growth and development of seeds. Rehman et al. (2021) reported that osmoprimed seeds had a larger embryonic surface area thereby increasing the availability of nutrients for the developing radicle and increasing the embryo axis during germination compared to control seeds.

An increase in α-amylase and β-amylase activity during the early stages of germination is associated to improved root anatomical structure, which then enhances the availability of energy from starch metabolism and stimulates root growth (Farooq et al., 2019). Priming treatment can also promote root viability and reduce damage to root cells and tissues by maintaining the integrity of root cell membranes.

Table 4. Epidermis thickness, cortex thickness, and stele diameter of red amaranth (*A. tricolor*) aged 5 weeks after PEG osmopriming and NaCl stress

Parameters	Osmopriming (% PEG)	NaCl concentration (mM)			Average
		0	50	100	
Epidermis thickness (μm)	0	33.34±4.18[abc]	31.27±2.76[ab]	26.53±2.01[a]	30.38±2.98[p]
	5	37.02±0.92[bcd]	42.51±6.61[d]	39.64±6.44[cd]	39.72±13.97[q]
	10	41.57±5.38[d]	35.28±3.23[bcd]	30.60±3.77[ab]	35.81±4.13[q]
	Average	37.31±3.50[z]	36.35±4.20[xy]	32.25±4.07[x]	
Cortex thickness (μm)	0	204.67±35.96[bc]	158.63±11.60[ab]	117.26±20.97[a]	160.18±22.84[p]
	5	216.83±15.02[c]	205.68±42.56[bc]	194.82±16.51[bc]	205.77±24.70[q]
	10	220.87±18.24[c]	217.39±15.56[c]	201.55±43.27[bc]	213.27±25.70[q]
	Average	214.12±23.07[y]	192.57±23.24[xy]	171.21±26.91[x]	
Stele diameter (μm)	0	1,376.83±88.32[cd]	984.35±68.53[a]	808.59±174.65[a]	1,056.59±110.50[p]
	5	1,508.15±101.28[de]	1,387.17±54.39[cd]	1,011.47±100.72[ab]	1,302.26±85.46[q]
	10	1,649.29±192.67[e]	1,438.59±200.95[cde]	1,230.39±55.07[bc]	1,439.42±115.17[r]
	Average	1,511.42±127.42[z]	1,270.03±107.95[y]	1,016.81±110.14[x]	

The number followed by the same letter in row and column of each parameter has no significant difference based on DMRT α=0.05, n=5.

Increasing the concentration of NaCl causes changes in the shape of the epidermal cells (Figure 4). Under normal conditions, the epidermis is round and neatly arranged around the cortex, whereas when the plant is under salinity stress, the epidermis will be compressed, thereby the shape is slightly flattened with an irregular arrangement. This correlates with a decrease in the area of epidermal cells (Hasan and Miyake, 2017). The decrease in cortex thickness due to salinity stress is related to a strategy of plant adaptation to shorten the distance of water transport into the stele and xylem so that roots are more effective in transporting water and nutrients. Rosawanti et al. (2015) has reported that the decrease in cortex thickness occurs due to decreased food supply and cortical cell turgidity. The decrease in root conductivity to water and minerals that occurs in response to high NaCl concentrations results in a reduction in the ability of the roots to absorb nutrients. Stele diameter decreases because the stele parenchyma shrinks during salt stress (Hasan and Miyake, 2017). A decrease in xylem and phloem area can also occur, causing obstacles to the transportation of water and important substances which have an impact on structure of the roots (Atabayeva et al., 2013).

P0

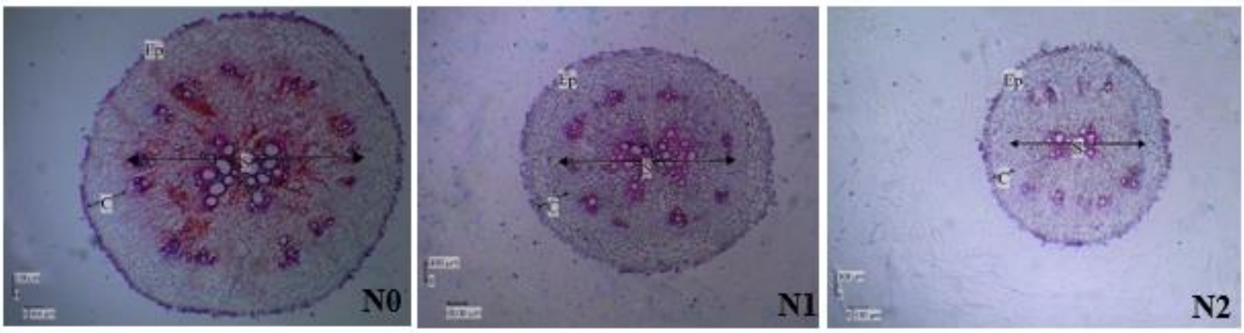

Figure 4. Cross section of red amaranth root (*A. tricolor*) plants aged 5 weeks after osmopriming application with PEG (P0: 0%; P1: 5%; P2: 10%) and NaCl stress (N0: 0 mM; N1: 50 mM; N2: 100 mM). Bar=100 μm. (Note: Ep=Epidermis, C=Cortex, S=Stele)

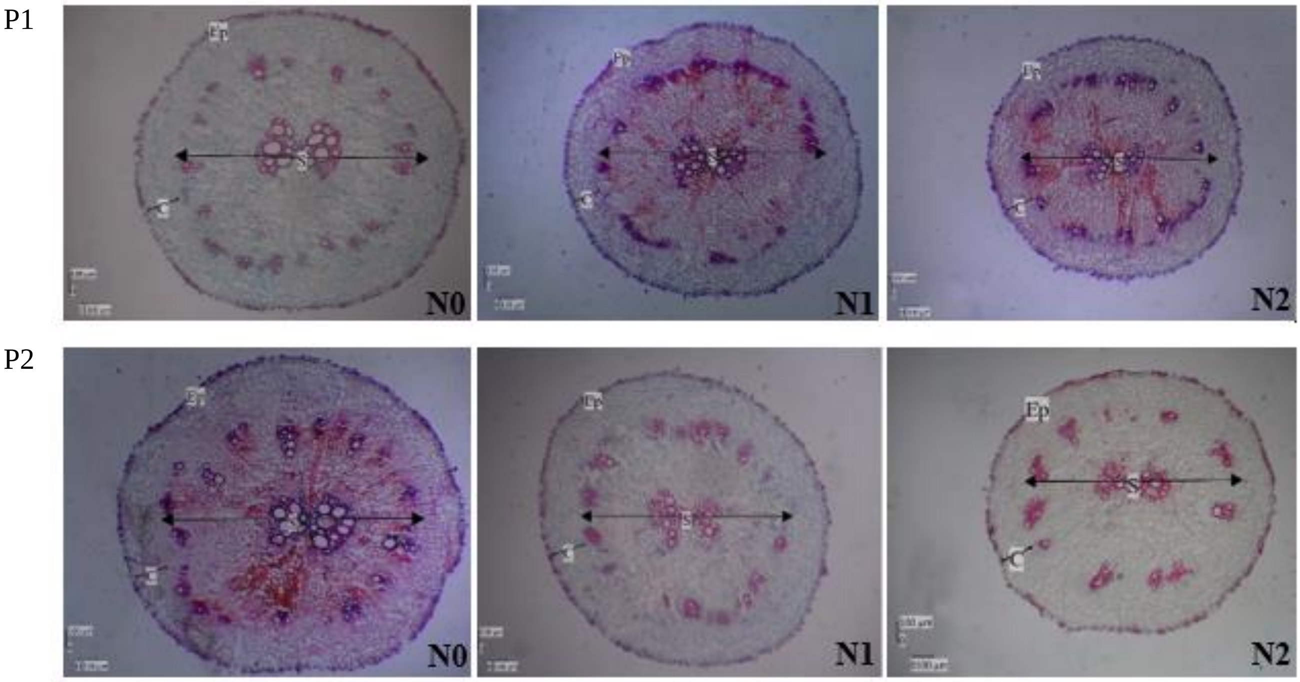

Figure 4. Cross section of red amaranth root (*A. tricolor*) plants aged 5 weeks after osmopriming application with PEG (P0: 0%; P1: 5%; P2: 10%) and NaCl stress (N0: 0 mM; N1: 50 mM; N2: 100 mM). Bar=100 µm. (Note: Ep=Epidermis, C=Cortex, S=Stele) (cont.)

4. CONCLUSION

According to the study's results, priming with PEG 6000 improved germination percentage, mean germination rate, germination rate index, plant height, leaf number, root length, chlorophyll content, and characteristics of red amaranth roots (epidermis thickness, cortex thickness, and stele diameter) under salinity stress conditions, but decreased proline, soluble oxalate, and Ca-oxalate crystal density levels. It indicates that priming with PEG 6000 reduces salinity stress in red amaranth.

ACKNOWLEDGEMENTS

This research was supported by the Research Directory of Universitas Gadjah Mada through Final Project Recognition Programs (RTA). Letter Task No. 3550/UN1.P.III/Dit-Lit/PT.01.05/2022. The authors extend our gratitude to the Faculty of Biology Universitas Gadjah Mada for supporting this research.

REFERENCES

Abdelaziz MN, Xuan TD, Mekawy AMM, Wang H, Khanh TD. Relationship of salinity tolerance to Na^+ exclusion, proline accumulation, and antioxidant enzyme activity in rice seedlings. Agriculture 2018;8(166):1-12.

Abdelhamid MT, El-Masry RR, Saleh DD, Mazhar MF, Ragab R, Oba S, et al. Mechanisms of seed priming involved in salt stress amelioration. In: Hasanuzzaman M, Fotopoulos V, editors. Priming and Pretreatment of Seeds and Seedlings Implication in Plant Stress Tolerance and Enhancing Productivity in Crop Plants. Singapore: Springer; 2019. p. 219-51.

Abid M, Hakeem A, Shao Y, Liu Y, Zahoor R, Fan Y, et al. Seed osmopriming invokes stress memory against post-germinative drought stress in wheat (*Triticum aestivum* L.). Environmental and Experimental Botany 2017;145:12-20.

Abid M, Zhang YJ, Li Z, Bai DF, Zhong YP, Fang JB. Effect of Salt stress on growth, physiological and biochemical characters of four kiwi fruit genotypes. Scientia Horticulturae 2020;271:1-12.

Ahmad P, Azooz MM, Prasad MNV. Ecophysiology and Responses of Plants under Salt Stress. New York: Springer; 2013. p. 16.

Al-Mudaris MA. Notes on various parameters recording the speed of seed germination. Der Tropenlandwirt 1998;99:147-54.

Alleva K, Chara O, Amodeo G. Aquaporins: Another piece in the osmotic puzzle. FEBS Letters 2012;586:2991-9.

Alzahrani SM, Alaraidh IA, Migdadi H, Alghamdi S, Altaf KM, Ahmad P. Physiological, biochemical, and antioxidant properties of two genotypes of *Vicia faba* grown under salinity stress. Pakistan Journal of Botany 2019;51:786-98.

Amalia DR. The Effect of Seed Osmopriming with PEG 6000 (Polyethylene Glycol) on Growth and Morphophysiological of Red Amaranth (*Amaranthus tricolor* L.) in NaCl Stress [dissertation]. Faculty of Biology, Universitas Gadjah Mada; 2022.

Arjmand HS, Sharafi S, Jouyban Z, Akhlaghi S. Effects of osmopriming on seed germination, emergence and field performance. Journal of Applied Science and Agriculture 2014;9(4):1569-73.

Atabayeva S, Nurmahanova A, Minocha S, Ahmetova A, Kenzhebayeva S, Aidosova S, et al. The effect of salinity on growth and anatomical attributes of Barley seedling (*Hordeum* *vulgare* L.). African Journal of Biotechnology 2013; 12(18):2366-77.

Bates LS, Waldran RP, Teare ID. Rapid determination of free proline for water-stress studies. Plant Soil 1973;39:Article No. 205.

Battaglia M, Covarrubias AA. Late embryogenesis abundant (LEA) proteins in legumes. Frontiers in Plant Science 2014;4(190):1-11.

Benincasa P, Pace R, Quinet M, Lutts S. Effect of salinity and priming on seedling growth in Rapeseed (*Brassica napus* var oleifera Del.). Acta Scientiarum Agronomy 2013;35(4):479-86.

Boughalleb F, Denden M, Tiba B. Anatomical changes induced by increasing NaCl salinity in three fodder shrubs, *Nitraria retusa*, *Atriplex halimus*, and *Medicago arborea*. Acta Physiologiae Plantarum 2009;31:947-60.

Boughalleb F, Abdellaoui R, Nbiba N, Mahmoudi M, Neffati M. Effect of NaCl stress on physiological, antioxidant enzymes and anatomical responses of *Astragalus gombiformis*. Biologia 2017;72(12):1454-66.

Cai X, Ge C, Xu C, Wang X, Wang S, Wang Q. Expression analysis of oxalate metabolic pathway genes reveals oxalate regulation patterns in Spinach. Molecules 2018;23(6):Article No. 1286.

Chaudhry AH, Nayab S, Hussain SB, Ali M, Pan Z. Current understandings on magnesium deficiency and future outlooks for sustainable agriculture. International Journal of Molecular Sciences 2021;22(4):1-18.

Chen X, Zhang R, Xing Y, Jiang B, Li B, Xu X. The efficacy of different seed osmopriming agents for promoting sorghum germination under salt stress. PLoS ONE 2021;16(1):1-14.

da Silva JG, Bianchini A, Costa PMC, de Almeida Lobo F, de Ameida JPM, de Moraes MF. Amaranth response to water stress. Journal of Experimental Agricultural International 2019;40(1):1-9.

Das K, Roychoudhury A. Reactive oxygen species (ROS) and response of antioxidants as ROS-scavengers during environmental stress in plants. Frontiers in Environmental Science 2014;2(53):1-13.

Debbarma M, Das SP. Priming of seed: Enhancing growth and development. International Journal of Current Microbiology and Applied Sciences 2017;6(12):2390-6.

Fang S, Hou X, Liang X. Response mechanisms of plants under saline-alkali stress. Frontiers in Plant Science 2021; 12(667458):1-20.

Farooq M, Usman M, Nadeem F. Seed priming in field crops: Potential benefits, adoption and challenges. Crop and Pasture Science 2019;70:731-71.

Fitriani H, Nurlailah D, Rakhimna. Oxalic acid content in spinach. Medical Laboratory Technology Journal 2016;2(2):51-5. (in Indonesian).

Fort F, Jouany C, Cruz P. Root and leaf functional trait relations in Poaceae species: Implications of differing resource-acquisition strategies. Journal of Plant Ecology 2013; 6(3):211-9.

Ghiyasi M, Tajbakhsh M. Osmopriming alleviates drought stress in Soybean (*Glycine max* L.) seeds during germination and early growth stages. Journal of Applied Biological Sciences 2013;7(1):27-32.

Harijati N, Arumingtyas EL, Handayani R. The effect of calcium on the size and density of crystal of calcium oxalate in Porang (*Amorphophallus muelleri* Blume). Jurnal Pembangunan dan Alam Lestari 2011;1:72-139. (in Indonesian)

Hasan R, Miyake H. Salinity stress alters nutrient uptake and causes the damage of root and leaf anatomy in maize. KnE Life Sciences 2017;3(4):219-25.

Hasanuzzaman M, Parvin K, Anee TI, Masud AAC, Nowroz F. Salt stress responses and tolerance in soybean. In: Hasanuzzaman M, Nahar K, editors. Plant Stress Physiology-Perspectives in Agriculture. IntechOpen; 2022. p. 1-37.

Hoang HL, Guzman C, Cadiz N, Dang HT. Physiological and phytochemical responses of red amaranth (*Amaranthus tricolor* L.) and green amaranth (*Amaranthus dubius* L.) to different salinity levels. Agricultural Research Communication Centre 2019;2(9):1-7.

Hussian I, Ahmad R, Farooq M, Rehman A, Amin M, Bakar MA. Seed priming: A tool to invigorate the seeds. Scientia Agriculturae 2014;7(3):122-8.

Kaur S, Gupta AK, Kaur N. Seed priming increase crop yield possibly by modulating enzymes of sucrose metabolism in chickpea. Journal of Agronomy and Crop Science 2005;191:81-7.

Khan AH, Singh AK, Maurya KN, Yadava RK. Effect of different seed priming treatments on germination, growth, biochemical changes, and yield of wheat varieties under sodic soil. International Journal of Science and Research 2015; 4(7):Article No. 14061502 .

Kibria MG, Hoque Md A. A Review on plant responses to soil salinity and amelioration strategies. Open Journal of Soil Science 2019;9:219-31.

Kim SH, Su YL, Jae YH. The effect of seed priming on the germination properties of *Aruncus dioicus*. Seed Science and Technology 2022;50(2):221-6.

Kotagiri D, Kolluru VC. Effect of salinity stress on the morphology and physiology of five different coleus species. Biomedical and Pharmacology Journal 2017;10(4):1639-49.

Kubala S, Garnczarska M, Wojtyla Ł, Clippe A, Kosmala A, Żmieńko A, Quinet M. Deciphering priming-induced improvement of rapeseed (*Brassica napus* L.) germination through an integrated transcriptomic and proteomic approach. Plant Science 2015;231:94-113.

Latifa A, Rachmawati D. The effect of seed osmopriming on growth and morphophysiology of Kangkoong (*Ipomoea reptans* Poir) in drought stress. Jurnal Agronomi Indonesia 2020;48(2):165-72. (in Indonesian).

Lei C, Bagavathiannan M, Wang H, Sharpe S, Meng W, Yu J. Osmopriming with polyethylene glycol (PEG) for abiotic stress tolerance in germinating crop seeds: A Review. Agronomy 2021;11(11):Article No. 2194.

Li G, Meng X, Zhu M, Li Z. Research progress of betalain in response to adverse stresses and evolutionary relationship compared with anthocyanin. Molecules 2019;24(17):Article No. 3078.

Maksimov IV, Surina OB, Sakhabutdinova AR, Troshina NB, Shakirova FM. Changes in the phytohormone levels in wheat calli as affected by salicylic acid and infection with *Tilletia caries*, a bunt pathogenic agent. Plant Physiology 2004; 51:228-33.

Mane AV, Karadge BA, Samant JS. Salinity induced changes in photosynthetic pigments and polyphenols of *Cymbopogon Nardus* (L.) Rendle. Journal of Chemical and Pharmaeutical Research 2010;2:338-47.

Menezes RV, Azevedo Neto ADD, Ribeiro MDO, Cova AMW. Growth and contents of organic and inorganic solutes in amaranth under salt stress. Pesquisa Agropecuária Tropical 2017;47:22-30.

Morales SG, Trejo-Tellez LI, Merino FCG, Caldana C, Espinosa-Victoria D, Cabrera BEH. Growth, photosynthetic activity, and potassium and sodium concentration in rice plants under salt stress. Acta Scientiarum-Agronomy 2012;34(3):317-24.

Nakata P. Plant calcium oxalate crystal formation, function, and its impact on human health. Frontiers in Biology 2012; 7:254-66.

Nxele X, Klein A, Ndimba BK. Drought and salinity stress alters ROS accumulation, water retention, and osmolyte content in sorghum plants. South African Journal of Botany 2017; 108:261-6.

Omami EN, Hammes PS, Robbertse PJ. Differences in salinity tolerance for growth and water-use efficiency in some amaranth (*Amaranthus* spp.) genotypes. New Zealand Journal of Crop and Horticultural Science 2006;34(1):11-22.

Pallaoro DS, Camili EC, Guimarães S, de Figueiredo e Albuquerque MC. Methods for priming maize seeds. Journal of Seed Science 2016;38(2):148-54.

Parera CA, Cantliffe DJ. Pre-sowing seed priming. Horticultural Reviews 1994;16:109-41.

Pospíšil P. Production of reactive oxygen species by photosystem II as a response to light and temperature stress. Frontiers in Plant Science 2016;7:1-11.

Price CA, Wright IJ, Ackerly DD, Niinemets U, Reich PB, Veneklaas EJ. Are leaf functional traits 'invariant' with plant size and what is 'invariance' anyway? Functional Ecology 2014;28:1330-43.

Puvanitha S, Mahendran S. Effect of salinity on plant height, shoot and root dry weight of selected rice cultivars. Scholars Journal of Agriculture and Veterinary Sciences 2017;4(4):126-31.

Rachma TNS, Damanhuri, Saptadi D. Viability and vigor of Cacao (*Theobroma cacao* L.) in some different invigoration media. Plantropica Journal of Agricultural Science 2016;1(2):72-80. (in Indonesian).

Raj AB, Raj SK. Seed priming: An approach towards agricultural sustainability. Journal of Applied and Natural Science 2019;11:227-34.

Rehman A, Nadeem F, Farooq M. Role of seed priming in root development and crop production. In: Rengel Z, Djalovic I, editors. The Root Systems in Sustainable Agricultural Intensification. United States: John Wiley and Sons Ltd.; 2021. p. 221-5.

Rosawanti P, Ghulamahdi M, Khumaida N. Anatomical and physiological responses of soybean root to drought stress. Jurnal Agronomi Indonesia 2015;43(3):186-92. (in Indonesian).

Ruzin SE. Plant Microtechnique and Microscopy. New York: Oxford University Press; 1999.

Tooulakou G, Giannopoulos A, Nikolopoulos D, Bresta P, Dotsika E, Orkoula MG, et al. Alarm photosynthesis: Calcium oxalate crystals as an internal CO_2 source in plants. Plant Physiology 2016;171:2577-85.

Uddin S, Nafees M. Effect of seed priming on growth and performance of *Vigna radiata* L. under induced drought stress. Journal of Agriculture and Food Research 2021;4:1-8.

Wang X, Geng S, Ri YJ, Cao D, Liu J, Shi D, et al. Physiological responses and adaptive strategies of tomato plants to salt and alkali stresses. Scientia Horticulturae 2011;130:248-55.

Wulandari Y, Triadiati T, Sulistyaningsih Y, Suprayogi A, Rahminiwati M. Salinity stress affects growth and physiology of mulberry (*Morus* sp.). IOP Conference Series: Earth and Environmental Science 2021;948:1-11.

Xu HW, Ji XM, He ZH, Shi WP, Zhu GH, Niu JK, et al. Oxalate accumulation and regulation is independent of glycolate oxidase in rice leaves. Journal of Experimental Botany 2006;57(9):1899-908.

Yildiz M, Poyraz I, Caudar A, Ozgen Y, Beyaz R. Plant response to salt stress. In: Abdurakhmonov IY, editor. Plant Breeding: Current and Future Views. IntechOpen; 2020. p. 1-19.

Yoshida S, Forno DA, Cock JH, Gomez KA. Laboratory Manual for Physiological Studies of Rice. 3rd ed. Philippines: The International Rice Research Institute. 1976.

Distribution and Characteristics of Microplastics in Nhue - Day River Basin, Vietnam

Huu Thang Nguyen[1,2,*], Thi Ha Nguyen[2], To Thi Hien[3,4], and Minh Trang Hoang[2]

[1]*Centre for Environmental Monitoring, Vietnam Environment Administration, Ministry of Natural Resources and Environment, Hanoi, Vietnam*
[2]*Faculty of Environmental Sciences, University of Science, Vietnam National University, Hanoi, Vietnam*
[3]*Faculty of Environment, University of Science, Vietnam National University, Ho Chi Minh City, Vietnam*
[4]*Vietnam National University, Ho Chi Minh City, Vietnam*

ARTICLE INFO

Received: 11 Nov 2022
Received in revised: 17 Feb 2023
Accepted: 22 Feb 2023
Published online: 11 Apr 2023
DOI: 10.32526/ennrj/21/202200244

Keywords:
Distribution/ Microplastics/ Nhue - Day River Basin/ Particle size

*** Corresponding author:**
E-mail: thangqtmt@gmail.com

ABSTRACT

The prevalence of microplastics (MPs) in the environment has had a significant impact on ecosystems and posed a major threat to human health. This study investigated the distribution and characteristics of MPs in the Nhue - Day River basin in Vietnam, which is a critical source of biodiversity and used to support the economic growth of about 12 million people. The effect of seasonal variation and anthropogenic activities on the MP abundance was assessed. The findings revealed that the MPs abundance was significant in this study area. The average abundance of MPs in the dry season (754 items/m^3) was insignificantly higher than that in the rainy season (706 items/m^3) with n=9. The range in the abundance of MPs in the dry and rainy seasons was 49-2,827 and 400-1,133 items/m^3, respectively. Microplastics in fiber forms were dominant in both seasons. The majority of the collected MPs were in the 0.5-2.0 mm size range, varying from 71% to 100% of the total MPs depend on sampling point. The total percentage of MPs size 0.3-0.5 mm in the dry season was 56.97% compared to 119.85% in the rainy season, indicating that the MPs were broken into smaller pieces due to UV exposure and weather conditions. Colored items occupied the majority of the MPs. This study can be used to gain a better knowledge of MP pollution in Vietnam's river water.

1. INTRODUCTION

Due to its potential harm to aquatic ecosystems and human health, MP contamination has recently become a much more concerned issue on a global scale (Wanner, 2021). Microplastics (MPs) are defined as plastic particles with a diameter of less than 5.0 mm, comprising primary MPs discharged during industrial production and secondary MPs produced during the breakdown of more substantial plastic products (De Falco et al., 2019). Because of the ability to absorb toxic chemicals or pathogens that can then be transferred to living organisms through the food chain, MPs are considered as a contaminant (Baldwin et al., 2020; Dai et al., 2022; Sulistyowati et al., 2022). Wang et al. (2018a) examined the chemical distribution and adsorption behavior of MPs. In China, Greece, and Portugal, polychlorinated biphenyl (PCB) congeners, polycyclic aromatic hydrocarbon isomers, hexa-chlorocyclohexane isomers, and dichloro-diphenyl-trichloroethane metabolites were discovered in plastic pellets. Chemical PCB congeners are more concentrated on black or aged MPs than on colored or white MPs (Beckingham and Ghosh, 2017). It has been reported that MPs can travel long distances in the water flow because of their small size and their ability to remain in the environment for long periods of time due to their resistance to degradation. Microplastics have recently been discovered and traced in a variety of environments, including drinking water (Schymanski et al., 2018), the atmosphere (Liu et al., 2019), soil (Nizzetto et al., 2016), food (Vitali et al., 2022), and even human bodies (Wright and Kelly, 2017). Therefore, it is critical to understand the occurrence, abundance, behavior, and fate of MPs in the natural environment.

Numerous studies on MPs in the marine environment (water, sediment, and biota) have been conducted. However, it remains limited for freshwater

Citation: Nguyen HT, Nguyen TH, Hien TT, Hoang MT. Distribution and characteristics of microplastics in Nhue - Day River Basin, Vietnam. Environ. Nat. Resour. J. 2023;21(3):245-255. (https://doi.org/10.32526/ennrj/21/202200244)

environments, particularly in Asia, where significant plastic pollution has been observed because of rapid economic and demographic growth, as well as urbanization development (Wang et al., 2018b). Furthermore, it has been demonstrated that rivers are not only important sinks of MPs in urban areas, but they are also one of the major sources of MPs in the oceans (Eerkes-Medrano et al., 2015). The Changjiang River in China is estimated to transfer 16-20 trillion MPs weighing 537.6-905.9 tons to the ocean through the surface water layer each year (Zhao et al., 2019); the Saigon River in Vietnam annually transports 115-164×10^{12} items of synthetic fibers to the sea (Strady et al., 2020). As a result, it is obvious that knowledge of MP pollution in urban freshwater bodies is essential for establishing efficient plastic waste management methods in both metropolitan regions and the oceans. Nonetheless, evidence of MP pollution in inland freshwater bodies is more restricted than in marine areas (Eerkes-Medrano et al., 2015).

Vietnam is one of the top 20 countries in terms of plastic waste input into the ocean, with approximately 1.8 million tons of plastic waste discharged each year, which is 10% more than the global average (Jambeck et al., 2015). The abundance of MP in aquatic systems in Vietnam has been reported in previous studies with the MP abundance ranging from 0.35 to 2,522 items/m^3 (Chau et al., 2020; Tran-Nguyen et al., 2022). In the Red River, the concentration of MP was 2.3 items/m^3, the lowest level among the investigated areas, while the highest concentrations were measured in urban and smaller rivers: 93.7 items/m^3 in the Nhue River and 2,522 items/m^3 in the To Lich River (Strady et al., 2021). In Danang City, the Phu Loc Channel it was reported as a MP pollution hotspot with a MP concentration of 1,482.0±1,060.4 items/m^3 in water (Tran-Nguyen et al., 2022). In the south of Vietnam, the Saigon River basin has high concentrations of fibers and fragments, 172,000 to 519,000 items/m^3 and 10 to 223 items/m^3, respectively (Lahens et al., 2018).

The Nhue - Day River flow through Hanoi and four other provinces (Hoa Binh, Ha Nam, Ninh Binh, and Nam Dinh) before joining at Phu Ly City in Ha Nam Province. This river basin, which has a length of 236 km and an area of around 7,655 km^2, is a source of critical biodiversity and is used to support the economic growth of about 12 million people. The effluents from large residential areas like Hanoi, which has over 4,000 industrial facilities, about 500 traditional artisan villages, and roughly 1,400 hospitals and healthcare facilities, have a negative impact on the water quality of these rivers (Le et al., 2022). This river system provides most of the freshwater for agriculture and aquaculture in the region. The presence of MPs in this river system has been reported by Strady (Strady et al., 2021). However, information on MP pollution in these systems is still rather limited to exploring the source of MPs in the investigated area. Therefore, investigating MP pollution in this river basin is very important for a comprehensive understanding of MP content situation to provide information to trace the sources and pathways of MPs in the aquatic environment. In this study, the MPs in surface water along the Nhue - Day River Basin was investigated with an aim to explore the effects of seasonal variation and anthropogenic activities on MP contamination and characteristics in the Nhue - Day River basin. Understanding the presence of MPs in river water will help to develop workable solutions and strategies to reduce the conflicting effects of MP contamination on the ecosystem and public health. The findings from this study can be used as trustworthy support for future research on the effects of MP pollution on human health in Northern Vietnam.

2. METHODOLOGY

2.1 Sampling points and sample collection

The Nhue - Day River Basins are one of the ten major river systems in Vietnam. It includes two large rivers: Nhue - Day River. The Nhue River has a length of 74 km, taking water from the Red River and flows into the Day River at Ha Nam Province. The Day River has a length of 237 km, also taking water from the Red River and flows into East Sea. Surface water samples were collected at nine points along the Nhue - Day River Basin, including four points on Nhue River and five points on Day River. The samples were collected in March 2021 represented for dry season samples and November 2021 for the rainy season in the North Central region. Figure 1 and Table 1 describe the details of the nine sampling points.

2.2 Sample preparation

River water samples were collected using a Manta mesh (mesh size 300 µm, mouth width 15×30 cm) fitted with a General Oceanic flowmeter (ensuring the mouth of the net was completely under the surface of the water) (Dris et al., 2018) for 120-240 seconds. Depending on the conditions at the sampling location, the two below methods were applied:

- At monitoring points with large currents and wide riverbeds, samples were collected in the middle of the stream from a boat. Sampling time and boat speed are calculated to ensure that the sample volume in the net is at least 1 m^3.

- For the point with low flow and narrow riverbed area that cannot be netted, a 100-200 L sample was collected into a bucket and slowly pour into the sampling device or through a sieve with 0.3 mm mesh size.

- The sampling device, after being taken from the river, was washed with clean water from the outside to wash away the dirt as well as the MPs (if any) on the mesh wall and move to the cup at the bottom of the device. This process is repeated several times until the sampler is clean of MPs. After that, water samples were transferred to 100 mL glass vials, kept refrigerated and dark before being transported to the laboratory. Then, the water sample was refrigerated at 4°C in the field for immediate analysis or stored in the refrigerator at 20°C for further analysis (stored time within 15-20 days).

Map of Microplastic Monitoring Points
in the Nhue - Day River Basin

Figure 1. Microplastic sampling points in Nhue - Day River Basin

Table 1. The basic information of surface water sampling points in Nhue - Day River Basin

No	Province/city	Sample symbol	River name	Coordinate		Sampling point description
				X	Y	
1	Hanoi	ND1	Nhue River	580499.178	2332119.309	Upstream monitoring point of Nhue River to get water from the Red River
2	Hanoi	ND2	Nhue River	583181.017	2315161.439	Area receiving domestic wastewater in Cau Giay District and surrounding areas
3	Hanoi	ND3	Day River	574060.905	2300545.244	Evaluation of MP pollution at Hanoi City
4	Hanoi	ND4	Nhue River	587598.865	2298950.196	Assessment of MP pollution in Nhue River

Table 1. The basic information of surface water sampling points in Nhue - Day River Basin (cont.)

No	Province/city	Sample symbol	River name	Coordinate		Sampling point description
				X	Y	
5	Hanoi	ND5	Day River	578284.590	2287467.761	Assessment of MP pollution in Day River
6	Ha Nam	ND6	Nhue River	594284.270	2282200.214	Evaluation of MP pollution at Hanoi City
7	Ha Nam	ND7	Nhue - Day River Basin	596439.229	2269667.671	Assessment of MP pollution for Nhue - Day River in Ha Nam Province
8	Ninh Binh	ND8	Nhue - Day River Basin	597954.548	2247725.092	Assessment of MP pollution for Nhue - Day River at Ninh Binh Province
9	Nam Dinh	ND9	Nhue - Day River Basin	615060.390	2239898.168	Assessment of MP pollution for Nhue - Day River Basin at Nam Dinh Province

2.3 Sample analysis

A volume of 100 mL of water sample was put into a 500-mL glass beaker and dried at 40°C for 24 to 48 h. Then, 50-70 mL of 30% H_2O_2 and $FeSO_4$ 0.05 M were added to dissolve the organic matters, until the appearance of the solution was clear. After that, the solution was redried to remove water. The carbonate compounds in samples were eliminated by adding 10-20 mL of HCl 1 M solution to the glass beaker and shaking well until no bubbling before letting it dry at 40°C for 12 h.

After the drying step, a volume of 30 mL of $ZnCl_2$ solution d=1.6 g/mL was slowly added to the beaker and mixed well, then the whole mixture was transferred into 50 mL PE centrifuge plastic tubes. The mixture in the canister was centrifuged at a rotational speed of 3,000 Relative Centrifugal Force (RCF) per min to separate MPs and other solids remaining in the water. Microplastics with light density float on the surface of the $ZnCl_2$ solution. The solution at the top of the test tube will be filtered to separate the MP particles from the remaining solid layer. The $ZnCl_2$ solution containing the supernatant MPs was collected by the overflow method, placed in a 500 mL Nalgene filter cup, and then filter through grid paper with 47 mm diameter, 0.45 µm filter pore size, each piece of paper has 100 cells with the size of each cell 3.1×3.1 mm. With the smallest MP particle size of 0.35 mm, filter paper with the above pore size can be used. Filter paper was gently removed and stored in aluminum foil bags, dried at 45°C for about six hours before determining the quantity and composition of MPs.

The number of MPs in dried samples were determined using a Euromex stereo microscope, with a maximum focal length of 40x, and a DC5.0 Stereo Camera with ImageFocus 4 English Version software to determine the size, shape, color, and quantity of suspected MPs.

3. RESULTS AND DISCUSSION

3.1 Microplastic abundance

In this study, MPs in surface water were detected at each sampling and in both dry and rainy seasons. The results shown in Figure 2 and Figure 3 indicated that the distribution and abundance of MP in Nhue - Day River system was significantly affected by season and geographical location. In the dry season, the concentration of MPs in surface water ranged from 49 to 2,827 items/m^3, with an average abundance of 754 items/m^3. The sampling area with the highest abundance of MPs was the ND3. The ND3 point is at the confluence of the Day River, the section of Hoa Vien Bridge, and near ND3 market, Ung Hoa District, Hanoi. This is a high population density area. Moreover, in recent years, various kinds of trading activities along the river in ND3 point have produced untreated wastes and the survey area pollution has been quite serious. In addition, various kinds of small, scattered enterprises and industrial activities such as wool and fabric factories, garment factories, and some manufacturers and traders of plastic products have been recorded as sources of MP discharge in the area. Point ND6 was also reported to have high levels of MPs in surface water (1,423 items/m^3). Previous studies connected the presence of MPs in the aquatic environment to the effects of human activity (Zhao et al., 2020). It explained the reason for the highest MP concentration at ND6 is because it runs through a high population density area and industrial area related to engineering, electronics, assembly, food production and some light industry. Additionally, the close distance between ND6 and rubbish dumping indicated a high MP concentration at this point. The fact that intense economic activities, such as industrial discharge and land use, can cause poor water quality to some extent has raised alarm. The idea that MP abundance is driven by economic activity is indirectly supported by the potential positive association between poor water quality and high MP content.

In the rainy season, the abundance of MP in Nhue - Day River ranged from 400 to 1,133 items/m^3, with an average abundance of 706.67 items/m^3 which was lower than that in the dry season. It is clear that the MPs are distributed more evenly along the river basin due to the influence of the river flow in rainy season instead of concentrating at some points in dry season. This phenomenon indicates that the abundance of MPs was gradually diluted when the water volume increased. The two survey points with the largest concentration of MPs were recorded at ND2 and ND6 with the corresponding value of 1,133 and 1,066 items/m^3, respectively. This difference in distribution pattern of MPs may be due to hydraulic and flow conditions that were significantly affected by season factor. In the rainy season, tributaries, and overflows in residential areas on both sides of the river are formed. This may partly explain why in the rainy season the number of MPs at the lower limit increases and the recorded upper limit decreases. The increase in hydrology is also a factor governing the distribution of these plastics.

(a)

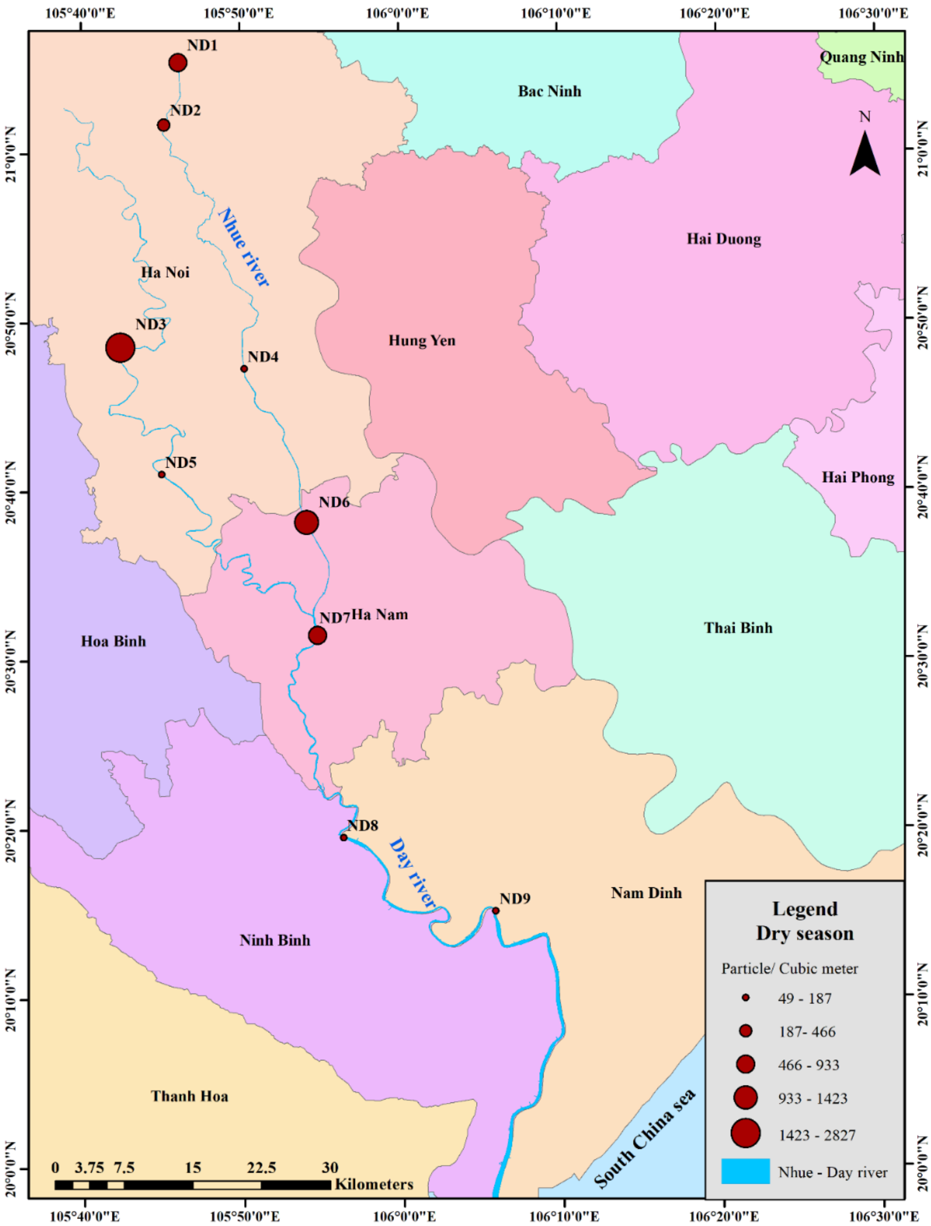

Figure 2. Distributions of MP contamination in surface water of Nhue - Day River Basin in dry season (a) and rainy season (b)

(b)

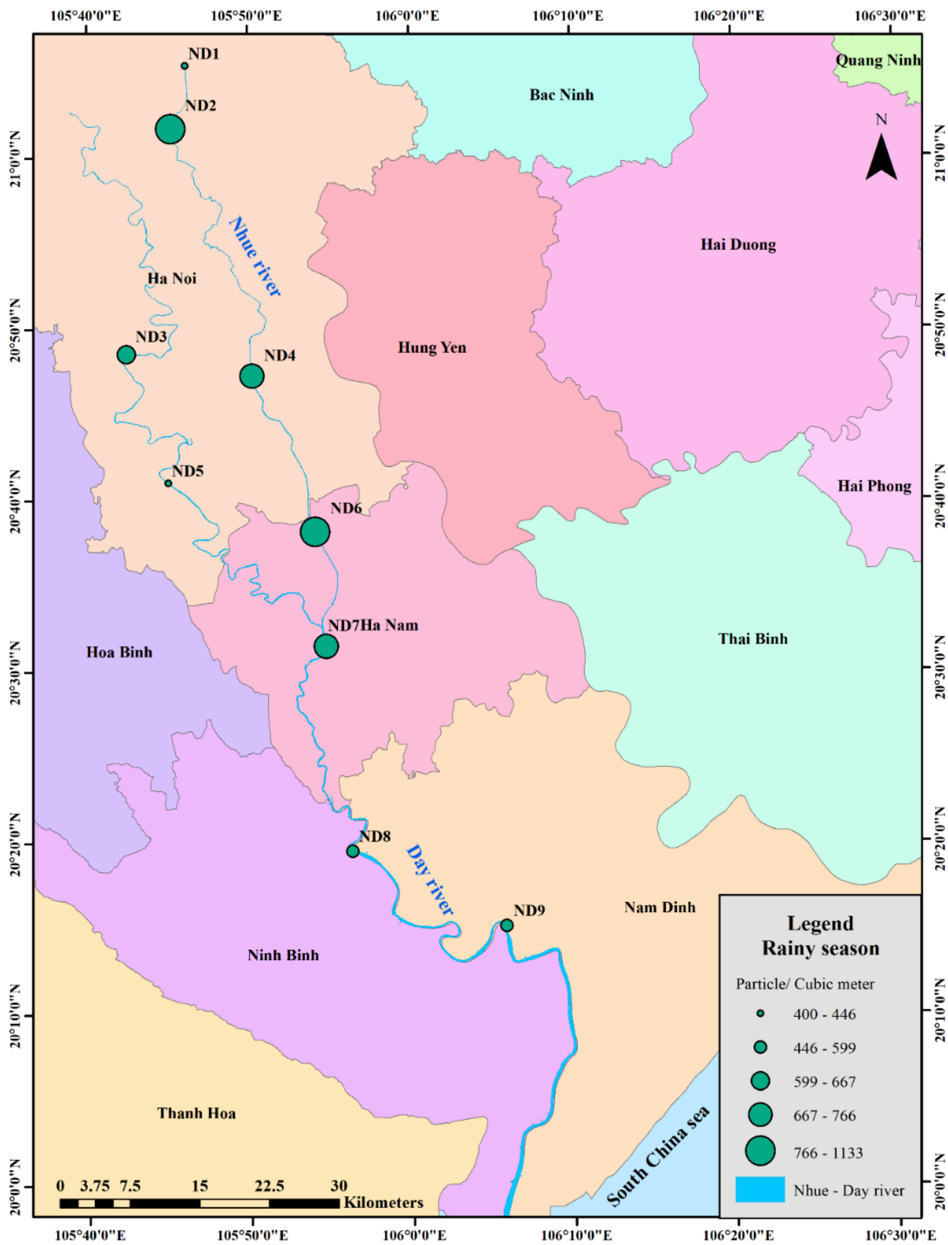

Figure 2. Distributions of MP contamination in surface water of Nhue - Day River Basin in dry season (a) and rainy season (b) (cont.)

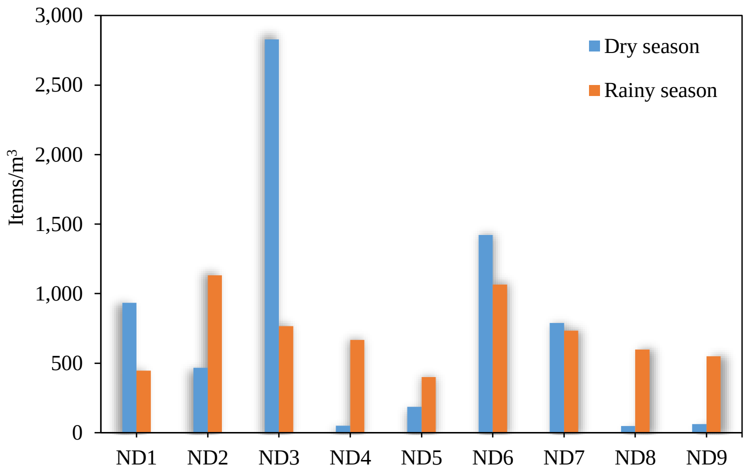

Figure 3. Microplastics abundance in surface water of Nhue - Day River Basin during dry and rainy season

The abundance of MPs in the surface water from urban areas in other parts of Vietnam and over the world is displayed in Table 2. The results in this study were compared with those in other rivers in Vietnam such as the Red River, Han River (which runs through Da Nang), and Dong Nai River. It is clear that, except for the To Lich River (2,522 items/m^3; (Strady et al., 2021)), the MPs concentration in the surface waters of the Nhue - Day River is in high levels. In particular, the average value of microplastics recorded in a m^3 of surface water in the study area is 327 times greater than the number of microplastics recorded in the Red River, nearly 280 times greater than the number of microplastics received from Han River water, and more than 193 times greater than the number of microplastics received from Dong Nai River. Especially, compared to Nhue - Day River itself in 2020, there is a significant increase in the microplastics abundance in 2021 (sample collected time of this study) alarming the polluted issue of this area.

The Nhue - Day River Basin has a greater MP concentration in waters than some rivers in Asian countries, such as Duong Tu River of China (8.6 items/m^3) and Surabaya River in Indonesia (1.47-43.11 items/m^3). The same situation happened when comparing with Rhine River in Europe, and Los Angeles River or San Gabriel River in the USA, where barely a few items per m^3 were found.

Table 2. Distribution of MPs in surface water in Vietnam and some countries in the world

Location	Size (mm)	Average abundance (items/m^3)	Abundant range (items/m^3)	References
Vietnam				
Nhue - Day River, rainy season	0.3-5.0	706	400-1,133	This study
Nhue - Day River, dry season	0.3-5.0	754	49-2,827	This study
Red River	0.3-5.0	2.3		Strady et al. (2021)
Han River	0.3-5.0	2.7		Strady et al. (2021)
Dong Nai River	0.3-5.0	3.9		Strady et al. (2021)
Nhue River (2020)	0.3-5.0	93.7		Strady et al. (2021)
To Lich River (2020)	0.3-5.0	2,522		Strady et al. (2021)
Saigon River	<5		22,812-251,000	Strady et al. (2020)
Other countries				
Hoang Ha River, China, dry season	<0.5	930	623-1,392	Han et al. (2020)
Maozhou River, China	0.001-5.000		4,000- 25,500	Wu et al. (2020)
Duong Tu River, China	0.3-5.0	8.6		Zhao et al. (2014)
Surabaya River, Indonesia	0.3-5.0		1.47-43.11	Lestari et al. (2020)
Han River, Korea	0.1-5.0		0-42.9	Park et al. (2020)
Danube River, Austia	0.5-5.0	17		Lechner et al. (2014)
Ravi River, Pakistan, rainy season	0.3-5.0	768		Aslam et al. (2022)
Ravi River, Pakistan, dry season	0.3-5.0	1,324		Aslam et al. (2022)
Rhine River, Europe	0.3-5.0	3.9		Mani et al. (2015)
Seine River, France	0.1-5.0	108		Dris et al. (2015)
Marne River, France	<5	398		Dris et al. (2018)
Los Angeles River, USA	0.3-5.0	13.7		Moore et al. (2005)
San Gabriel River, USA	0.3-5.0	0.6		Moore et al. (2005)
Hudson River, USA	0.1-5.0	0.98		Miller et al. (2017)
Ottawa River, Canada	0.1-5.0	0.2		Vermaire et al. (2017)

3.2 Morphology of MPs

3.2.1 Shape distribution

Figures 4 and 5 show the composition of MP pollution based on different types. In both seasons, fibers identified as the most dominant type of MPs collected from the sampling points was similar to those of other studies on freshwater MP (Koelmans et al., 2019). Fibers come from a variety of sources, such as washing clothes, using and wearing plastic objects, and the waste plastic produced during industrial production (Browne et al., 2011). Furthermore, fiber-like MPs are likely to be formed from huge blocks of plastic during migration, which are subject to wind, water flow, temperature, and abrasion by hard things

(Peters and Bratton, 2016). Indeed, in both seasons, this form of plastic produced much more fibrous MPs than other types of MPs. Fibers were 93.26% of all MP types, while fragments were 6.47% in dry season. In rainy season, there was a light increase in the number of fragmented MP. Fragment MPs have a higher density than fibers, some types of density can increase to 1.2 g/L. In the rainy season the river water discharge increases causing a high-water velocity which facilitated the transportation of fragment in the flow. Therefore, the concentration of MP in fragment shape in dry season was higher than that in rainy season.

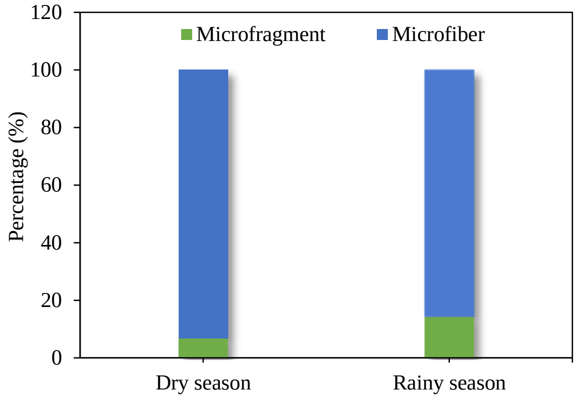

Figure 4. Shape distribution and pictures of MPs in surface water of Nhue - Day River Basin during dry and rainy season

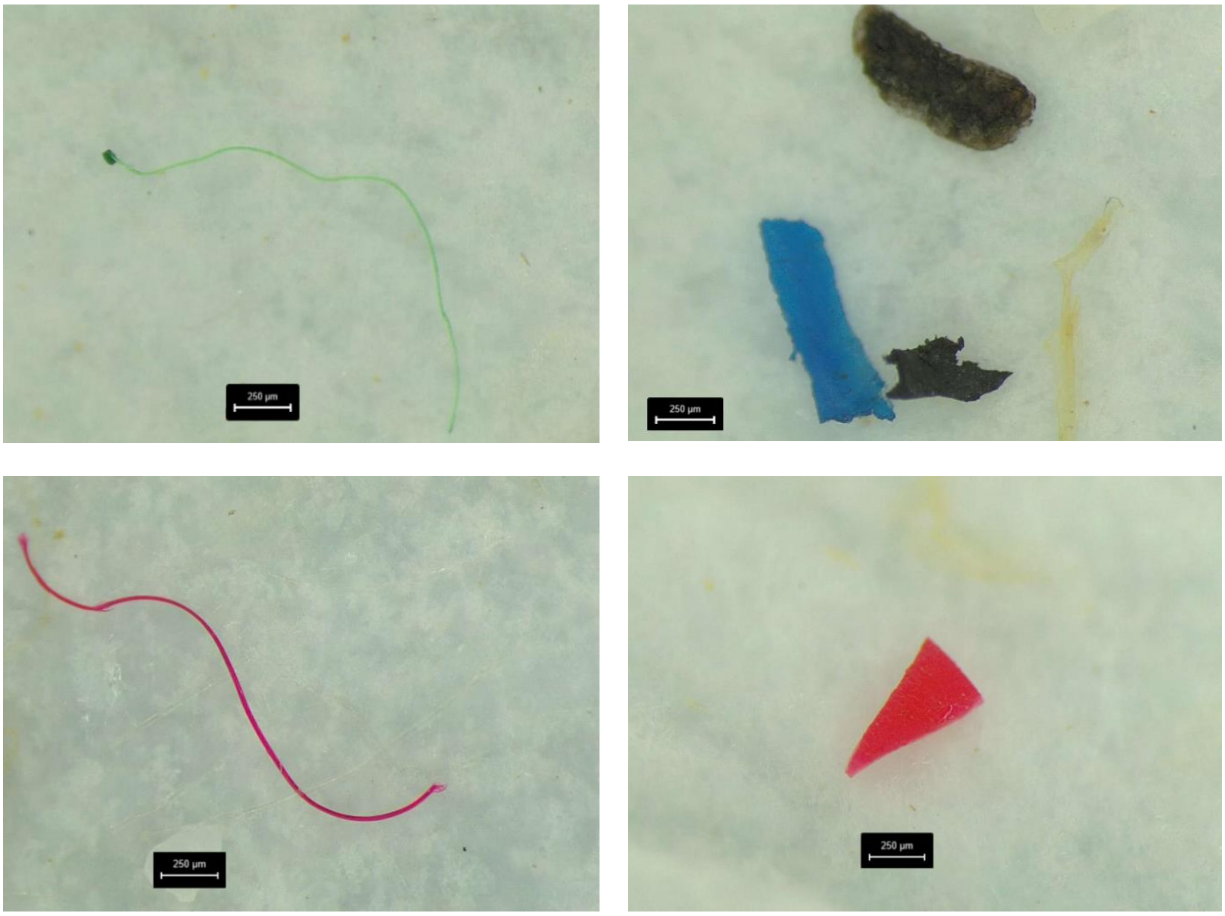

Figure 5. Photomicrographs of the MPs found in Nhue - Day River water

3.2.2 Colors distribution

Microplastics with different colors are presented in Figure 6. In dry season, black was seen to be the dominant color (33.6%), followed by blue (31.6%) and red (18.5%). Other pigmented particles, such as green (4.46%), yellow (1.53%), grey (0.03%), occurred only at low proportions. The colored particles are more likely to be mistaken for food by aquatic biota because they resemble low-trophic-level organisms (Browne et al., 2008). Furthermore, green MPs with irregular forms may be formed because of the breakdown of single-use plastic products containing colorants (Wang et al., 2018b). In contrast, in rainy season, white was the most common MP color with a percentage reaching 49.6%, followed by blue (31.6%). In both seasons, grey is the least common one. This result agreed with number of previous studies which high proportion of colorless MPs (transparent and white) was found (Phuong et al., 2018; Lestari et al., 2020; Wu et al., 2020). In addition, it was reported that the reason may be caused by the overflow of plastic manufacture from nearby companies, as well as fading during significant weathering processes such as wave action by tidal currents.

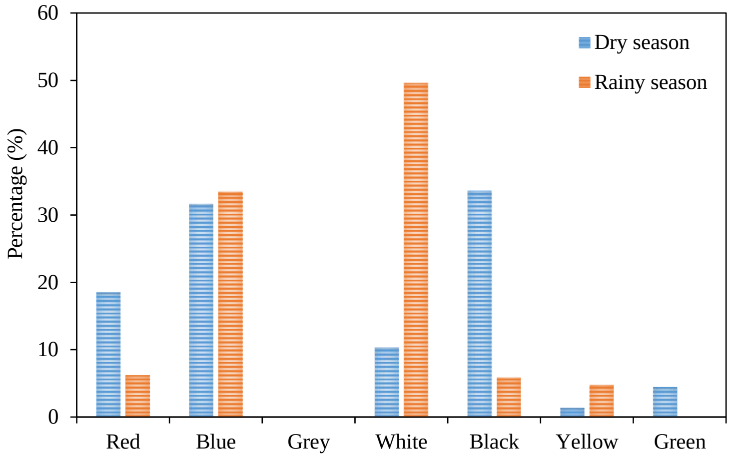

Figure 6. Colors distribution of MPs in surface water of Nhue - Day River Basin during dry and rainy season

3.2.3 Size distribution

Figure 7 shows the size distribution of MPs in both dry season (a) and rainy season (b). The microplastics tend to be unevenly concentrated in sizes as MPs with the size of 0.5-2.0 mm accounted for 71% to 100% in both seasons. In the dry season, the recorded MPs size values ranged from 0.301 mm to 4.71 mm. While in the rainy season, those numbers were 0.306 mm and 4.453 mm.

Even though there were no significant differences in the size range and the size majority of the MPs between two seasons, the sum of the percentage of MPs size 0.3-0.5 mm from all nine points in the dry season is smaller than in the rainy season, 56.97% compared to 119.85%, respectively. This can be explained by the fact that MPs in the dry season are subjected to adverse weather conditions with prolonged high temperatures, as well as the influence of UV, causing these MPs to break into smaller pieces. In the rainy season, these particles are transported everywhere by the water flow, so the encountering of small-sized pieces of MPs is more frequent.

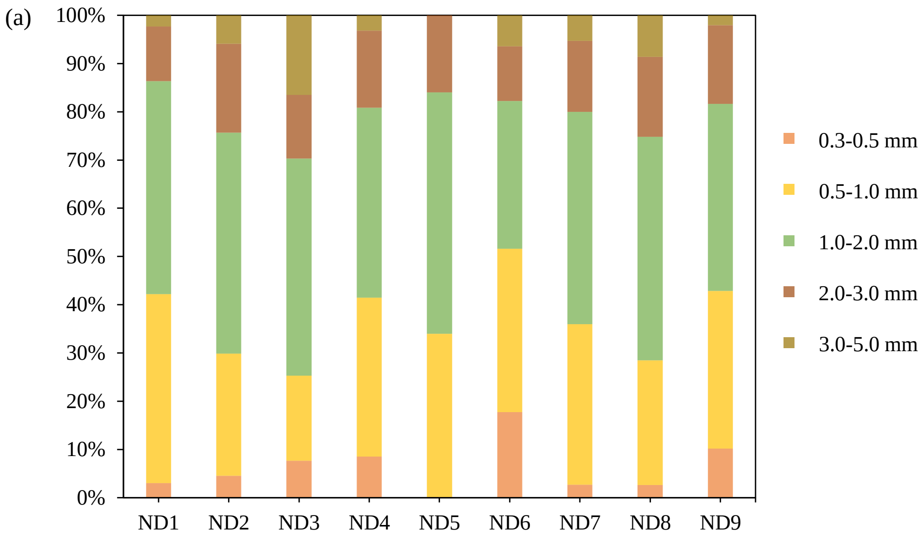

Figure 7. Size distribution of MPs in surface water of Nhue - Day River Basin during dry (a) and rainy (b) seasons

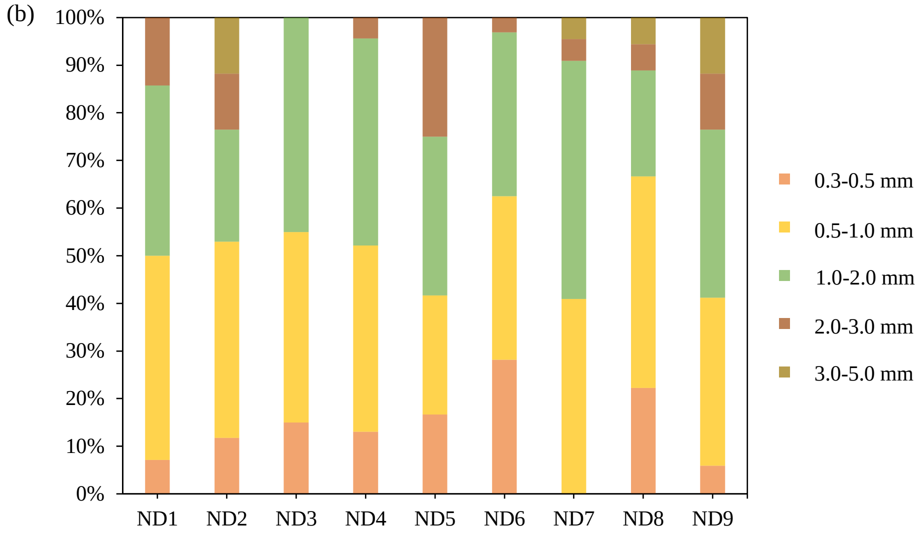

Figure 7. Size distribution of MPs in surface water of Nhue - Day River Basin during dry (a) and rainy (b) seasons (cont.)

4. CONCLUSION

In this study, the microplastic (MP) contamination, and MP characteristics in surface water along the Nhue - Day River Basin were investigated. The results showed the presence of MPs at different levels in water samples of all sampling points along the study area. Although there is no significant difference in abundance of MP between dry season and rainy season, the MPs were distributed more evenly along the river basin in the rainy season due to the influence of the river flow instead of concentrating at some specific points as in the dry season. In terms of shape, fiber was the dominant form of MP in both seasons.

The majority of the collected MPs were in the 0.5-2.0 mm size range, varying from 71% to 100% of the total MPs depending on the sampling point. The sum of the percentage of MPs size 0.3-0.5 mm from all nine sample points in the dry season was 56.97%, compared to 119.85% in the rainy season, indicating that the MPs were broken into smaller pieces due to UV exposing and weather condition. The results allow us to conclude that the Nhue - Day River is highly polluted with MPs compared to some other rivers in Vietnam, as well as in the world. It is of practical significance to understand the sources and sinks of MPs in inland freshwater environments.

REFERENCES

Aslam M, Qadir A, Hafeez S, Aslam HMU, Ahmad SR. Spatiotemporal dynamics of microplastics burden in River Ravi, Pakistan. Journal of Environmental Chemical Engineering 2022;10:Article No. 107652.

Baldwin AK, Spanjer AR, Rosen MR, Thom T. Microplastics in lake mead national recreation area, USA: Occurrence and biological uptake. PLoS ONE 2020;15:e0228896.

Beckingham B, Ghosh U. Differential bioavailability of polychlorinated biphenyls associated with environmental particles: Microplastic in comparison to wood, coal and biochar. Environmental Pollution 2017;220:150-8.

Browne MA, Crump P, Niven SJ, Teuten E, Tonkin A, Galloway T, et al. Accumulation of microplastic on shorelines woldwide: Sources and sinks. Environmental Science and Technology 2011;45:9175-9.

Browne MA, Dissanayake A, Galloway TS, Lowe DM, Thompson RC. Ingested microscopic plastic translocates to the circulatory system of the Mussel, *Mytilus edulis* (L.). Environmental Science and Technology 2008;42:5026-31.

Chau MQ, Hoang AT, Truong TT, Nguyen XP. Endless story about the alarming reality of plastic waste in Vietnam. Energy Sources, Part A: Recovery, Utilization, and Environmental Effects 2020:1-9. DOI: 10.1080/15567036.2020.1802535.

Dai L, Wang Z, Guo T, Hu L, Chen Y, Chen C, et al. Pollution characteristics and source analysis of microplastics in the Qiantang River in southeastern China. Chemosphere 2022;293:Article No. 133576.

De Falco F, Di Pace E, Cocca M, Avella M. The contribution of washing processes of synthetic clothes to microplastic pollution. Scientific Reports 2019;9:Article No. 6633.

Dris R, Gasperi J, Rocher V, Saad M, Renault N, Tassin B. Microplastic contamination in an urban area: A case study in Greater Paris. Environmental Chemistry 2015;12:592-9.

Dris R, Gasperi J, Tassin B. Sources and fate of microplastics in urban areas: A focus on Paris Megacity. In: Wagner M, Lambert S, editors. Freshwater Microplastics: Emerging Environmental Contaminants? Switzerland: Springer International Publishing; 2018. p. 69-83.

Eerkes-Medrano D, Thompson RC, Aldridge DC. Microplastics in freshwater systems: A review of the emerging threats, identification of knowledge gaps and prioritisation of research needs. Water Research 2015;75:63-82.

Han M, Niu X, Tang M, Zhang BT, Wang G, Yue W, et al. Distribution of microplastics in surface water of the lower

Yellow River near estuary. Science of the Total Environment 2020;707:Article No. 135601.

Jambeck JR, Geyer R, Wilcox C, Siegler TR, Perryman M, Andrady A, et al. Plastic waste inputs from land into the ocean. Science 2015;347:768-71.

Koelmans AA, Mohamed Nor NH, Hermsen E, Kooi M, Mintenig SM, De France J. Microplastics in freshwaters and drinking water: Critical review and assessment of data quality. Water Research 2019;155:410-22.

Lahens L, Strady E, Kieu-Le TC, Dris R, Boukerma K, Rinnert E, et al. Macroplastic and microplastic contamination assessment of a tropical river (Saigon River, Vietnam) transversed by a developing megacity. Environmental Pollution 2018;236: 661-71.

Le ND, Hoang TTH, Duong TT, Lu X, Pham TMH, Phung TXB, et al. First observation of microplastics in surface sediment of some aquaculture ponds in Hanoi City, Vietnam. Journal of Hazardous Materials Advances 2022;6:Article No. 100061.

Lechner A, Keckeis H, Lumesberger-Loisl F, Zens B, Krusch R, Tritthart M, et al. The Danube so colourful: A potpourri of plastic litter outnumbers fish larvae in Europe's second largest river. Environmental Pollution 2014;188:177-81.

Lestari P, Trihadiningrum Y, Wijaya BA, Yunus KA, Firdaus M. Distribution of microplastics in Surabaya River, Indonesia. Science of the Total Environment 2020;726:Article No. 138560.

Liu K, Wu T, Wang X, Song Z, Zong C, Wei N, et al. Consistent transport of terrestrial microplastics to the ocean through atmosphere. Environmental Science and Technology 2019; 53:10612-9.

Mani T, Hauk A, Walter U, Burkhardt-Holm P. Microplastics profile along the Rhine River. Scientific Reports 2015; 5:Article No. 17988.

Miller RZ, Watts AJR, Winslow BO, Galloway TS, Barrows APW. Mountains to the sea: River study of plastic and non-plastic microfiber pollution in the northeast USA. Marine Pollution Bulletin 2017;124:245-51.

Moore C, Lattin G, Zellers A. A brief analysis of organic pollutants sorbed to pre and post production plastic particles from the Los Angeles and San Gabriel River Watersheds. Proceedings of the Plastic Debris, Rivers to Sea Conference; September 2005; Redondo Beach, California: USA; 2005.

Nizzetto L, Langaas S, Futter M. Pollution: Do microplastics spill on to farm soils? Nature 2016;537:Article No. 488.

Park T-J, Lee S-H, Lee M-S, Lee J-K, Lee S-H, Zoh K-D. Occurrence of microplastics in the Han River and riverine fish in South Korea. Science of the Total Environment 2020;708:Article No. 134535.

Peters CA, Bratton SP. Urbanization is a major influence on microplastic ingestion by sunfish in the Brazos River Basin, Central Texas, USA. Environmental Pollution 2016;210:380-7.

Phuong NN, Poirier L, Lagarde F, Kamari A, Zalouk-Vergnoux A. Microplastic abundance and characteristics in French Atlantic coastal sediments using a new extraction method. Environmental Pollution 2018;243:228-37.

Schymanski D, Goldbeck C, Humpf H-U, Fürst P. Analysis of microplastics in water by micro-Raman spectroscopy: Release of plastic particles from different packaging into mineral water. Water Research 2018;129:154-62.

Strady E, Dang TH, Dao TD, Dinh HN, Do TTD, Duong TN, et al. Baseline assessment of microplastic concentrations in marine and freshwater environments of a developing Southeast Asian country, Viet Nam. Marine Pollution Bulletin 2021;162:Article No. 111870.

Strady E, Kieu-Le T-C, Gasperi J, Tassin B. Temporal dynamic of anthropogenic fibers in a tropical river-estuarine system. Environmental Pollution 2020;259:Article No. 113897.

Sulistyowati L, Nurhasanah, Riani E, Cordova MR. The occurrence and abundance of microplastics in surface water of the midstream and downstream of the Cisadane River, Indonesia. Chemosphere 2022;291:Article No.133071.

Tran-Nguyen QA, Vu TBH, Nguyen QT, Nguyen HNY, Le TM, Vo VM, et al. Urban drainage channels as microplastics pollution hotspots in developing areas: A case study in Da Nang, Vietnam. Marine Pollution Bulletin 2022;175:Article No.113323.

Vermaire JC, Pomeroy C, Herczegh SM, Haggart O, Murphy M. Microplastic abundance and distribution in the open water and sediment of the Ottawa River, Canada, and its tributaries. FACETS 2017;2:301-14.

Vitali C, Peters R, Janssen H-G, W.F.Nielen M. Microplastics and nanoplastics in food, water, and beverages; part I. Occurrence. TrAC Trends in Analytical Chemistry 2022:159:Article No. 116670.

Wang F, Wong CS, Chen D, Lu X, Wang F, Zeng EY. Interaction of toxic chemicals with microplastics: A critical review. Water Research 2018a;139:208-19.

Wang W, Yuan W, Chen Y, Wang J. Microplastics in surface waters of Dongting Lake and Hong Lake, China. Science of the Total Environment 2018b;633:539-45.

Wanner P. Plastic in agricultural soils - A global risk for groundwater systems and drinking water supplies?: A review. Chemosphere 2021;264:Article No. 128453.

Wright SL, Kelly FJ. Plastic and human health: A micro issue? Environmental Science and Technology 2017;51:6634-47.

Wu P, Tang Y, Dang M, Wang S, Jin H, Liu Y, et al. Spatial-temporal distribution of microplastics in surface water and sediments of Maozhou River within Guangdong-Hong Kong-Macao Greater Bay Area. Science of the Total Environment 2020;717:Article No. 135187.

Zhao S, Wang T, Zhu L, Xu P, Wang X, Gao L, et al. Analysis of suspended microplastics in the Changjiang Estuary: Implications for riverine plastic load to the ocean. Water Research 2019;161:560-9.

Zhao S, Zhu L, Wang T, Li D. Suspended microplastics in the surface water of the Yangtze Estuary System, China: First observations on occurrence, distribution. Marine Pollution Bulletin 2014;86:562-8.

Zhao W, Huang W, Yin M, Huang P, Ding Y, Ni X, et al. Tributary inflows enhance the microplastic load in the estuary: A case from the Qiantang River. Marine Pollution Bulletin 2020;156:Article No. 111152.

Feasibility Study of Plastic Waste Pyrolysis from Municipal Solid Waste Landfill with Spent FCC Catalyst

Jiraphan Chotiratanasak[1,2], Tharapong Vitidsant[3], and Maneerat Khemkhao[1,*]

[1]Rattanakosin College for Sustainable Energy and Environment, Rajamangala University of Technology Rattanakosin, Phutthamonthon, Nakhon Pathom 73170, Thailand
[2]E-Square Green Innovation Co., Ltd., Ramkhamhaeng Road, Bangkapi, Bangkok 10240, Thailand
[3]Department of Chemical Technology, Faculty of Science, Chulalongkorn University, Pathumwan, Bangkok 10330, Thailand

ARTICLE INFO

Received: 15 Dec 2022
Received in revised: 22 Feb 2023
Accepted: 26 Feb 2023
Published online: 21 Apr 2023
DOI: 10.32526/ennrj/21/202200270

Keywords:
Municipal solid waste/ Plastic waste/ Pyrolysis/ Spent FCC catalyst/ Samui Island

*** Corresponding author:**
E-mail:
maneerat.khe@rmutr.ac.th;
maneeratkhemkhao@gmail.com

ABSTRACT

Globally, there is growing concern about the problem of plastic waste. The majority of plastic waste is dumped into landfills, where it occupies space, reducing landfill capacity and causing a variety of environmental issues. Plastic waste pyrolysis has gained popularity because it can reduce the volume of plastic waste while also producing alternative fuels. This study assessed the feasibility of producing fuel oil from plastic waste using the catalytic pyrolysis process. Polyethylene (PE), polypropylene (PP), and polystyrene (PS) waste samples were collected from municipal solid waste (MSW) landfills on Samui Island, Surat Thani Province, Thailand. Pyrolysis was carried out in a 3-L bench-scale reactor at 450ºC using a 3% spent FCC catalyst. PE, PP, PS, and mixed plastic waste were used as feedstocks. The results showed that the pyrolysis of PS produced the most liquid product (91.44 wt%), whereas the pyrolysis of PE produced the highest percentage of diesel range product (36.60 wt%). Furthermore, the results of the analysis revealed that the characteristics of diesel from improved PE pyrolysis oil by naphtha removal were similar to those of commercial diesel B7. According to the cost-benefit analysis, the operating costs of pyrolysis oil and improved diesel were 0.37 and 0.65 USD/L, respectively, which were lower than the current market price of diesel B7. The findings of the study demonstrated the feasibility of converting plastic waste from MSW on Samui Island into alternative energy using eco-friendly and cost-effective technology.

1. INTRODUCTION

Samui Island is one of Thailand’s most popular tourist destinations. The increasing number of residents and visitors contributes to a large volume of solid waste. According to the report of the TISTR (2020), the major component of municipal solid waste (MSW) on Samui Island was plastic waste, which accounted for 40.4% and 64.4% of new and old MSW, respectively. Since plastics degrade slowly, they take up a lot of space, resulting in overflowing landfills. In addition, leachate, toxic dyes, and additives in plastic products have a negative impact on the environment (Miandad et al., 2017a; Yansaneh and Zein, 2022).

Although several approaches have been implemented for MSW management on Samui Island, there are still many problems and obstacles. These include landfills that have reached their maximum capacity, leachate contamination from landfill sites to the nearby environment, and the MSW incinerator that has been out of order since 2012. To solve the problems, the municipality has transported the waste to be disposed of outside the area with a large budget. However, the accident in which a ferry capsized during MSW transportation from Samui Island to Surat Thani Province in August 2020, causing 60 tons of MSW to sink into the sea (Bangkok Post, 2020; Thai PBS, 2020), has raised concerns.

Currently, pyrolysis technology is growing in interest. This technology involves the thermal degradation of complex molecules into smaller molecules at temperatures ranging from 300 to 600°C in the absence of oxygen (Singh et al., 2019; Zhang et al., 2020; Lee et al., 2021). This method reduces a massive amount of MSW and can potentially convert

Citation: Chotiratanasak J, Vitidsant T, Khemkhao M. Feasibility study of plastic waste pyrolysis from municipal solid waste landfill with spent FCC catalyst. Environ. Nat. Resour. J. 2023;21(3):256-265. (https://doi.org/10.32526/ennrj/21/202200270)

plastics to more valuable chemicals and fuels (Hakeem et al., 2018; Maafa, 2021).

A number of studies have been documented on the factors affecting the yield and distribution of pyrolysis products. Miandad et al. (2017b) conducted the pyrolysis of polystyrene (PS), polypropylene (PP), polyethylene (PE), and polyethylene-terephthalate (PET) at 450°C for 75 min of retention time and found PS provided the maximum liquid yield, while PE pyrolysis converted plastic into wax instead of liquid products. While the thermal and kaolin catalytic pyrolysis of PP waste was conducted in a horizon glass reactor at 450°C for 30 min of retention time, 67.48 wt% and 79.85 wt% of the liquid products were obtained, respectively (Hakeem et al., 2018), whereas plastic bag pyrolysis in a fixed bed reactor at 500°C with three catalysts (ZSM-5, dolomite, and kaolin) showed that non-catalytic pyrolysis provided the largest amount of liquid products (Chaiphet et al., 2022). These studies demonstrated that the distribution and yield of pyrolysis oil depend on several factors, such as temperature, type of catalyst, reactor type, and feedstock characteristics.

According to the above-mentioned MSW management issue on Samui Island, pyrolysis could be an alternative method for Samui Island MSW management. However, since the yield and characteristics of liquid products and the cost-effectiveness of this approach have not been evaluated, this research aimed to determine the feasibility of using catalytic pyrolysis to convert plastic waste from Samui Island's MSW into fuel. The results provided the information necessary for the relevant organizations to select the appropriate means of MSW management that facilitate the environmental and economic sustainability of Samui Island.

2. METHODOLOGY

2.1 Study site

Samui Island, Thailand's third-largest island, is a municipality in Surat Thani Province. The island is situated off the east coast of Thailand between latitudes N9°24' to N9°36' and longitudes E99°54' to E100°06', which cover an area of around 227 km^2 as shown in Figure 1 (Nazaruddin, 2020). In 2021, the population in the Samui Island municipality was 68,698 (Koh Samui City, 2021).

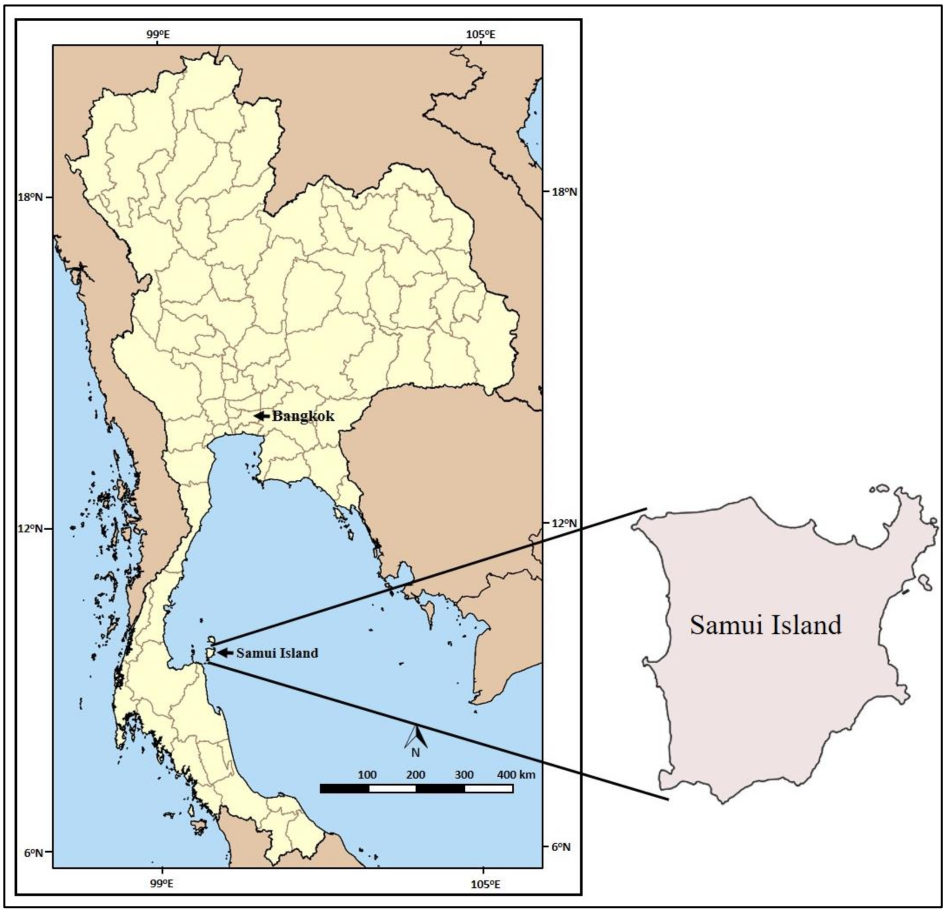

Figure 1. Map of Samui Island, Surat Thani Province, Thailand

2.2 Raw material survey and preparation

Municipal plastic waste samples were randomly collected from Samui Island Landfill in April 2022. PE, PP, and PS were the three major types of plastic in the landfill in the ratio of 80:15:5 wt%. Thus, this study conducted the pyrolysis based on the types of plastic and the mixed plastic ratio in terms of mixed plastic waste. All samples were shredded to less than 3 cm and dried to less than 1% moisture content.

2.3 Reactor system and experimental set-up

The pyrolysis experiments were carried out in a 3-L bench-scale horizontal cylindrical reactor comprised of 316 stainless steel materials with a 10 cm internal diameter, 2 cm thickness, and 39 cm length. The center shaft was equipped with an agitator and a compartment for inserting a thermocouple to monitor the temperature inside the reactor. The reactor was heated via an electrical furnace, and nitrogen gas was used to carry the obtained product vapor to the condenser. A counter-current heat exchanger and the chiller were installed to support cool water for the heat exchanger. The schematic diagram of the reactor is shown in Figure 2.

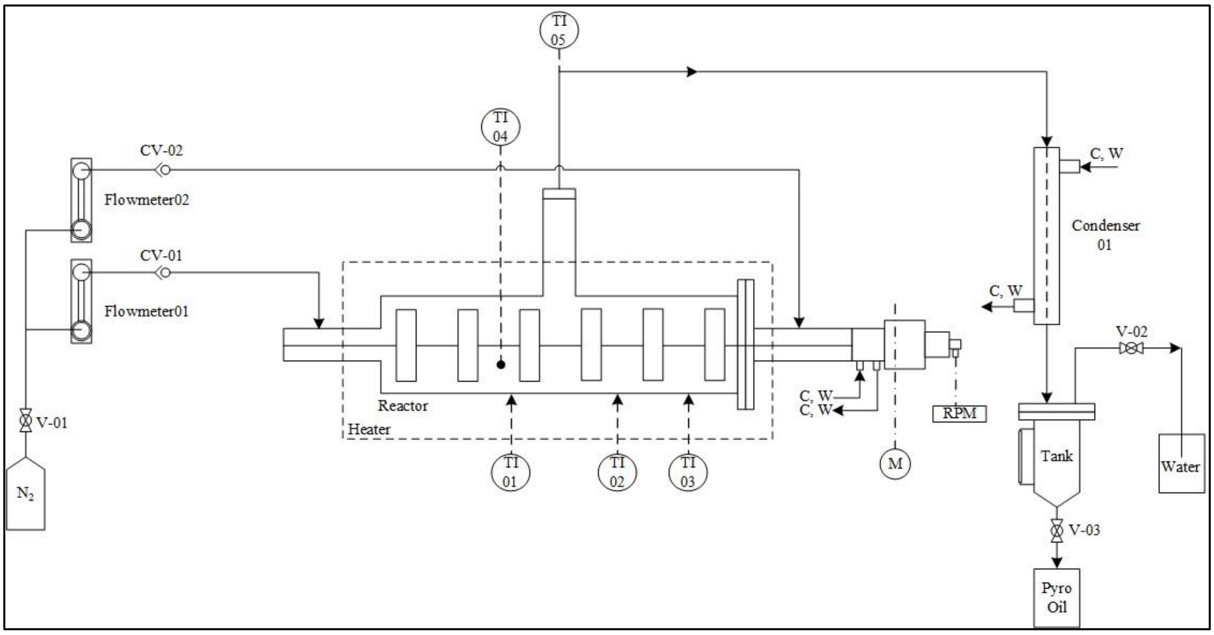

Figure 2. The schematic diagram of the reactor

The pyrolysis experiment was carried out at a reaction temperature of 450°C with 3 wt% spent FCC catalyst in the feed. A total of 250 g of PE, PP, and PS and mixed plastics of PE, PP, and PS in a ratio of 80:15:5, which was the plastic ratio in the Samui Island Landfill, were used to determine the effect of the plastic types on the yield and selectivity of the product. Two thermocouples were used to indicate the reaction temperature (RT) and the oil vapor's temperature (VT) over time at TI04 and TI05, respectively. The pyrolysis oil product was collected gradually until the reaction ended. The carbon residues that remained in the reactor were collected and weighed. Finally, the mass balance was used to calculate the gas product.

2.4 Analytical methods

Ash content, moisture content, volatile matter, and fixed carbon of plastic waste samples were determined by proximate analysis according to ASTM D3172-3175. Carbon, hydrogen, nitrogen, and sulfur were determined by ultimate analysis according to ASTM D5373. Meanwhile, heating value and thermal degradation temperature were determined via the bomb calorimeter and TGA, respectively.

The composition of liquid products from the pyrolysis process was analyzed by a Simulated Distillation Gas Chromatography (DGC; Agilent 7890 model) equipped with a DB-1 column (J&W Scientific) and simulation distillation software. The heating value, viscosity, and acidity of pyrolysis liquid products were analyzed following the ASTM standards. The quality of improved pyrolysis oil was compared with diesel standards to assess the possibility of using it as an alternative fuel.

2.5 Cost-benefit evaluation of plastic waste pyrolysis

The cost-benefit analysis focused only on the pyrolysis of plastic waste to produce a liquid product with the same quality and characteristics as diesel fuel. The cost-benefit analysis was based solely on the estimated monthly operational costs of the plastic waste pyrolysis process and income from diesel sales. PE plastic waste with a moisture content of 0.77 wt% was used as the feedstock for the pyrolysis process at a rate of one ton per day.

3. RESULTS AND DISCUSSION

3.1 Characteristic of plastic waste samples

In April 2022, 30 kg of plastic waste samples were randomly collected from the landfill. The plastic waste samples contained 80% PE, 15% PP, and 5% PS. Table 1 presents the proximate and ultimate results of plastic waste samples. The PP had the highest gross calorific value, fixed carbon, and hydrogen content, whereas the PS had the highest volatile matter and carbon content. In the meantime, the moisture content, ash, nitrogen content, and sulfur content of mixed plastic waste were the highest among PP, PS, and PE.

Table 1. Proximate and ultimate analysis of plastic waste samples

Parameters	Methods	Unit	PP	PS	PE	Mixed plastic
Gross calorific value	ASTM D5865	cal/g	10,381.47	9,843.51	9,824.28	9,718.4
Moisture content	ASTM D3172	wt%	0.77	0.22	1.03	1.11
Volatile matter	ASTM D3173	wt%	95.19	99.57	93.24	93.05
Ash	ASTM D3174	wt%	2.03	0.11	5.66	5.68
Fixed carbon	ASTM D3175	wt%	2.01	0.10	0.07	0.16
Carbon content	ASTM D5373	wt%	82.22	92.00	77.55	78.97
Hydrogen content	ASTM D5373	wt%	13.84	8.34	12.81	12.77
Nitrogen content	ASTM D5373	wt%	0.14	0.05	0.21	0.24
Sulfur content	ASTM D4239	wt%	UD	0.002	0.015	0.024

Remark: UD refers to Undetectable

3.2 Thermogravimetric analysis of plastic wastes

The degradation temperatures of individual and mixed plastic wastes were determined using TGA. In Figure 3, all plastic degradation temperatures began around 300°C (as shown on the TG line in solid lines). PE degraded slowly initially until it reached 450°C then the degradation occurred rapidly. While PP, PS, and mixed PE/PP/PS degradation occurred rapidly after reaching 440, 425, and 390°C, respectively. As shown on the DTG line, the peaks of the dashed lines showed that the maximum temperatures for PS, PP, PE, and mixed PE/PP/PS degradation were 414.0, 467.7, 480.2, and 470.3°C, respectively. PE had the highest maximum degradation temperature, followed by mixed PE/PP/PS, PP, and PS. The differences in pyrolysis temperatures between plastic types are caused by the polymer structures of each plastic (Gałko and Sajdak, 2022).

Figure 4 depicts the RT and VT against the reaction time. The PS experimental results showed that when the desired RT (solid line) was reached at 450ºC, the VT rapidly rose (dashed line). A rapid increase in the oil vapor temperature in PS pyrolysis indicated that PS cracked easily to produce pyrolysis oil and gas products when compared to PP, PE, and mixed PE/PP/PS; corresponding to TGA results, the PS degradation reaction occurred at a lower temperature when compared to other plastics. Figure 5 depicts the differential oil and accumulative oil against reaction times. It was clearly observed that the differential oil receiving of all samples conformed to the oil vapor's temperature with time, as mentioned in Figure 4. PS had a reaction termination time of 120 min, whereas PP, PE, and mixed plastics had times of 210, 240, and 225 min, respectively.

PS degrades more easily than other plastics (Maafa, 2021). As shown in Figure 6, PS has a long-chain hydrocarbon molecular structure with alternating carbon centers attached to phenyl groups. PS plastic degradation is typically caused by end-chain scission, followed by beta scission, which can occur at low temperatures (Singh et al., 2019). Meanwhile, PE had the highest peak pyrolysis temperature compared to the others. PE requires higher temperatures to degrade than other plastics (Rizzarelli et al., 2016; Miandad et al., 2017b) due to its structure being linear and symmetrical without a functional group, resulting in a higher crystalline structure. Furthermore, cracking may occur only on both sides of the polymer chain's end, resulting in small molecular hydrocarbon products (Cheng et al., 2022). The study results also exhibited that the reaction temperature of mixed PE/PP/PS (80:15:5) was higher than PS and comparable to PP and PE. This is caused by the composition of the plastics used as feedstock, which contributes to the interaction of the mixed polymers that affects the onset temperature, peak decomposition temperature, and endset temperature (Yu et al., 2016; Anene et al., 2018).

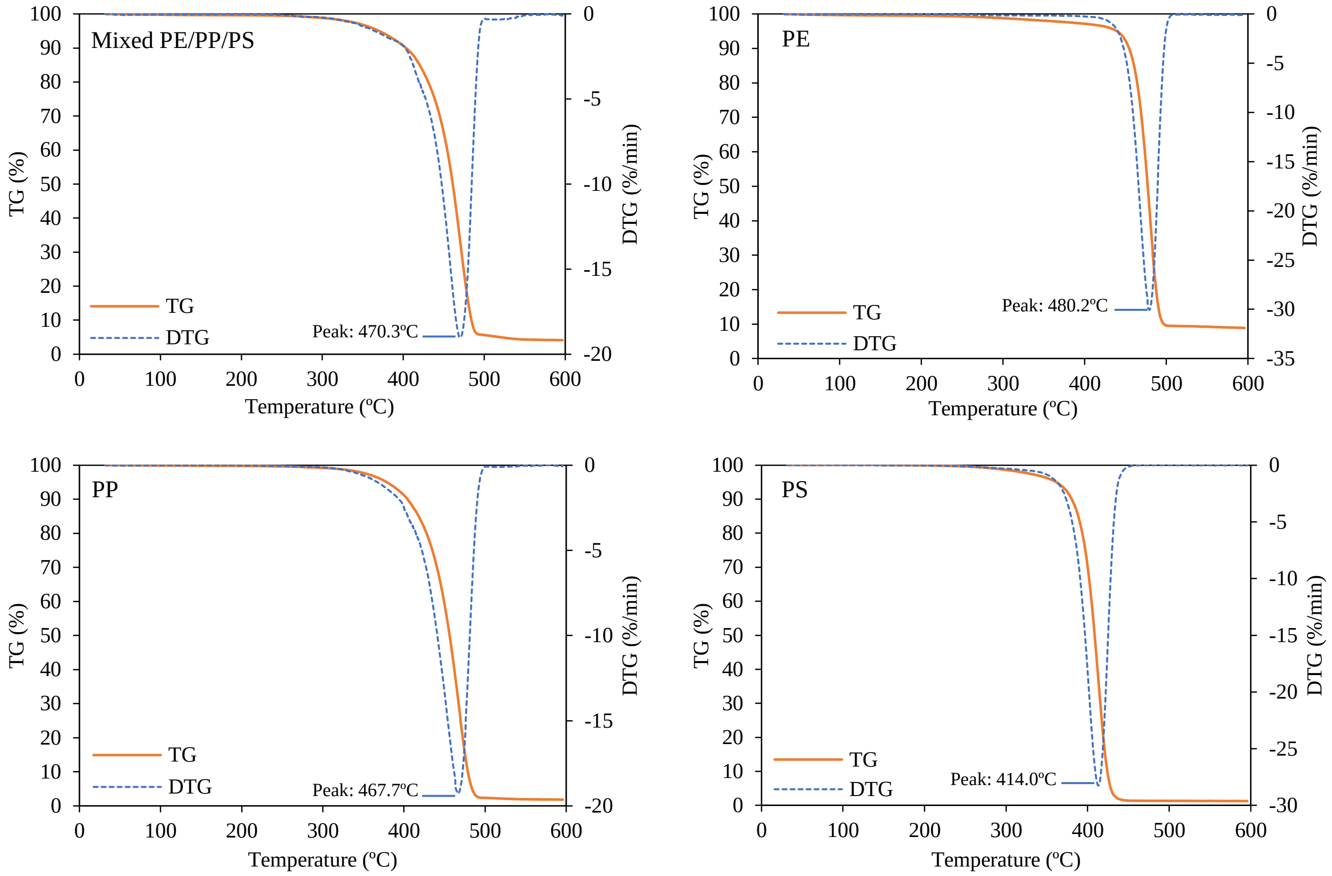

Figure 3. The TGA results (TG refers to Thermogravimetric; DTG refers to Differential Thermogravimetric)

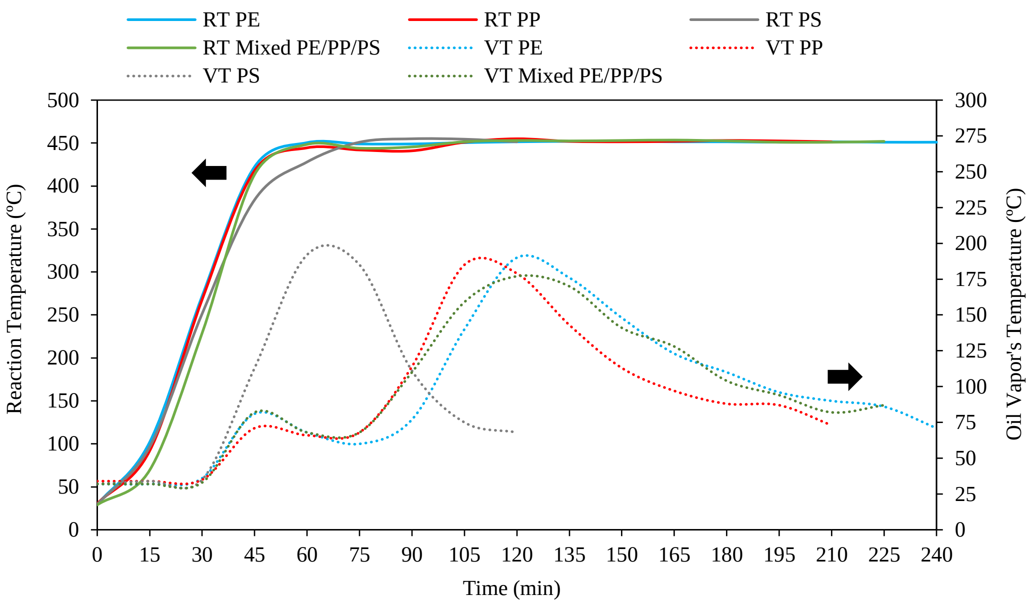

Figure 4. The reaction temperature (RT) and the oil vapor's temperature (VT) against reaction time

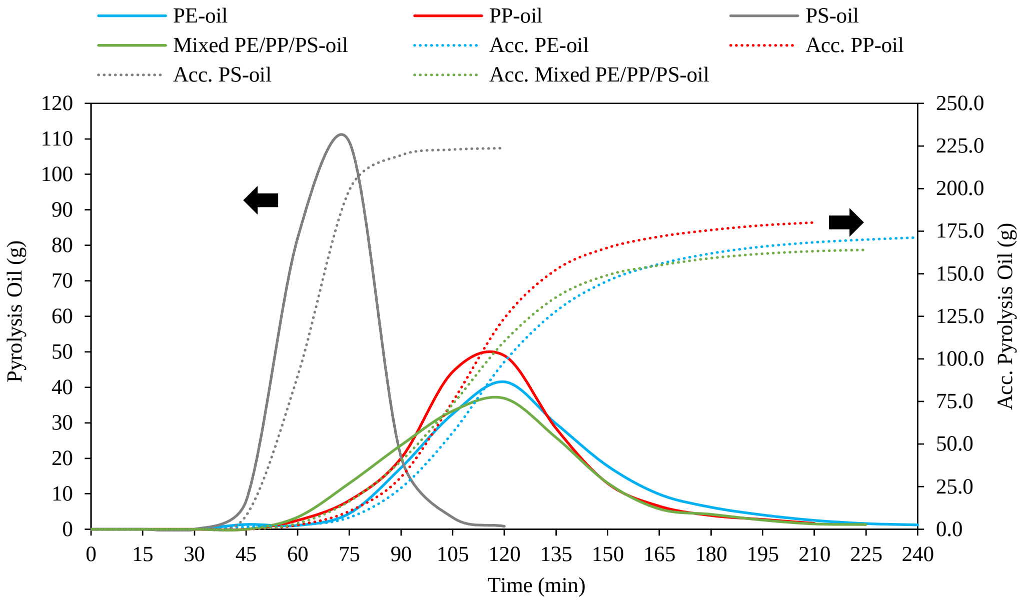

Figure 5. Differential and accumulative oil against reaction time

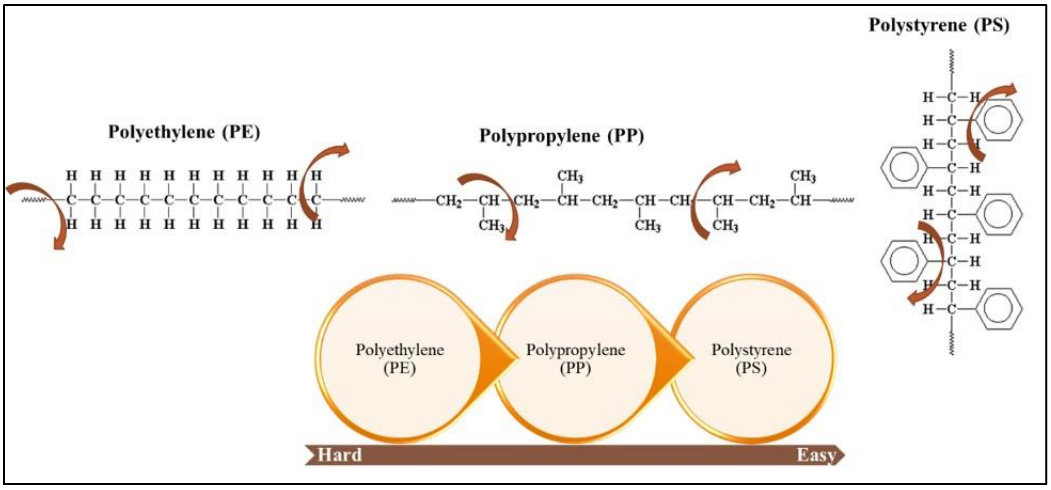

Figure 6. Molecular structures of PE, PP, and PS (Maafa, 2021)

Plastic molecular structures also influence reaction times. In this study, the time required for the complete pyrolysis reaction of PS was the shortest, which was 120 min, whereas the time required to complete the pyrolysis reactions of PP, PE, and mixed PE/PP/PS was 210, 240, and 225 min, respectively. Furthermore, a 3% catalyst was used in the reaction condition, which improved the cracking of polymers, particularly PS, leading to the conversion into styrene over catalysts at relatively low temperatures via simple thermal cracking (Maafa, 2021).

3.3 Yield and distribution of pyrolysis products

Figure 7 presents the maximum liquid yield from the pyrolysis of PS at 91.44 wt%, while the pyrolysis of PE, PP, and mixed PE/PP/PS yielded 72.65, 73.75, and 69.19 wt%, respectively. Furthermore, PS plastic waste produced the least amount of gas and carbon residue. This is consistent with previous research showing that pyrolysis of PS produced the most liquid product with the least amount of gas and char when compared to PE and PP (Miandad et al., 2017b; Palmay et al., 2022). However, when compared to individual plastics, mixed plastic waste pyrolysis produced the lowest yield of liquid product and the highest yield of carbon residue and gas products. The proportion of plastic types in the mixed feedstock has a significant impact on the oil yield of mixed plastic waste (Kusenberg et al., 2022; Palmay et al., 2022; Zein et al., 2022).

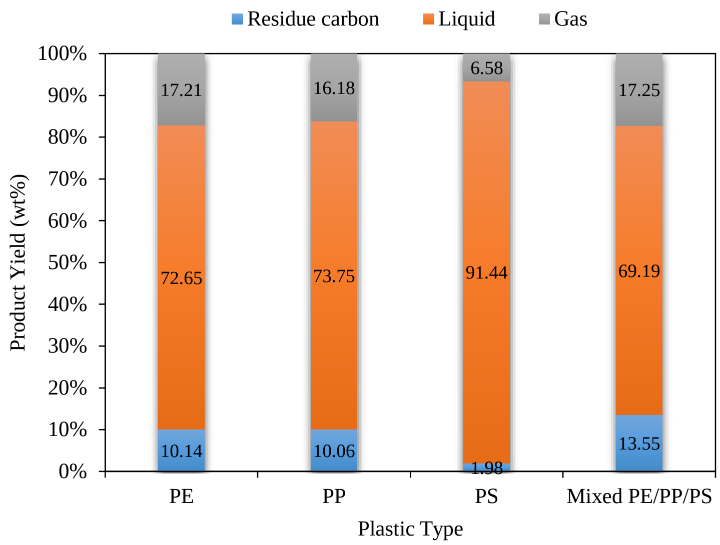

Figure 7. Effect of the plastic types on yield of pyrolysis product

Figure 8 exhibits the variation in the composition of pyrolysis oil derived from each feedstock type. The percentage of naphtha (C_5-C_{12}), kerosene (C_{12}-C_{15}), diesel (C_{15}-C_{33}), and long residue varies in the range of 39.55-72.25%, 0.35-18.70%, 24.00-36.60%, and 3.40-6.80%, respectively. In liquid products, pyrolysis of PS yielded the highest percentage of naphtha range, followed by diesel range, long residue, and kerosene range, whereas pyrolysis of PE yielded the highest percentage of naphtha range, followed by diesel range, kerosene range, and long residue. When PS was mixed with PE and PP, the light hydrocarbon molecule decreased while the heavy hydrocarbon molecule increased. These findings confirmed the previously reported influence of plastic type and plastic waste composition on the yield and formation of certain hydrocarbon groups (Al-Salem et al., 2017; Miandad et al., 2017a; Santaweesuk and Janyalertadun, 2017).

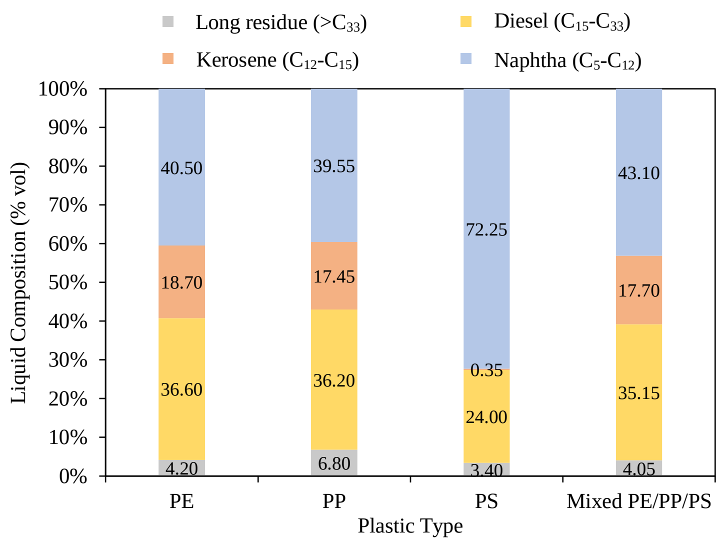

Figure 8. Effect of the plastic types on selectivity of pyrolysis product

3.4 Characteristic of improved diesel from pyrolysis oil

Normally, the naphtha composition in commercial diesel B7 is around 10 wt%, which contributes to high performance in diesel engines. In this study, the pyrolysis oil of PE contained 40.50 percent naphtha. Excess naphtha was evaporated at temperatures ranging from 120 to 150°C in the same reactor. Naphtha vapor was condensed by keeping the condenser temperature at 20°C until the naphtha product was obtained. The remaining pyrolysis oil in the reactor was a diesel product with a naphtha content similar to diesel B7 (around 10 wt%). Furthermore, the liquid diesel composition from the pyrolysis process, as shown in Table 2, had a relative value to commercial diesel B7.

3.5 Application of pyrolysis oil from plastic waste

According to the improved pyrolysis oil, its properties were close to those of diesel B7, so the oil could be used as a fuel for diesel engines. However, before use, pyrolysis liquid oils should be upgraded through various methods such as distillation, refining, and blending with conventional diesel. Various studies have reported on the use of pyrolysis oil in diesel engines for electricity generation (Rehan et al., 2016; Kassargy et al., 2018; Lee et al., 2021) and the use of pyrolysis oil or blended pyrolysis oil with conventional diesel as a transportation fuel (Faussone, 2018; Jahirul et al., 2022; Uebe et al., 2022). Furthermore, because of the high-value chemical potentials of pyrolysis oils, they could be used in industries such as the browning and flavoring of wood adhesives (Kunwar et al., 2016) and could be a source of precursor chemicals in plastic, including biocompatible and biodegradable plastic industries (Lu et al., 2021; Mahari et al., 2022).

Table 2. Characteristics of diesel after improvement and commercial diesel

Characteristic	Methods	Diesel after improvement	Commercial diesel B7
1. Density at 15°C (kg/m^3)	ASTM D 1298	809.60	827.48
2. Kinematic viscosity at 40°C	ASTM D 445	1.45	3.74
3. Heat value (MJ/kg)	ASTM D 240	45.376	44.864±0.295
4. API gravity	ASTM D 1298	43.10	39.5
5. Distillation (°C)	ASTM D 86		
• IBP		140.00	206.59
• T10		191.00	251.70
• T50		280.00	316.18
• T90		364.00	375.34
• FBP		435.00	398.21
6. Cetane index	ASTM D 976	63.58	68.89
7. Flash point (°C)	ASTM D 93	55.00±1.20	81.50±0.70
8. Acid value (mg KOH/g)	ASTM D 664	0.15	0.3
9. Liquid composition	ASTM D 2887		
• Naphtha		12.70	12.20
• Kerosene		23.30	21.10
• Diesel		55.40	57.20
• Long Residue		8.60	9.50

IBP=Initial Boiling Point; FBP=Final Boiling Point; T10, T50, T90=10, 50, 90 % recovery temperature (°C), respectively (ASTM International, 2020)

3.6 Cost-benefit evaluation of plastic waste pyrolysis

As previously mentioned, the study's target pyrolysis product is diesel. In terms of the cost-benefit analysis presented in Table 3, it was focused only on the cost of pyrolysis operations and the income from diesel based on the current diesel price. A total of 21,795 L of pyrolysis oil were produced from 1 ton/day, or 30 tons/month, of PE plastic waste pyrolysis. Following the removal of the excess naphtha, the process will produce 13,730 L/month of diesel fuel (with a 10% loss during operation). The total operating cost of pyrolysis oil will be 8,144.69 USD/month, or 0.37 USD/L. While the operating cost for diesel production will be added up for naphtha separation and additives, the total cost will be 8,859.89 USD/month or 0.65 USD/L. Based on the current market price of diesel, which is 1.01 USD/L, the monthly income from selling diesel will be 13,931.96 USD (PTT OR, 2023). However, this benefit is not included in the naphtha revenue evaluation. In addition, the carbon residue and gas products, mainly ethane and propane, can be recycled as fuel for heating the reactor on pilot and commercial scales, leading to a lower operation cost.

Furthermore, because a large amount of plastic waste will be pyrolyzed, this project will assist Samui Municipality in overcoming solid waste problems, resulting in sustainable solid waste management, which corresponds to SDG 6: Water and Sanitation and SDG 11: Sustainable Cities and Communities.

Table 3. Monthly expenditure and income

Items	Quantity	Cost per unit	Total (USD)
PE plastic waste1 (ton/day × 30 days)	30tons	877.12 USD/ton	2,613.73
Catalyst	900 kg	0.15 USD/kg	130.69
Bleach substances	763 kg	0.87 USD/kg	664.6
Electricity	692.15 units	0.13 USD/unit	88.87
Workforce	4persons	726.04 USD/month/person	2,904.15
Maintenance cost			871.24
Others			871.24
Total cost for pyrolysis oil			8,406.06
Cost per liter of pyrolysis oil (USD/L)			0.37
Adding up cost of improvement from pyrolysis oil to diesel grade			
Separating	21,795 L	0.15 USD/L	316.47
Additives (Cetane improver, PPD)	13,730 L	0.029 USD/L	398.74
Total cost for diesel			8,859.79
Cost per liter of diesel product (USD/L)			0.65

Remark: Monthly expenditure and income calculated based on 1-month pyrolysis operation with 30 tons/month of PE plastic waste. 1 baht=0.029 USD (January 3rd, 2023)

4. CONCLUSION

The pyrolysis of municipal plastic wastes from Samui Island landfill was carried out in a 3-L bench-scale reactor at a temperature of 450ºC with a 3 wt% spent FCC catalyst loading. PE, PP, PS, and mixed plastic waste were used as feedstock. Although catalytic pyrolysis of PS plastic waste yielded the most liquid products, catalytic pyrolysis of PE plastic waste yielded the most diesel-range products. The properties of the improved pyrolysis oil after naphtha removal were quite similar to commercial diesel B7. Furthermore, the operation cost of plastic waste pyrolysis and liquid product improvement was less than the market price of diesel fuel. This study demonstrated that plastic pyrolysis is a feasible and cost-effective intervention for addressing Samui Island's plastic waste problem.

ACKNOWLEDGEMENTS

The authors would like to express their gratitude to the Center of Fuels and Energy from Biomass at Chulalongkorn University for kindly supporting this research project. The authors are also deeply grateful to the Samui municipality for providing examples of plastic waste.

REFERENCES

Al-Salem SM, Antelava A, Constantinou A, Manos G, Dutta A. A review on thermal and catalytic pyrolysis of plastic solid waste (PSW). Journal of Environmental Management 2017;197:177-98.

Anene AF, Fredriksen SB, Sætre KA, Tokheim LA. Experimental study of thermal and catalytic pyrolysis of plastic waste components. Sustainability 2018;10:Article No. 3979.

ASTM International. Test Method for Distillation of Petroleum Products and Liquid Fuels at Atmospheric Pressure [Internet]. 2020 [cited 2023 Feb 17]. Available from: http://www.astm.org/cgi-bin/resolver.cgi?D86-20.

Bangkok Post. Last two bodies from Samui ferry sinking retrieved [Internet]. 2020 [cited 2023 Feb 15]. Available from: https://www.bangkokpost.com/thailand/general/1970391/last-two-bodies-from-samui-ferry-sinking-retrieved.

Chaiphet K, Turakarn C, Duanguppama K, Sasen C, Khamsuwan S, Promphipha P. The product yields and fuel properties from catalytic pyrolysis of plastic bag. Journal of Materials Science and Applied Energy 2022;11:16-23.

Cheng L, Zhang Y, Wang Y, Gu J, Yuan H, Chen Y. Pyrolysis of long chain hydrocarbon-based plastics via self-exothermic effects: The origin and influential factors of exothermic processes. Journal of Hazardous Materials 2022;424: Article No. 127476.

Faussone GC. Transportation fuel from plastic: Two cases of study. Waste Management 2018;73:416-23.

Gałko G, Sajdak M. Trends for the thermal degradation of polymeric materials: Analysis of available techniques, issues, and opportunities. Applied Sciences 2022;12Article No. 9138.

Hakeem IG, Aberuagba F, Musa U. Catalytic pyrolysis of waste polypropylene using Ahoko kaolin from Nigeria. Applied Petrochemical Research 2018;8:203-10.

Jahirul MI, Rasul MG, Schaller D, Khan MMK, Hasan MM, Hazrat MA. Transport fuel from waste plastics pyrolysis: A review on technologies, challenges and opportunities. Energy Conversion and Management 2022;258:Article No. 115451.

Kassargy C, Awad S, Burnens G, Kahine K, Tazerout M. Gasoline and diesel-like fuel production by continuous catalytic pyrolysis of waste polyethylene and polypropylene mixtures over USY zeolite. Fuel 2018;224:764-73.

Koh Samui City. General information [Internet]. 2021 [cited 2023 Feb 16]. Available from: https://www.kohsamuicity.go.th/content/general. (in Thai).

Kunwar B, Cheng HN, Chandrashekaran SR, Sharma BK. Plastics to fuel: A review. Renewable and Sustainable Energy Reviews 2016;54:421-8.

Kusenberg M, Zayoud A, Roosen M, Thi HD, Abbas-Abadi MS, Eschenbacher A, et al. A comprehensive experimental investigation of plastic waste pyrolysis oil quality and its dependence on the plastic waste composition. Fuel Processing Technology 2022;227:Article No. 107090.

Lee D, Nam H, Wang S, Kim H, Kim JH, Won Y, et al. Characteristics of fractionated drop-in liquid fuel of plastic wastes from a commercial pyrolysis plant. Waste Management 2021;126:411-22.

Lu C, Xiao H, Chen X. Simple pyrolysis of polystyrene into valuable chemicals. e-Polymers 2021;21:428-32.

Maafa IM. Pyrolysis of polystyrene waste: A review. Polymers 2021;13:Article No. 225.

Mahari WAW, Kee SH, Foong SY, Amelia TSM, Bhubalan K, Man M, et al. Generating alternative fuel and bioplastics from medical plastic waste and waste frying oil using microwave co-pyrolysis combined with microbial fermentation. Renewable and Sustainable Energy Reviews 2022;153:Article No. 111790.

Miandad R, Barakat MA, Rehan M, Aburiazaiza AS, Ismail IMI, Nizami AS. Plastic waste to liquid oil through catalytic pyrolysis using natural and synthetic zeolite catalysts. Waste Management 2017a;69:66-78.

Miandad R, Barakat MA, Aburiazaiza AS, Rehan M, Ismail IMI, Nizami AS. Effect of plastic waste types on pyrolysis liquid oil. International Biodeterioration and Biodegradation 2017b;119:239-52.

Nazaruddin DA. Granite landforms of Samui Island (southern Thailand) from geoheritage, geoconservation and geotourism perspectives. International Journal of Geoheritage and Parks 2020;8:75-86.

Palmay P, Haro C, Huacho I, Barzallo D, Bruno JC. Production and analysis of the physicochemical properties of the pyrolytic oil obtained from pyrolysis of different thermoplastics and plastic mixtures. Molecules 2022;27:Article No. 3287.

PTT Oil and Retail Business Public Company Limited (PTT OR). Oil price [Internet]. 2023 [cited 2023 Feb 15]. Available from: https://www.pttor.com/th/oil_price.

Rehan M, Nizami AS, Shahzad K, Ouda OKM, Ismail IMI, Almeelbi T, et al. Pyrolytic liquid fuel: A source of renewable electricity generation in Makkah. Energy Sources, Part A: Recovery, Utilization, and Environmental Effects 2016; 38:2598-603.

Rizzarelli P, Rapisarda M, Perna S, Mirabella EF, La Carta S, Puglisi C, et al. Determination of polyethylene in biodegradable polymer blends and in compostable carrier bags by Py-GC/MS and TGA. Journal of Analytical and Applied Pyrolysis 2016;117:72-81.

Santaweesuk C, Janyalertadun A. The production of fuel oil by conventional slow pyrolysis using plastic waste from a municipal landfill. International Journal of Environmental Science and Development 2017;8:168-73.

Singh RK, Ruj B, Sadhukhan AK, Gupta P. Thermal degradation of waste plastics under non-sweeping atmosphere: Part 1: Effect of temperature, product optimization, and degradation mechanism. Journal of Environmental Management 2019; 239:395-406.

Thai PBS. Recovering the municipal solid waste (MSW) of Samui Island from a capsized ferry accident during transportation [Internet]. 2020 [cited 2023 Feb 7]. Available from: https://www.thaipbs.or.th/news/content/296474. (in Thai).

Thailand Institute of Scientific and Technological Research (TISTR). The Suitability Study of the Model and the Approach for Municipal Solid Waste Disposal in Koh Samui Municipality. Pathum Thani, Thailand: Thailand Institute of Scientific and Technological Research; 2020. (in Thai).

Uebe J, Kryzevicius Z, Majauskiene R, Dulevicius M, Kosychova L, Zukauskaite A. Use of polypropylene pyrolysis oil in alternative fuel production. Waste Management and Research 2022;40:1220-30.

Yansaneh OY, Zein SH. Recent advances on waste plastic thermal pyrolysis: A critical overview. Processes 2022;10:Article No. 332.

Yu J, Sun L, Ma C, Qiao Y, Yao H. Thermal degradation of PVC: A review. Waste Management 2016;48:300-14.

Zein SH, Grogan CT, Yansaneh OY, Putranto A. Pyrolysis of high-density polyethylene waste plastic to liquid fuels: Modelling and economic analysis. Processes 2022;10:Article No. 1503.

Zhang Y, Ji G, Chen C, Wang Y, Wang W, Li A. Liquid oils produced from pyrolysis of plastic wastes with heat carrier in rotary kiln. Fuel Processing Technology 2020;206:Article No. 106455.

Investigation of Some Physicochemical Parameters and Heavy Metals for Monitoring the Groundwater Quality of Savar Upazila of Dhaka, Bangladesh

Meherun Nesha[1*], Zeenath Fardous[1], Hasibul Islam[2], Priyanka Das Pinkey[3], Md. Abdur Rahman[1], and M. Alamgir Zaman Chowdhury[1]

[1]Agrochemical and Environmental Research Division, Institute of Food and Radiation Biology, Atomic Energy Research Establishment, Ganakbari, Savar, Dhaka, Bangladesh
[2]Department of Biochemistry and Molecular Biology, Jahangirnagar University, Dhaka, Bangladesh
[3]Department of Environmental Science and Management, North South University, Dhaka, Bangladesh

ARTICLE INFO

Received: 28 Apr 2022
Received in revised: 22 Sep 2022
Accepted: 26 Sep 2022
Published online: 28 Apr 2023
DOI: 10.32526/ennrj/21/202200264

Keywords:
Groundwater/ Water quality index/ Heavy metals/ Savar/ Bangladesh

*** Corresponding author:**
E-mail: meher.bmb@gmail.com

ABSTRACT

Safe and clean water is an indispensable component for all kinds of living beings. An attempt was taken to examine the drinking water, particularly the groundwater quality of Savar Upazila under the Dhaka District of Bangladesh by assessing some physicochemical parameters such as pH, total dissolved solids (TDS), electrical conductivity (EC), and temperature and the levels of different heavy metals (Cu, Cd, Cr, Fe, Mn, and Zn). To measure the concentration of the six selected metals from the groundwater samples collected from 38 different locations of Savar Upazila, Atomic Absorption Spectrophotometry (AAS) was used. Our results showed that the pH, TDS, EC, and temperature ranged from (6.56-7.72), (73-437 mg/L), (117-654 µS/cm), and (27.7-30.5ºC), respectively which were found within the limit of water standards recommended by national and global regulatory authorities. The mean concentration of different studied metals in the reported water samples of Savar Upazila followed the order of Fe > Zn > Mn > Cr > Cu > Cd. The average concentration was 0.136±0.188 mg/L, 0.121±0.289 mg/L, 0.033±0.060 mg/L, 0.015±0.0096 mg/L, 0.0104±0.005 mg/L, and 0.0022±0.0019 mg/L for Fe, Zn, Mn, Cr, Cu, and Cd, respectively. In this study, Water quality index (WQI) was also calculated for the studied samples and it was observed that the groundwater of Savar Upazila belonged in the good to excellent categories and can be recommended as suitable for drinking purposes.

1. INTRODUCTION

Water plays a pivotal role in the existence of all known forms of life on the earth's surface. A large number of sources of drinking water like rivers, ponds, lakes, wells, and tube wells are present in our environment and it is highly desirable to keep these sources safe and secure from any kind of pollution. If these resources of essential drinking water become contaminated, they may pose the greatest risk to human health. The random and misuse of agricultural, industrial, and various natural activities throughout Bangladesh have led to the degradation of the quality of groundwater resources over the past few decades (Bhuiyan et al., 2015; Bodrud-Doza et al., 2016; Islam et al., 2017; Islam et al., 2018). This deterioration of groundwater quality is highly threatening as it is very difficult to control the severity of groundwater contamination which causes environmental as well as human health hazards (Gupta et al., 2008). In recent days, industrial growth is occurring rapidly which expedites the discharge of chemical toxins along with heavy metals into the environment (Saha et al., 2017). The waste from the industries and factories is usually discharged into the ponds, rivers, lakes, and into the ocean if the industry is located near seaside zones with or without proper treatment and causes surface water as well as groundwater contamination (Bakis and Tuncan, 2011; Lu et al., 2016).

Heavy metals are defined as metallic elements which are found in the nature and have a very high

Citation: Nesha M, Fardous Z, Islam H, Pinkey PD, Rahman MA, Chowdhury MAZ. Investigation of some physicochemical parameters and heavy metals for monitoring the groundwater quality of Savar Upazila of Dhaka, Bangladesh. Environ. Nat. Resour. J. 2023;21(3):266-278. (https://doi.org/10.32526/ennrj/21/202200264)

density which is greater than 5 g/cm^3 (Singh et al., 2018). Heavy metals in water are toxic to the human body even in trace levels which are related to several health problems such as nutritional deformities, immunological disfigurement, deficient intrauterine growth, imperfect psycho-social behavior, and many more (Nweke and Sanders, 2009; Khan et al., 2011). Generally, these metals are not degradable with any kind of environmental chemicals or microbial attack and remain in the environment for a very long time. They are often transported from soil and water sources and deposited into various tissues of plants and animals causing long-term deleterious effects on recipient species. Various human organs such as the liver, kidneys, lungs, bones, and brain can be highly affected due to chronic exposure to heavy metals (Tchounwou et al., 2012). Both essential and toxic elements if excessively present are of concern in groundwater investigations. Long-time exposure to copper (Cu) in potable water can lead to copper toxicities which results in liver and kidney damage, anemia, hepatic cirrhosis, and corrosion of the basal ganglia (Harris and Gitlin, 1996). High levels of zinc (Zn) in the drinking water can lead to stomach cramps, neurological problems, vomiting (Hooper et al., 1980). Manganese (Mn) is an essential element for human body which is a significant cofactor for a variety of enzymes in the brain (Hurley and Keen, 1987). In a study of the rural area Araihazar in Bangladesh, it was found that elevated levels of Mn exposure in drinking water may hinder learning mathematics in elementary school children (Khan et al., 2012). An extreme level of iron (Fe) accumulation is associated with Parkinson disease, hyperkeratosis, cardiovascular disease, Huntington disease, diabetes mellitus, pigmentation changes, Alzheimer disease, kidney, liver, respiratory, and neurological disorders (Powers et al., 2003; Kell, 2010; Farina et al., 2013). Over consumption of chromium (Cr) in the body may create health risks including the damage of liver, kidney, nose, lungs, and possible asthma attacks (Kleefstra et al., 2004). Cadmium toxicity is linked with the damage to the cardiovascular system, kidneys, and bones (Fang et al., 2014). The types of the bedrock and the pH value also play important roles for the presence of such elements (Gore et al., 2010). According to WHO, 80% of diseases arise due to contaminated groundwater (Smith et al., 2000). Therefore, it is necessary to protect the quality of water particularly groundwater as this is mostly used for drinking purposes.

The UN Agenda 2030 and the Sustainable Development Goals (SDGs) have given fair significance to the goals that are “by 2030, improve water quality by reducing pollution, eliminating dumping and minimizing release of hazardous chemicals and materials, halving the proportion of untreated wastewater and substantially increasing recycling and safe reuse globally” (UN, 2017). Population growth led to a demand for resources for industrialization and urbanization worldwide (Boojhawon and Surroop, 2021). In a developing country like Bangladesh, groundwater pollution by heavy metals causes environmental risk which may have a negative impact on the environment, and the effects may be irreparable. Savar is a rapidly growing industrial area of Bangladesh which is located near the capital city of Dhaka and many industries like garments, textile mills, electronic equipment, leather materials, chemicals, paper, fertilizers, metals, and miscellaneous manufactures have been established in the area. Industrial development causes pollution in both surface and groundwater in many areas of Bangladesh (Rahman et al., 2020). As an economic zone of Bangladesh, Savar Upazila is expanding its industrial area very quickly which may pose a great threat to the groundwater due to untreated and contaminated industrial wastes and debris. This necessitates the investigation of the quality of the groundwater used for drinking purposes by the inhabitants of Savar Upazila. The aim of the present study was to monitor the physicochemical properties and the levels of different elements (Cu, Cd, Cr, Fe, Mn, and Zn) for assessing the groundwater quality of Savar Upazila of Dhaka of Bangladesh.

2. METHODOLOGY

2.1 Description of the study area and water sampling

Our study sites were in the Savar Upazila which has an area of about 280 km^2 and is the second largest Upazila of Dhaka District located on the northern side of the district. The geographical position of the studied area lies between 23°44'N and 24°12'N latitude and between 90°11'E and 128 90°22'E longitude. This is one of the most densely populated areas in the country which consists of a total population of about 1.39 million people. The northern side of the Upazila is bounded by Kaliakair and Gazipur Sadar Upazilas, Keraniganj Upazila is on the south side, Dhamrai and Singair Upazilas are found on the West and on the eastern side, Mirpur, Mohammadpur, Pallabi, and Uttara thanas are found. This studied region is a rapidly growing industrial and urbanized area of the country and surrounded by the Bangshi, Dhaleswari, Karnatali, and Turag Rivers.

2.2 Sample collection and preservation

A total of 38 groundwater samples (S1-S38) from different places of Savar Upazila adjacent to Dhaka City of Bangladesh were collected in the month of July, 2022 (Figure 1). The geographical positions of the selected sampling points were determined by Global Positioning System (GPS). To get fresh groundwater samples free from any kind of unwanted debris, the tap was run for 10 min before sampling and then the representative water samples (500 mL) were taken in acid-washed, cleaned plastic bottles which were rinsed three times with sampled water. The collected samples were shifted immediately to the Laboratory. The pH of the studied samples was measured by Hanna Instrument and some other physicochemical parameters such as total dissolved solids (TDS), electrical conductivity (EC), and temperature were analyzed by using a multiparameter analyzer EZDO 7200. For the analysis of six selected heavy metals (Cu, Cd, Cr, Fe, Mn, and Zn), the collected samples were then filtered using Whatman filter paper (number 42), acidified with 2 mL of 65% nitric acid (Merck, Germany) per litre of water for the removal of microbial growth, chemical absorption and precipitation (Singare et al., 2013), and then preserved in a refrigerator at 4ºC until final analysis.

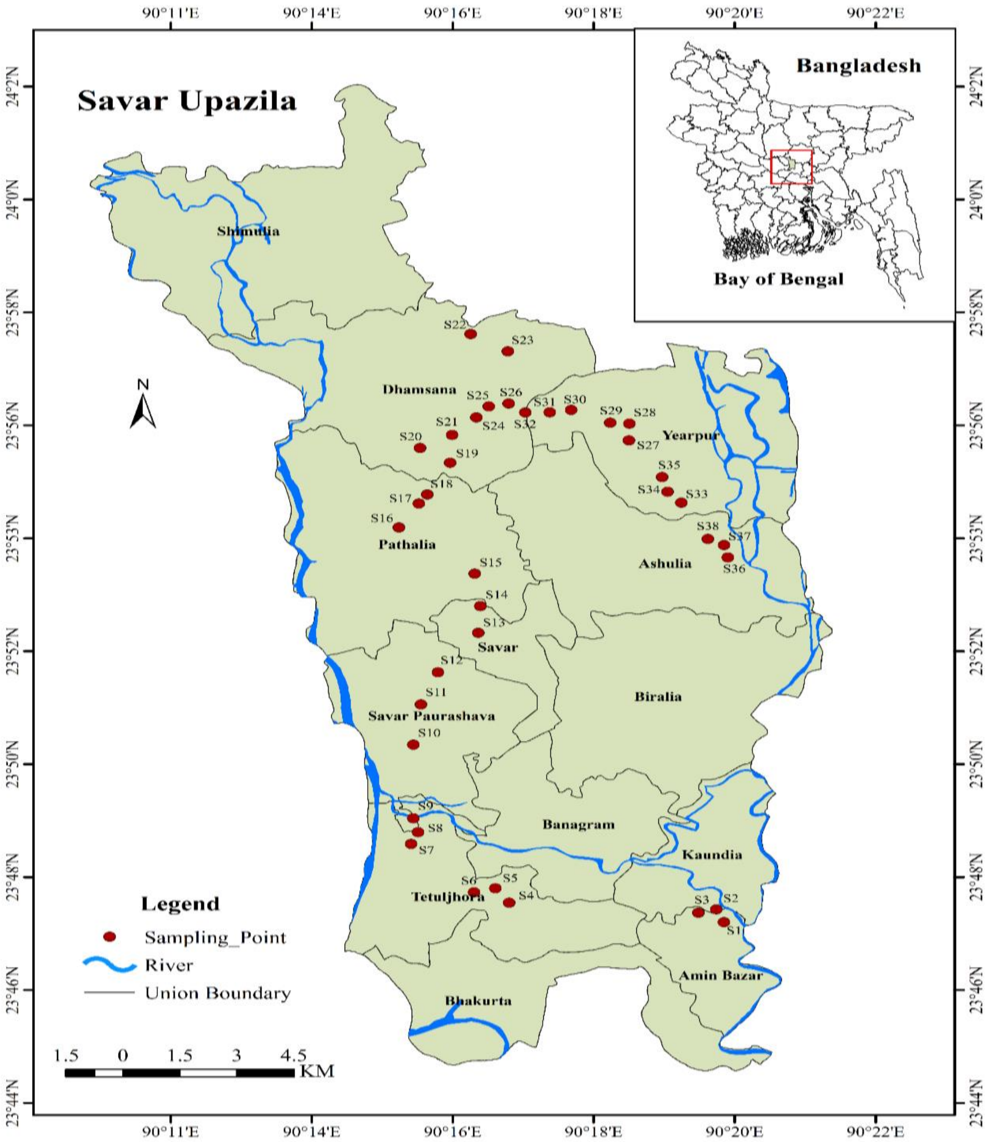

Figure 1. Map of the sampling points of the Savar Upazila, Dhaka, Bangladesh

2.3 Reagents and standards

Analytical grade reagents and calibration standards without any further treatment were used throughout the study. The six different metal standards of Fe, Zn, Mn, Cr, Cu, and Cd with a concentration of 1,000 mg/L were obtained from inorganic ventures, USA. Reference standards with different concentrations and the reagent blank solution for escaping the risk of contamination during sample preparation and analysis were prepared with deionized distilled water.

2.4 Analysis of metals

The selected groundwater samples were analyzed by flame atomic absorption spectroscopy (AAS) (Model: AA-7000, Shimadzu Corporation, Japan) for this study. Background correction of the machine was done using the deuterium-arc lamp. An aliquot of the samples was injected into the air acetylene flame for six chosen metals (Fe, Zn, Mn, Cr, Cu, and Cd) using a Shimadzu auto sampler ASC-7000. The operating conditions (shown in Table 1) for the Flame AAS were followed by the instrument manufacturer's specifications. A blank reading was taken to allow background correction and necessary corrections were made during the calculation of concentration of our desired elements. The value of the blank sample was deducted from the studied groundwater samples to make sure that the equipment read only the particular values of heavy metals.

Table 1. The instrumental settings of AAS for metal analysis of groundwater samples of Savar Upazila

Elements	Wavelength	Lamp current	Slit width	Gas flow rate
Cd	228.8 nm	8 mA	0.7 nm	1.8 L/min
Cr	357.9 nm	10 mA	0.7 nm	2.8 L/min
Mn	279.5 nm	10 mA	0.2 nm	2.0 L/min
Cu	324.8 nm	6 mA	0.7 nm	1.8 L/min
Fe	248.3 nm	12 mA	0.2 nm	2.2 L/min
Zn	213.9 nm	8 mA	0.7 nm	2.0 L/min

2.5 Groundwater quality index (WQI) analysis

The Department of Environment's (DoE) standard for Bangladesh groundwater quality was used to determine the WQI using four steps (Rahaman et al., 2020). Firstly, the weight (w_i) was assigned on a scale of 1 to 5 based on the likelihood that each parameter (pH, TDS, EC, Fe, Mn, Cu, Zn, Cd, and Cr) would have an adverse effect on human health (Tabrez et al., 2022). Secondly, the following equation was used to obtain the relative weight (W_i).

$$W_i = \frac{w_i}{\sum_{i=1}^{n} w_i} \quad (1)$$

Where; w_i=each parameter's weight and n=total number of parameters.

Thirdly, the quality rating scale (q_i) was derived by using the formula:

$$q_i = \frac{C_i}{S_i} \times 100$$

Where; C_i=each parameter's concentration in mg/L and S_i=groundwater standard value for a specific parameter as set by the DoE in mg/L. Finally, after calculating the sub index (SI) for each parameter, the WQI was computed by summing the SIs. The equations are:

$$SI_i = W_i \times q_i \quad (2)$$

$$WQI = \sum SI_i \quad (3)$$

Where; SI_i=subindex for i^{th} parameter, q_i=quality rating scale for i^{th} parameter, and W_i=relative weight of i^{th} parameter. Each parameter's relative weights (W_i) have been calculated and given in Table 2.

2.6 Statistical analysis

Data for different physicochemical parameters and heavy metals of groundwater samples of the studied region of Dhaka were analyzed statistically using the Microsoft Excel 2016 software and the analyzed data were presented as mean±standard deviation (SD).

Table 2. Relative weight of drinking water quality parameters

Chemical parameters	DoE standard	Weight (w_i)	Relative weight (W_i)	Reference
pH	8.5	4	0.1176	Tabrez et al. (2022)
TDS	1,000	4	0.1176	Tabrez et al. (2022)
EC	1,000	4	0.1176	Tabrez et al. (2022)
Fe	1	4	0.1176	Tabrez et al. (2022)
Mn	0.1	4	0.1176	Tabrez et al. (2022)
Cu	1	3	0.0882	Tabrez et al. (2022)
Zn	5	1	0.0294	Tabrez et al. (2022)
Cd	0.005	5	0.1471	Tabrez et al. (2022)
Cr	0.05	5	0.1471	Tabrez et al. (2022)

3. RESULTS AND DISCUSSION

3.1 Physicochemical characteristics of groundwater of Savar Upazila

Different physicochemical parameters (pH, TDS, EC, and temperature) of the studied groundwater samples of Savar Upazila were analyzed and the obtained results were presented in Table 3. In our present study, the pH of the water samples from different regions of Savar Upazila ranged from 6.99-7.62. The value of pH is a traditional measuring parameter for water that affects biological and chemical reactions. The solubility and toxicity of chemicals and heavy metals in the water can be highly affected based on the level of pH in the water (EPA, 2012). Low level of pH in drinking water has a profound effect on pipes which may be degraded and may increase the level of toxic metals in the water supply, causing health issues if consumed. Besides, water containing high pH provides an unpleasant taste and has certain concerns such as skin and eye irritations (Fink, 2005). The average (±SD) pH value of groundwater samples of Savar was obtained at 7.24 (±0.28) which is slightly alkaline in nature. According to the water quality standards of WHO (2011) and DPHE, Bangladesh (2019), the pH of drinking water should be between 6.5 and 8.5 and the measured pH of the water of the studied region is within the allowable limit. A similar study in Savar Upazila documented the mean pH value of 6.90 which also followed the standard range of WHO (2011) and DPHE, Bangladesh (2019) (Hasan et al., 2022). The level of pH in the water of Dhaka metropolitan city was obtained (6.54±0.42) which was found slightly acidic in nature (Sharmin et al., 2020) while the mean pH was characterized as alkaline (8.07±0.51) in an industrial area of Narayanganj City (Rahman et al., 2020).

One of the most important parameters for drinking water quality assessment is TDS which is comprised of dissolved substances and organic matter in water. The mean±SD of TDS value in this study was reported 181.63±82.69 mg/L which was under the permissible limit proposed by different national and international authorities. The highest TDS was obtained in the S1 site and the value was 437 mg/L, while the lowest TDS value was 73 mg/L obtained in the S24 site. The mean TDS was reported at 270.80 mg/L in groundwater samples of Savar Upazilla in another study done by Hasan et al. (2022). In other recent studies, the mean TDS value was reported 321.30 mg/L, 242.25 mg/L, 237.5 mg/L, and 162.2 mg/L in Dhaka Metropolitan City, Rangpur, Gazipur, and Jamalpur area of Bangladesh, respectively (Bakali et al., 2014; Zakir et al., 2018; Saha et al., 2019; Sharmin et al., 2020). Another essential water quality assessment parameter is EC which was measured in the collected water samples of our studied region and it was observed that the EC varies from 117-654 µS/cm which was within the standard limit set by WHO (2011) and USEPA (2009). EC has a strong relationship with TDS. The mean value of EC in the studied area was 265.47 µS/cm which was lower than the studies performed in Chittagong, Rajshahi, and Sylhet (Ahmed et al., 2010; Mostafa et al., 2017; Ahmed et al., 2019). As TDS and EC values are interdependent, high values are a sign of salt in the groundwater (Hasan et al., 2022). According to Bangladesh standards, the water temperature (ºC) should be ranged between 28 and 30, and in our study done in Savar Upazila, it varies from 27.7-30.5ºC with a mean of 29.40±0.70ºC which was within the safe limit of DPHE, Bangladesh (2019) standard.

Table 3. The physicochemical properties of studied groundwater samples of Savar Upazila

Sampling station	Longitude	Latitude	pH	TDS (mg/L)	EC (µS/cm)	Temperature (ºC)
S1	90.3277	23.7876	6.94	437	654	28.9
S2	90.3268	23.7881	7.01	247	361	29.6
S3	90.3259	23.7887	7.04	312	470	29.6
S4	90.2802	23.7951	7.25	204	308	29.6
S5	90.2798	23.7942	7.00	215	327	29.7
S6	90.2713	23.7933	7.22	227	342	29.8
S7	90.2573	23.8116	7.15	222	334	29.6
S8	90.2575	23.8140	7.52	213	317	29.5
S9	90.2569	23.8165	7.68	250	376	29.5
S10	90.2574	23.8391	7.30	182	274	29.8
S11	90.2592	23.8510	6.92	257	385	29.7
S12	90.2632	23.8605	6.80	212	315	29.5
S13	90.2727	23.8721	7.02	137	203	29.6
S14	90.2732	23.8800	7.62	105	164	29.5
S15	90.2719	23.8896	6.85	103	160	29.1
S16	90.2539	23.9032	7.72	87	131	29.8
S17	90.2592	23.9115	7.29	177	263	29.7
S18	90.2603	23.9128	6.56	97	147	30.5
S19	90.2661	23.9223	7.51	106	157	28.5
S20	90.2589	23.9267	7.40	112	165	27.7
S21	90.2665	23.9305	7.55	104	156	27.8
S22	90.2709	23.9603	7.66	78	117	28.2
S23	90.2797	23.9551	7.58	86	132	27.7
S24	90.2723	23.9368	7.36	73	119	30.0
S25	90.2757	23.9362	7.30	107	163	29.8
S26	90.2768	23.9364	7.00	236	393	29.6
S27	90.2927	23.9367	7.30	252	376	29.7
S28	90.2896	23.9372	7.30	170	255	29.7
S29	90.2838	23.93715	7.20	171	256	29.9
S30	90.3080	23.9308	7.10	157	236	29.7
S31	90.3074	23.9321	7.02	158	238	29.6
S32	90.3039	23.9341	7.02	158	237	29.6
S33	90.3207	23.9105	7.69	396	265	28.7
S34	90.31874	23.9131	7.10	184	274	28.7
S35	90.3187	23.9136	7.20	205	312	28.6
S36	90.3309	23.8972	7.60	183	282	28.6
S37	90.3308	23.8980	7.40	192	291	28.8
S38	90.3296	23.8989	7.05	90	133	30.0
Mean			7.24	181.63	265.47	29.4
SD			0.28	82.69	112.07	0.71
DPHE, Bangladesh (2019)			6.5-8.5	1,000	-	20-30
BIS (2012)			6.5-8.5	500-2,000	-	20-30
WHO (2011)			6.5-8.5	500	1,500	-
USEPA (2009)			6.5-8.5	500	750	-

3.2 Concentration of different heavy metals in groundwater of Savar Upazila

The concentrations of the six selected heavy metals (Cu, Cd, Cr, Fe, Mn, and Zn) in the studied groundwater of 38 different locations of Savar Upazila of Dhaka are shown in Table 4. Figure 2 illustrates the average concentration of the studied heavy metals found in collected groundwater samples of the Savar

Area of Dhaka, Bangladesh. The obtained results for heavy metals concentration showed the decreasing order of Fe > Zn > Mn > Cr > Cu > Cd and the Fe was detected in the highest amount with an average (±SD) of 0.136 (±0.188) mg/L. The value of Fe in the selected locations of the Upazila ranged from Below the Detection Limit (BDL) to 0.756 mg/L, where the maximum Fe was detected in the S9 site of the Upazila. The maximum acceptable limit of Fe in drinking water is 1 mg/L according to the drinking water standard set by the DPHE, Bangladesh (2019) and all the samples showed lower levels of Fe than the DPHE, Bangladesh (2019) standard, though groundwater from four different locations, S7, S9, S11, and S12, of Savar crossed the international regulations which is 0.3 mg/L set by Health Canada (2001), USEPA (2009), BIS (2012), and WHO (2011). The obtained concentration of Fe in studied groundwater ties well with the previous study done in the Savar Upazila wherein the content of Fe in groundwater was 0.18 mg/L which was also lower than the standard water quality guideline values (Hasan et al., 2022). The reported Fe level was compared with other studies done in different cities of Bangladesh and it was observed that the level of Fe in the groundwater of the Savar Area was comparatively lower than Sylhet, Rajshahi, Chittagong, Lakshipur, which exceeded the standard limits, while studies from Dhaka Metropolitan City, Gazipur which are near to our studied region also maintained drinking water standards (Table 5). From the study of Sharmin et al. (2020) and Bodrud-Doza et al. (2020), it was clearly seen that the Fe level in Dhaka City was 0.0896 mg/L, and 0.208 mg/L, respectively, which was also within the safe limit of drinking water quality.

Table 4. Concentration (mg/L) of heavy metals and estimated WQI value with the classification of studied groundwater of Savar Upazila

Sampling station	Zn	Fe	Mn	Cr	Cd	Cu	WQI	Classification
S1	0.4891	0.0078	0.0126	0.0358	BDL	0.0077	34.90	Excellent
S2	0.0524	0.0563	0.0108	0.0358	BDL	0.0115	29.45	Excellent
S3	0.0460	BDL	0.0042	0.0393	BDL	0.0045	31.06	Excellent
S4	0.0588	0.0089	0.3213	0.0184	BDL	0.0071	59.47	Good
S5	0.0615	BDL	0.0135	0.0271	BDL	0.0071	25.72	Excellent
S6	0.0830	0.0606	0.0130	0.0289	BDL	0.0090	27.56	Excellent
S7	0.0654	0.4020	0.0387	0.0098	0.0017	0.0052	33.69	Excellent
S8	0.1368	0.2448	0.0515	0.0150	0.0037	0.0083	41.03	Excellent
S9	0.0691	0.7564	0.2320	0.0202	0.0012	0.0052	63.74	Excellent
S10	0.0190	0.0002	0.0343	0.0011	0.0019	0.0102	25.52	Excellent
S11	0.1407	0.6681	0.0232	0.0098	0.0019	0.0127	36.39	Excellent
S12	0.0668	0.5862	0.0179	0.0115	0.0030	0.0096	36.94	Excellent
S13	0.1107	0.2943	0.0303	BDL	0.0015	0.0285	25.47	Excellent
S14	0.0185	BDL	0.0011	0.0011	0.0019	0.0096	19.85	Excellent
S15	0.1272	0.1015	0.0090	0.0011	0.0012	0.0228	18.96	Excellent
S16	0.5229	0.0218	0.0128	0.0092	0.0039	0.0228	29.70	Excellent
S17	0.0194	BDL	0.0076	0.0116	0.0026	0.0071	27.29	Excellent
S18	0.0493	0.0175	0.0053	0.0092	0.0027	0.0064	23.51	Excellent
S19	0.0119	BDL	0.0222	0.0116	0.0031	0.0071	28.70	Excellent
S20	0.0133	BDL	0.0121	0.0139	0.0032	0.0083	28.51	Excellent
S21	0.0119	BDL	0.0083	0.0116	0.0029	0.0071	26.50	Excellent
S22	0.2928	0.0724	0.0098	0.0185	0.0031	0.0127	29.74	Excellent
S23	1.7110	0.2071	0.0290	0.0162	0.0038	0.0096	35.94	Excellent
S24	0.0488	0.1723	0.0152	0.0140	0.0075	0.0117	42.57	Excellent
S25	BDL	0.1845	0.0167	0.0089	0.0060	0.0103	37.77	Excellent
S26	BDL	0.1740	0.0203	0.0073	0.0052	0.0075	39.03	Excellent
S27	BDL	0.1671	0.0191	0.0174	0.0013	0.0167	27.75	Excellent
S28	0.0303	0.0017	0.0195	0.0089	0.0037	0.0110	30.30	Excellent
S29	BDL	0.1340	0.0235	0.0073	0.0009	0.0117	23.60	Excellent
S30	0.1066	0.0313	0.0215	0.0089	BDL	0.0096	23.15	Excellent

Table 4. Concentration (mg/L) of heavy metals and estimated WQI value with the classification of studied groundwater of Savar Upazila (cont.)

Sampling station	Zn	Fe	Mn	Cr	Cd	Cu	WQI	Classification
S31	BDL	0.0278	0.0211	0.0106	BDL	0.0089	21.11	Excellent
S32	0.0550	0.0174	0.0215	0.0140	BDL	0.0082	21.95	Excellent
S33	0.0677	0.1793	0.0627	0.0056	0.0045	0.0103	42.92	Excellent
S34	BDL	0.1462	0.0199	0.0123	0.0037	0.0082	33.85	Excellent
S35	0.0303	0.2558	0.0223	0.0157	0.0039	0.0103	37.88	Excellent
S36	0.0860	0.0609	0.0215	0.0292	0.0005	0.0110	29.44	Excellent
S37	BDL	0.0696	0.0255	0.0190	0.0037	0.0110	36.31	Excellent
S38	0.0147	0.0296	0.0203	0.0174	BDL	0.0103	20.33	Excellent
Mean	0.1210	0.1360	0.0335	0.0146	0.0022	0.0104	31.78	
S.D.	0.2890	0.1880	0.0600	0.0096	0.0019	0.0049	9.644	

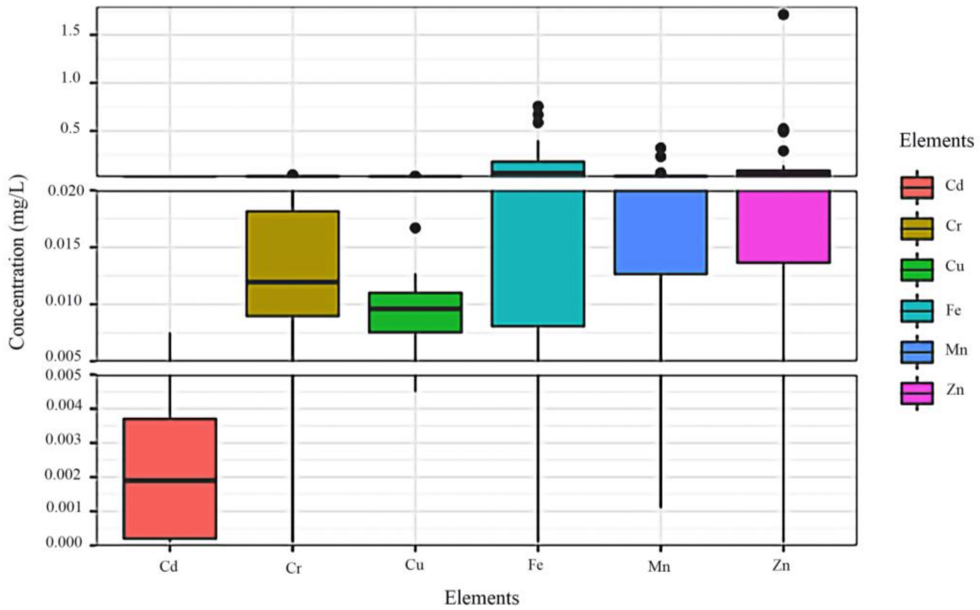

Figure 2. Comparison of the mean concentration (mg/L) of heavy metals in groundwater of Savar

The level of Zn was also analyzed in studied groundwater samples and it was detected in the highest amount followed by Fe. The mean concentration of Zn in the Upazila was documented as 0.121±0.289 mg/L which was far below the tolerable limit provided by both national and international regulatory bodies. The range for Zn in the groundwater of our study area in Upazila was BDL-1.711 mg/L. The location S23 contained the maximum level of Zn (1.711 mg/L) in the present study. Our study clearly showed that there is no risk in the consumption of water on the basis of the concentration of Zn. A similar study in a coastal area in Bangladesh showed the mean concentration of Zn (0.17333±0.12146) mg/L that followed the standard range of Health Canada (2001), USEPA (2009), BIS (2012), and WHO (2011) (Deeba et al., 2021). Another study showed the average concentration of Zn (0.010383±0.010199) mg/L that was absolutely fine according to drinking water quality standards and consistency with our study (Bodrud-Doza et al., 2016). Previous studies from Rakib et al. (2020), Bhuiyan et al. (2016), and Sharmin et al. (2020) detected the concentration of Zn in different cities in Bangladesh and the value was 0.420, 0.02164, and 0.0053 mg/L, respectively, which were all within the water quality guidelines.

The concentration of Mn in the groundwater of the Savar area varied from 0.0011-0.3213 mg/L, reaching an average of 0.0335 mg/L. The maximum allowed limit of Mn in drinking water is 0.4 mg/L and 0.1 mg/L set by WHO (2011) and DPHE, Bangladesh (2019) respectively. In addition, Health Canada (2001) and USEPA (2009) determined a maximum limit of 0.05 mg/L for Mn. Though the samples from S4

(0.3213 mg/L) and S9 (0.232 mg/L) sites exceeded the limit of DPHE, Bangladesh (2019), Health Canada (2001), and USEPA (2009), the level of Mn was still within the permissible limit of WHO (2011). The Mn content from the present investigation was compared with recent past findings. Our data are consistent with other studies done on the groundwater samples of Dhaka city nearby Savar Upazila. The mean concentration of Mn was determined to be 0.057 mg/L, and 0.058 mg/L in Dhaka city groundwater samples studied by Bodrud-Doza et al. (2020) and Sharmin et al. (2020), respectively. Another study described the mean Mn value as 0.22693 mg/L which was under the permissible limit of WHO (2011), but exceeded the DPHE, Bangladesh (2019) standard (Deeba et al., 2021) (Figure 3).

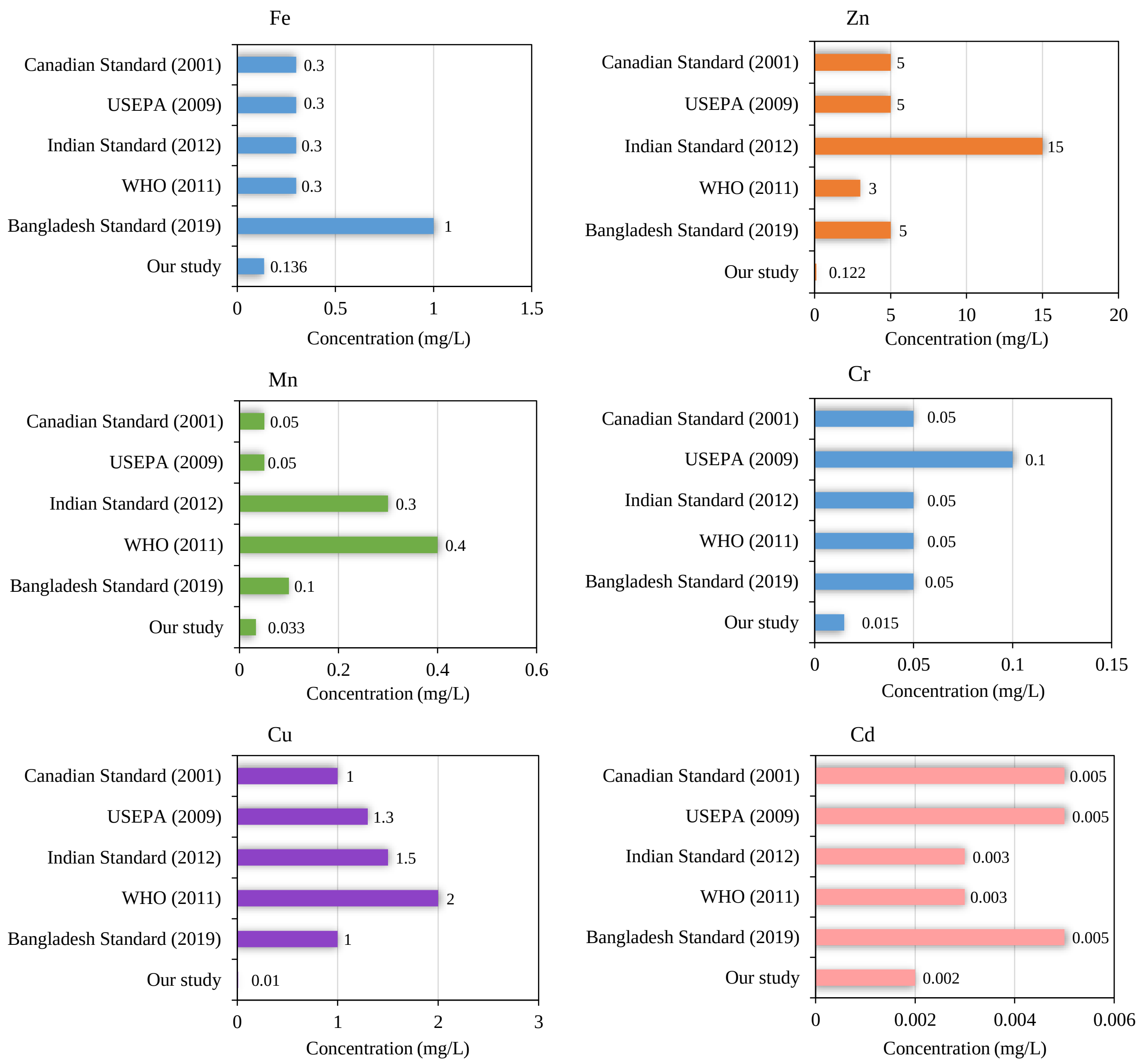

Figure 3. Maximum permitted limits of heavy metals (mg/L) for drinking water quality

The concentrations of Cr and Cu in the groundwater of the Savar Upazila of Dhaka varied among the sampling locations (S1-S38) and the mean±SD of the metals were 0.0146±0.0096 and 0.010±0.0049 mg/L, respectively. Hasan et al. (2022) found a similar amount of Cr from the groundwater samples of Savar Upazila and it was reported as 0.01152 mg/L. Cr is a vital ingredient for the human metabolism of sugar and fat, but excessive amounts from eating, inhalation, or skin contact may be harmful to one's health (Rahman et al., 2020). Both the Cr and Cu levels in the studied Upazila were found

Table 5. Comparison of measured parameters of studied groundwater of Savar Upazila with other different locations of Bangladesh

Locations	Physicochemical parameters				Mean concentration (mg/L) of heavy metals						Ref
	pH	TDS (mg/L)	EC (µS/cm)	Temperature (ºC)	Fe	Zn	Mn	Cr	Cu	Cd	
Present Study	7.24	181.63	265.47	29.4	0.136	0.121	0.0335	0.015	0.0104	0.002	
Savar	6.90	270.80	-	20.1-22.7	0.18	-	0.24	0.01152	-	-	Hasan et al. (2022)
Dhaka City	6.54	321.30	459	-	0.0896	0.0053	0.0588	0.0015	0.0096	-	Sharmin et al. (2020)
Dhaka City	7.32	72.22	120.64	-	0.208	0.021	0.057	-	-	-	Bodrud-Doza et al. (2020)
Gazipur	6.70	237.5	38.25	-	0.08	0.20	0.29	-	0.08	-	Bakali et al. (2014)
Narayangonj	8.068	554.5	1350	-	-	-	-	0.0709		0.0067	Rahman et al. (2020)
Chuadanga	6.47	-	686.10	-	1.303	0.0801	0.284		0.3347	0.03316	Bodrud-Doza et al. (2019)
Kushtia	-	-	-	-	5.072	1.501	1.614	0.031	1.078	0.0019	Islam and Mostafa (2021)
Faridpur	6.9122	-	788.7667	-	5.952	0.0103	0.00064	-	-	-	Bodrud-Doza et al. (2016)
Joypurhat	6.74	222.0	336.1	-	0.42	-	-	3.10	0.76	-	Kumar et al. (2017)
Tangail	6.6	243.66	-	-	2.7265	-	0.97	-	-	-	Uddin et al. (2013)
Gopalganj	7.53	1,635.04	3,206.95	27.41	5.12	-	0.20	-	-	-	Rahman et al. (2018)
Lakshmipur	7.0369	1,135.086	-	-	3.235	0.02164	0.652	-	-	-	Bhuiyan et al. (2016)
Rajshahi	7.0	241.65	454.98	-	2.23	0.18	2.2	-	0.39	0.016	Mostafa et al. (2017)
Sylhet	6.64	-	302.47	25.53	5.91	-	0.30	-	-	-	Ahmed et al. (2019)
Chittagong	7.38	787.0	2,822.1	-	1.67	0.015	0.19	0.005	0.010	-	Ahmed et al. (2010)
Khulna	7.8	1,043	1,777	-	1.21	-	-	-	-	-	Adhikary et al. (2012)
Cox's Bazar	7.69	522.61	804	27.95	1.255	0.173	0.227	0.068	0.057	0.017	Deeba et al. (2021)
Rangpur	6.63	361.58	242.25	28.32	-	-	-	-	-	-	Saha et al. (2019)
Sathkhira	6.03	3,691	7,135.67	-	4.9	0.42	-	-	-	-	Rakib et al. (2020)
Jamalpur	6.87	162.2	270.5	-	0.363	0.020	1.075	0.006	0.008	-	Zakir et al. (2018)

under the permissible limit of drinking water quality. The observed data, therefore, indicated that the groundwater samples of Savar Upazila were not contaminated with Cr and Cu. A minor quantity of Cu is required for maintaining sound health and if exposed to excess concentration, these may cause various health complications such as gastrointestinal distress, anemia, and disrupt liver and kidney functions. A similar kind of research on Dhaka City detected almost the same amount of Cu (0.0096 mg/L) in groundwater (Sharmin et al., 2020). Deeba et al. (2021) reported a high level of Cu (0.05680±0.01522 mg/L) at the South Eastern Coastal Area, Cox Bazar District which was beyond the limit of both WHO (2011) and DPHE, Bangladesh (2019). Most of the cities of Bangladesh showed a higher level of Cu than the present report, while in the Jamalpur Area of Bangladesh, the amount of Cu was detected at a low level in groundwater (Table 5). In a study of the Chittagong area, the level of Cu (0.010 mg/L) was found in a similar amount that was obtained in our present study. Except for Kushtia, the concentration of Cd (0.0022 mg/L) in our study was lower than the other cities of Bangladesh (Table 5). In the studied location of S24, the maximum amount (0.0075 mg/L) of Cd was detected and the level exceeded the maximum allowable limit of drinking water which is a great concern. Among all the samples of groundwater, only two samples (S24 and S25) were beyond the limit of DPHE, Bangladesh (2019) as the standard determined the maximum level as 0.005 mg/L.

3.3 Water quality index (WQI)

The suitability for human consumption of our studied groundwater was assessed by measuring the Water quality index (WQI) value. The results indicated that the range varied from location to location of Savar Upazila of Dhaka of Bangladesh. Following the standard equations, the obtained result was presented in Table 4 and the result revealed that the WQI for the selected samples ranged between 18.96 and 63.74 with a mean value of 31.78. WQI is usually categorized into five different classes from excellent to unsuitable for drinking (Table 6). The method used for WQI indicated that the permissible WQI value for drinking is considered 100 and the water quality will be categorized as poor and hence unsuitable for drinking if the value surpassed this tolerable limit. Our study reported that almost all the studied groundwater quality was excellent while a sample from the site S4 was categorized as good (59.47) and hereafter, it can be inferred that the groundwater is safe and suitable for drinking purposes by the dwellers of the Savar Upazila of Dhaka, Bangladesh.

Table 6. Drinking water categories based on WQI values (Ramakrishnaiah et al., 2009; Tabrez et al., 2022).

WQI range	Category of water	Number of location	Percentage of groundwater samples
<50	Excellent water	37	97.44
50-100	Good water	1	2.56
100-200	Poor water	-	-
200-300	Very poor water	-	-
>300	Unsuitable for drinking	-	-

4. CONCLUSION

The major focus of the present investigation was to monitor the groundwater quality of Savar Upazila of Dhaka for evaluating its suitability for drinking purposes. Safe drinking water is obligatory for human health which will save us from many water-borne diseases. The residents of the Upazila almost entirely rely on groundwater for their daily activities such as drinking, bathing, washing, and other household activities. The obtained physicochemical parameters (pH, TDS, EC, and temperature) and the level of six different metals (Cu, Cd, Cr, Fe, Mn, and Zn) in almost all the studied water were within the guideline values proposed by different regulatory authorities. The level of Mn in two different sites of Savar exceeded the desirable standard limit of Bangladesh while the limit was within the maximum allowed level of WHO (2011). Though the concentration of Cd in two different locations was beyond the maximum residue limit, the measured WQI values of the groundwater samples of Savar area revealed that all the water samples were in the good to excellent category and recommended as suitable for drinking and may be considered as safe reserves of water for future use. Therefore, it can be concluded that our studied groundwater quality is considered suitable for drinking on the basis of the level of our studied physicochemical parameters and WQI analysis. This study can help the national authorities of Bangladesh to know the current status of the drinking water quality of the Savar Upazila and may aide taking appropriate measures for maintaining the standard quality of drinking water for safe consumption in the future. It is recommended that seasonal variation should be measured in the regions and periodic monitoring should be carried out to retain the standards of the water and, thus, to maintain functional human health.

ACKNOWLEDGEMENTS

The authors are thankful to Agrochemical and Environmental Research Division, Institute of Food and Radiation Biology, Atomic Energy Research Establishment, Bangladesh Atomic Energy Commission, Dhaka, Bangladesh for providing laboratory support during the study.

REFERENCES

Adhikary SK, Elahi MM, Hossain AI. Assessment of shallow groundwater quality from six wards of Khulna City Corporation, Bangladesh. International Journal of Applied Sciences and Engineering Research 2012;1(3):488-98.

Ahmed MJ, Ahsan A, Haque MR, Siraj S, Bhuiyan MH, Bhattacharjee SC, et al. Physicochemical assessment of surface and groundwater quality of the greater Chittagong region of Bangladesh. Pakistan Journal of Analytical and Environmental Chemistry 2010;11(2):Article No. 11.

Ahmed N, Bodrud-Doza M, Islam SD, Choudhry MA, Muhib MI, Zahid A, et al. Hydrogeochemical evaluation and statistical analysis of groundwater of Sylhet, North-Eastern Bangladesh. Acta Geochimica 2019;38:440-55.

Bakali B, Mia MY, Zakir HM. Water quality evaluation of Tongi Area in Bangladesh: An impact of industrialization. Journal of Chemical, Biological and Physical Sciences 2014;4(2): 1735-52.

Bakis R, Tuncan A. An investigation of heavy metal and migration through groundwater from the landfill area of Eskisehir in Turkey. Environmental Monitoring and Assessment 2011;176:87-98.

Bhuiyan MA, Bodrud-Doza M, Islam AT, Rakib MA, Rahman MS, Ramanathan AL. Assessment of groundwater quality of Lakshimpur District of Bangladesh using water quality indices, geostatistical methods, and multivariate analysis. Environmental Earth Sciences 2016;75:1-23.

Bhuiyan MA, Ganyaglo S, Suzuki S. Reconnaissance on the suitability of the available water resources for irrigation in Thakurgaon District of northwestern Bangladesh. Applied Water Science 2015;5:229-39.

Bodrud-Doza M, Islam SD, Hasan MT, Alam F, Haque MM, Rakib MA, et al. Groundwater pollution by trace metals and human health risk assessment in central west part of Bangladesh. Groundwater for Sustainable Development 2019;9:Article No. 100219.

Bodrud-Doza M, Islam SD, Rume T, Quraishi SB, Rahman MS, Bhuiyan MA. Groundwater quality and human health risk assessment for safe and sustainable water supply of Dhaka City dwellers in Bangladesh. Groundwater for Sustainable Development 2020;10:Article No. 100374.

Bodrud-Doza MD, Islam AT, Ahmed F, Das S, Saha N, Rahman MS. Characterization of groundwater quality using water evaluation indices, multivariate statistics and geostatistics in central Bangladesh. Water Science 2016;30(1):19-40.

Boojhawon A, Surroop D. Impact of climate change on vulnerability of freshwater resources: A case study of Mauritius. Environment, Development and Sustainability 2021;23(1):195-223.

Bureau of Indian Standard (BIS). Indian Standard for Drinking Water as Per BIS Specifications (IS 10500). 2nd ed. New Delhi, India: BIS; 2012.

Health Canada. Canadian Council of Ministers of the Environment: Water Quality Guidelines for the Protection of Aquatic Life: Canadian or B.C. Health Act Safe Drinking Water Regulation BC Reg 230/92, and 390 Sch 120. Health Canada; 2001.

Deeba F, Rahman SH, Kabir MZ, Dina NT, Das SC, Sultana S, et al. Heavy metals distribution and contamination in groundwater of the South Eastern Coastal Area of Bangladesh. Journal of Water and Environment Technology 2021; 19(5):267-82.

Department of Public Health Engineering (DPHE). Guidelines for Water Quality Standards in Bangladesh Perspective. Dhaka, Bangladesh: Ministry of Health of Bangladesh; 2019.

Environmental Protection Agency (EPA). Guidelines for Water Reuse, EPA/600/R-12/004. Washington, United States: USEPA Office of Wastewater Management; 2012.

Fang Y, Sun X, Yang W, Ma N, Xin Z, Fu J, et al. Concentrations and health risks of lead, cadmium, arsenic, and mercury in rice and edible mushrooms in China. Food Chemistry 2014; 147:147-51.

Farina M, Avila DS, Da Rocha JB, Aschner M. Metals, oxidative stress and neurodegeneration: A focus on iron, manganese and mercury. Neurochemistry International 2013;62(5):575-94.

Fink JC. Establishing a Relationship between Sediment Concentrations and Turbidity. the Effects of Urbanization on Baird Creek [dissertation]. Green Bay, University of Wisconsin; 2005.

Gore F, Fawell J, Bartram J. Too much or too little? A review of the conundrum of selenium. Journal of Water and Health 2010;8(3):405-16.

Gupta N, Khan D, Santra S. An assessment of heavy metal contamination in vegetables grown in wastewater-irrigated areas of Titagarh, West Bengal, India. Bulletin of Environmental Contamination and Toxicology 2008;80(2): 115-8.

Harris ZL, Gitlin JD. Genetic and molecular basis for copper toxicity. The American Journal of Clinical Nutrition 1996; 63(5):836S-841S.

Hasan M, Islam MA, Alam MJ, Rahman M, Hasan MA. Hydrogeochemical characterization and quality assessment of groundwater resource in Savar: An industrialized zone of Bangladesh. Environmental Monitoring and Assessment 2022;194(8):Article No. 549.

Hooper PL, Visconti L, Garry PJ, Johnson GE. Zinc lowers high-density lipoprotein-cholesterol levels. Jama 1980;244(17): 1960-1.

Hurley LS, Keen CL. Manganese: Trace Elements in Human and Animal Nutrition. New York: Academic Press; 1987.

Islam MA, Rahman MM, Bodrud-Doza M, Muhib MI, Shammi M, Zahid A, et al. A study of groundwater irrigation water quality in south-central Bangladesh: A geo-statistical model approach using GIS and multivariate statistics. Acta Geochimica 2018;37:193-214.

Islam MS, Mostafa M. Groundwater quality and risk assessment of heavy metal pollution in middle-west part of Bangladesh. Journal of Earth and Environmental Science Research 2021;143:Article No. 3.

Islam SD, Majumder RK, Uddin MJ, Khalil MI, Alam MF. Hydrochemical characteristics and quality assessment of groundwater in Patuakhali District, southern coastal region of Bangladesh. Exposure and Health 2017;9:43-60.

Kell DB. Towards a unifying, systems biology understanding of large-scale cellular death and destruction caused by poorly liganded iron: Parkinson's, Huntington's, Alzheimer's, prions, bactericides, chemical toxicology and others as examples. Archives of Toxicology 2010;84:825-89.

Khan SA, Uddin Z, Ihsanullah ZA. Levels of selected heavy metals in drinking water of Peshawar City. International Journal of Science and Nature 2011;2(3):648-52.

Khan K, Wasserman GA, Liu X, Ahmed E, Parvez F, Slavkovich V, et al. Manganese exposure from drinking water and children's academic achievement. Neurotoxicology 2012; 33(1):91-7.

Kleefstra N, Bilo HJ, Bakker SJ, Houweling ST. Chromium and insulin resistance. Nederlands Tijdschrift Voor Geneeskunde 2004;148(5):217-20.

Kumar D, Zakir H, Maleque M, Seal H. Evaluation of groundwater quality with special emphasis on heavy metal contamination in major areas of Joypurhat District. Journal of Chemical, Biological and Physical Sciences 2017;7(4):819-34.

Lu Y, Tang C, Chen J, Yao H. Assessment of major ions and heavy metals in groundwater: A case study from Guangzhou and Zhuhai of the Pearl River Delta, China. Frontiers of Earth Science 2016;10(2):340-51.

Mostafa MG, Uddin S, Haque A. Assessment of hydro-geochemistry and groundwater quality of Rajshahi City in Bangladesh. Applied Water Science 2017;7(8):4663-71.

Nweke OC, Sanders III WH. Modern environmental health hazards: A public health issue of increasing significance in Africa. Environmental Health Perspectives 2009;117(6): 863-70.

Powers KM, Smith-Weller T, Franklin GM, Longstreth WT, Swanson PD, Checkoway H. Parkinson's disease risks associated with dietary iron, manganese, and other nutrient intakes. Neurology 2003;60(11):1761-6.

Rahaman MF, Ali MS, Arefin R, Mazumder QH, Majumder RK, Jahan CS. Assessment of drinking water quality characteristics and quality index of Rajshahi City, Bangladesh. Environment, Development and Sustainability 2020;22:3957-71.

Rahman MA, Paul M, Bhoumik N, Hassan M, Alam M, Aktar Z. Heavy metal pollution assessment in the groundwater of the Meghna Ghat industrial area, Bangladesh, by using water pollution indices approach. Applied Water Science 2020;10(8):1-15.

Rahman MM, Islam MA, Bodrud-Doza M, Muhib MI, Zahid A, Shammi M, et al. Spatio-temporal assessment of groundwater quality and human health risk: A case study in Gopalganj, Bangladesh. Exposure and Health 2018;10:167-88.

Rakib M, Sasaki J, Matsuda H, Quraishi SB, Mahmud MJ, Bodrud-Doza M, et al. Groundwater salinization and associated co-contamination risk increase severe drinking water vulnerabilities in the southwestern coast of Bangladesh. Chemosphere 2020;246:Articlw No. 125646.

Ramakrishnaiah C, Sadashivaiah C, Ranganna G. Assessment of water quality index for the groundwater in Tumkur Taluk, Karnataka State, India. E-Journal of Chemistry 2009;6(2): 523-30.

Saha N, Rahman MS, Ahmed MB, Zhou JL, Ngo HH, Guo W. Industrial metal pollution in water and probabilistic assessment of human health risk. Journal of Environmental Management 2017;185:70-8.

Saha S, Reza A, Roy MK. Hydrochemical evaluation of groundwater quality of the Tista floodplain, Rangpur, Bangladesh. Applied Water Science 2019;9(8):1-12.

Sharmin S, Mia J, Miah MS, Zakir H. Hydrogeochemistry and heavy metal contamination in groundwaters of Dhaka metropolitan city, Bangladesh: Assessment of human health impact. HydroResearch 2020;3:106-17.

Singare PU, Talpade MS, Dagli DV, Bhawe VG. Heavy metal content in water of Bhavan's College Lake of Andheri, Mumbai. International Letters of Chemistry, Physics and Astronomy 2013;8(2):94-104.

Singh R, Ahirwar NK, Tiwari J, Pathak J. Review on sources and effect of heavy metal in soil: Its bioremediation. International Journal of Research in Applied, Natural and Social Sciences 2018;2008:1-22.

Smith AH, Lingas EO, Rahman M. Contamination of drinking-water by arsenic in Bangladesh: A public health emergency. Bulletin of the World Health Organization 2000;78(9): 1093-103.

Tabrez S, Zughaibi TA, Javed M. Water quality index, *Labeo rohita*, and *Eichhornia crassipes*: Suitable bio-indicators of river water pollution. Saudi Journal of Biological Sciences 2022;29(1):75-82.

Tchounwou PB, Yedjou CG, Patlolla AK, Sutton DJ. Heavy metal toxicity and the environment. In: Molecular, Clinical and Environmental Toxicology. Volume 3: Environmental Toxicology. Springer Basel; 2012. p. 133-64.

Uddin M, Rahaman M, Mondal M. Assessment of ground water quality at Mawlana Bhashani Science and Technology University Campus, Tangail, Bangladesh. Journal of Environmental Science and Natural Resources 2013;6(2): 177-80.

United Nations (UN). Sustainable Development Goal 6: Clean Water and Sanitation in the Sustainable Development Goals Report. UN; 2017.

United States Environmental Protection Agency (USEPA). National Primary Drinking Water Regulations. US EPA; 2009.

World Health Organization (WHO). Guidelines for Drinking-Water Quality: Volume 38. 4th ed. WHO; 2011.

Zakir HM, Akter A, Rahman A, Sharmin S, Arafat MY. Groundwater quality evaluation for irrigation and drinking utilities collected from Sadar Upazila of Jamalpur District, Bangladesh. Asian Journal of Applied Chemistry Research 2018:2(1); 1-13.

Examining Soil Erodibility, Soil pH, and Heavy Metal Accumulation in a Nickel Ore Mine: A Case Study in Tubay, Agusan del Norte, Philippines

Jobelle Capilitan[1,2*], Abigael Balbin[1,2], Ian Dominic Tabañag[1,3], and Evelyn Taboada[1]

[1]School of Engineering, University of San Carlos, Talamban, Cebu City 6000, Philippines
[2]Caraga State University, Butuan City, Agusan del Norte 8600, Philippines
[3]Philippine Council for Industry, Energy, and Emerging Technology Research and Development, Department of Science and Technology (DOST-PCIEERD), Bicutan, Taguig City 1631, Philippines

ARTICLE INFO

Received: 15 Dec 2022
Received in revised: 1 Mar 2023
Accepted: 12 Mar 2023
Published online: 8 May 2023
DOI: 10.32526/ennrj/21/202200271

Keywords:
Agusan del Norte Province/ Heavy metals accumulation/ Nickel ore mine/ Soil erodibility/ Soil pH/ USLE

*** Corresponding author:**
E-mail: jjcapilitan@carsu.edu.ph

ABSTRACT

Mining activity always presents threats to soil and water pollution. As an extractive industry, it disturbs the ground and the biodiversity associated with soil and plants. Its operations have led to severe geological and environmental problems, including the depletion of land and water resources, geological dangers, and ecological landscape devastation that may have accelerated the desertification of mining areas. This case study analyzed the soil's physical and chemical properties in a nickel laterite mine, including soil erodibility K factor, soil pH, and heavy metal accumulation, as a basis for establishing mine management protocol during and post-mining operations in Tubay, Agusan del Norte, Philippines. Results determined a slightly alkaline pH level. An estimate of soil erodibility ranging from 0.016 to 0.066 was determined using the USLE-K factor, with the highest erodibility at Mine 7, where % silt is high and % sand is lowest. X-ray fluorescence (XRF) spectroscopy was used to analyze soil samples. The findings show that Ni, Fe, Co, and Mn in the soil were above the WHO-permitted limits. The surface soil had mean values of 9,239 ppm for nickel, 302,618 ppm for iron, 639 ppm for cobalt, and 5,203 for manganese. Heavy metals in soil may be consumed by crops and pollute land and water.

1. INTRODUCTION

Nickel ore mining plays an immense role in the global nickel industry (Trescases, 1997) by creating valuable technologies and infrastructure, including operations in agriculture. They are Mg-rich or ultramafic rocks with primary Ni contents ranging from 0.2 to 0.4 percent through a lateritisation process (Golightly, 1981). The depth of a nickel laterite profile usually ranges from 10 meters to 50 meters below the surface (Nahon, 1986) and is excavated through open-cut mining methods, removing wasteful overburden.

Mining has long been vital to human economic prosperity; however, the economic and technological demands have increased mining disturbance over the years. Its operations have resulted in severe geological and environmental issues, such as the degradation of land and water supplies, geologic hazards, and ecological landscape destruction, potentially contributing to the desertification of mining areas (Jha, 2020; Lei et al., 2016; Wu, 2017; Zhang et al., 2011). Generally, nickel extraction significantly impacts water and sediment quality (Schmidt et al., 2012) if left uncontrolled and improperly managed.

The Philippines possesses vast copper, gold, nickel, and other minerals. Its economic expansion is fueled by the mining sector, both directly and indirectly. Approximately 24 nickel ore mines are active in the country. As of 2021, Region XIII - Caraga has fourteen (14) companies focused on exploring Nickel ore mines, with one location in Tubay, Agusan del Norte. The Tubay nickel ore mining site is about 10 km south of Lake Mainit, with rolling mountains, dense flora on the sidehills, and flatlands that encircle the coastline area. It receives 2,125.7 millimeters of precipitation annually with an average of 157 days with precipitation, according to climatic normal data

Citation: Capilitan J, Balbin A, Tabañag ID, Taboada E. Examining soil erodibility, soil pH, and heavy metal accumulation in a nickel ore mine: A case study in Tubay, Agusan del Norte, Philippines. Environ. Nat. Resour. J. 2023;21(3):279-289. (https://doi.org/10.32526/ennrj/21/202200271)

from 1991 to 2021. The mining site is in a nearby community where the livelihood of the locals is mainly rice farming and fishing. Due to its proximity, the co-existence of mining and agriculture poses harm, especially in extreme rainfall events where erosion and sediment transfer can be a significant threat.

Soil erodibility, K, as a measure of soil sensitivity to erosion, shows the intrinsic susceptibility or resistance of the soil to erosive action and is the most critical component in predicting soil loss (Huang et al., 2022; Ostovari et al., 2019; Salehi-Varnousfaderani et al., 2022). The K factor in Universal Soil Loss Equation or USLE (Wischmeier and Smith, 1986) is most adopted in soil erosion models (Auerswald et al., 2014; Kulikov et al., 2020), represented by Equation 1:

$$A = R \times K \times L \times S \times C \times P \qquad (1)$$

Where; A is average annual soil loss, R is the rainfall factor, K is the soil erodibility factor, LS is the topography factor, C is the crop factor, and P is the control practice factor.

USLE is a conservation tool generally accepted and widely used in various kinds of research regarding soil management. It includes the estimation of erosion for land use (Okorafor et al., 2018), upland erosion (Almasalmeh et al., 2021; National Institute of Hydrology, 2017), specific sediment yield (Rajbanshi and Bhattacharya, 2020), erosion patterns (Pijl et al., 2020), as well as estimating soil erosion in mining (Ramli et al., 2020). This model and its subsequent Revised (RUSLE) and Modified (MUSLE) variants are commonly used worldwide, with a significant number of developed models (Aksoy et al., 2019; Hajigholizadeh et al., 2018). It has inspired several other models, including LISEM (Limburg Soil Erosion Model) (de Roo et al., 1998), WEPP (Water Erosion Prediction Project) (Morgan and Nearing, 2011), EUROSEM (European Soil Erosion Model) (Morgan et al., 1998), EGEM (Ephemeral Gully Erosion Model), and PESERA (Pan European Soil Erosion Risk Assessment) (Okorafor et al., 2018) and EPIC - Erosion Productivity Impact Calculator (Williams et al., 1990).

Sediment mobility through runoff directly impacts land and water quality. They are classified as significant contaminants in the aquatic environment (Frey et al., 2015; Milligan and Law, 2013). In a scenario where there is an anthropogenic activity like mining, heavy metals such as Ni, Fe, and Al are present in high concentrations (Apodaca et al., 2018; Gavhane et al., 2021) in mine waste (tailings dams and overburden waste rock sites) (El Azhari et al., 2017; Chileshe et al., 2020; Lei et al., 2016). In turn, heavy metals could endanger agricultural resources due to surface or groundwater pollution, offsite contamination via water erosion, and uptake by plants (Chileshe et al., 2020; Shirani et al., 2020). Additionally, fishes tend to experience sublethal stress from suspended sediments (Binet et al., 2018; Wang et al., 2020) rather than lethality. Additionally, natural weathering, such as wind erosion, rainfall flushing, and sulfide oxidation in the discarded overburden, may release heavy metals into soils, surface water, and groundwater, posing environmental hazards (Bartzas et al., 2021).

It is crucial to understand the possible impacts of the open-pit nickel mining site on its surrounding environment. Hence, the USLE-K factor is used in this study to examine the soil erodibility in Tubay, Agusan del Norte. Heavy metal accumulation in the soil is determined using X-ray fluorescence (XRF) spectroscopy. XRF spectroscopy has proven to be a dependable method for an in-situ soil analysis to evaluate metal pollution (Peralta et al., 2020). This study can produce insight that gives awareness to the locality, better mine management, and a decision tool for policymaking in the local government unit.

2. METHODOLOGY

2.1 Study site background

The research area (Figure 1) is a nickel ore mining facility located in the northern part of Agusan del Norte, Mindanao, Philippines, under the jurisdiction of the municipalities of Tubay, Jabonga, and Santiago, Agusan del Norte. The mine site lies within 9°10'30" and 9°19'30" north latitude and 125°29'30" to 125°33'30" east longitude. It is within a 4,995-hectare Mineral Production Sharing Agreement (MPSA) contract area. Boundaries of the mining site include the western range approximately 10 km south of Lake Mainit, rolling mountains with thick and varied vegetation on the sidehills, and flatlands that encompass the coastal area. According to the soil order classification by the Bureau of Soil and Water Management (BSWM) (DA-BSWM, 2017), the soil study site falls under Acrisols. The subsurface of Acrisols has more clay than the topsoil due to pedogenetic processes (particularly clay migration) that result in an argic subsoil horizon. Acrisols have low-activity clays and low base saturation in the 50-100 cm deep range. They are most prevalent in tropical, subtropical, and warm temperate regions where forests dominate native vegetation (IUSS and WRB, 2015). Acrisols are taxonomically related to USDA soil order Oxisols. Oxisols are tropical and subtropical soils with a high level of weathering and are rich in minerals such as quartz, kaolinite, and iron oxides (USDA-NRCS, 2023).

The mining facility has twelve areas for exploration; however, during the study, four of the mining sites were inaccessible, and safety was at risk; hence this study focuses on seven mining sites: 1, 2, 3, 4, 5, 7, and 9. The discharge area (10) was also included. As of 2021, an estimated 20% of the mined area was undergoing rehabilitation leaving at most 80% bare soil.

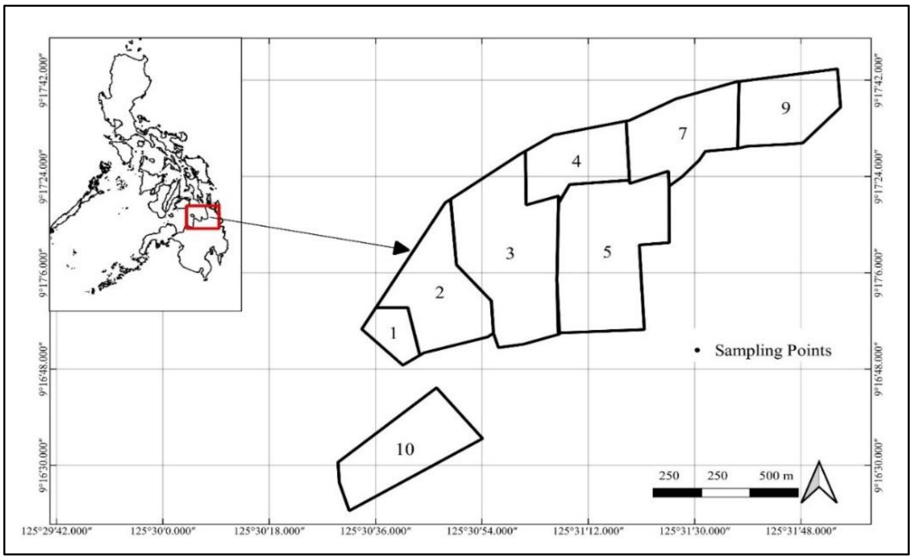

Figure 1. Study area for soil quality assessment

2.2 Soil sampling and analysis

A total of eight mine locations served as test zones for soil samples, including the discharge area, to evaluate the soil composition in the nickel laterite mine. This research utilized a composite soil sampling method. Each mine site had 18 subsamples taken, totaling 144 subsamples. Each subsample was mixed and blended to create three homogenous samples, while large rocks and other elements were removed. Forty-eight (48) composite samples, 24 at the mine surface and 24 at the settling ponds, were analyzed for this study.

Soil samples were collected from 0 to 15 centimeters from the top surface. Each sample was air-dried and sieved through a 2 mm mesh for analysis, including particle size distribution of sand, silt, clay, soil texture, organic matter content, and pH. Table 1 presents the summary of the soil analysis conducted in this study.

Particle Size Analysis (PSA) determines the soil's relative sand, silt, and clay amounts. These size fractions constitute the mineral component of the soil when combined. The particle distribution of sand (0.05-2.00 mm), silt (0.05-2.00 mm), clay (<2 mm), and clay were determined using the sieve analysis and hydrometer method (Gee and Or, 2004) and USDA triangle (USDA, 1987) for soil texture. Table 2 presents the common soil textural classes according to USDA.

Table 1. Summary of soil analysis conducted in this study

Parameter	Method	Reference
% Sand	Sieve analysis	Gee and Or (2004)
% Silt	Sieve analysis/ Hydrometer test	Gee and Or (2004)
% Clay	Sieve analysis/ Hydrometer test	Gee and Or (2004)
Organic matter	Loss of ignition	Nelson and Sommers (2018); ASTM D7348 (Webster, 2003)
Soil pH	Electrochemical	ASTM D4972-19
Heavy metals (Ni, Co, Fe, Mn)	XRF	
Soil erodibility factor, K	USLE	Wischmeier and Smith (1986)

Table 2. USDA textural classes of soil (coarse and moderately coarse)

Common names of soils (general texture)	Sand	Silt	Clay	Textural class
Sandy soils (coarse texture)	86-100	0-14	0-10	Sand
	70-86	0-30	0-15	Loamy sand
Loamy soils (moderately coarse texture)	50-70	0-50	0-20	Sandy loam

Soil texture affects nutrient retention, water storage, drainability, and other agricultural variables. Clay soils hold more nutrients and water than sandy soils.

Soil organic matter plays a crucial role in soil quality and erodibility. It influences how soil particles aggregate to form a stable soil structure (Kumar and Kushwaha, 2013). It is measured using the Loss of Ignition (LOI) method (Nelson and Sommers, 2018), Equation 2:

$$\%OM = \frac{W_{105} - W_{450}}{W_{105}} \times 100 \qquad (2)$$

Soil samples (2mm) were carefully weighed and put into a 450°C preheated porcelain crucible. Samples were dried in the furnace at 105°C for 16 hours and left cool in a desiccator, establishing the initial weight (W_{105}). The samples were heated again to 450°C in the furnace for 16 hours. After cooling, the final weight (W_{450}) is determined. According to (Murphy et al., 2012), soil organic matter levels are based on the soil textural class, ranging from extremely low (1%) to average (2% to 4%) to very high (>5%) by weight.

Soil erodibility factor K of the Universal Soil Loss Equation (USLE) (Wischmeier and Smith, 1986) determines the estimated soil erodibility in the area. Soil erodibility is a critical indicator for assessing a soil's erosion vulnerability, with a mathematical formula shown in Equation 3:

$$K = 2.1\, M^{1.14} \times 10^{-4}\,(12 - OM) + 3.25(S - 2) + 2.5(P - 3) \qquad (3)$$

Where; M, Equation 4, is the texture of the top 15 cm of soil, Equation 4, relating to soil particles, OM is the organic matter content determined in the laboratory, as described in Table 2 using the Loss of Ignition (LOI) method (Nelson and Sommers, 2018), and S and P are codes for soil structure and permeability, respectively. The percentage of clay is 0.002 mm, the percentage of silt is 0.002-0.050 mm, and the percentage of extremely fine sand is 0.05-0.10 mm (USDA, 1987).

$$M = (100 - \%\text{ clay})\,(\%\text{ very fine sand} + \%\text{ silt}) \qquad (4)$$

As the soil texture becomes finer, soil erodibility increases. Increased erodibility readings imply that the soil is more prone to erosion (Kumar and Kushwaha, 2013). Soil erodibility factor ranges from 0.02, the least erodible, to 0.64, for most erodible soils (IWR, 2002). Clay-rich fine-textured soils have low K values ranging from 0.02 to 0.15, while sandy soils range from 0.05 to 0.20. Medium textured soils, including silt loam, have moderate K values, 0.25 to 0.40. Silty soils are the most erodible, crust readily, and have a high drainage rate (Pijl et al., 2020).

Soil samples at MS and SP passing through a 2 mm sieve were evaluated for pH level. Soil pH measures soil acidity or alkalinity and is crucial in agricultural productivity management (Gozukara et al., 2022). Nutrient mobilization, microbial activity, and plant uptake increase with ideal pH. In this study, soil pH determination used an electrochemical method described by (Webster, 2003) and ASTM D4972-19. Twenty (20) g of air-dried soil was added with 20 mL of reagent water, covered, and continuously stirred at 240 rpm for 5 min. The soil suspension was allowed to stand for about 1 hour to allow most of the suspended clay to settle out from the suspension. After which, the electrodes for pH reading was immersed into the suspension. Soil pH ranges from <5.5 as strongly acidic to strongly alkaline at >9.2. The ideal soil pH is between 6.5 and 7.5, approaching neutral (Khan et al., 2022).

X-ray fluorescence (XRF) spectroscopy, a non-destructive method in determining the elemental makeup of substances, was used to analyze heavy metals in the soil samples, including Ni, Co, Fe, and Mn. Powdered soil samples (approximately 50 µm) were placed in a 30 mm outer ring cup with holes lined with a 3.6 µm Mylar film and were analyzed using the Epson 1 EDXRF machine. The maximum permissible limits for Ni, Co, Fe, and Mn according to World Health Organization (WHO, 1996) are listed in Table 3.

Table 3. Maximum allowable limit of heavy metals concentrations in soil by WHO (1996)

Heavy metal	Maximum permissible level in soil in ppm
Ni	50
Fe	50,000
Co	50
Mn	2,000

2.3 Statistical analyses

Pearson's correlation analysis determined the relationships between the soil erodibility indicators and their influencing factors. The linear regression method evaluated the correlations between soil erodibility indicators and soil surface characteristics.

3. RESULTS AND DISCUSSION

3.1 Particle size distribution, soil texture, organic matter, and K factor

Table 4 displays the soil particle distribution (% sand, % silt, % clay) and organic matter content within the research region's 0-15 cm topsoil. The study region has an average sand content of 90.61 percent, 7.76 percent silt, 1.33 percent clay, and an average organic matter content of 4.33 percent, classified as sandy soil (USDA, 1987). Categorizing by each mine site, each was classified as sandy except for Mine site 7. Mine site 7 falls under the loamy sand classification, which recorded the most significant percentage of silt and the lowest percentage of sand.

Mine site 4 recorded the highest % of sand at 94.46% and the lowest at Mine site 7 (84.78%). Percent silt is also highest at Mine site 4 (8.43%) and lowest in Mine site 2 at 4.07%. Clay concentration in the mining site is generally low, ranging from the highest at 2.72% (discharge) and the least at 1.21% (Mine site 1). By Murphy rating, the site has a high to extremely high OM rating (Murphy et al., 2012), with the highest value at site 5 (7.42%) and the lowest at mine 1 (2.3%). The estimated K values are generally low due to the high sand concentration (Pijl et al., 2020). K factors are most significant at mine site 7, where the percentage of sand is lowest, and silt is the most abundant.

Table 4. Summary data on particle size distribution, soil texture, organic matter, and K factor

Site	Elevation (m)	% Sand	% Silt	% Clay	Soil Texture	% OM	USLE-K
Mine 1	209	92.99	5.80	1.21	Sandy	2.38	0.027
Mine 2	245	94.46	4.07	1.47	Sandy	3.45	0.017
Mine 3	265	93.23	5.15	1.62	Sandy	2.29	0.016
Mine 4	262	90.27	8.43	1.30	Sandy	6.52	0.025
Mine 5	277	91.86	6.90	1.24	Sandy	7.42	0.016
Mine 7	130	84.78	13.54	1.68	Loamy sand	3.38	0.066
Mine 9	238	89.49	8.72	1.79	Sandy	5.91	0.033
Discharge	17	87.83	9.45	2.72	Sandy	3.28	0.045
Mean		90.61	7.76	1.63	Sandy	4.33	0.031

Figure 2 presents the variation of the K factor and the elevation change. The estimated K factor generally decreases at higher altitudes and increases as elevation decrease. Also exhibiting the lowest projected soil erodibility are mines 3 and 5 at higher elevations.

By correlation, as shown in Table 5, the USLE-K factor value correlates positively with silt and clay percentages in the soil and negatively with sand and organic matter. Regression analysis revealed a significant positive relationship between USLE-K and % silt (r=0.78, p=1.93E-05). Consequently, USLE-K has a significant negative correlation between % sand (r=0.80, p=9.44E-06). The indices of soil erodibility and susceptibility to erosion are impacted by soil aggregates (Khanchoul and Boubehziz, 2019; Kumar and Kushwaha, 2013; Madubuike et al., 2020). Given that sandy soils have a low drainage rate, the findings of this study indicating that sand content has a significant negative correlation with the erodibility factor suggest that soils high in the sand can achieve lower erodibility since sand content decreases soil erodibility (Khanchoul and Boubehziz, 2019; Madubuike et al., 2020; Radziuk and Switoniak, 2021).

In contrast, there is a clear positive link between clay and silt. High silt-content soils are more prone to erode due to their ease of detachment and high runoff rate, while clay particles create clumping (Ghosal and Das Bhattacharya, 2020; Radziuk and Switoniak, 2021). As a binder for the aggregates needed for soil structure analysis, clay is essential for calculating the K factor. Clay particles, however, might not combine with water, increasing soil loss.

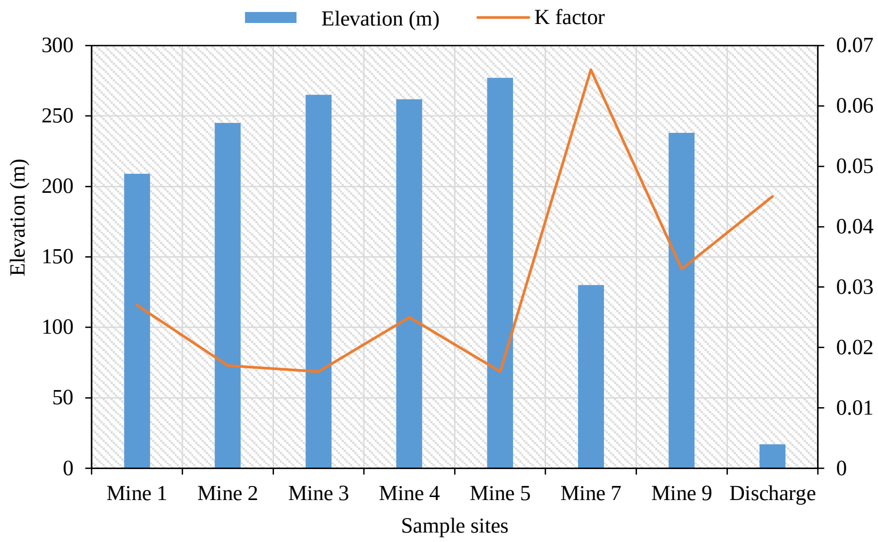

Figure 2. Site elevation (m) vs. K factor

Table 5. The correlation coefficient of soil properties and erodibility factor, K

	% Sand	% Silt	% Clay	Organic matter
1. % Sand	-			
2. % Silt	-0.98	-		
3. % Clay	-0.81	0.68	-	
4. OM	0.09	-0.07	-0.13	-
5. USLE-K	-0.80	0.78	0.65	-0.29

This study shows a significant positive correlation between the percent clay and soil erodibility (r=0.65, p=0.0011), suggesting that a higher percentage of clay in the soil may increase erodibility. Clay-rich soils, however, seem to show considerable resilience to erosion in other studies (Khanchoul and Boubehziz, 2019; Madubuike et al., 2020; Ostovari et al., 2019). The only likely direct source of a positive correlation between clay content and K factor value is a contemporaneous decline in sand content (Radziuk and Switoniak, 2021). The clay content in the soil samples under examination is likely insufficient to generate an aggregate resistant to erosion, but it is sufficient to decrease the soil's permeability and raise the likelihood of surface runoff (Radziuk and Switoniak, 2021).

The association between OM and K is not as strong as in this study's other soil characteristics. OM shows no significant correlation between OM and K (r=0.29, p=0.19). A related study shows that OM in the soil properties may reduce soil erodibility (Madubuike et al., 2020) at the mine site. Higher OM concentrations suggest that soil detachment susceptibility and erosion will decrease (IWR, 2002; Khanchoul and Boubehziz, 2019).

3.2 Soil pH

Overall, the mine site is generally classified as slightly alkaline, as in Figure 3. Soil pH in the settling pond is relatively higher than at the surface, ranging from 7.2 to 8.6 and 7.0 to 8.4, respectively. SP shows a strong alkaline pH value (8.6) in mine 1 and gradually decreases to a moderately alkaline value of 8.2 at the exit. Meanwhile pH level at the surface also recorded a moderately alkaline value of 8.4 at the exit area.

Nevertheless, the surface and settling pond's pH level generally shows values within the acceptable pH. The result suggests that soil at this level is calcareous (Thomas, 1996). Hence, soil acidity and the addition of lime are not a concern. Carbonate-rich soil is said to have the ability to stabilize organic materials due to chemical stabilization mechanisms (Virto et al., 2017). A strong alkaline observed at the settling pond of mine site 1 corroborates an initial high pH level and decreases when mine residues pass through a series of settlings ponds. A correlation coefficient of r=0.70, p=0.0013 suggests a significant positive relationship between pH at the surface and the settling pond.

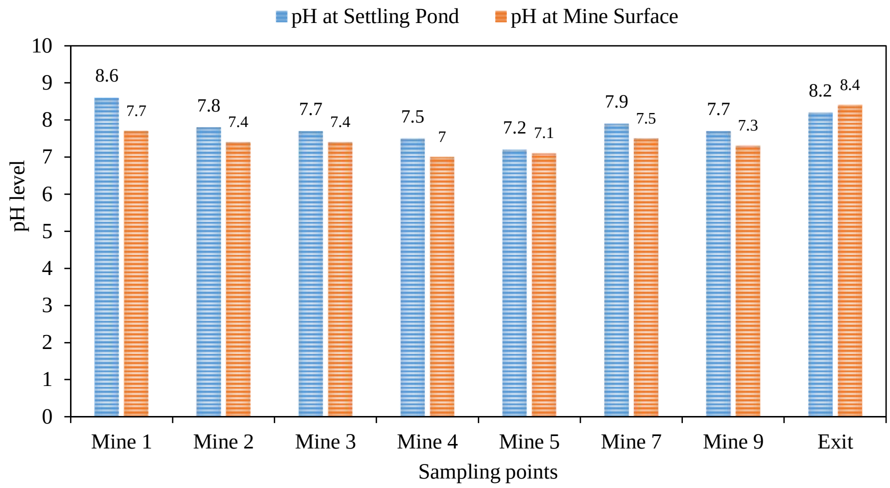

Figure 3. pH Level at the settling ponds (SP) and mine surface (MS)

3.3 Heavy metal concentration

3.3.1 Nickel (Ni)

Nickel concentrations were recorded from a minimum of 6,980 ppm to a maximum of 11,350 ppm at the mine surface, while nickel in settling ponds ranged from 5,000-11,000 ppm, illustrated in Figure 4. These values exceeded the maximum allowable limit (MAL) by WHO at 50 ppm for all mine sites. The recorded concentrations are approximately 130-200 times higher than the allowable limit.

3.3.2. Iron (Fe)

The permissible allowable limit of Fe content in the soil is 50,000 ppm, as recommended by WHO. In Figure 5, the iron concentration recorded higher values than the limit for all mine sites. Fe is found to have a concentration of 185,650-443,100 ppm at MS and 95,250-463,775 ppm at SP.

3.3.3. Cobalt (Co)

WHO recommends a Co concentration of 50 ppm maximum allowable limit in soil. By XRF analysis, the sampling sites exceeded the limit by 8 to 22 times more. The highest Co accumulation at MS was found in Mine sites 3 and 5 at 700 ppm, while 1,125 ppm was recorded in Mine site 5 (SP), as shown in Figure 6.

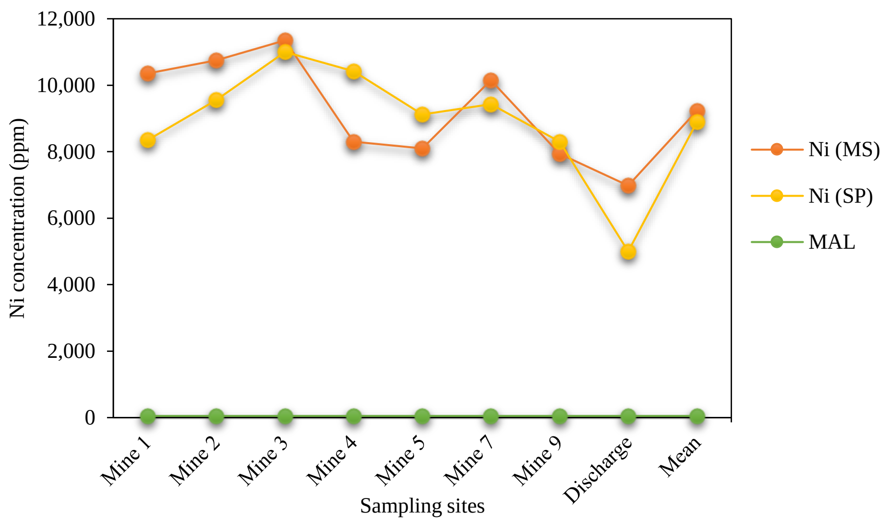

Figure 4. Nickel concentration in the mine surface (MS) and settling pond (SP)

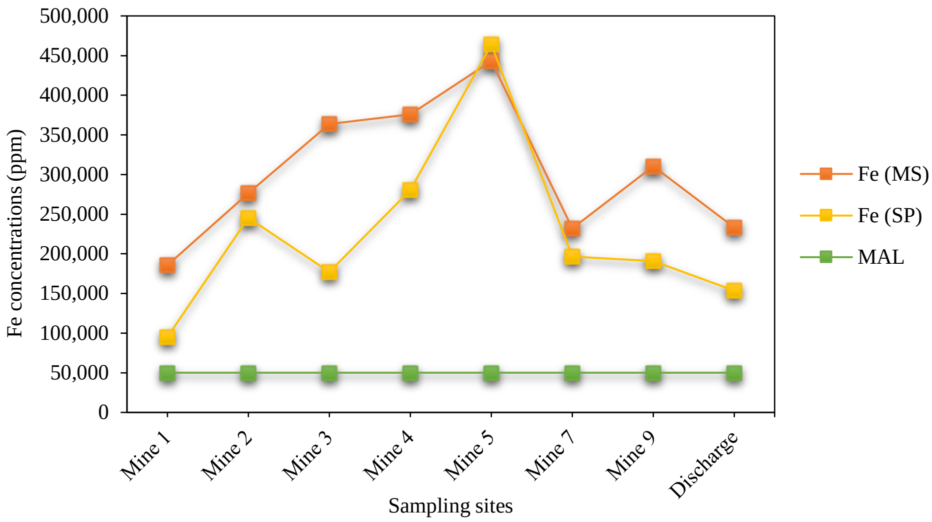

Figure 5. Fe concentrations in the mine surface (MS) and settling pond (SP)

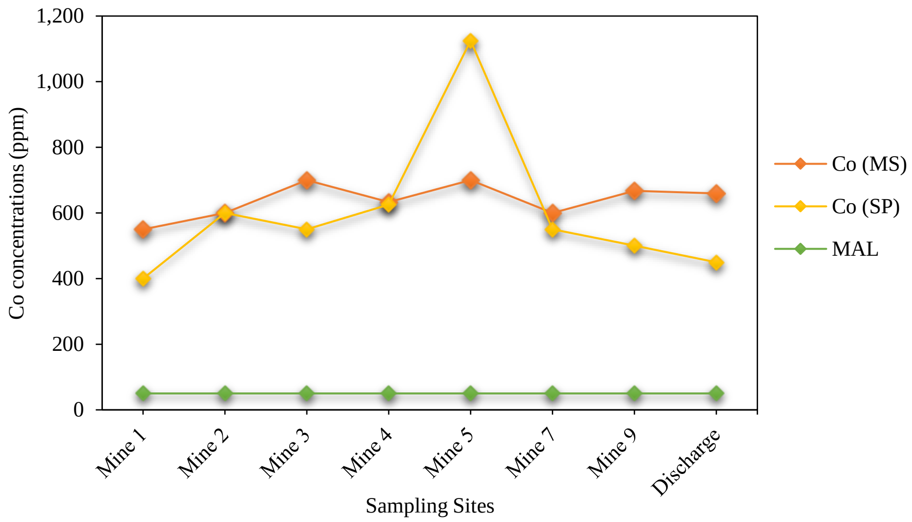

Figure 6. Co concentrations in the mine surface (MS) and settling pond (SP)

3.3.4. Manganese (Mn)

Manganese (Mn) recorded the lowest concentrations compared to WHO values (2,000 ppm), ranging from 3,850-7,500 ppm and 3,300-8,475 ppm at the mine surface and settling pond, respectively, Figure 7. However, the values still exceeded the allowable limit as recommended by WHO, except at Mine site 1 (SP), which has 2,000 ppm, just equivalent to the maximum allowable limit.

3.4. Implications and future work

It is well established that soil is more prone to erosion in areas with a high silt concentration. Due to their ease of detachment and fast flow rate, silt is more sensitive to soil erodibility (IWR, 2002; Radziuk and Switoniak, 2021), while organic matter and a high sand content reduce soil erosion impacts (Chen et al., 2021; Kumar and Kushwaha, 2013; Tian et al., 2022). The area with the highest silt concentration had the highest significant value for K; as a result, soil conservation management has to be given more consideration in this area. However, calibration and validation can improve the K-factor estimations' accuracy. An area-specific map of the soil erodibility may also help plan soil conservation strategies, modeling, and forecasting erosion. Correspondingly, accurate information on the site data is beneficial to prevent soil loss and minimize the consequences on its surroundings, particularly in high rainfall events.

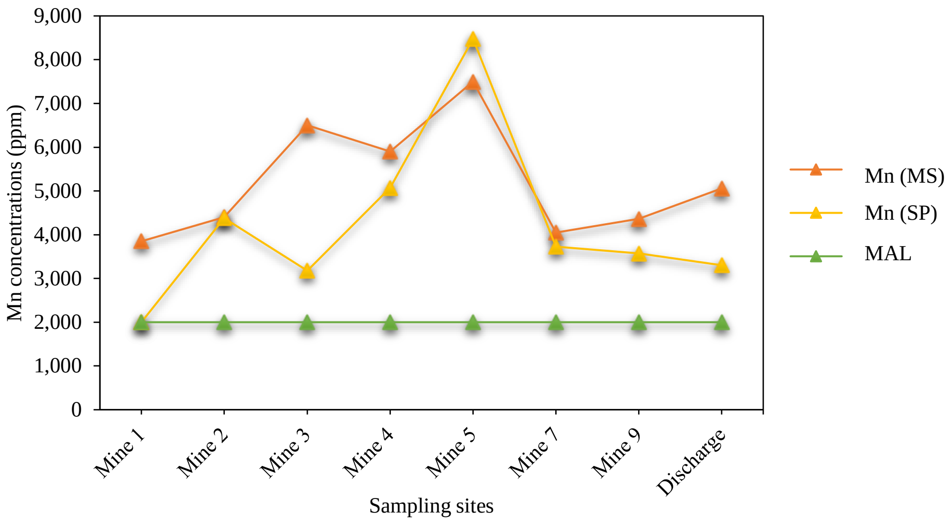

Figure 7. Mn concentrations in the mine surface (MS) and settling pond (SP)

Although the soil pH level in the area is ideal, the overly high presence of heavy metals is alarming. It causes plant growth inhibition, chlorosis, necrosis, and wilting (Bhalerao et al., 2015; Prematuri et al., 2020; Sreekanth et al., 2013). When considering the impact on the food chain, the ingestion of plants from soils with significant levels of heavy metals could be dangerous to human health. Ni also adversely affects marine plants and organisms (Gavhane et al., 2021). Hence, natural farming is not an option before any mine rehabilitation is applied. Post-mining remediation and revegetation may be carefully planned to remove the excess presence of heavy metal in the soil, specifically Ni, Fe, Co, and Mn, and reduce harmful environmental effects and possible re-utilization of the site. Further research should be carried out to study the accumulation of heavy metals in the surrounding environment, especially in crops and waters.

Due to the significant residues of Ni, the possibility of phytomining in the area can also be considered as part of a progressive rehabilitation strategy to re-vegetate huge areas stripped by lateritic nickel mining and generate income by “harvesting” nickel metal. Developing plant-based remediation technologies for Ni-contaminated soils has garnered much interest due to its cost-effectiveness, environmental friendliness, and lack of adverse side effects (He et al., 2012). Hyperaccumulators, plants accumulating high heavy metal concentrations, make excellent models for investigating metals’ uptake, movement, and storage and their evolution and environmental adaptation.

4. CONCLUSION

The nickel ore mining site in Tubay, Agusan del Norte, was subjected to soil erodibility estimate, pH value determination, and heavy metal accumulation (Ni, Fe, Co, Mn). This study has determined an erodibility estimate of 0.016 to 0.066 using the USLE-K erodibility factor formula. The k factor is highest at mining site 7, where sand is the lowest (84.78%), and silt is highest (13.54%). The nickel ore mine has a slightly alkaline pH level at an average soil pH of 7.4 and 7.8 at the surface and settling pond, respectively, within the acceptable range. The heavy metal accumulation of Ni, Fe, Co, and Mn exceeded the recommended permissible limit by WHO. The excessive heavy metal levels in the soil are potentially available for crop intake and may pose a threat to land and water environment pollution, including humans.

ACKNOWLEDGEMENTS

This work is supported by the Department of Science and Technology (DOST) through the Engineering Research and Development for Technology (ERDT) program.

REFERENCES

Aksoy H, Mahe G, Meddi M. Modeling and practice of erosion and sediment transport under change. Water (Switzerland) 2019;11(8):1-9.

Almasalmeh O, Saleh AA, Mourad KA. Soil erosion and sediment transport modelling using hydrological models and remote sensing techniques in Wadi Billi, Egypt. Modeling Earth Systems and Environment 2021;8:1215-26.

Apodaca DC, Domingo JPT, David CPC, David SD. Siltation load contribution of nickel laterite mining on the coastal water quality of Hinadkaban Bay, Surigao Provinces, Philippines.

IOP Conference Series: Earth and Environmental Science 2018;191(1):Article No. 012048.

Auerswald K, Fiener P, Martin W, Elhaus D. Use and misuse of the K factor equation in soil erosion modeling: An alternative equation for determining USLE nomograph soil erodibility values. Catena 2014;118:220-5.

El Azhari A, Rhoujjati A, El Hachimi ML, Ambrosi J-Paul. Pollution and ecological risk assessment of heavy metals in the soil-plant system and the sediment-water column around a former Pb/Zn-mining area in NE Morocco. Ecotoxicology and Environmental Safety 2017;144:464-74.

Bartzas G, Tsakiridis PE, Komnitsas K. Nickel industry: Heavy metal(loid)s contamination - sources, environmental impacts and recent advances on waste valorization. Current Opinion in Environmental Science and Health 2021;21:Article No. 100253.

Bhalerao SA, Sharma AS, Poojari AC. Toxicity of nickel in plants. International Journal of Pure and Applied Bioscience 2015; 3(2):345-55.

Binet MT, Adams MS, Gissi F, Golding LA, Schlekat CE, Garman ER, et al. Toxicity of nickel to tropical freshwater and sediment biota: A critical literature review and gap analysis. Environmental Toxicology and Chemistry 2018;37(2):293-317.

Chen S, Zhang G, Luo Y, Zhou H, Wang K, Wang C. Soil erodibility indicators as affected by water level fluctuations in the Three Gorges Reservoir Area, China. Catena 2021; 207:Aticle No. 105692.

Chileshe MN, Syampungani S, Festin ES, Tigabu M, Daneshvar A, Odén PC. Physico-chemical characteristics and heavy metal concentrations of copper mine wastes in Zambia: Implications for pollution risk and restoration. Journal of Forestry Research 2020;31(4):1283-93.

Department of Agriculture - Bureau of Soil and Water Management (DA-BSWM). Soil map of the Philippines: Soil order [Internet]. 2017 [cited 2023 Feb 18]. Available from: http://farmersguidemap.da.gov.ph/.

Frey SK, Gottschall N, Wilkes G, Grégoire DS, Topp E, Pintar KDM, et al. Rainfall-induced runoff from exposed streambed sediments: An important source of water pollution. Journal of Environmental Quality 2015;44(1):236-47.

Gavhane SK, Sapkale JB, Susware NK, Sapkale SJ. Impact of heavy metals in riverine and estuarine environment: A review. Research Journal of Chemistry and Environment 2021;25(5): 226-33.

Gee GW, Or D. Methods of soil analysis. Part 4: Physical Methods. Vadose Zone Journal 2004;3(2):722-3.

Ghosal K, Bhattacharya SD. A review of RUSLE model. Journal of the Indian Society of Remote Sensing 2020;48(4):689-707.

Golightly JP. Nickeliferous laterite deposits. In: Skinner BJ, editor. Seventy-Fifth Anniversary Volume. Society of Economic Geologists; 1981. p. 710-35.

Gozukara G, Altunbas S, Dengiz O, Adak A. Assessing the effect of soil to water ratios and sampling strategies on the prediction of EC and pH using pXRF and Vis-NIR spectra. Computers and Electronics in Agriculture 2022;203:Article No. 107459.

Hajigholizadeh M, Melesse AM, Fuentes HR. Erosion and sediment transport modelling in shallowwaters: A review on approaches, models and applications. International Journal of Environmental Research and Public Health 2018;15(3): Article No. 518.

He S, He Z, Yang X, Baligar VC. Mechanisms of nickel uptake and hyperaccumulation by plants and implications for soil remediation. Advances in Agronomy 2012;117:117-89.

Huang X, Lin L, Ding S, Tian Z, Zhu X, Wu K, et al. Characteristics of soil erodibility K value and its influencing factors in the Changyan Watershed, Southwest Hubei, China. Land 2022;11(1):Article No. 134.

Institute of Water Research (IWR). RUSLE - K factor Soil. Erosion Assessment Tool [Internet]. 2002 [cited 2022 Mar 4]. Available from: http://www.iwr.msu.edu/rusle/kfactor.htm.

International Union of Soil Sciences (IUSS), Working Group for World Reference Base for Soil Resources (WRB). World Reference Base for Soil Resources 2014, update 2015 International Soil Classification System for Naming Soils and Creating Legends for Soil Maps. 3rd ed. World Soil Resources Reports. Rome (Italy): FAO; 2015.

Jha MK. Impacts of landscape changes on water resources. Water (Switzerland) 2020;12(8):10-5.

Khan J, Singh R, Upreti P, Yadav RK. Geo-statistical assessment of soil quality and identification of heavy metal contamination using integrated GIS and multivariate statistical analysis in industrial region of Western India. Environmental Technology and Innovation 2022;28:Article No. 102646.

Khanchoul K, Boubehziz S. Spatial Variability of soil erodibility at El Hammam Catchment, Northeast of Algeria. Environment and Ecosystem Science 2019;3(1):17-25.

Kulikov M, Schickhoff U, Gröngröft A, Borchardt P. Modelling soil erodibility in mountain rangelands of southern Kyrgyzstan. Pedosphere 2020;30(4):443-56.

Kumar S, Kushwaha SPS. Modelling soil erosion risk based on RUSLE-3D using GIS in a Shivalik Sub-Watershed. Journal of Earth System Science 2013;122(2):389-98.

Lei K, Pan H, Lin C. A landscape approach towards ecological restoration and sustainable development of mining areas. Ecological Engineering 2016;90:320-5.

Madubuike CN, Nwachukwu PI, Emerson KU, Asuzu CC. Comparative assessment of selected erodibility indices for erosion prediction of soils of Imo State, Southeast, Nigeria. International Journal of Agriculture, Environment and Bioresearch 2020;5(05):198-209.

Milligan TG, Law BA. Contaminants at the sediment-water interface: Implications for environmental impact assessment and effects monitoring. Environmental Science and Technology 2013;47(11):5828-34.

Morgan RPC, Nearing MA. Handbook of Erosion Modelling. Blackwell Publishing, Ltd; 2011.

Morgan RPC, Quinton JN, Smith RE, Govers G, Poesen JWA, Auerswald K, et al. The european soil erosion model (EUROSEM): A dynamic approach for predicting sediment transport from fields and small catchments. Earth Surface Processes and Landforms 1998;23(6):527-44.

Murphy S, Ciménez D, Muldowney LS, Heckman JR. Soil Organic Matter Level and Interpretation. Fact Sheet FS1136. Rutgers, The State University of New Jersey; 2012. p. 1-3.

Nahon D. Evolution of iron crusts in tropical landscapes. In: Rates of Chemical Weathering of Rocks and Minerals. London: Academic Press; 1986. p. 169-91.

National Institute of Hydrology. Hydrological modeling: Current status and future directions. Environmental Earth Sciences 2017;77:Article No. 242.

Nelson DW, Sommers LE. Total carbon, organic carbon, and organic matter. Methods of Soil Analysis, Part 3: Chemical Methods 2018;(5):961-1010.

Okorafor OO, Akinbile CO, Adeyemo AJ. Determination of soils erodibility factor (K) for selected sites in Imo State, Nigeria. Resources and Environment 2018;8(1):6-13.

Ostovari Y, Ghorbani-Dashtaki S, Kumar L, Shabani F. Soil erodibility and its prediction in semi-arid regions. Archives of Agronomy and Soil Science 2019;65(12):1688-703.

Peralta E, Pérez G, Ojeda G, Alcañiz JM, Valiente M, López-Mesas M, et al. Heavy metal availability assessment using portable X-ray fluorescence and single extraction procedures on former vineyard polluted soils. Science of the Total Environment 2020;726:Article No. 138670.

Pijl A, Reuter LEH, Quarella E, Vogel TA, Tarolli P. GIS-based soil erosion modelling under various steep-slope vineyard practices. Catena 2020;193:Article No.104604.

Prematuri R, Turjaman M, Sato T, Tawaraya K. The impact of nickel mining on soil properties and growth of two fast-growing tropical trees species. International Journal of Forestry Research 2020;2020:Article No. 8837590.

Radziuk H, Switoniak M. Soil erodibility factor (K) in soils under varying stages of truncation. Soil Science Annual 2021; 72(1):1-8.

Rajbanshi J, Bhattacharya S. Assessment of soil erosion, sediment yield and basin specific controlling factors using RUSLE-SDR and PLSR approach in Konar River Basin, India. Journal of Hydrology 2020;587:Article No. 124935.

Ramli M, Purwanto, Thamrin M, Maemuna, Asrafil M. Analysis of soil erosion on mine area. IOP Conference Series: Materials Science and Engineering 2020;875(1):Article No. 012052.

de Roo A, Jetten V, Wesseling C, Ritsema C. LISEM: A physically-based hydrologic and soil erosion catchment model. In: Modelling Soil Erosion by Water. Berlin, Heidelberg: Springer; 1998. p. 429-40.

Salehi-Varnousfaderani B, Honarbakhsh A, Tahmoures M, Akbari M. Soil erodibility prediction by Vis-NIR spectra and environmental covariates coupled with GIS, regression and PLSR in a watershed scale, Iran. Geoderma Regional 2022; 28:e00470.

Schmidt TS, Clements WH, Wanty RB, Verplanck PL, Church SE, Juan CAS, et al. Geologic processes influence the effects of mining on aquatic ecosystems. Ecological Applications 2012;22(3):870-9.

Shirani M, Afzali KN, Jahan S, Strezov V, Soleimani-Sardo M. Pollution and contamination assessment of heavy metals in the sediments of Jazmurian playa in southeast Iran. Scientific Reports 2020;10(1):1-11.

Sreekanth TVM, Nagajyothi PC, Lee KD, Prasad TNVKV. Occurrence, physiological responses and toxicity of nickel in plants. International Journal of Environmental Science and Technology 2013;10(5):1129-40.

Thomas GW. Soil pH and soil acidity. In: Sparks DL, Page AL, Helmke PA, Loeppert RH, Soltanpour PN, Tabatabai MA, et al, editors. Methods of Soil Analysis: Part 3 Chemical Methods, 53. Soil Science Society of America, Inc., American Society of Agronomy, Inc.; 1996. p. 393-400.

Tian Z, Liu F, Liang Y, Zhu X. Mapping soil erodibility in southeast China at 250 m resolution: Using environmental variables and random forest regression with limited samples. International Soil and Water Conservation Research 2022; 10(1):62-74.

Trescases JJ. The lateritic nickel-ore deposits. In: Soils and Sediments. Berlin, Heidelberg: Springer; 1997. p. 125-38.

United States Department of Agriculture - Natural Resources Conservation Service (USDA-NRCS). Oxisols [Internet]. 2023 [cited 2023 Feb 16]. Available from: https://www.nrcs.usda.gov/conservation-basics/natural-resource-concerns/soils/oxisols.

United States Department of Agriculture (USDA). Soil Mechanics Level I Module 3 - USDA Textural Soil Classification. Natural Resources Conservation Service, USDA; 1987. p. 1-53.

Virto I, Antón R, Apesteguía M, Plante A. Role of Carbonates in the Physical Stabilization of Soil Organic Matter in Agricultural Mediterranean Soils. Soil Management and Climate Change: Effects on Organic Carbon, Nitrogen Dynamics, and Greenhouse Gas Emissions. Elsevier; 2017.

Wang Z, Yeung KWY, Zhou GJ, Yung MMN, Schlekat CE, Garman ER, et al. Acute and chronic toxicity of nickel on freshwater and marine tropical aquatic organisms. Ecotoxicology and Environmental Safety 2020;206:Article No. 111373.

Webster D. Ph - Principles and measurement. In: Encyclopedia of Food Sciences and Nutrition. 2nd ed. 2003. p. 4501-7.

Williams JR, Jones CA, Dyke PT. EPIC - Erosion/Productivity Impact Calculator: 1. Model Documentation. United States Department of Agriculture Technical Bulletin. United States Department of Agriculture (USDA); 1990.

Wischmeier WH, Smith DD. Predicting Rainfall Erosion Losses-A Guide to Conservation Planning. Washington DC, USA: U.S. Department of Agriculture; 1986.

World Health Organization (WHO). Permissible Limits of Heavy Metals in Soil and Plants. Switzerland: Geneva: WHO; 1996.

Wu B. Study on Renewal Strategy of Ecological Restoration in an Abandoned Mining Area Based on the View of Loess Civilization. In: Land Reclamation in Ecological Fragile Areas. CRC Press; 2017. p. 51-3.

Zhang Z, Shen N, Wang Y, Li Y, Song Y, He T. Geological environment problems and countermeasures of Shijiaying mine in western Beijing. Procedia Environmental Sciences 2011;11:1245-52.

INSTRUCTION FOR AUTHORS

Publication and Peer-reviewing processes of Environment and Natural Resources Journal

Environment and Natural Resources Journal is a peer reviewed and open access journal that is published in six issues per year. Manuscripts should be submitted online at https://ph02.tci-thaijo.org/index.php/ennrj/about/submissions by registering and logging into this website. Submitted manuscripts should not have been published previously, nor be under consideration for publication elsewhere (except conference proceedings papers). A guide for authors and relevant information for the submission of manuscripts are provided in this section and also online at: https://ph02.tci-thaijo.org/index.php/ennrj/author. All manuscripts are refereed through a **single-blind peer-review** process.

Submitted manuscripts are reviewed by outside experts or editorial board members of **Environment and Natural Resources Journal**. This journal uses double-blind review, which means that both the reviewer and author identities are concealed from the reviewers, and vice versa, throughout the review process. Steps in the process are as follows:

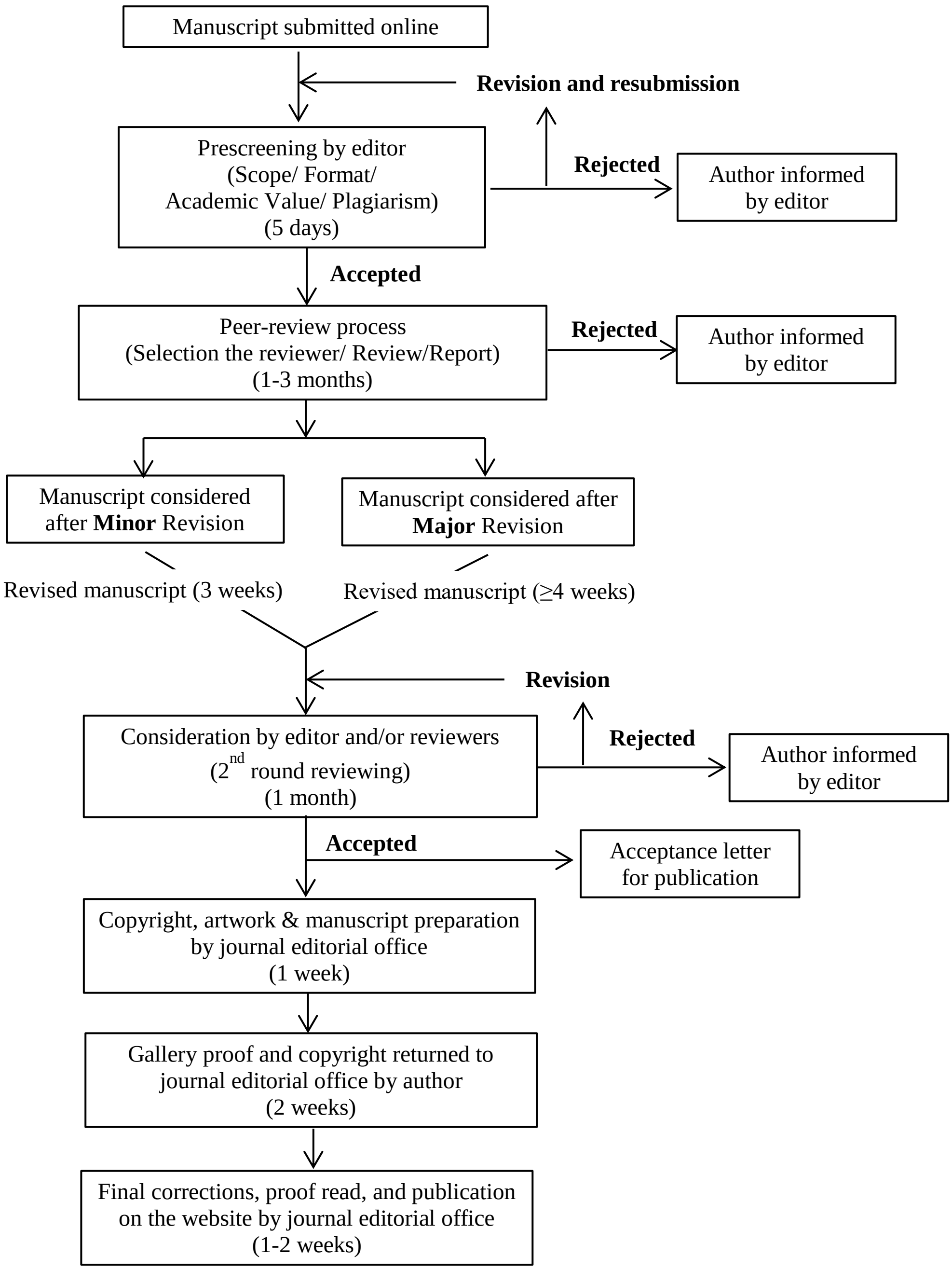

The Environment and Natural Resources Journal (EnNRJ) accepts 2 types of articles for consideration of publication as follows:

- *Original Research Article:* Manuscripts should not exceed 3,500 words (excluding references).
- *Review Article (by invitation):* This type of article focuses on the in-depth critical review of a special aspect in the environment and also provides a synthesis and critical evaluation of the state of the knowledge of the subject. Manuscripts should not exceed 6,000 words (excluding references).

Submission of Manuscript

Cover letter: Key points to include:

- Statement that your paper has not been previously published and is not currently under consideration by another journal
- Brief description of the research you are reporting in your paper, why it is important, and why you think the readers of the journal would be interested in it
- Contact information for you and any co-authors
- Confirmation that you have no competing interests to disclose

Manuscript-full: Manuscript (A4) must be submitted in Microsoft Word Files (.doc or .docx). Please make any identifying information of name(s) of the author(s), affiliation(s) of the author(s). Each affiliation should be indicated with superscripted Arabic numerals immediately after an author's name and before the appropriate address. Specify the Department/School/Faculty, University, Province/State, and Country of each affiliation.

Manuscript-anonymized: Manuscript (A4) must be submitted in Microsoft Word Files (.doc or .docx). Please remove any identifying information, such as authors' names or affiliations, from your manuscript before submission and give all information about authors at title page section.

Reviewers suggestion *(mandatory)*: Please provide the names of 3 potential reviewers with the information about their affiliations and email addresses. *The recommended reviewers should not have any conflict of interest with the authors. Each of the reviewers must come from a different affiliation and must not have the same nationality as the authors.* Please note that the editorial board retains the sole right to decide whether or not the recommended potential reviewers will be selected.

Preparation of Manuscript

Manuscript should be prepared strictly as per guidelines given below. The manuscript (A4 size page) must be submitted in Microsoft Word (.doc or .docx) with Times New Roman 12 point font and a line spacing of 1.5. *The manuscript that is not in the correct format will be returned and the corresponding author may have to resubmit*. The submitted manuscript must have the following parts:

Title should be concise and no longer than necessary. Capitalize first letters of all important words, in Times New Roman 12 point bold.

Author(s) name and affiliation must be given, especially the first and last names of all authors, in Times New Roman 11 point bold.

Affiliation of all author(s) must be given in Times New Roman 11 point italic.

Abstract should indicate the significant findings with data. A good abstract should have only one paragraph and be limited to 250 words. Do not include a table, figure or reference.

Keywords should adequately index the subject matter and up to six keywords are allowed.

Text body normally includes the following sections: 1. Introduction 2. Methodology 3. Results and Discussion 4. Conclusions 5. Acknowledgements 6. References

Reference style must be given in Vancouver style. Please follow the format of the sample references and citations as shown in this Guide below.

Unit: The use of abbreviation must be in accordance with the SI Unit.

Format and Style

Paper Margins must be 2.54 cm on the left and the right. The bottom and the top margin of each page must be 1.9 cm.

Introduction is critically important. It should include precisely the aims of the study. It should be as concise as possible with no sub headings. The significance of problem and the essential background should be given.

Methodology should be sufficiently detailed to enable the experiments to be reproduced. The techniques and methodology adopted should be supported with standard references.

Headings in Methodology section and Results and Discussion section, no more than three levels of headings should be used. Main headings should be typed (in bold letters) and secondary headings (in bold and italic letters). Third level headings should be typed in normal and no bold, for example;

2. Methodology
2.1 Sub-heading
2.1.1 Sub-sub-heading

Results and Discussion can be either combined or separated. This section is simply to present the key points of your findings in figures and tables, and explain additional findings in the text; no interpretation of findings is required. The results section is purely descriptive.
<u>Tables</u> Tables look best if all the cells are not bordered; place horizontal borders only under the legend, the column headings and the bottom.
<u>Figures</u> should be submitted in color; make sure that they are clear and understandable. Please adjust the font size to 9-10, no bold letters needed, and the border width of the graphs must be 0.75 pt. *(Do not directly cut and paste them from MS Excel.)* Regardless of the application used, when your electronic artwork is finalized, please 'save as' or convert the images to TIFF (or JPG) and separately send them to EnNRJ. The images require a resolution of at least 300 dpi (dots per inch). If a label needed in a figure, its font must be "Times New Roman" and its size needs to be adjusted to fit the figure without borderlines.

All Figure(s) and Table(s) should be embedded in the text file.

Conclusions should include the summary of the key findings, and key take-home message. This should not be too long or repetitive, but is worth having so that your argument is not left unfinished. Importantly, don't start any new thoughts in your conclusion.

Acknowledgements should include the names of those who contributed substantially to the work described in the manuscript but do not fulfill the requirements for authorship. It should also include any sponsor or funding agency that supported the work.

References should be cited in the text by the surname of the author(s), and the year. This journal uses the author-date method of citation: the last name of the author and date of publication are inserted in the text in the appropriate place. If there are more than two authors, "et al." after the first author' name must be added. Examples: (Frits, 1976; Pandey and Shukla, 2003; Kungsuwas et al., 1996). If the author's name is part of the sentence, only the date is placed in parentheses: "Frits (1976) argued that . . ."

Please be ensured that every reference cited in the text is also present in the reference list (and vice versa).

In the list of references at the end of the manuscript, full and complete references must be given in the following style and punctuation, arranged alphabetically by first author's surname. Examples of references as listed in the References section are given below.

Book
Tyree MT, Zimmermann MH. Xylem Structure and the Ascent of Sap. Heidelberg, Germany: Springer; 2002.

Chapter in a book
Kungsuwan A, Ittipong B, Chandrkrachang S. Preservative effect of chitosan on fish products. In: Steven WF, Rao MS, Chandrkachang S, editors. Chitin and Chitosan: Environmental and Friendly and Versatile Biomaterials. Bangkok: Asian Institute of Technology; 1996. p. 193-9.

Journal article
Muenmee S, Chiemchaisri W, Chiemchaisri C. Microbial consortium involving biological methane oxidation in relation to the biodegradation of waste plastics in a solid waste disposal open dump site. International Biodeterioration and Biodegradation 2015;102:172-81.

Published in conference proceedings
Wiwattanakantang P, To-im J. Tourist satisfaction on sustainable tourism development, amphawa floating marketSamut songkhram, Thailand. Proceedings of the 1st Environment and Natural Resources International Conference; 2014 Nov 6-7; The Sukosol hotel, Bangkok: Thailand; 2014.

Ph.D./Master thesis

Shrestha MK. Relative Ungulate Abundance in a Fragmented Landscape: Implications for Tiger Conservation [dissertation]. Saint Paul, University of Minnesota; 2004.

Website

Orzel C. Wind and temperature: why doesn't windy equal hot? [Internet]. 2010 [cited 2016 Jun 20]. Available from: http://scienceblogs.com/principles/2010/08/17/wind-and-temperature-why-doesn/.

Report organization:

Intergovernmental Panel on Climate Change (IPCC). IPCC Guidelines for National Greenhouse Gas Inventories: Volume 1-5. Hayama, Japan: Institute for Global Environmental Strategies; 2006.

Remark

** Please be note that manuscripts should usually contain at least 15 references and some of them must be up-to-date research articles.*

** Please strictly check all references cited in text, they should be added in the list of references. Our Journal does not publish papers with incomplete citations.*

Changes to Authorship

This policy of journal concerns the addition, removal, or rearrangement of author names in the authorship of accepted manuscripts:

Before the accepted manuscript

For all submissions, that request of authorship change during review process should be made to the form below and sent to the Editorial Office of EnNRJ. Approval of the change during revision is at the discretion of the Editor-in-Chief. The form that the corresponding author must fill out includes: (a) the reason for the change in author list and (b) written confirmation from all authors who have been added, removed, or reordered need to confirm that they agree to the change by signing the form. Requests form submitted must be consented by corresponding author only.

After the accepted manuscript

The journal does not accept the change request in all of the addition, removal, or rearrangement of author names in the authorship. Only in exceptional circumstances will the Editor consider the addition, deletion or rearrangement of authors after the manuscript has been accepted.

Copyright transfer

The copyright to the published article is transferred to Environment and Natural Resources Journal (EnNRJ) which is organized by Faculty of Environment and Resource Studies, Mahidol University. The accepted article cannot be published until the Journal Editorial Officer has received the appropriate signed copyright transfer.

Online First Articles

The article will be published online after receipt of the corrected proofs. This is the official first publication citable with the Digital Object Identifier (DOI). After release of the printed version, the paper can also be cited by issue and page numbers. DOI may be used to cite and link to electronic documents. The DOI consists of a unique alpha-numeric character string which is assigned to a document by the publisher upon the initial electronic publication. The assigned DOI never changes.

Mahidol University

Wisdom of the Land

Research and Academic Service Section, Faculty of Environment and Resource Studies, Mahidol University
999 Phutthamonthon 4 Rd, Salaya, Nakhon Pathom 73170, Phone +662 441-5000 ext. 2108 Fax. +662 441 9509-10
E-mail: ennrjournal@gmail.com Website: https://www.tci-thaijo.org/index.php/ennrj